UNCLASSIFIED

AD NUMBER

AD277163

LIMITATION CHANGES

TO:

Approved for public release; distribution is unlimited.

FROM:

**Distribution authorized to U.S. Gov't. agencies and their contractors;
Administrative/Operational Use; FEB 1962. Other requests shall be referred to Wright Aeronautical Development Division, Wright-Patterson AFB, OH 45433.**

AUTHORITY

WL/AFSC (IST) ltr dtd 28 Mar 1991

THIS PAGE IS UNCLASSIFIED

AD0277163

[redacted]

WADD TR 60-411
PART 2

PREDICTION OF CREEP EFFECTS IN AIRCRAFT STRUCTURES

TECHNICAL REPORT WADD-TR-60-411, PART 2

FEBRUARY 1962

20080818 026

FLIGHT DYNAMICS LABORATORY
AERONAUTICAL SYSTEMS DIVISION
AIR FORCE SYSTEMS COMMAND
WRIGHT-PATTERSON AIR FORCE BASE, OHIO

Project No. 1367, Task No. 14002

(Prepared under Contract AF 33(616)-6567
by General Dynamics/Convair, San Diego, California.
Authors: C. W. Alesch, B. Klein, and W. Robe)

NOTICES

When Government drawings, specifications, or other data are used for any purpose other than in connection with a definitely related Government procurement operation, the United States Government thereby incurs no responsibility nor any obligation whatsoever; and the fact that the Government may have formulated, furnished, or in any way supplied the said drawings, specifications, or other data, is not to be regarded by implication or otherwise as in any manner licensing the holder or any other person or corporation, or conveying any rights or permission to manufacture, use, or sell any patented invention that may in any way be related thereto.



ASTIA release to OTS not authorized.

Qualified requesters may obtain copies of this report from the Armed Services Technical Information Agency, (ASTIA), Arlington Hall Station, Arlington 12, Virginia.



Copies of WADD Technical Reports and Technical Notes should not be returned to the Wright Air Development Division unless return is required by security considerations, contractual obligations, or notice on a specific document.

300 - June 1962 - 35-1518 & 1519

AD277163

FOREWORD

This report was prepared by the Engineering Structures Group, Engineering Department, General Dynamics/Convair, San Diego, California under Contract AF 33(616)-6567, Project No. 1367, "Structural Design Criteria," Task No. 14002, "Structural Analysis Methods." This contract was administered under the direction of the Flight Dynamics Laboratory, Wright Air Development Division, now designated Aeronautical Systems Division, with Lt. J. M. O'Connor, Mr. R. M. Bader and Mr. Laszlo Berke acting as Project Engineers.

This report covers the period of work from April 15, 1960 to April 15, 1961.

The Convair personnel who contributed to the project were: Dr. W. H. Steurer, Chief of Engineering Materials, B. Klein, Structural Research Design Specialist, C. W. Alesch, Engineering Metallurgy Design Specialist, W. Robe, Structural Engineer, G. de Vries, Design Engineer, H. H. Stier, J. M. Harvey and W. M. Parker, Metallurgists, and A. C. Carlson, Structural Test Engineer.

ABSTRACT

The method presented in WADD TR 60-411 Part I for predicting deformations in aircraft structures undergoing creep is reviewed. Modifications and simplifications of this method are considered and a simplified version of the original method is presented. Box beam tests were used to investigate the simplified method. The outcome of these tests indicated the accuracy of the method in predicting deformations in aircraft structures undergoing creep was in the same order of accuracy as that usually experienced in redundant analysis procedures.

The power law for expressing creep relations is found redundant in solution. Its usefulness appears chiefly in the display of creep test data. Current creep prediction methods, such as the Larson-Miller and Manson Haferd methods, appear as linearizing approximations for creep-relations with the result that inaccuracies in predicting very long and very short creep life restrict their usefulness. An approach to creep prediction based on creep-rupture history for establishment of creep laws is proposed. Relationships between tension - and creep - test data are examined experimentally with respect to single and repetitive load applications. General relationships are examined with the outcome that a general approach to creep prediction in all metallic materials appears improbable.

PUBLICATION REVIEW

This report has been reviewed and is approved.

FOR THE COMMANDER



WILLIAM C. NIELSEN
Colonel, USAF
Chief, Flight Dynamics Laboratory

TABLE OF CONTENTS

PAGE

SECTION I. NUMERICAL METHOD

Introduction 1
Limitations 1
Review of General Method 2
Illustrative Examples 7
Plane Stress 9
Plate Elements Subject to Bending 10
Proposed Procedure 14
Modifying Theories 15
Age Hardening Theory 15
Generalized Superposition Theory 15
Strain Hardening Theory 17
Combined Strain and Age Hardening Theory 18
Representation of Creep 18
Simplifying Changes in Proposed Method 22
Box Beam Tests - Design 22
Idealization of Structure for Analysis 23
Box Beam Tests - Procedure 24
Outcome of Tests 26
Comparison Criteria 26
Summary and Conclusions 26
References 27

SECTION II. MATERIAL CHARACTERISTICS

Introduction 28
Basic Limitations Upon the Structural Stability of Materials . . . 28
Structurally Significant Variables Operative in Heated Environments 29
The Deformation Variable 29
Stress Strain Relations 30
Strain Rate Effects 30
The Power Law Expression for Creep Relations 32
The Exponential Law Expression for Creep Relations 34
Linearizations 36
Cumulative Creep Curves 37
Non-Dimensional Creep Curves 38
Incremental Load Applications and Release Effects 38
Effect of Decremental Loading at Various Temperatures 41
Effect of Decremental Loading at Varying Stresses and Constant Temperature 42

TABLE OF CONTENTS (Cont'd)

PAGE

Creep Initiation 42
Effect of Stainless Steel Alloy Change on Creep Stability 44
Effect of Base Metal Change on Creep Stability 45
Effect of a "Non-Hardening" Material on Creep Stability 47
Summary and Conclusions 49
References 50

APPENDIX I - VERIFICATIONS OF ELECTRIC RESISTANCE STRAIN GAGES FOR USE WITH STAINLESS STEEL AT ELEVATED TEMPERATURES. . 204

APPENDIX II - EXAMPLE PROBLEM ILLUSTRATING USE OF PROPOSED METHOD FOR INTRODUCING CREEP INTO AIRFRAME ANALYSIS 206

APPENDIX III- BIBLIOGRAPHY 211

LIST OF FIGURES

FIGURE	TITLE	PAGE
1.	Tensile Stress Strain Time Curves for .050 Inch Thick Armco PH 15-7 Mo, Condition RH 950 Steel	95
2.	Tensile Stress Strain Time Curves (log-log) .050 Inch Thick Armco PH 15-7 Mo, Condition RH 950 Steel	96
3.	Temperature - Mach Number Speed Data	97
4.	Methods for Presenting Creep Data (2 pages)	98
5.	Test Box Idealization - General	100
6.	Test Box Idealization - Spars and Bulkheads - Box II and III	101
7.	Test Box Idealization - Plate Surfaces - Box II	102
8.	Test Box Idealization - Plate Surfaces - Box III	103
9.	Predicted Elastic Strains in Box II Cover Plates	104
10.	Predicted Elastic Stresses in Box II Cover Plates	105
11.	Predicted Elastic Strains in Box III Cover Plates	106
12.	Predicted Elastic Strains in Box III Cover Plates	107
13.	Predicted Elastic Stresses in Box III Cover Plates	108
14.	Predicted Creep Strain in Lower Cover Plate of Box III	109
15.	Fabrication Drawing for Test Box (2 pages)	110
16.	Test Box	112
17.	Test Box Failure - Box II	113
18.	Test Box Failure - Box III	114
19.	Test Box Installation	115
20.	Test Temperatures - Box II (3 pages)	116
21.	Thermocouple Locations - Box III	119
22.	Test Load Spectrum - Box II	120
23.	Test Load Spectrum - Box III	121
24.	Strain Gage and Node Locations - Box III	122
25.	Test Strains, Box II (2 pages)	123
26.	Test Strains - Box III (2 pages)	125

LIST OF FIGURES (Cont'd)

FIGURE	TITLE	PAGE
27.	Strain Comparison - Box II Tension Surface	127
28.	Strain Comparison - Box III	128
29.	Curvature Comparison - Box III	129
30.	Schematic Stress Strain Curve with Derived Plastic Strain Curve	130
31.	Stress Strain Curves for Armco 17-7 PH Condition TH 1050 Stainless Steel at Various Strain Rates at 1200°F	131
32.	Plastic Stress Strain Curves for Armco 17-7 PH Condition TH 1050 Stainless Steel at Various Strain Rates at 1200°F	132
33.	Plastic Stress Strain Curves for Armco 17-7 PH Stainless Steel at Various Strain Rates at 1200°F	133
34.	Schematic Stress Strain Curves Resulting from Load Applications at Different Strain Rates	134
35.	Schematic Creep Time versus Creep Strain Plot	135
36.	Schematic Rupture Time Fraction versus Creep Strain Plot	136
37.	Non-Dimensional Creep Curves (Schematic)	137
38.	Program for Incremental Loading Test (Schematic)	138
39.	Typical Deformation Activity upon Incremental Loading Armco PH 15-7 Mo at Elevated Temperature	139
40.	Time-Deformation Data, Incremental Loading, Armco PH 15-7 Mo	140
41.	Time-Deformation Data, Incremental Loading, Armco PH 15-7 Mo	141
42.	Program for Decremental Loading Test	142
43.	Time-Deformation Data, Decremental Loading, Armco PH 15-7 Mo, 700°F	143
44.	Time-Deformation Data, Decremental Loading, Armco PH 15-7 Mo, 700°F	144
45.	Time-Deformation Data, Decremental Loading, Armco PH 15-7 Mo, 800°F	145
46.	Time-Deformation Data, Decremental Loading, Armco PH 15-7 Mo, 800°F	146
47.	Time-Deformation Data, Decremental Loading, Armco PH 15-7 Mo, 900°F	147

LIST OF FIGURES (Cont'd)

FIGURE	TITLE	PAGE
48.	Time-Deformation Data, Decremental Loading, Armco PH 15-7 Mo, 900° F	148
49.	Time-Deformation Data, Decremental Loading, Armco PH 15-7 Mo, 1000° F	149
50.	Time-Deformation Data, Decremental Loading, Armco PH 15-7 Mo, 1000° F	150
51.	Time-Deformation Data, Decremental Loading, Armco PH 15-7 Mo, 185 KSI	151
52.	Time-Deformation Data, Decremental Loading, Armco PH 15-7 Mo, 185 KSI	152
53.	Time-Deformation Data, Decremental Loading, Armco PH 15-7 Mo, 188 KSI	153
54.	Time-Deformation Data, Decremental Loading, Armco PH 15-7 Mo, 188 KSI	154
55.	Time-Deformation Data, Decremental Loading, Armco PH 15-7 Mo, 191 KSI	155
56.	Time-Deformation Data, Decremental Loading, Armco PH 15-7 Mo, 191 KSI	156
57.	Time-Deformation Data, "Standard" Creep Test, Armco PH 15-7 Mo, 700° F	157
58.	Time-Deformation Data, "Standard" Creep Test, Armco PH 15-7 Mo, 700° F	158
59.	Time-Deformation Data, "Standard" Creep Test, Armco PH 15-7 Mo, 700° F	159
60.	Time-Deformation Data, "Standard" Creep Test, Armco PH 15-7 Mo, 700° F	160
61.	Time-Deformation Data, "Standard" Creep Test, Armco PH 15-7 Mo, 700° F	161
62.	Time-Deformation Data, "Standard" Creep Test, Armco PH 15-7 Mo, 800° F	162
63.	Time-Deformation Data, "Standard" Creep Test, Armco PH 15-7 Mo, 800° F	163

LIST OF FIGURES (Cont'd)

FIGURE	TITLE	PAGE
64.	Time-Deformation Data, "Standard" Creep Test, Armco PH 15-7 Mo, 800°F	164
65.	Time-Deformation Data, "Standard" Creep Test, Armco PH 15-7 Mo, 800°F	165
66.	Time-Deformation Data, "Standard" Creep Test, Armco PH 15-7 Mo, 800°F	166
67.	Time-Deformation Data, "Standard" Creep Test, Armco PH 15-7 Mo, 900°F	167
68.	Time-Deformation Data, "Standard" Creep Test, Armco PH 15-7 Mo, 900°F	168
69.	Time-Deformation Data, "Standard" Creep Test, Armco PH 15-7 Mo, 900°F	169
70.	Time-Deformation Data, "Standard" Creep Test, Armco PH 15-7 Mo, 900°F	170
71.	Time-Deformation Data, "Standard" Creep Test, Armco PH 15-7 Mo, 900°F	171
72.	Time-Deformation Data, "Standard" Creep Test, Armco PH 15-7 Mo, 1000°F	172
73.	Time-Deformation Data, "Standard" Creep Test, Armco PH 15-7 Mo, 1000°F	173
74.	Time-Deformation Data, "Standard" Creep Test, Armco PH 15-7 Mo, 1000°F	174
75.	Time-Deformation Data, "Standard" Creep Test, Armco PH 15-7 Mo, 1000°F	175
76.	Stress Strain Diagram, Allegheny Ludlum AM 355, Condition SCT Stainless Steel, 700°F	176
77.	Creep Curve, Allegheny Ludlum AM 355, Condition SCT Stainless Steel.	177
78.	Creep Curve, Allegheny Ludlum AM 355, Condition SCT Stainless Steel.	178
79.	Creep Curve, Allegheny Ludlum AM 355, Condition SCT Stainless Steel	179
80.	Creep Curve, Allegheny Ludlum AM 355, Condition SCT Stainless Steel	180
81.	Creep Curve, Allegheny Ludlum AM 355, Condition SCT Stainless Steel	181
82.	Creep Curve, Allegheny Ludlum AM 355, Condition SCT Stainless Steel	182

LIST OF FIGURES (Cont'd)

FIGURE	TITLE	PAGE
83.	Creep Curve, Allegheny Ludlum AM 355, Condition SCT Stainless Steel . .	183
84.	Creep Curve, Allegheny Ludlum AM 355, Condition SCT Stainless Steel . .	184
85.	Creep Curve, Allegheny Ludlum AM 355, Condition SCT Stainless Steel . .	185
86.	Creep Curve, Allegheny Ludlum AM 355, Condition SCT Stainless Steel . .	186
87.	Creep Curve, Allegheny Ludlum AM 355, Condition SCT Stainless Steel . .	187
88.	Creep Curve, Allegheny Ludlum AM 355, Condition SCT Stainless Steel . .	188
89.	Stress Strain Curves, Rene 41 Alloy	189
90.	Creep Curve, Rene 41 Alloy 1300° F	190
91.	Creep Curve, Rene 41 Alloy, 1300° F	191
92.	Creep Curves, Rene 41 Alloy, 1300° F	192
93.	Creep Curves, Rene 41 Alloy, 1300° F	193
94.	Creep Curve, Rene 41 Alloy, 1300° F	194
95.	Creep Curves, Rene 41 Alloy, 1300° F	195
96.	Creep Curves, Rene 41 Alloy, 1300° F	196
97.	Stress Strain Curves, HS-25 Alloy	197
98.	Creep Curves, HS-25 Alloy, 1600° F	198
99.	Creep Curves, HS-25 Alloy, 1600° F	199
100.	Electric Resistance Strain Gage Calibration Test Specimen	200
101.	Strain Gage Calibration - Room Temperature	201
102.	Strain Gage Calibration - 800° F	202
103.	Illustrative Example Scheme	203

LIST OF TABLES

TABLE	TITLE	PAGE
1.	Element Stiffness Matrix	51
2.	Box Stiffness Matrix - Representation of Columns of T_1	53
3.	Box Stiffness Matrix - Transformation Matrix T_1	55
4.	Box Stiffness Matrix	56
5.	Box Deflections for Unit Loads	57
6.	Predicted Elastic Strains and Curvatures	61
7.	Stress and Strain Redistribution For ϵ_c = .000100 in./in.	63
8.	Load Spectrum - Predicted and Final - Box I, II and III.	68
9.	Temperatures for Discreet Load Levels - Box III	69
10.	Predicted Creep Strain, Box II and III	70
11.	Strain Redistribution in Box III	71
12.	Stress Redistribution in Box III	73
13.	Stress Redistribution in Box III Due to Creep	75
14.	Summation of Stress and Strain Redistribution in Box III	76
15.	Predicted Creep Curvature, Box III	77
16.	Deflections and Curvatures, Box II	80
17.	Deflections and Curvatures, Box III	82
18.	Strain Comparison, Box II	85
19.	Strain Comparison, Box III	86
20.	Curvature Comparison, Box III	88
21.	Empirical Creep Power Law Expressions for 7075-T6 Aluminum Alloy	89
22.	Comparison of Permanent Sets - Incremental Loading Condition	90
23.	Comparison of Permanent Sets - Decremental Loading Condition	91
24.	Comparison of Permanent Sets - Decremental Loading Condition.	92
25.	Creep Test Data Summary	93
26.	Stresses Arising From Creep Strain Increments	94

LIST OF SYMBOLS

SYMBOL		REPRESENTATION
$\epsilon_{x_c}, \epsilon_{y_c}, \epsilon_{z_c}$	=	creep strain in x, y and z directions
$\dot{\epsilon}_{x_c}, \dot{\epsilon}_{y_c}, \dot{\epsilon}_{z_c}$	=	creep strain rate in x, y and z directions
$\sigma_x, \sigma_y, \sigma_z$	=	stress in x, y and z directions
σ_p	=	hydrostatic stress
λ	=	threshold stress at which creep strain becomes apparent
n	=	a constant
$\dot{\epsilon}_c$	=	creep strain rate
ϵ_c	=	creep strain
A	=	a constant
p	=	a constant
t	=	time or thickness
T	=	temperature, °K
J	=	invariant of stress
I	=	moment of inertia
F	=	function
γ	=	shear strain
τ	=	shear stress

SYMBOL		REPRESENTATION
E	=	modulus of elasticity
ν	=	Poisson's ratio
α	=	coefficient of linear expansion
M_x, M_y	=	bending moments in x and y directions
M_{xy}	=	twisting moment
W	=	normal deflection
D	=	flexural rigidity of a plate
h	=	hydrostatic without displacement
$(\phi)_{(t)}$	=	function of time
$\varphi_{(eq)}$	=	function of equivalent uniaxial strain
$K_{(x)}$	=	function of x
K^*	=	an integral operator
S	=	a constant
$\triangle H$	=	activation energy
g_1, g_2	=	function of $\cdots$

PREDICTION OF CREEP EFFECTS
IN
AIRCRAFT STRUCTURES
SECTION I. NUMERICAL METHOD

INTRODUCTION

The primary objective of this creep prediction study is to develop a method to predict with reasonable accuracy the deformations in aircraft structures undergoing creep. Such a method must be capable of accounting for both constant and varying temperatures and, or loads which produce strains up to but not necessarily including the failed state.

A basic method for predicting creep effects in aircraft structures was presented in WADD TR 60-411, Part I. Although tests were performed in support of certain criteria used in the method and illustrative examples worked out, no major tests were performed in support of the method. In order to perform these tests, a program utilizing built-up boxes subject to bending and torsion as well as high temperatures was set up for test. The purpose of these tests was to determine the accuracy of the predicted creep effects in comparison with experimentally derived creep effects for typical aircraft construction. In addition attempts were made to correct and simplify any part of the method as the need appeared desirable.

LIMITATIONS

In order to obtain useful results only certain ranges of plastic deformation, load or stress and temperature was considered with certain materials. The primary effort in the investigation centered on the Armco PH 15-7 Mo, Condition RH 950 stainless steel. The heat treatments involved in obtaining Condition RH 950 material were those considered conducive to both good tensile and creep properties. Pertinent creep data for this material are shown in Figures 1 and 2.

Because available strain gages operate reliably within the ranges of 900°F and under, and, 8 percent strain, experimental correlations were held within these limits.

It is difficult to see a need at present for predicting total strains greater than about one percent. In any case this is sufficient to change the general geometry of a structure. The absolute upper limit for investigation is limited by the strain to failure of the material itself.

Manuscript released by the authors June 1961 for publication as a WADD Technical Report

This strain is about six percent. Under this condition and assuming a possible strain concentration factor of about four, the average strain in sections would be limited to about one and one-half percent strain. It is difficult to set arbitrary limits for strain from an aerodynamic standpoint since these limits would depend on the uses of the structures involved. Hence, aerodynamic limitations are ignored.

The temperature on a structure necessarily is less than the stagnation temperature caused by friction in the air surrounding the structure. As Figure 3 shows, the temperature of 900° F is equivalent to a speed of about Mach 4 at 70,000 feet. This temperature accordingly was taken as a reasonable limit for an investigation considering airframe structures.

REVIEW OF GENERAL METHOD

The method of procedure advanced for predicting creep effects in aircraft structures consists of two parts:

1. Prediction of creep effects in elements of structures

2. Prediction of the effect of creep in an element upon a structure.

Structural elements are arbitrarily considered to be stringers or plates. Structures are considered to be redundant or statically determinate assemblies of structural elements. In actual practice it is necessary to consider structural elements that are loaded and, or heated so as to produce multi-axial states of stress and strain in the presence of creep. Such elements would exist in wings and shell bodies of air breathing supersonic aircraft, ascending missiles or re-entry gliders such as the Dyna Soar. Much attention in the past has been devoted to uniaxial creep behavior. This subject in itself is quite formidable. At the same time several formulations have been and are being proposed to treat the general conditions of multiaxial creep behavior. The various methods hinge on various assumptions and hypotheses. It is the purpose here to discuss various of these approaches to determine what underlying principles may be common to them and what the engineer might do in actual practice.

Practically all investigators use certain simplifying assumptions regarding material behavior. These include the following:

1. Materials are initially isotropic and remain so under creep conditions.

2. Materials behave the same in compression as in tension.

3. Materials are incompressible for small strains.

4. The directions of principal stress and strain increments coincide.

5. a. Maximum shear creep strains are proportional to corresponding maximum shear stresses, or as an alternate,

   b. Creep strain rates are proportional to corresponding components of stress deviators, i.e., hydrostatic stress does not affect creep.

6. The multiaxial state is related to a uniaxial state by use of notions of equivalent stress and strain. These notions are embodied in the so-called effective, intensity or second invariant notions of stress and strain.

7. Steady state conditions prevail, i.e., stress and temperature are constants.

At this point it will be convenient to define and discuss some of the terms and ideas appearing in the above statements. Incompressibility of materials means that

$$\epsilon_{x_c} + \epsilon_{y_c} + \epsilon_{z_c} = 0 \tag{1}$$

and

$$\dot{\epsilon}_{x_c} + \dot{\epsilon}_{y_c} + \dot{\epsilon}_{z_c} = 0 \tag{2}$$

where the epsilons represent three rectangular strains at any point and the superscript dot indicates time rate of change. The subscript c refers to creep. A stress deviator is defined as the difference between a stress and a hydrostatic or pressure stress,

$$\sigma_p = \frac{1}{3}(\sigma_x + \sigma_y + \sigma_z) \, . \tag{3}$$

Notice that σ_p is independent of the rectangular axes, since $\sigma_x + \sigma_y + \sigma_z$ is an invariant. σ_p is also the same as the so called octahedral normal stress that acts on the octahedral plane containing the octahedral shear stress. Now the stress deviators are:

$$\sigma_x - \sigma_p = \frac{2}{3}\left[\sigma_x - \frac{1}{2}(\sigma_y + \sigma_z)\right] \tag{4}$$

$$\sigma_y - \sigma_p = \frac{2}{3}\left[\sigma_y - \frac{1}{2}(\sigma_x + \sigma_z)\right] \tag{5}$$

$$\sigma_z - \sigma_p = \frac{2}{3}\left[\sigma_z - \frac{1}{2}(\sigma_x + \sigma_y)\right] \tag{6}$$

It is interesting to note that these stress deviators have the same mathematical form as the elastic stress strain relations but with Poisson's ratio put equal to 1/2.

According to assumption 5b one may write

$$\dot{\epsilon}_{x_c} = \left[\sigma_x - \frac{1}{2}(\sigma_y + \sigma_z) \right] f; \quad \dot{\gamma}_{xy_c} = 3\,\tau_{xy}\, f \tag{7}$$

$$\dot{\epsilon}_{y_c} = \left[\sigma_y - \frac{1}{2}(\sigma_x + \sigma_z) \right] f; \quad \dot{\gamma}_{yz_c} = 3\,\tau_{yz}\, f \tag{8}$$

$$\dot{\epsilon}_{z_c} = \left[\sigma_z - \frac{1}{2}(\sigma_x + \sigma_y) \right] f; \quad \dot{\gamma}_{xz_c} = 3\,\tau_{xz}\, f \tag{9}$$

where f is some function yet to be determined. The same relations may be derived starting with assumption 5a and then using assumption 3. Notice that strain deviators are the same as strains because of the assumption of incompressibility, i.e.,

$$\epsilon_{x_c} - \frac{1}{3}\left(\epsilon_{x_c} + \epsilon_{y_c} + \epsilon_{z_c} \right) = \epsilon_{x_c}, \text{etc.} \tag{10}$$

So far most of the investigators agree. The conjecture appears to be in the choice of the function f. These differences are understandable because of the variance in creep law functions even for uniaxial loading. Let us consider then some of the proposed forms of uniaxial creep laws. Assume first that temperature is constant. One of the first and simplest rules is due to Bailey and Norton. It considers only what we call steady creep, or secondary creep, and is written

$$\dot{\epsilon}_c = (\sigma/\lambda)^n \qquad 3 < n < 10 \tag{11}$$

Notice that λ here has the significance of a threshold stress. Another possibility for predicting steady creep is

$$\dot{\epsilon}_c = A \sinh (\sigma/\lambda) \, . \tag{12}$$

Primary creep may be expressed by

$$\epsilon_c = (\sigma/\lambda)^n t^{1/p}, \quad 2 < p < 3 \, , \tag{13}$$

which becomes upon differentiation

$$\dot{\epsilon}_c = (1/p)\,(\sigma/\lambda)^n t^{(1/p)-1} \, . \tag{14}$$

One could eliminate time

$$t = \epsilon_c^p \, (\sigma/\lambda)^{-np} \tag{15}$$

and get

$$\dot{\epsilon}_c = (1/p) \, (\sigma/\lambda)^{np} / \epsilon_c^{p-1} \, . \tag{16}$$

One may generalize the above as well as the steady creep equations to the form

$$\dot{\epsilon}_c = F(\sigma, \, \epsilon_c, \, t, \, T) \, . \tag{17}$$

This expression means that the creep strain rate is in general a function of stress, creep strain, time and temperature.

Let us return to the multiaxial condition and the function f. In order to determine this function, the ideas stated in assumption 6 are used. This requires relating the multiaxial to the uniaxial state. This is accomplished by means of the quantities of equivalent stress and strain. These quantities physically are proportional to the shear stress acting on the octahedral plane and the corresponding shear strain. When shear stress and shear strain acting on the octahedral plane reach certain magnitudes, shear slippage or yielding is assumed to begin. Mathematically the square of the equivalent stress is defined as three times the deviated second stress invariant, J_2:

$$J_2 = \frac{1}{6} \left[(\sigma_x - \sigma_y)^2 + (\sigma_y - \sigma_z)^2 + (\sigma_z - \sigma_x)^2 \right] + (\tau_{xy}^2 + \tau_{xz}^2 + \tau_{yz}^2) \tag{18}$$

$$\sigma_{eq} = (3 J_2)^{\frac{1}{2}} = (3/\sqrt{2}) \, \tau_{oct} \tag{19}$$

Also the square of the equivalent strain is defined as 2/3 times the deviated second strain invariant, I_2:

$$I_2 = \frac{1}{3} \left[(\epsilon_x - \epsilon_y)^2 + (\epsilon_y - \epsilon_z)^2 + (\epsilon_z - \epsilon_x)^2 \right] + \frac{1}{2} \left(\gamma_{xy}^2 + \gamma_{yz}^2 + \gamma_{zx}^2 \right) \tag{20}$$

$$\epsilon_{eq} = (2/3 \, I_2)^{\frac{1}{2}} = 1/\sqrt{2} \, \gamma_{oct} \tag{21}$$

The relationship between the multiaxial and uniaxial states is found by using σ_{eq} and ϵ_{eq} or J_2 and I_2 in place of σ and ϵ appearing in uniaxial creep expressions or functions. Thus

$$\dot{\epsilon}_{eq_c} = F \, (\sigma_{eq}, \, \epsilon_{eq_c}, \, t, \, T) \tag{22}$$

Returning to the equations involving the functions, f, the special case of uniaxial loading is considered. Then the Equation (17) becomes

$$\dot{\epsilon}_{x_c} = \sigma_x f \, . \tag{23}$$

Replacing ϵ_{x_c} and σ_{x_c} with ϵ_{eq} and σ_{eq}

$$\dot{\epsilon}_{eq_c} = \sigma_{eq} f \tag{24}$$

is found. But $\dot{\epsilon}_{eq_c}$ is defined by F above. Thus

$$f = F\,(\sigma_{eq}, \epsilon_{eq_c}, t, T)/\sigma_{eq} \, . \tag{25}$$

Now the expressions for the creep rates in rectangular coordinates may be written:

$$\dot{\epsilon}_{x_c} = \left[\sigma_x - \frac{1}{2}(\sigma_y + \sigma_z)\right] \frac{F}{\sigma_{eq}}; \quad \dot{\gamma}_{xy_c} = 3\,\tau_{xy} \cdot \left(\frac{F}{\sigma_{eq}}\right) \tag{26}$$

$$\dot{\epsilon}_{y_c} = \left[\sigma_y - \frac{1}{2}(\sigma_x + \sigma_z)\right] \frac{F}{\sigma_{eq}}; \quad \dot{\gamma}_{yz_c} = 3\,\tau_{yz} \cdot \left(\frac{F}{\sigma_{eq}}\right) \tag{27}$$

$$\dot{\epsilon}_{z_c} = \left[\sigma_z - \frac{1}{2}(\sigma_x + \sigma_y)\right] \frac{F}{\sigma_{eq}}; \quad \dot{\gamma}_{xz_c} = 3\,\tau_{xz} \cdot \left(\frac{F}{\sigma_{eq}}\right) \tag{28}$$

The procedure to follow in actual problem solution is as follows:

1. Given σ_x, σ_y, σ_z, τ_{xy}, τ_{xz}, τ_{yz}, ϵ_{x_c}, ϵ_{y_c}, ϵ_{z_c}, γ_{xy_c}, γ_{yz_c}, γ_{zx_c}

   calculate

$$\sigma_{eq} = \left\{\frac{1}{2}\left[(\sigma_x - \sigma_y)^2 + (\sigma_y - \sigma_z)^2 + (\sigma_z - \sigma_x)^2\right] + 3\left(\tau_{xy}^2 + \tau_{xz}^2 + \tau_{yz}^2\right)\right\}^{\frac{1}{2}} \tag{29}$$

$$\epsilon_{eq_c} = \left\{\frac{2}{9}\left[(\epsilon_{x_c} - \epsilon_{y_c})^2 + (\epsilon_{y_c} - \epsilon_{z_c})^2 + (\epsilon_{z_c} - \epsilon_{x_c})^2\right] + \frac{1}{3}\left(\gamma_{xy_c}^2 + \gamma_{yz_c}^2 + \gamma_{zx_c}^2\right)\right\}^{\frac{1}{2}} \tag{30}$$

2. If an analytic function F is not available, use σ_{eq} and ϵ_{eq_c} to read $\dot{\epsilon}_{eq_c}$ from appropriate graphs.

3. Lastly calculate

$$\dot{\epsilon}_{x_c} = \left[(\sigma_x - \sigma_y) + (\sigma_x - \sigma_z) \right] \frac{F}{2\sigma_{eq}}, \quad \dot{\gamma}_{xy_c} = 3\ \tau_{xy} \frac{F}{\sigma_{eq}} \tag{31}$$

$$\dot{\epsilon}_{y_c} = \left[(\sigma_y - \sigma_z) + (\sigma_y - \sigma_z) \right] \frac{F}{2\sigma_{eq}}, \quad \dot{\gamma}_{yz_c} = 3\ \tau_z \frac{F}{\sigma_{eq}} \tag{32}$$

$$\dot{\epsilon}_{z_c} = \left[(\sigma_z - \sigma_x) + (\sigma_z - \sigma_y) \right] \frac{F}{2\sigma_{eq}}, \quad \dot{\gamma}_{xz_c} = 3\ \tau_{xz} \frac{F}{\sigma_{eq}} \tag{33}$$

ILLUSTRATIVE EXAMPLES

1. Assuming steady creep under constant stress, Norton's Law may be applied.

$$\dot{\epsilon}_c = (\sigma/\lambda)^n \tag{11}$$

and

$$\dot{\epsilon}_{eq_c} = (\sigma_{eq}/\lambda)^n \tag{34}$$

thus

$$\dot{\epsilon}_{x_c} = \left[(\sigma_x - \sigma_y) + (\sigma_x - \sigma_z) \right] \frac{(\sigma_{eq_c}/\lambda)^{n-1}}{2\lambda}, \quad \dot{\gamma}_{xy_c} = 3\ \tau_{xy} \cdot \frac{(\sigma_c/\lambda)^{n-1}}{2\lambda}. \tag{35}$$

This result has been obtained or used by several authors, such as Timoshenko, Poritsky, Odqvist, Calladine and others.

2. When primary creep at constant stress is considered,

$$\dot{\epsilon}_c = (1/p)\ (\sigma/\lambda)^n\ t^{(1/p)\ -\ 1} \tag{36}$$

and

$$\dot{\epsilon}_{eq_c} = (1/p)(\sigma_{eq}/\lambda)^n\ t^{(1/p)\ -\ 1}. \tag{37}$$

Values for $\dot{\epsilon}_{x_c}$, $\dot{\epsilon}_{y_c}$, $\dot{\epsilon}_{z_c}$, $\dot{\gamma}_{xy_c}$, $\dot{\gamma}_{yz_c}$ and $\dot{\gamma}_{xz_c}$ may be calculated as before.

Creep phenomena will tend to change stresses in general. Therefore σ_x, σ_y, σ_z, τ_{xy}, τ_{xz}, τ_{yz} will change with time because of creep. Thus,

$$\dot{\sigma}_x = \frac{E}{(1-\nu^2)} \left[\dot{\epsilon}_x - \dot{\epsilon}_{x_c} + \nu \left(\dot{\epsilon}_y - \dot{\epsilon}_{y_c} + \dot{\epsilon}_z - \dot{\epsilon}_{z_c} \right) \right],$$

$$\dot{\tau}_{xy} = \frac{E}{2(1+\nu)} \left(\dot{\gamma}_{xy} - \dot{\gamma}_{xy_c} \right); \tag{38}$$

$$\dot{\sigma}_y = \frac{E}{(1-\nu^2)} \left[\dot{\epsilon}_y - \dot{\epsilon}_{y_c} + \nu \left(\dot{\epsilon}_x - \dot{\epsilon}_{x_c} + \dot{\epsilon}_z - \dot{\epsilon}_{z_c} \right) \right],$$

$$\dot{\tau}_{yz} = \frac{E}{2(1+\nu)} \left(\dot{\gamma}_{yz} - \dot{\gamma}_{yz_c} \right); \text{ and} \tag{39}$$

$$\dot{\sigma}_z = \frac{E}{(1-\nu^2)} \left[\dot{\epsilon}_z - \dot{\epsilon}_{z_c} + \nu \left(\dot{\epsilon}_x - \dot{\epsilon}_{x_c} + \dot{\epsilon}_y - \dot{\epsilon}_{y_c} \right) \right],$$

$$\dot{\tau}_{zx} = \frac{E}{2(1+\nu)} \left(\dot{\gamma}_{xz} - \dot{\gamma}_{xz_c} \right). \tag{40}$$

Here elastic considerations were used because $\dot{\epsilon}_x - \dot{\epsilon}_{x_c}$ represents elastic strain. When a thermal expansion term αT is introduced where temperature changes with time and E and ν are assumed to be proportional to the temperature, T,

$$\dot{\sigma}_x = \frac{E}{(1-\nu^2)} \left[\dot{\epsilon}_x - \dot{\epsilon}_{x_c} - \frac{\dot{}}{\alpha T} + \nu \left(\dot{\epsilon}_y - \dot{\epsilon}_{y_c} - \frac{\dot{}}{\alpha T} + \dot{\epsilon}_z + \dot{\epsilon}_{z_c} - \frac{\dot{}}{\alpha T} \right) \right] \tag{41}$$

. . .

Occasionally it is desirable to use the alternate form

$$\dot{\epsilon}_x - \dot{\epsilon}_{x_c} = 1/E \left[\dot{\sigma}_x - \nu \left(\dot{\sigma}_y + \dot{\sigma}_z \right) \right] + \frac{\dot{}}{\alpha T} \tag{42}$$

. . .

PLANE STRESS

A condition where $\sigma_z = \dot{\sigma}_z = 0$ and $\tau_{yz} = \tau_{xz} = 0$ could occur in thin plates or shells. Under these conditions

$$\dot{\sigma}_x = \frac{E}{1-\nu^2}\left[\dot{\epsilon}_x - \dot{\epsilon}_{x_c} - \frac{\dot{}}{\alpha T} + \nu\left(\dot{\epsilon}_y - \dot{\epsilon}_{y_c} - \frac{\dot{}}{\alpha T}\right)\right] \tag{43}$$

$$\dot{\sigma}_y = \frac{E}{1-\nu^2}\left[\dot{\epsilon}_y - \dot{\epsilon}_{y_c} - \frac{\dot{}}{\alpha T} + \nu\left(\dot{\epsilon}_x - \dot{\epsilon}_{x_c} - \frac{\dot{}}{\alpha T}\right)\right] \tag{44}$$

$$\dot{\tau}_{xy} = \frac{E}{2(1+\nu)}\left(\dot{\gamma}_{xy} - \dot{\gamma}_{xy_c}\right) \tag{45}$$

where

$$\dot{\epsilon}_{x_c} = \left(2\sigma_x - \sigma_y\right)\frac{F}{2\sigma_{eq}} \tag{46}$$

$$\dot{\epsilon}_{y_c} = \left(2\sigma_y - \sigma_x\right)\frac{F}{2\sigma_{eq}} \tag{47}$$

$$\dot{\gamma}_{xy} = 3\tau_{xy} \cdot \left(\frac{F}{\sigma_{eq}}\right) \tag{48}$$

$$\sigma_{eq} = \left(\sigma_x^2 - \sigma_x\sigma_y + \sigma_y^2 + 3\tau_{xy}^2\right)^{\frac{1}{2}} \tag{49}$$

In general in solving stress problems, the actual deformations of the structure are to be considered. This is true in treating problems involving creep. Thus, the total strains in terms of displacements are obtained by double integration as:

$$u = \int_x \int_t \left\{\dot{\epsilon}_{x_c} + \frac{1}{E}\left[\dot{\sigma}_x - \nu\left(\dot{\sigma}_y + \dot{\sigma}_z\right)\right] + \frac{\dot{}}{\alpha T}\right\} \partial x \, dt \tag{50}$$

$$v = \int_y \int_t \left\{ \dot{\epsilon}_{y_c} + \frac{1}{E}\left[\dot{\sigma}_y - \nu \left(\dot{\sigma}_x + \dot{\sigma}_z \right) \right] + \dot{\alpha T} \right\} \partial y \, dt \tag{51}$$

$$w = \int_z \int_t \left\{ \dot{\epsilon}_{z_c} + \frac{1}{E}\left[\dot{\sigma}_z - \nu \left(\dot{\sigma}_x + \dot{\sigma}_y \right) \right] + \dot{\alpha T} \right\} \partial z \, dt \tag{52}$$

At time zero, before creep starts

$$u = \int \left\{ \frac{1}{E}\left[\sigma_x - \nu \left(\sigma_y + \sigma_z \right) \right] + \alpha \Delta T \right\} \partial x \tag{53}$$

.
.
.

PLATE ELEMENTS SUBJECT TO BENDING

Heretofore only states of stress involving no bending have been considered. It is of interest to consider how creep problems when bending is present may be treated. Only initially flat plates are considered here. Where x and y represent a rectangular coordinate system, M_x, M_y may be used to denote bending moments and M_{xy} a twisting moment. Then

$$\frac{\partial^2 w}{\partial x^2}, \frac{\partial^2 w}{\partial y^2} \text{ and } \frac{\partial^2 w}{\partial x \partial y} \tag{54}$$

can denote curvature changes where w is normal deflection at any point and plane sections can be assumed to remain plane during creep. Under these conditions the following equations may be derived:

$$\frac{\partial^2 \dot{w}}{\partial x^2} = -\frac{1}{EI}\left(\dot{M}_x - \nu \dot{M}_y \right) - \dot{K}_{x_c} \tag{55}$$

$$\frac{\partial^2 \dot{w}}{\partial y^2} = -\frac{1}{EI}\left(\dot{M}_y - \nu \dot{M}_x \right) - \dot{K}_{y_c} \tag{56}$$

$$\frac{\partial^2 \dot{w}}{\partial x \partial y} = \frac{(1+\nu)}{EI} \dot{M}_{xy} - \dot{K}_{xy_c} \tag{57}$$

where

$$\dot{K}_{x_c} = \frac{1}{I} \int z \dot{\epsilon}_{x_c} \, dz \tag{58}$$

$$\dot{K}_{y_c} = \frac{1}{I} \int z \dot{\epsilon}_{y_c} \, dz \tag{59}$$

$$\dot{K}_{xy_c} = \frac{1}{2I} \int z \dot{\gamma}_{xy} \, dz \tag{60}$$

$$I = \frac{1}{12} t^3, \text{ where } t = \text{plate thickness} \tag{61}$$

These preceding equations are derived by the following steps. According to the assumptions made regarding plane sections,

$$\dot{\epsilon}_x = - \frac{\partial^2 \dot{w}}{\partial x^2} z \tag{62}$$

$$\dot{\epsilon}_y = - \frac{\partial^2 \dot{w}}{\partial y^2} z \tag{63}$$

$$\dot{\gamma}_{xy} = - 2 \frac{\partial^2 \dot{w}}{\partial x \partial y} z. \tag{64}$$

When these expressions are multiplied by z and integration over the thickness of the plate in the range $- t/2 \leq z \leq t/2$ is performed,

$$\int \dot{\epsilon}_x z \, dz = - \frac{\partial^2 \dot{w}}{\partial x^2} \cdot \frac{t^3}{12} \tag{65}$$

$$\int \dot{\epsilon}_y z \, dz = - \frac{\partial^2 \dot{w}}{\partial y^2} \cdot \frac{t^3}{12} \tag{66}$$

$$\int \dot{\gamma}_{xy}\, z\, dz = -2\left(\frac{\partial \dot{w}}{\partial x \partial y}\right) \cdot \frac{t^3}{12} \,. \tag{67}$$

Substituting

$$\dot{\epsilon}_x = \dot{\epsilon}_{x_c} + \frac{1}{E}\left(\dot{\sigma}_x - \nu\, \dot{\sigma}_y\right) \tag{68}$$

$$\dot{\epsilon}_y = \dot{\epsilon}_{y_c} + \frac{1}{E}\left(\dot{\sigma}_y - \nu\, \dot{\sigma}_x\right) \tag{69}$$

$$\dot{\gamma}_{xy} = \dot{\gamma}_{xy_c} + \frac{2}{E\,(1+\nu)}\, \dot{\tau}_{xy} \tag{70}$$

and using the relations

$$\dot{M}_x = \int \dot{\sigma}_x\, z\, dz,\ \dot{M}_y = \int \dot{\sigma}\, z\, dz,\ \dot{M}_{xy} = -\int \dot{\tau}_{xy}\, z\, dz \tag{71}$$

the following solutions for moments are obtained

$$\dot{M}_x = -\left(\frac{EI}{1-\nu^2}\right)\left[\left(\frac{\partial^2 \dot{w}}{\partial x^2} + \dot{K}_{x_c}\right) + \nu\left(\frac{\partial^2 \dot{w}}{\partial y^2} + \dot{K}_{y_c}\right)\right] \tag{72}$$

$$\dot{M}_y = -\left(\frac{EI}{1-\nu^2}\right)\left[\left(\frac{\partial^2 \dot{w}}{\partial y^2} + K_{y_c}\right) + \nu\left(\frac{\partial^2 \dot{w}}{\partial x^2} + \dot{K}_{x_c}\right)\right] \tag{73}$$

$$\dot{M}_{xy} = \left(\frac{EI}{1+\nu}\right)\left[\frac{\partial^2 \dot{w}}{\partial x \partial y} + \dot{K}_{xy_c}\right]. \tag{74}$$

In the solution of creep bending problems, the solution proceeds as before using the fiber stresses to determine the creep rates through the cross section. In this solution $\dot{\epsilon}_x$, $\dot{\epsilon}_y$ and $\dot{\gamma}_{xy}$ are assumed to be linear functions of z. The stresses, σ_x, σ_y, σ_z will not be linear because the creep action will tend to cause parabolic shapes for the stresses through the cross section. This phenomenon is the same as in plastic bending.

In dealing with creep problems, it is advantageous to write the following moment curvature relations,

$$\dot{M}_x + D\left(\dot{K}_{x_c} + \nu \dot{K}_{y_c}\right) = \dot{M}_{x_{eff}} = -D\left(\frac{\partial^2 \dot{w}}{\partial x^2} + \nu \frac{\partial^2 \dot{w}}{\partial y^2}\right) \tag{75}$$

$$\dot{M}_y + D\left(\dot{K}_{y_c} + \nu \dot{K}_{x_c}\right) = \dot{M}_{y_{eff}} = -D\left(\frac{\partial^2 \dot{w}}{\partial y^2} + \nu \frac{\partial^2 \dot{w}}{\partial x^2}\right) \tag{76}$$

$$\dot{M}_{xy} - D(1-\nu)\dot{K}_{xy_c} = \dot{M}_{xy_{eff}} = D(1-\nu)\frac{\partial^2 \dot{w}}{\partial x \partial y} \tag{77}$$

and the following stress relations,

$$\dot{\sigma}_x = |z/I|\,\dot{M}_{x_{eff}} - D\left(\dot{\epsilon}_{x_c} + \nu\,\dot{\epsilon}_{y_c}\right) \tag{78}$$

$$\dot{\sigma}_y = |z/I|\,\dot{M}_{y_{eff}} - D\left(\dot{\epsilon}_{y_c} + \nu\,\dot{\epsilon}_{x_c}\right) \tag{79}$$

$$\dot{\tau}_{xy} = |z/I|\,\dot{M}_{xy_{eff}} - G\,\dot{\gamma}_{xy_c} \tag{80}$$

Thus effective moments are used in calculating stresses due to bending in the presence of creep. The actual moments acting in the plate, however, are $\dot{M}_x$, $\dot{M}_y$ and $\dot{M}_{xy}$. At a simply supported edge no bending moment can exist. Assuming that $\dot{w}$ is determined so that

$$\frac{\partial^2 \dot{w}}{\partial x^2} + \nu \frac{\partial \dot{w}}{\partial y^2} = 0 \tag{81}$$

at an edge parallel to the y-axis, creep will then cause a moment

$$-D\left(\dot{K}_{x_c} + \nu \dot{K}_{y_c}\right) \tag{82}$$

at the edge. Therefore, a moment equal but opposite in sense must be applied to insure zero moment at the edge, i.e.,

$$D\left(\dot{K}_{x_c} + \nu \dot{K}_{y_c}\right) . \tag{83}$$

PROPOSED PROCEDURE

On the basis of creep taking place in elements of a structure, the effects of creep upon the structure can be computed in two steps.

1. A fictitious load is calculated. This load would cause the same strains in a completely elastic element as those present in an element undergoing creep.

2. The fictitious loads are applied to the boundary of the element represented in the structure. The deflections and internal forces then are calculated for the structure. The stresses resulting from these loads are the "redistribution stresses" or the effect on the structure arising out of creep in an element. The change in stress in the element that creeps is then the difference between the stress before creep takes place and the redistribution stress minus the change of stress in an element due to creep with the boundary fixed.

The proposed procedure can be detailed in the following steps.

1. All the structural nodes are locked in a jig of infinite rigidity. The temperature increment, ΔT, corresponding to the time interval Δt is applied at each structural element. The corresponding "hydrostatic" stress terms are computed. These have the form

$$\Delta \sigma_h = - E \alpha \Delta T \tag{84}$$

for bars and stringers and the form

$$\Delta \sigma_x = \Delta \sigma_y = - \frac{E \alpha}{1 - \nu} \Delta T \tag{85}$$

for panels. These stresses are replaced with equivalent forces at the nodes. Then increments of external loads are applied during the same time interval and these are replaced with equivalent concentrated forces at the nodes. Finally the resultant forces at the nodes and their components in the directions of the chosen coordinate axes are computed.

2. Node displacements adequate to reestablish equilibrium in the unlocked structure are determined. The corresponding stresses are computed. When this is done, stress analysis considering thermal effects but neglecting creep in the time interval considered is performed.

3. Proceeding into creep considerations, the average stresses in the time interval taken into consideration are estimated according to the creep rates which are read off from a calibration diagram and which depend on the stresses.

As an alternative a stress increment corresponding to a convenient fraction of the overstress may be chosen and a time interval consistent with it may be assigned.

In this step it is necessary to account for the "weight" of the section areas under creep in relation to the remaining section areas.

4. The structure is again locked at the nodes and force increments corresponding to the stress relaxation terms over the whole time interval are introduced.

5. The deformation analysis of the structure is repeated, as in step 2, on the basis of the force increments determined in step 4. The corresponding stress increments due to relaxation are added to those found in step 2.

MODIFYING THEORIES

The method of analysis described in WADD TR 60-411 Part I does not account for the effects of strain hardening except as defining a threshold value for determining a boundary wherein negligible creep takes place. Some of the theories in popular use to account for the strain hardening effect are pointed out in the following discussions.

AGE HARDENING THEORY

According to the age hardening theory, the total strain due to creep is the sum of the values occurring in each loading condition obtained by time integration for each period. Thus

$$\left(\epsilon_{x_c}\right)_1 = \left[\left(\sigma_{x_1} - \sigma_{y_1}\right) + \left(\sigma_{x_1} - \sigma_{z_1}\right)\right]\left(\frac{F}{2\sigma_{eq}}\right)_1 \int_o^{t_1} \phi(t)\, dt \qquad (86)$$

$$\left(\epsilon_{x_c}\right)_2 = \left(\epsilon_{x_c}\right)_1 + \left[\left(\sigma_{x_2} - \sigma_{y_2}\right) + \left(\sigma_{x_2} - \sigma_{z_2}\right)\right]\left(\frac{F}{2\sigma_{eq}}\right)_2 \int_{t_1}^{t_2} \phi(t)\, dt \qquad (87)$$

$$\vdots$$

$$\left(\epsilon_{x_c}\right)_n = \left(\epsilon_{x_c}\right)_{n-1} + \left[\left(\sigma_{x_n} - \sigma_{y_n}\right) + \left(\sigma_{x_n} - \sigma_{z_n}\right)\right]\left(\frac{F}{2\sigma_{eq}}\right)_n \int_{t_{n-1}}^{t_n} \phi(t)\, dt \qquad (88)$$

GENERALIZED SUPERPOSITION THEORY

According to the generalized superposition theory the total strain due to creep is the sum of the values integrated for the periods o to t_n, t_1 to t_n, t_2 to t_n ... t_{n-1} to t_n due to the stress function differences existing between successive conditions. Thus

$$\left(\epsilon_{x_c}\right)_1 = \left[\left(\sigma_{x_1} - \sigma_{y_1}\right) + \left(\sigma_{x_1} - \sigma_{z_1}\right)\right]\left(\frac{F}{2\sigma_{eq}}\right)_1 \int_0^{t_1} \phi(t)\, dt \tag{86}$$

$$\left(\epsilon_{x_c}\right)_2 = \left[\left(\sigma_{x_1} - \sigma_{y_1}\right) + \left(\sigma_{x_1} - \sigma_{z_1}\right)\right]\left(\frac{F}{2\sigma_{eq}}\right)_1 \int_0^{t_2} \phi(t)\, dt + \tag{89}$$

$$+ \left\{\left[\left(\sigma_{x_2} - \sigma_{y_2}\right) + \left(\sigma_{x_2} - \sigma_{z_2}\right)\right]\left(\frac{F}{2\sigma_{eq}}\right)_2 -$$

$$- \left[\left(\sigma_{x_1} - \sigma_{y_1}\right) + \left(\sigma_{x_1} - \sigma_{z_1}\right)\right]\left(\frac{F}{2\sigma_{eq}}\right)_1\right\} \int_{t_1}^{t_2} \phi(t)\, dt .$$

$$\vdots$$

$$\epsilon_{x_{c_n}} = \left[\left(\sigma_{x_1} - \sigma_{y_1}\right) + \left(\sigma_{x_1} - \sigma_{z_1}\right)\right]\left(\frac{F}{2\sigma_{eq}}\right)_1 \int_0^{t_n} \phi(t)\, dt \tag{90}$$

$$+ \left\{\left[\left(\sigma_{x_2} - \sigma_{z_2}\right) + \left(\sigma_{x_2} - \sigma_{z_2}\right)\right]\left(\frac{F}{2\sigma_{eq}}\right)_2 -$$

$$- \left[\left(\sigma_{x_1} - \sigma_{y_1}\right) + \left(\sigma_{x_1} - \sigma_{z_1}\right)\right]\left(\frac{F}{2\sigma_{eq}}\right)_1\right\} \int_{t_1}^{t_n} \phi(t)\, dt +$$

$$+ \cdots \left\{\left[\left(\sigma_{x_n} - \sigma_{y_n}\right) + \left(\sigma_{y_n} - \sigma_{z_n}\right)\right]\left(\frac{F}{2\sigma_{eq}}\right)_n -\right.$$

$$\left. - \left[\left(\sigma_{x_{n-1}} - \sigma_{y_{n-1}}\right) + \left(\sigma_{x_{n-1}} - \sigma_{z_{n-1}}\right)\right]\left(\frac{F}{2\sigma_{eq}}\right)_{n-1}\right\} \int_{t_{n-1}}^{t_n} \phi(t)\, dt .$$

STRAIN HARDENING THEORY

In the strain hardening theory time is first eliminated. When the relation

$$\phi(t) = mt^{m-1} \tag{91}$$

is assumed, then

$$\epsilon_{x_c} = \left[\left(\sigma_x - \sigma_y\right) + \left(\sigma_x - \sigma_z\right)\right]\left(\frac{F}{2\sigma_{eq}}\right) t^m , \tag{92}$$

$$t = \left(\epsilon_{x_c}\right)^{\frac{1}{m}} \left\{\left[\left(\sigma_x - \sigma_y\right) + \left(\sigma_x - \sigma_z\right)\right]\left(\frac{F}{2\sigma_{eq}}\right)\right\}^{-\frac{1}{m}} \tag{93}$$

$$\dot{\epsilon}_{x_c} = \left[\left(\sigma_x - \sigma_y\right) + \left(\sigma_x - \sigma_z\right)\right]\left(\frac{F}{2\sigma_{eq}}\right) mt^{m-1} \tag{94}$$

$$= m \frac{\left\{\left[\left(\sigma_x - \sigma_y\right) + \left(\sigma_x - \sigma_z\right)\right]\left(\frac{F}{2\sigma_{eq}}\right)\right\}^{\frac{1}{m}}}{\left(\epsilon_{x_c}\right)^{\frac{1}{m} - 1}}$$

Then the total strain due to creep is obtained by integrating with respect to ϵ_{x_c} in each loading condition. Thus

$$\left(\epsilon_{x_c}\right)_1^{\frac{1}{m}} = \left\{\left[\left(\sigma_{x_1} - \sigma_{y_1}\right) + \left(\sigma_{x_1} - \sigma_{z_1}\right)\right]\left(\frac{F}{2\sigma_{eq}}\right)\right\}^{\frac{1}{m}} t_1 \tag{95}$$

$$\left(\epsilon_{x_c}\right)_2^{\frac{1}{m}} = \left(\epsilon_{x_c}\right)_1^{\frac{1}{m}} + \left\{\left[\left(\sigma_{x_2} - \sigma_{y_2}\right) + \left(\sigma_{x_2} - \sigma_{z_2}\right)\right]\left(\frac{F}{2\sigma_{eq}}\right)\right\}^{\frac{1}{m}} (t_2 - t_1) \tag{96}$$

$$\vdots$$

$$\left(\epsilon_{x_c}\right)_m^{\frac{1}{m}} = \left(\epsilon_{x_c}\right)_{n-1}^{\frac{1}{m}} + \left\{\left[\left(\sigma_{x_n} - \sigma_{y_n}\right) + \left(\sigma_{x_n} - \sigma_{z_n}\right)\right]\left(\frac{F}{2\sigma_{eq}}\right)\right\}^{\frac{1}{m}} (t_n - t_{n-1}) \tag{97}$$

COMBINED STRAIN AND AGE HARDENING THEORY

In the combined strain and age hardening theory a number, N, is introduced and the strain is raised to the Nth power. When $\phi(t)$ is taken as a power term in t, the following relations are obtained

$$\left(\epsilon_{x_c}\right)_1^N = \left\{\left[\left(\sigma_{x_1} - \sigma_{y_1}\right) + \left(\sigma_{x_1} - \sigma_{z_1}\right)\right]\left(\frac{F}{2\sigma}\right)\right\}^N t_1^{N_m} \tag{98}$$

$$\left(\epsilon_{x_c}\right)_2^N = \left(\epsilon_{x_c}\right)_1^N + \left\{\left[\left(\sigma_{x_2} - \sigma_{y_2}\right) + \left(\sigma_{x_2} - \sigma_{z_1}\right)\right]\left(\frac{F}{2\sigma}\right)_2\right\}^N \left(t_2^{N_m} - t_1^{N_m}\right) \tag{99}$$

$$\vdots$$

$$\left(\epsilon_{x_c}\right)_n^N = \left(\epsilon_{x_c}\right)_{n-1}^N + \left\{\left[\left(\sigma_{x_n} - \sigma_{y_n}\right) + \left(\sigma_{x_n} - \sigma_{z_n}\right)\right]\left(\frac{F}{2\sigma}\right)_n\right\}^N \left(t_n^{N_m} - t_{n-1}^{N_m}\right) \tag{100}$$

Now when N = 1, the foregoing reduces to the age hardening theory and when N = 1/m, it reduces to the strain hardening theory.

REPRESENTATION OF CREEP

Several empirical and semi-empirical formulas for representing creep have come into existence. Many of these relations appear to be reasonably accurate for particular materials or particular values of stress and, or temperature. Several of these representations are treated in the following discussion.

Rabotnov (Reference 1) proposed the creep law

$$\phi\left(\epsilon_{eq}\right) = \left(1 + K^*\right)\sigma_{eq} \tag{101}$$

where

$$K^*(\sigma) = \int_o^t K(t-\tau)\,\sigma(\tau)\,d\tau \tag{102}$$

in general is the integral operator of Volterra. In the simplest form

$$\phi\left(\epsilon_{eq}\right) = \left(1 + a t^p\right)\sigma_{eq} \tag{103}$$

where a = constant
p = 0.3.

Here $\phi(\epsilon_{eq})$ is the ordinary stress strain law for the material in the absence of creep, i.e. for $t = o$. In the above notation ϵ represents total strain, the elastic plus the plastic plus the creep strain. Further when

$$\phi(\epsilon_{eq}) = B\epsilon_{eq}^{q} \tag{104}$$

for the condition where $at^{p} >> 1$

$$\epsilon_{eq} = c\,\sigma_{eq}^{n}\,t^{\alpha} \tag{105}$$

which already has been quoted.

As regards ϕ (t) Marin (Reference 2) suggests

$$\int \phi(t)\,dt = \sigma_o^{n}\left[k_1 + k_2(1-e^{-qt}) + k_3 t\right] \tag{106}$$

where k_1 = initial creep strain, i.e., at $t = o$

$k_2(1-e^{-qt})$ = transient creep strain

$k_3 t$ = constant "minimum creep rate" strain.

More complex forms for ϕ (t) have been suggested by Mac Donald (Reference 3).

$$\phi_{(t)} = \left(\frac{q}{\tau_o}\right)\left\{\left[1+\left(\frac{t}{\tau_o}\right)\right]^{1-\nu} + \left(\frac{t}{\tau_\infty}\right)^{2}\right\}^{-1} \tag{107}$$

or

$$\phi_{(t)} = \left(\frac{q}{\tau_o}\right)\left(e^{-t/\tau_\infty}\right)\left[1+\left(\frac{t}{\tau_o}\right)\right]^{\nu-1} \tag{108}$$

Permanent set in a creep specimen upon release of stress is

$$(\epsilon_{set}) = (\epsilon_c)_{t=t_1} - \frac{\sigma}{E} - \frac{\sigma}{E}\left[G(t_1) + G(t_2 - t_1) - G(t_2)\right] \tag{109}$$

where G = Rabotnov's time function

t_1 = time stress is removed

t_2 = time for permanent set

When in the above expression $t_2 \gg t_1$, then

$$\epsilon_{set} = \epsilon_c - \epsilon_c \frac{E_{sec}}{E} = \left(1 - \frac{E_{sec}}{E}\right) \epsilon_c \tag{110}$$

since

$$\epsilon_c E_{sec} = \varphi(\epsilon_c) = \left[1 + G(t)\right] \sigma \tag{111}$$

where in the above expressions E_{sec} is the modulus taken from the instantaneous stress-strain curve.

Stowell suggests the viscous creep term

$$\dot{\epsilon} = 2 s T e^{\frac{-\triangle H}{RT}} \sinh\left(\frac{\sigma}{\sigma_o}\right) \tag{112}$$

to account for effects of temperature.

Warner and Mahmoodi (Reference 4) suggest stress strain flow laws which become for the case of plane stress

$$\dot{\epsilon}_x = \frac{1}{E}\left(\dot{\sigma}_x - \nu \dot{\sigma}_y\right) + n_x \dot{\sigma}_x + 2 \tau_{xy} n \dot{\tau}_{xy} - \tfrac{1}{2}(n_x - n_y) \dot{\sigma}_y \tag{113}$$

$$\dot{\epsilon}_y = \frac{1}{E}\left(\dot{\sigma}_y - \nu \dot{\sigma}_x\right) + n_y \dot{\sigma}_y - 2 \tau_{xy} n \dot{\tau}_{xy} - \tfrac{1}{2}(n_x - n_y) \dot{\sigma}_x \tag{114}$$

$$\dot{\gamma}_{xy} = \frac{1}{G} \dot{\tau}_{xy} + 4 n_{xy} \dot{\tau}_{xy} \tag{115}$$

where

$$n_x = f_1(\sigma_x, \sigma_y), \quad n_y = f_2(\sigma_x, \sigma_y) \tag{116}$$

$$n = g_1(\tau_{xy}),\ n_{xy} = g_2(\tau_{xy}) \tag{117}$$

These functions, n_x, n_y, n_{xy} and n,need to be determined by tests. In conditions where $\dot{\sigma}_x = o$, $\dot{\sigma}_y = o$ and $\dot{\tau}_{xy} = o$ no creep can occur.

Narasimhamurthy (Reference 5) found that constant creep rates could be expressed as

$$\dot{\epsilon}_x = a\left(\frac{\epsilon_{eq}}{\sigma_{eq}}\right)^N \left\{\sigma_x - \tfrac{1}{2}(\sigma_y + \sigma_z)\right\} \tag{118}$$

where $N \approx 0.6$ for aluminum alloy. This means that the uniaxial creep law should be

$$\dot{\epsilon}_x = a\left(\frac{\epsilon_x}{\sigma_x}\right)^N \sigma_x \tag{119}$$

Johnson, Henderson, and Mathur (Reference 6) showed that under sets of loadings involving increased magnitudes and at constant temperature,

$$f = \left[F(\sigma_{eq}) - G\left(\int \gamma_{oct}\, dt\right)\right] \tag{120}$$

Where

$$F(\sigma_{eq}) = A_1(\sigma_{eq})^{p_1} + A_2(\sigma_{eq})^{p_2} \tag{121}$$

$$G\left(\int \gamma_{oct}\, dt\right) = A_3\left(\int \gamma_{oct}\, dt\right)^{p_3},\ \gamma_{oct} = \frac{2}{\sqrt{3}}\sqrt{I_2} \tag{122}$$

The integral of octahedral creep strain, γ_{oct},is taken from time zero to a time greater than the first period of loading.

For the purposes of this investigation actual results from uniaxial elements are plotted. Many methods of plotting creep data are in use. These are recapitulated in Figure 4. The specific method used involves increments of creep strain plotted against stress and time as shown in Figure 4, Mark K.

SIMPLIFYING CHANGES IN PROPOSED METHOD

In the case of redundant structures the use of elastic stress to predict creep rate results in overprediction of creep. The prediction of redistribution stress on the basis of areas is difficult in the case of non-symmetric sections. Because of this, certain minor modifications have been introduced into the proposed method. These changes consist of the following steps.

1. After those elements which will probably creep have been determined, unit amounts of creep are applied to these elements.

2. The change of stress due to this unit creep is computed in the same manner as in Step 5 of the proposed method.

3. The average stress is found for the element that creeps for the interval of time in which this unit creep takes place by averaging the stress before the unit creep and after this creep.

4. The average stress in the element that creeps during the interval of creep is used to find the time necessary to arrive at the creep strain.

In the case of several elements which creep at the same time, an iteration technique is used. This iteration consists of several steps. The initial step is to calculate the change of stress throughout the structure caused by unit creep in one element. This element should be the one most likely to have the greatest amount of creep. The time for the element to creep its unit amount is then used to calculate the creep strain in the next element under the action of the average stress applied to that element. The process is repeated for every element in the structure subject to loading that would cause creep. The average load for the first element is then recalculated on the basis of the effects of creep in all the elements and the time for unit creep to take place is then recalculated from graphs of material properties.

The procedure is repeated until the creep strain changes less than some predetermined percent. Since creep is localized in some region such as the leading edge of a wing, the number of elements that creep should not be excessive and convergence should be rapid.

BOX BEAM TESTS - DESIGN

A built up box was designed and built for testing in bending and torsion. The box was intended to represent a typical element in aircraft construction. It was designed to resist buckling of the surface subjected to compression. The box was fabricated from Armco PH 15-7 Mo, Condition RH 950 stainless steel and was fastened together with spotwelds. The box components were first heat treated and then spotwelded in the heat treated condition. This resulted in some loss of strength in the area of the spotwelds due to annealing action resulting from localized heating. This technique was representative of construction practice

that would be followed in actual construction of an airplane or missile using this material. It was considered impractical to rivet a very high strength, limited ductility material and it is also considered impractical to heat treat very large elements or parts of an airplane.

The test box consisted of five beams connected by means of square diaphrams. This "egg crate" structure was then covered by plates. The load was introduced into the plates at their ends. These ends were built up by means of doublers spotwelded to the sheets at their ends. These built up sections were attached to a loading jig by means of bolts. One end of a test box was directly bolted to a jig while the other end was attached to a heavy beam. Two actuators were attached to this beam and were capable of introducing two equal and opposite loads which resulted in tension and compression loads being applied to the cover plates of the box. The doublers attached to the plates also were attached to the spars so as to introduce moments into the entire structure. When the actuators were applied to the center of the loading beam, pure moment was introduced to it. When the actuators were applied to some point other than the center of the beam, torsion plus bending was introduced into the test box. Dynamomenters were attached to the actuators and these were capable of recording loads applied to the beam and consequently the test box.

IDEALIZATION OF STRUCTURE FOR ANALYSIS

In order to predict the interaction of internal forces in the test box structure, it was treated as a combination of elements which have continuity at their boundaries and are in equilibrium at the joints in the structure where the loads of the elements are introduced. In common representations of structural elements, beams and stringers are taken as one dimensional elements. In the case of the test box, the flanges of the spars are represented as stringers and the plates connecting these flanges are represented as plates in which the strain is linear. This representation can be approximated by the "lattice analogy" in which the plate is represented as a truss.

The general method illustrated in Figures 5 through 14 and Tables 1 through 16 was used to solve for the interaction of the elements of the test box. This general method used the stiffness or unit deflection approach. In this method only one point or "node" is allowed to deflect at a time. The forces resulting from this unit deflection of the node on the structure then represent the line of the final array or matrix. The spar caps and the attached cover sheets were considered as acting as separate units. The cover plates were broken into four plates and the spar caps were treated as five individual caps. The areas of each section were allowed .000100 in per in creep strain interval and the load redistribution was calculated for unit creep in each element. The test box was uniformly heated and the action of any fiber in the longitudinal direction was taken to be the same throughout its length. This meant that restraint forces could be treated as forces and moments applied at the ends of the sections as shown in Table 7.

In the analysis of the box certain modifications were made in the preceding formulas. Equations (46) and (47) were modified as follows:

$$\Delta\epsilon_{x_c} = \left(\sigma_x - \frac{\sigma_y}{2}\right)\frac{\Delta\epsilon_{eq_c}}{\sigma_{eq}} \tag{123}$$

$$\Delta\epsilon_{y_c} = \left(\sigma_y - \frac{\sigma_x}{2}\right)\frac{\Delta\epsilon_{eq_c}}{\sigma_{eq}} \tag{124}$$

This is justified because the principal stresses are assumed not to change direction. The strain hardening theory is then used, Equation (97), to estimate strain rate and hence incremental strain-time relationships.

BOX BEAM TESTS - PROCEDURE

The test boxes were designed to give uniform or nearly uniform stress and strain distribution across the surfaces of the box. The compression surface was designed to be completely buckle resistant. Further creep buckling was considered beyond the range of conditions incorporated into study.

Failure took place in the first box submitted to test before any useful results could be obtained. This failure was traced to loss of strength beyond that predicted in the net section as a result of strength deterioration attendant to spot welding. Also, certain warping effects inherent in the box were constrained from taking place because of the stiff jig used. This gave rise to local stress risers in the areas where the box was attached to the jig. In order to utilize remaining boxes of this initial design, a thin annealed stainless steel reinforcement was attached to the attachment area by means of stainless steel blind bolts. Those test boxes which were assembled subsequent to the initial failure incorporated tension covers which were reduced to test section thickness by means of chemical milling. The doublers in the boxes incorporating the chemically milled cover plates were redesigned to reduce concentration effects of spot welds on the net section. The revised design is shown in Figures 15 and 16. The failures which occurred with the revised design are shown in Figures 17 and 18.

The test jig used consisted of a heavy rectangular frame constructed of "I" beams. This is shown in Figure 19. One end of the test box was attached to the jig by means of heavy steel plates and angles. Equal actuators were attached to the frame and the loading beam in order to introduce loads. A platform was rigidly attached to the jig to firmly position the dial gages used to measure normal deflections. An aluminum oven was attached to the jig to concentrate the heat produced by the quartz lamps used to heat the specimens. This oven contained interior baffles to regulate the heat input by directing the heat to local regions of the test box

as required. The thermocouple arrays used with the box beam tests and the temperature distributions observed with them are shown in Figures 20 and 21. Hydraulic pressure was introduced to the load actuators by means of hand pumps. The loads applied by this means are shown in Figures 22 and 23. All loads were monitored by dynamometers attached to the actuators.

Three types of gages were used to determine strains and temperatures within the test boxes. Strains and deflections were measured with weld attached electrical resistance strain gages and dial gages. The temperatures were measured by means of thermocouples attached to the surfaces of the boxes by welding. The observed temperatures are shown in Figures 20 and 21.

The resistance strain gages as originally delivered were found unsatsifactory for use in the range temperatures encountered in the tests. This required return of these gages to the manufacturer for heat treatments intended to increase the stability of the gage readings. In order to test the reliability of the heat treated strain gages, several of them were welded to metallic coupons and heated. Stress strain relationships were then determined by loading the heated coupons. The outcome of these electric strain gage verifications are given in Appendix I. Strain gages were mounted in different locations in each test. Although the gage locations used in the first test were adequate, additional gages were used in subsequent tests to insure provision of useful data in the event of failure of one or more of the electric strain gages during test. The increased number of gages also provided greater opportunity for comparison of results obtained from the various gages. The locations of the strain gages on the test boxes is shown in Figures 20 and 24. The observed strains are shown in Figures 25 and 26.

Dial gages were connected to the boxes to determine deflections occurring at various points on the box surfaces. Twelve of these gages were used to measure normal deflections on the boxes. Four of them were used to measure longitudinal deflections on the box surfaces. The mode of attachment of these gages is shown in Figure 19.

The general procedure followed in all bending tests was to load the specimens to a predetermined "tare load" well within the elastic range, hold for sufficient time to calibrate drift in the electric and mechanical strain gages and determine the relations present between the loads and strains within the elastic limit. After this the load was then increased into the plastic or creep range and was held at this increased load for a predetermined time. At the end of this time interval, the loads were reduced to the tare load level. At this load level recalibration of the strain gages was done to ascertain strain gage drift. Photographs of the mechanical dial gages were taken at the tare load condition, at the instant creep loads were reached and at the instant preceding release of creep load. Photographic recording was used to obtain readings in the shortest time under uniform conditions of observation. This was necessary because the dial gage indications did vary with time when loads on the test boxes were sufficient to cause creep.

OUTCOME OF TESTS

The creep data obtained were the normal deflections and strains at specific locations. These strains were plotted for specific times on graphs scaled in time. This permitted extrapolation of the elastic strain and the difference between the extrapolated elastic strain and the indicated gage strain was taken to be the result of creep. Where gages were not mounted back to back, certain errors due to local bending may be included in the apparent strain. This error decreases as the thickness of the plate to which gages are mounted is decreased. Where the plate is restrained against local bending, the error in apparent strain is decreased even further. In any case, the strains should be proportional to loads and divergence should be due to non-linear response of the material. The observed strains are shown in Figures 25 and 26. Comparisons of predicted and observed strains are shown in Figures 27 and 28.

The deflections recorded from the dial gages contained the rigid body motion obtained at the joint of the box to the jig. The conditions present at these joints are difficult to analyze. Therefore the deflections were reduced to curvature and rates of change of curvature. The deflections and the reductions of these deflections to curvatures are shown in Tables 6, 16 and 17. The comparison of predicted and observed curvature for test box III is shown in Figure 29.

COMPARISON CRITERIA

It is difficult to set arbitrary criteria for evaluations of the adequacy of comparisons between theoretical predictions and test outcomes aimed toward their verification. Because structures and their uses vary an adequate comparison in one case can easily be inadequate in a different case. In any event the ultimate criterion must be the percent divergence between the theoretical and the test values of deflection, stress or strain.

It is generally considered that redundant analysis can represent a structure with reasonable accuracy when the divergence between theoretical and test outcomes indicate less than ten percent error. It appears therefore that a divergence of creep predictions in the same order of magnitude would be acceptable in most cases. Accordingly in this study those predicted values of creep that deviated ten percent or less from test indications were arbitrarily considered adequate.

SUMMARY AND CONCLUSIONS

1. On the basis of data displayed in Tables 18, 19 and 20 and Figures 27, 28 and 29, it is concluded that the effects of creep within structures can be predicted with reasonable accuracy.

2. Great difficulty exists in evaluating the interaction loads of structural elements and the internal loads of a structure with sufficient accuracy to enable precise predictions

of the effects of creep upon a structure. This difficulty arises out of approximating nature of redundant analysis methods themselves which result in a compounding of approximations when the approximations attendant to creep prediction are multiplied into the overall outcome. A need exists in the refinement of redundant analysis for elucidation of interactions between structural elements. This may be achieved by tests which provide elastic loading conditions and corrections for elastic analysis methods in conformance with test data.

REFERENCES

1. Rabotnov, Y. N., "The Effect of Changing Loads During Creep," Chapter in Creep And Fracture of Metals at High Temperature, Philosophical Library, New York, 1957.

2. Marin, J., "Mechanics of Creep and Combined Stress," Paper in Colloquium on Creep in Structures Sponsored by the International Union on Theoretical and Applied Mechanics, June 11-12, 1960, Stanford University, Palo Alto, California, 1960.

3. McDonald, J. R., "Modification of Lammitz - Jeffrey Law of Creep," Journal of Applied Physics, Vol. 30, No. 3, p. 453, March 1959.

4. Warner, W. H. and Mahmoodi, P., "The Plastic Coefficients for Work Hardening," WADC TR 59-674.

5. Narasimhamurthy, P., "An Analytical Investigation of Creep Under Combined Loadings," Aircraft Engineering, Vol. 29, No. 345, p. 346, November 1957.

6. Johnson, A. E., Henderson, E. J. and Mathur, V., "Creep Under Changing Complex Stress System," The Engineer, Vol. 206, No. 5350, 5351 and 5352, p. 209, 258 and 287, August 8, 15 and 22, 1958.

SECTION II. MATERIAL CHARACTERISTICS

INTRODUCTION

Subsonic aircraft structural designs are characterized as a special case because they utilize materials under limited environmental conditions. This limitation is concerned with the narrow temperature range of about -100°F to 200°F in which these aircraft operate. In this range aircraft structural materials behave generally in a unique condition of stability so far as their engineering properties are concerned. This has resulted in the establishment of methods of structural analysis with a tacit assumption that structural materials are in the practical sense stable and homogeneous.

The appearance of supersonic aircraft and of liquefied gas propellant materials broadened the conceivable range of structural temperatures from about -420°F to 3500°F and beyond. The immediate result of this broadening was to widen the demand for structural analysis techniques beyond those required to cope with a -100° to 200°F temperature range. The broadening of operating temperature range also resulted in removal of most aircraft structural materials from lists of stable materials and placed them in lists of unstable materials.

BASIC LIMITATIONS UPON THE STRUCTURAL STABILITY OF MATERIALS

In a nutshell structural analysis techniques are rooted in two basic material characteristics, elastic action and inherent material stiffness. Elastic action capability is an explicit characteristic of structural materials in that specific capability at a given time is a product of the processing and environmental history which the material has experienced. Inherent material stiffness, on the other hand, is an implicit material characteristic not governed by processing or environmental history but by temperature alone.

The importance of elastic action in structural design can be appreciated when it is realized that no aircraft structure has yet been designed which permits plastic deformation beyond .002 strain considered negligible. This in essence defines an aircraft structure as an elastic structure which loads and unloads in a reversible fashion and resembles a spring in that it is able to resume its original shape upon removal of the deforming force.

STRUCTURALLY SIGNIFICANT VARIABLES OPERATIVE IN HEATED ENVIRONMENTS

Four apparent variables assert themselves in structural designs aimed for use in heated environments. They are load, temperature, time and deformation. Three of these variables, load, temperature and time, define environments. The remaining one, deformation, defines a reaction of materials upon exposure to environmental factors which can be regulated. The deformation variable cannot be regulated in any way other than adjustment of load, temperature and time variables. The deformation variable is a dependent variable which relies upon the magnitude of the environmental factors, load, temperature and time, in the determination of its magnitude. A further distinguishing characteristic of the deformation variable is that it is the one of the four variables listed which expresses a material rather than an environmental characteristic.

THE DEFORMATION VARIABLE

The deformation present in an element of a structure exposed to heating for a period of time is comprised of three components, thermal expansion, elastic deformation and plastic deformation. Thermal expansion is temperature dependent, independent of load and time and is reversible. Elastic deformation is temperature and load dependent, independent of time and is reversible. Plastic deformation is temperature, time and load dependent and is irreversible.

From this it can be deduced that thermal expansion is an intrinsic material characteristic inherently present in materials as a consequence of interatomic spacial arrangements which can be altered only by thermal activation and observed only as a consequence of temperature change. Empirical deduction indicates that elastic deformations are present from the time load is applied to a material and until such time that the maximum or ultimate strength of the material is attained. In the presence of load applications, elastic action in a "pure" form occurs up to some load where plastic action initiates. From this point elastic and plastic actions progress concurrently up to the attainment of maximum load conditions. The time independence of elastic action is readily checked in creep tests wherein elastic spring-back is observed upon completion of test. This spring-back is comparable with the elastic component of the loading deformation which can be computed as a quotient of stress divided by modulus of elasticity.

Empirical deduction indicates that plastic deformations originate in metals at a load application level at which pure elastic action halts. This occurs because in pure elastic action inter-atomic positional readjustments take place in the absence of the movement of atomic units from one spatial site to another. As these readjustments proceed a resistance to continuing readjustment accumulates and finally a condition is attained where further readjustment is not possible in the absence of movement of the atomic units from their original sites. When this condition is reached plastic action sets in and further pure elastic action does not take place in the material.

In that interval where elastic action takes place in conjunction with plastic action a see-saw of balance between the forces resisting inter-atomic positional rearrangement in elastic action and those resisting movement from one site to another in plastic action goes on. At some level where the forces resisting inter-atomic positional rearrangement increase at a rate which continuously exceeds that at which the forces resisting movement from one site increase, elastic action comes to a halt and that action which continues is exclusively plastic.

This visualization indicates that the halting of pure elastic action which takes place upon the initiation of plastic action can be accounted for in terms of a physical process. Conversely it indicates, in terms of apparent disappearance of elastic action, a physical basis for the maximum strength phenomenon in materials. The association of elastic action with displacement phenomena suggests that this action is involved with potential energy. Similarly the association of plastic action with phenomena involved with relative motions suggests that this action is involved with kinetic energy.

Energy summations appear attractive as means for evaluating the importance of individual effects entering into a culminating event such as creep rupture. However when present capabilities for measuring energy inputs involved in a creep rupture history are taken into consideration, the impracticality of such attempts is apparent. In the present state of technology then, it is of importance to realize that although energy relations constitute the full reality of creep history, the present state of advance allows only for assessment of certain factors entering into these relations. Accordingly the assumption of some factor chosen to represent energy summation is made. The factor which represents creep deformation energies in this discussion is plastic strain.

STRESS STRAIN RELATIONS

Figure 30 schematically displays a stress strain curve and shows, for a constant stress condition, the elastic and plastic components of deformation present when loading is effective, elastic spring-back appearing upon load release and permanent set resulting from the load application. This figure displays, in addition to the stress strain curve, the plastic strain curve which results from deducting the elastic strain component from the stress strain curve. The exponential nature of the plastic strain curve is not evident in this schematic diagram, however its nature is demonstrated clearly in experiment. This discussion relative to inter-atomic structures and their relations with load-deformation mechanisms stem from A. H. Cottrell discussions in his "Theoretical Structural Metallurgy" (Reference 1). The approach taken with respect to load-deformation diagrams stems from F. R. Shanley's "Strength of Materials " (Reference 2).

STRAIN RATE EFFECTS

In testing experience it is not uncommon to find that creep and creep rupture tests which have been made with carefully prepared and controlled materials, and, according to closely supervised test procedures, fail to produce results which are in agreement from test to test.

Such results are distressing because the deformations at which creep originates vary considerably, and, concurrently creep rates vary to such an extent that the use of such test data for establishing design numbers is questionable.

Foregoing discussion pertaining to plastic deformations intimates that the plastic deformation process is a step by step operation requiring finite time of infinitesimal duration for the accomplishment of each individual step. The overall process then is a time dependent and rate controlled one. Hence the conception that time independent plastic deformation takes place in creep test loading appears erroneous.

Figure 31 shows replots of stress-strain curves given in W A D D Technical Report No. 59-199, Part 2, page 80 (Reference 3). These stress strain curves were obtained with Armco 17-7 PH, Condition TH-1050 at strain rates of 1.0, 0.01 and 0.00005 inches per inch per minute at 1200°F. These curves show that a thigher rates of strain higher proportional limits are demonstrated by the metal, and, as strain rates diminish the proportional limits dimish. Figure 32 shows the plastic stress strain plots obtained from the stress strain curves. The shapes of these curves indicate that strain hardening, a manifestation of plastic action is more intense, once it is initiated, in material strained rapidly than in that which is strained slowly. Figure 33 plots the data shown in Figure 32 in the range of .0001 to .001 strain in logarithmic coordinates. The straight line nature of these plots indicates that the increase in strain attendant to increases in stress proceeds in an exponential manner. The slopes of these logarithmic curves indicate also that the rate at which strain increases as stress increases in plastic action is greater in materials which are rapidly strained than those which are strained slowly.

The foregoing as well as the remaining data in the referenced report, are difficult to apply further. The reason for this is that the range of strain rate magnitudes reported is too great to permit desired comparisons. To study the effect of strain rates operative in creep loadings, it appears that data from tension tests wherein strain rate variations are held within one order of magnitude, 0.001 to 0.0001 inch per inch per minute for example, are required. This occurs because under conditions of this creep study stress strain curves diverge and because comparisons must be based on a single stress level. The schematic diagram shown in Figure 34 illustrates the point. Here the curves OP′ R′ and OPR represent outcomes of loadings at high and low strain rates. As indicated previously, high strain rates result in the more intense work hardening and accordingly stress strain curves obtained under differing strain rates will diverge. The differences in strain rate for creep study purposes thus need be small to provide data which fall into an area where comparisons are possible. In the conduct of creep tests involving load applications at differing strain rates at a given temperature and a given stress level, the temperature variable is recognized as a parameter and the stress as an independent variable, the application of which results in the appearance of strain, a dependent variable. Hence if cause and effect are to be studied, the comparisons desired must be made at a single stress level in order to observe the differences in plastic action resulting as consequence of variations in strain-rate.

In Figure 34 the line OA′ represents the course of elastic action involved in attaining the stress OX. Since elastic action is reversible, the elastic action involves a storage of potential energy. Here also the curve OP′ R′ represents the total action taken in attaining the stress, OX. This is composed of the elastic and plastic action comprising the total action represented. Thus the curve representing the difference between the total action and the elastic action is the curve resulting from deducting the curve OP′ A′ from the curve OP′ B′. This difference curve represents the plastic action present. Because plastic action is irreversible, it involves the expenditure of kinetic energy. The curves shown in Figure 34 do not represent energy quantities. They merely index changes in energy quantities and in the acceptance of the index concept, assumptions are involved. These are to the effect that volume changes do not occur throughout stress strain testing and that up to the ultimate stress area changes are so small that they may be considered negligible. Thus on the basis of these assumptions, the line OA in Figure 34 represents the strain index of the elastic action involved in attaining the stress OX. The line AB represents the strain index of plastic action involved in attaining the stress OX at a high strain rate, and, the line AC represents the strain index of plastic action involved in attaining the stress OX at a low strain rate. The implications from this are that creep tests which are initiated by loading at differing strain rates enter into creep under varying conditions of energy content and accordingly can be expected to display variations in creep behavior, and, that relatively small differences in strain rate result in comparatively large differences in energy content once a given stress is reached.

THE POWER LAW EXPRESSION FOR CREEP RELATIONS

The power law or parabolic expression for creep relations is given as

$$\epsilon = Kt^N \tag{125}$$

where ϵ = creep strain

t = time

K = an arbitrary coefficient

N = an arbitrary power,

is frequently encountered in discussions of creep phenomena and creep prediction method. The main attraction of this expression is its simplicity. In its logarithmic form

$$\log \epsilon = \log K + N \log t . \tag{126}$$

This expression plots as a straight line. In this form numerical values for K are easily found by reading the ordinate at the point where the straight line intercepts it and those for N are easily found by directly measuring the slope of the line. When found the numerical values for K and N can be directly substituted into the power law expression.

Figures 17 through 21 of Reference 4 show creep strain versus time data derived from tests with 7075-T6 aluminum alloy. When these data are subjected to the evaluation steps described, the expressions listed in Table 21 result. This tabulation displays the individualistic nature of each expression listed and indicates that if generalizations are sought additional steps are required to ascertain relations between the K and N values of the expressions listed.

When the quantities t^N in the expressions of Table 21 are fixed for each of the five temperatures listed and relationships between the stresses and expression coefficients shown are sought in the relation

$$\log \sigma = \log K + \log C \tag{127}$$

where σ = stress, p.s.i.

K = coefficient of $\epsilon = Kt^N$ expression

C = fixed value of t^N according to temperature,

the following values for K emerge:

Temperature	K
200°F	$8.7 \times 10^{-13}\ \sigma^{10}$
250°F	$2.0 \times 10^{-11}\ \sigma^{11.1}$
300°F	$4.6 \times 10^{-11}\ \sigma^{10}$
350°F	$1.4 \times 10^{-8}\ \sigma^{8.33}$
400°F	$1.3 \times 10^{-6}\ \sigma^{4.35}$

In the arithmetical sense the values given for K are of little consequence here since the true stress-strain relation has been ignored. However the step shown does indicate that moves to simplify the power function will result in the development of additional expressions incorporating a new correlation coefficient such as the one required to relate stress with strain in the step taken.

Figure 23 of Reference 4 presents results of an advanced plotting technique where stress is plotted against log K and where K represents the power law coefficient taken at the one hour creep strain condition. Straight line temperature parameter lines which are drawn on this chart suggest relations between stresses and temperatures at fixed values of creep strain. When stresses and temperatures are taken at creep strains of 0.1, 0.5, 1.0 and 1.5, plotted in logarithmic form and evaluated, the following expressions for stress in terms of temperature appear.

Creep Strain	$\sigma = CT^{D}$*
0.1	$\sigma = 82500\ T^{-18350}$
0.5	$\sigma = 86500\ T^{-18550}$
1.0	$\sigma = 93000\ T^{-18460}$
1.5	$\sigma = 97000\ T^{-18400}$

* where σ = stress, psi, T = temperature, °F and C and D are arbitrary numbers.

These expressions serve to show certain relations between stress and temperature at fixed values of creep strain and time. They represent a special case because the creep strain and times considered are singular values. When creep strains consistent with creep times differing from those involved in the foregoing special case are taken into consideration, corresponding changes in stress and temperature can be anticipated. Under these conditions a new set of expressions will be needed to relate stress and temperature at the new fixed values of creep strain and time. In order to generalize the various sets of expressions, additional steps relating them appear necessary. This indicates that moves such as these which attempt to simplify the power function relation also will result in the development of new sets of correlation numbers further attempting to relate creep stress, time, temperature and strain variables. Thus continuing need for redevelopment of correlation numbers diminishes confidence in the eventual utility of the power law expression for creep prediction extrapolations.

THE EXPONENTIAL LAW EXPRESSION FOR CREEP RELATIONS

The Larson-Miller approach toward establishing time-temperature relationships for rupture and creep stress (Reference 5) is based upon an expression which is a variant of the compound interest law. This assumes that creep strain, which can be indicated by some function, y, varies at a rate proportional to itself, with or without some constant term. Thus it follows that if

$$y = Ce^{ax} \tag{128}$$

then

$$\frac{dy}{dx} = be^{ax} \tag{129}$$

where a, b and C are constants and

$$b = aC \tag{130}$$

and C is the value of y when x equals zero.

Thus if

$$\frac{dy}{dx} = \pm ay \tag{131}$$

then

$$y = Ce^{ax} \text{ or } Ce^{-ax} \tag{132}$$

according as the function is increasing or decreasing in magnitude. The Larson-Miller approach is rooted in the idea that the creep rate is a function of the energy content of a system which is running down, hence the form in which they state the compound interest law employs a negative exponent, -ax, or in their terms -Q/RT where Q is the activation energy for the process, R is the universal gas constant and T is the absolute temperature. Considering the reasonable success the Larson-Miller approach has achieved in the prediction of creep and rupture, it can be judged that the basic assumption correctly indicates the direction in which energy moves and that like assumptions with regard to direction would not be erroneous.

The step Larson and Miller used in moving from an expression of the $dy/dx = be^{-ax}$ form, specifically, $r = Ae^{-Q/RT}$, to one of the $y = Ce^{ax}$ form, specifically, $\frac{1}{t} = Ae^{-Q/RT}$, is not clear. This step is explained on the basis that "the time to rupture depends on the summation of creep rates out to rupture." The expression for the Larson-Miller parameter is $T(C + \log t) = \frac{Q}{2.3R}$ = a constant for the constant stress condition where $C = \log A$, a "material" constant. The steps by which the Larson-Miller parameter are arrived at from $1/t = Ae^{-Q/RT}$ are

$$\frac{1}{t} = Ae^{-Q/RT} \tag{133}$$

$$\log \frac{1}{t} = \log A + \left(\frac{1}{2.3}\right)\left(-\frac{Q}{RT}\right) \tag{134}$$

$$-\log t = \log A + \left(\frac{1}{2.3}\right)\left(-\frac{Q}{RT}\right) \tag{135}$$

and taking $\log A = C$

$$-\log t = C + \left(\frac{1}{2.3}\right)\left(-\frac{Q}{RT}\right) \tag{136}$$

$$-T \log t = TC - \frac{Q}{2.3R} \tag{137}$$

$$T\ (C + \log t) = \frac{Q}{2.3R} = \text{Constant} \qquad (138)$$

Thus the process for arriving at the Larson-Miller parameter is straightforward algebraic solution of the $1/t = Ae^{-Q/RT}$ expression in terms of T and t. In the foregoing the presence of an integration constant implied in the integration step involved in the change from r to $1/t = Ae^{-Q/RT}$ is not evidenced.

The Larson-Miller parameter expression $T\ (C + \log t) = Q/2.3R$ = constant implies that C is constant only for constant stress, where as the relation was stated with the assertion that C is independent of stress and possibly material. This point is treated by Manson and Haferd (Reference 6) who examined the relations between the Larson-Miller parameter and stress with the results that they concluded that the method advanced in the Larson-Miller approach was subject to wide variations in error when used in general application.

The result from the Manson and Haferd study was the development of their time temperature relation for extrapolation of creep and stress rupture data. The approach employed was empirical. In essence this method was designed to reduce variation in error in creep prediction, especially at very short and very long times, by applying linerization procedures to a wide variety of experimental data dealing with stress, time and temperature relations observed in creep tests.

LINEARIZATIONS

The power law and exponential rate function approaches to creep phenomena characteristically attempt to linearize creep relations by use of the device of logarithmic transformation of power or exponential equations. The redundant conditions experienced in attempts to manipulate emperical power law expressions are indicated in preceding discussion. Manson and Haferd's work in relation to the Larson-Miller exponential rate function treatment of creep data indicates a degree of error in the Larson-Miller approach which is countered by the presentation of the Manson-Haferd linear time-temperature relation for extrapolating creep and stress rupture data. Linearization practices such as these tend to divert attention from the basic curve shapes which are contained in creep test data. In creep prediction it does not appear sufficient to learn for example what creep times may be observed in attaining a stated deformation when the stress is changed from one value to another at a constant temperature. It does appear that in experimental situations such as the one given in example that the significant information sought in the interest of creep prediction is expression of the effect a change in stress exerts on the change in time required to attain the stated deformation. Basic creep curve expressions derived from basic curve shapes suggest themselves as a means for indicating the interrelations involved in changes in the variables encountered in creep experiments.

The injection of linearity into treatments of creep phenomena apparently results from the practice of recording creep test data in the form of chronological records of strain versus

time. In this convention the chronology of strain history during creep appears in three stages. The first, designated primary creep, characteristically displays strain accrual at a decreasing rate as time accumulates. The second, designated secondary creep, displays strain accumulation at a constant rate as time passes and the third, designated tertiary creep, shows strain growing at an increasing rate as time elapses. Since in usual practice secondary creep, or minimum rate creep, conveniently plots as a straight line, secondary creep phenomena are taken to be those wherein a linear relation between creep time and creep deformation exists under conditions of constant stress and temperature present in test. This practice may be questioned relative to the existence of true linearity in the secondary stage of creep. In view of the special case nature of the straight line, the possibility of the secondary creep stage being one in which very slight curvature appears merits some consideration in the development of creep prediction techniques. The lack of direct physical evidence obtained from materials undergoing creep to support the discontinuties or transitions implied in conventional creep strain versus time records implies the continuity of creep activity and the continuity of curves depicting their progress.

CUMULATIVE CREEP CURVES

The idea that creep strain outwardly manifests accumulations of internal movements of one kind or another within a metal in a continuous manner appears consistent with evidence offered by materials as they undergo creep. The one certainty that can be assumed in the presence of creep, is that if creep is allowed to progress sufficiently, rupture will eventually result. In rupture the item undergoing creep will display its total capability for accepting those internal movements integrated into the strain present at the instant of rupture. At rupture certainty is evident and the probability of rupture is 1. In this concept, the role of time as an indicator of the probability with which internal movements take place within a metal suggests itself. Accordingly since strain is the integral of internal movements probable, time may be considered indicative of the probability of this integral. Thus plotting creep strain against time can express a cumulative creep function.

The importance of the creep probability conception lies in its application to prediction techniques. Here the probability of stress rupture can be interpreted to indicate that fraction of the total strain capability of a metal used up in attaining this probability. Thus the difference between unity and a used-up life fraction could be interpreted as an indication of creep life remaining.

Figure 35 schematically diagrams an idealized time versus creep-strain plot. Here the regions of primary, secondary and tertiary creep associated with conventional creep-strain versus time plots are referenced with respect to inflection points of the curve shown. Figure 36 is a replication of Figure 35 which shows relations obtaining between rupture time fractions, probability and creep strain. The curve shape displayed in Figures 35 and 36 is that for the cumulative normal distribution.

The entering of creep test data into charts of the kind shown in Figure 35 results in dimensioned number displays. In data comparisons presented in raw data form, the choice of scales selected for plotting convenience distort curve shapes. This makes comparison between different sets of charts unwieldy and conceals true curve shapes. When expression coefficients and amplification factors enter into data presentations, data comparison becomes difficult. This results in resort to empirical expressions which are difficult to interpret except on the base of the data from which they originated. These reasons thus make non-dimensional representations of data desirable especially where true curve shapes and a standard of reference are sought.

NON-DIMENSIONAL CREEP CURVES

The reduction of a dimensional time versus creep strain curve to a non-dimensional one is comparatively simple when recognition is given the fact that at stress rupture the time is indicative of the total number of internal movements which have occurred in arriving at stress rupture, and, that the strain at stress rupture represents the external displacement exhibited during creep as a result of all the internal movements within the material up to rupture. The non-dimensional curve takes the time to rupture and the strain to rupture at unity and proportions intermediate values on the basis of a scale ranging from 1 to zero. The non-dimensional creep curve thus derived (Figure 37) represents a pure curve shape indicative of the physical course of events occurring throughout the history of a creep-rupture test.

The non-dimensional creep curves shown in Figure 37 illustrate the special case where the plastic strain introduced at the beginning of creep is negligible. This condition can be visualized only when the creep stress is at or below the proportional limit stress. In cases where the creep stress exceeds the proportional limit stress, the origin of creep strain will move to the right along the abscissa of Figure 37 and the origin of plastic strain, which includes both the initial plastic strain and the creep strain, will remain at the origin shown in Figure 37. This inclusion of plastic strain present at the beginning of creep is necessary because this initial plastic strain is a portion of the total plastic strain present at rupture. When initial plastic strain effects are introduced into non-dimensional creep curves, these effects can be expected to modify the shape of these curves. Experimentally derived creep rupture test data are not immediately available to indicate whether initial plastic strain effects modify the general shape of creep curves or confine their modifications to those portions of creep curves ordinarily designated primary creep portions. Thus before curve fitting can be attempted data are required.

INCREMENTAL LOAD APPLICATIONS AND RELEASE EFFECTS

In view of the importance attached to stress in creep situations a series of incremental loading tests were made to determine those stress levels at which plastic deformation begins to assert itself, how this plastic deformation increases with increasing stress and how these plastic deformation characteristics reassert themselves in successive incremental re-loadings.

Figure 38 indicates the plan for the incremental loading tests run under conditions of constant temperature and repeated increasing stress applications. These tests were made with Armco Ph 15-7 Mo, Condition RH-950 stainless steel. They were run in an Arcweld Model JE creep testing machine and used an Arcweld Model 400 extensometer to observe deformations. The test specimens were 0.505 inch wide by 0.025 inch thick and were provided with 2.0 inch gage lengths conforming to Federal Standard 151A dimensions. The tests involved the initial application of a stress equal to 10 percent of a predetermined maximum stress, allowing this stress to be effective for 15 to 20 seconds and then releasing it. After allowing a 15 to 20 second recovery period subsequent to release, the succeeding stress of 20 percent of the predetermined maximum stress was applied. From this point on the stress application and loading proceeded as described with a 10 percent increase in the stress level being made at each reapplication of stress until the predetermined maximum stress was reached. Upon attaining the maximum stress, the entire procedure was repeated until five complete build-ups to the maximum stress were accomplished. Tests were made at 700°, 800°, 900° and 1000°F, in duplicate, to explore the effects of temperature variation.

Figure 39 shows the outcome of the first incremental loading test run at 700°F with material which was not stressed prior to test. The line AB in this chart shows the deformations attained upon application of the various stresses in a single cycle of build-up. The deformations remaining upon removal of stress are shown in the line CD. The deformations shown by the line CD result from plastic action and are not reversible.

In Figure 39 the incidence of permanent set occurs at about 50 percent of the maximum stress used or about 87.5 ksi. This stress approximates the proportional limit of the material. A 0.2 percent permanent set, the limit of plastic strain considered negligible, occurs at a stress of about 90 percent of the maximum stress used or about 166.5 ksi. This stress approximates the yield strength of the material. Thus when a 0.2 percent permanent set is taken as a limit, the yield strength is the limit for use and the total deformation at the yield stress also is limited. From the data in Figure 39 the limit of total deformation appears at 0.8 percent total deformation, the deformation at yield, in the material at hand at 700°F. The significant meaning in this is that the permanent set allowed into a material rather than the total deformation permitted can become the controlling factor in application. The case at hand shows that limiting permanent set can be attained in the course of initial loading provided stresses are allowed to go high enough. If however permanent set is allowed to enter from creep sources, for example, this can all be taken in creep provided the proportional limit is not exceeded. A holding of stresses at or below proportional limit stress levels conceivably can penalize weight conscious design. The alternative to this consists of a partitioning of the allowable permanent set between that acquired in consequence of initial loading and that acquired in creep.

Figure 40 displays the deformations arising out of repeated applications of incremental stress build-ups at 700°F. In the initial cycle shown about 1.1 percent total deformation was observed upon application of the maximum stress. This resulted in the introduction of about 0.48 percent permanent set into the material. In the repeat stress build-ups, the permanent set observed subsequent to each load release always exceeded the 0.48 percent permanent set

introduced during the initial stress build-up. Also in the repeat stress build-ups, the stress-strain relationships throughout the second to fifth repetitions were such that direct proportionality of stress to strain was in evidence. This indicated that work hardening occurred during the initial stress build-up and established a new proportional limit at the 185 ksi maximum stress level. Thus those stresses applied subsequent to the first maximum or 185 ksi stress application acted in an elastic manner. The cost involved in obtaining this elastic action subsequent to the initial maximum stress application was the 0.48 percent permanent set introduced in consequence of the initial loading.

The work hardening attendant to the initial maximum stress application, although it did force the material into behaving in an elastic manner, did not stabilize it with respect to its acquiring additional permanent set. The information shown in Figure 40 is not suggestive of deterioration of work hardening effects since the stress strain proportionality persisted throughout the repeated stress build-ups. The immediate cause of the permanent set build-up during the repeat stress build-ups appeared to be creep.

Figure 41 shows the outcome of the test duplicating the one whose results are shown in Figure 40. These outcomes closely resemble one another especially with regard to events during the repeat stress build-up cycles. They differ in two respects however. In the first test (Figure 40) the proportional limit appeared at about 50 percent of the maximum stress or 87.5 ksi. In the second test (Figure 41) the proportional limit appeared at about 60 percent of the maximum stress or 110 ksi. Also in the first test the permanent set increment occurring during the repeat stress build-ups totaled 0.12 percent and in the second test this increment totaled 0.03 percent. Close check of the temperatures present and the loads applied in these tests did not uncover significant differences. Also since the specimens came from the same sheet of material and were heat treated and machined together, differences from these sources was minimized. Accordingly in recognition of the sensitivity of the nickel-chronium austenitic steels as a class to strain hardening, attention was given this and the differences observed in the proportional limits exhibited by the Armco PH 15-7 Mo steel were attributed to differences in strain rates present during load application.

The differences in the test outcomes noted above intimate that as the proportional limit increases a strain rate increase would also be reflected and thus a smaller amount of plastic strain would be present upon reaching a given stress in excess of the proportional limit than would be the case if the strain rate were low. The test data at hand are in contradiction to this. Here the test displaying the lower proportional limit displayed least permanent set upon attaining maximum stress and the test displaying the higher proportional limit displayed greatest permanent set upon attaining maximum stress. The test data at hand are not taken to disprove the initial statement in this paragraph. However their inconsistency with this statement does indicate the importance of each load application in the accumulation of plastic strain present at the onset of creep, and, the desirability for assessment of load applications from the standpoint of magnitude and uniformity of strain rate so that estimates of the amount of plastic strain present at the onset of creep are made available.

Table 22 recapitulates the pertinent points of the incremental loading test data given in Part I of this report. In this table an initial tendency for a high initial permanent set to associate itself with greater creep set upon repetitive stress build-up cycling is shown at the lower temperature. In addition a tendency for this relation to diminish and tend to reverse as temperatures increase is suggested. Creep test data reporting results of tests run at constant temperature and varying stresses consistently show variation in initial strain present at the onset of creep. The increase of creep rate which associates itself with increased initial stress and increased initial strain indicates effects arising out of the initial strain which appear influential in ensuing creep history. This can be appreciated because when creep is taken as a process which follows an exponential growth law, the rate at which the plastic (creep) strain can be expected to proceed will be related to the plastic strain initially present in the same sense that the amount of initial principal governs the amount of interest accrued.

EFFECT OF DECREMENTAL LOADING AT VARIOUS TEMPERATURES

Figure 42 indicates the plan for decremental loading tests run under constant temperature conditions. These tests were made with the same material, specimens and apparatus used in the incremental loading tests described above. These tests differed from the former ones in that the predetermined maximum stress was applied initially and was followed by stress applications which diminished in 10 percent steps to zero. Figures 43 through 50 display outcomes from duplicate tests run at 700°F and 182 ksi stress, 800°F and 175 ksi stress, 900°F and 135 ksi stress, and, 1000°F and 77 ksi stress.

The data displayed in Figures 43 through 50 show that these tests as a group resulted in similar outcomes. The general behavior exhibited throughout was for the initial and highest stress application to work harden the material and increase its proportional limit to the applied stress level. This caused the material to work in an elastic manner throughout the several loading programs. In a general way the two specimens representing each test case displayed parallel elastic behavior.

The two specimens representing each test case differed in respect to their response to initial load application. The data given in Table 23 indicates the pertinent differences. In each test case the specimen displaying the lowest total deformation also exhibited the lowest permanent set resulting from the initial load application. By inference of the kind discussed in relation to the incremental loading tests, those tests showing the lowest loading deformations in the decremental loading tests displayed the highest proportional limits during loading. These were considered to be strained at the higher strain rate. In the relations observed between the permanent set acquired in loading to maximum stress and the creep set occurring from the beginning of the second to the end of the fifth repetition of decremental loading, consistent trends were not obvious. The general tendency was for the greater creep set to associate itself with the lower permanent set arising out of the initial loading. This association was not observed in those tests run at 800°F where the opposite trend appeared.

Although the incremental and decremental loading tests did not clearly demonstrate the relationships obtaining between strain rates present during loading, the permanent set occur-

ring during loading, and, the creep rates present subsequent to loading, they did bring attention to these items. These tests suggest that other tests embodying precise strain rate control can help illuminate understanding of creep action. These incremental and decremental tests did clearly demonstrate the role initial high stressings play in work hardening. High initial stresses induce elastic behavior which is effective at stress levels equal to or less than the high initial stress. This elastic action induction may alter but does not halt the progress of creep.

EFFECT OF DECREMENTAL LOADING AT VARYING STRESSES AND CONSTANT TEMPERATURE

The incremental and decremental loading tests already discussed were run at various temperatures as indicated. These temperatures were selected to span the range wherein aging or precipitation hardening activity could assert itself. At 700°F the likelihood of activation was considered slight. At 800°F activation in the long term was considered possible. At 900°F activation in the short term was considered possible and at 1000°F activation was considered certain upon attainment of temperature. Because of conflicting outcomes observed in the two preceding series of tests, a third set was run, using the same material, specimen preparation and testing apparatus used in the first two instances, at a constant temperature of 700°F and with varying stresses, 182, 185, 188 and 191 ksi, to learn if temperature variation exerted a significant influence upon the foregoing test outcomes.

Figures 43 and 44, and 51 through 56 show the outcome of tests run at 700°F, a temperature considered to be within a range wherein aging activation is remote. These tests like the preceding series resulted in similar outcomes. The general behavior exhibited throughout this series of tests again was for the initial and highest stress applications to work harden the material. This increased its proportional limit to the applied stress level and caused it to work in an elastic manner throughout the loading programs. In general the two specimens representing each test displayed parallel elastic behavior.

The two specimens representing each test case differed one from the other in their response to initial load application. The data given in Table 24 indicates the pertinent differences observed. In three test cases; 182, 185 and 191 ksi, the specimens displaying the lowest total deformation also exhibited the lowest permanent set as a result of the initial load application. In the fourth case, 188 ksi, both specimens exhibited about the same total deformations but acquired differing amounts of permanent set. In this series of tests, as in the preceding series, the tendency for those specimens which exhibited the least plastic or permanent set upon loading to accumulate creep strain at the greater rate generally reasserted itself.

CREEP INITIATION

The "standard" creep tests reported in Part I of this report were made to ascertain the utility of stress-rupture and creep data presented in vendor literature in the form of Larson-

Miller plots. These plots were used for estimating total deformations resulting from stresses and temperatures suggested for 50 hour creep life determined by the appearance of 1 percent total deformation in tests. The material used in these tests was Armco PH 15-7 Mo stainless steel heat treated to the RH 950 condition. The specimens used were 0.025 in by 0.125 by 15 in long and they were tested in a multiple station, specially built creep test machine employing dead weight loading, automatic temperature control and visual strain measurement aided by cathetometer equipment. All tests in the "standard" creep test series were run under constant load, constant temperature conditions. Pertinent data relating to test outcome are shown in Table 25.

In those "standard" creep tests run at 700°, 800° and 900°F, the secondary creep rates all were less than the rate of 3.33×10^{-4} in per minute estimated from vendor supplied Larson-Miller stress-rupture chart data. In view of the conservative creep rates observed in these tests, attention was turned to circumstances related to the initiation of conditions promoting these creep rates. Using a rule of thumb comparison base that total deformation of approximately 1 percent is permissible in airframe structures and a permanent set in excess of 0.2 percent is undesirable, all those tests which were run at 700°, 800° and 900 F with conservative secondary creep occurrence displayed total deformations upon loading which were greatly in excess of the rule of thumb limit. This indicated the critical nature of the initially applied load in a deformation sensitive situation.

When the spring back or recovery observed after removal of the creep load is deducted from the total deformation observed subsequent to loading at the beginning of test, the difference represents the permanent set introduced as a result of load application. Here the spring back or recovery is taken to represent the elastic deformation appearing during loading. In those tests run at 700°, 800° and 900°F. the permanent sets observed upon loading were either in excess of or consumed a substantial portion of the 0.2 percent limit considered under the rule of thumb comparison standard. In contrast with the conservatism of the secondary creep rates observed, the initial loading situation again was critical.

When primary creep deformations observed with those tests run at 700°, 800° and 900°F were compared with the conservative secondary creep rates and the 0.2 percent rule of thumb permanently set limit, they were great enough in themselves to indicate that the very early creep history would be critical with respect to deformation.

In the tests run at 700°, 800° and 900°F. two sets of specimens were tested at each temperature. The loading between the sets of specimens differed by about 1, 3 and 4 percent as each increasing temperature was considered in the tests. The object of this was to see if minor stress variations could give rise to significant differences in outcome. As the foregoing dicussion indicates all secondary creep outcomes were conservative and all loading and primary creep outcomes asserted the relatively slight effect arising out of minor stress differences. These tests again indicated the important role of initial loading in shaping the deformation pattern of creep history.

In order to extend considerations into the area of major stress differences, the stress difference between the two sets of specimens run at 1000°F was increased to about 40 percent.

The actual stresses used were taken at approximately 50 and 75 percent of yield strength. The test outcome indicated conservative secondary creep rates, all less than a 3.33×10^{-4} in per min estimated to produce 1 percent deformation in 50 hours. These resulted at both stress levels employed. Primary creep persisted also. In view of the temperature used, 1000°F., the possibility of overaging promoting primary creep action existed and suggested that tests run at a temperature where overaging was not probable would be informative with respect to associations between stress and primary creep incidence.

Figures 57 through 75 show test outcomes from "standard" creep tests run at 700°F, 800°F., 900°F. and 1000°F. at stresses chosen to represent the proportional limit stress, that stress required to produce 0.1 percent permanent set and the yield stress as indicated in vendor tensile test data. These tests, with the exception of the details mentioned above, were made with the same material, apparatus and procedure described earlier in this section. Table 25 lists the pertinent data derived from the tests detailed in Figures 57 through 75.

The Table 25 data indicate that temperature exerts the major influence in creep and stress exerts a secondary influence. At lower temperatures creep did not assert its presence until a stress in the neighborhood of the yield stress was reached. At the higher temperatures creep was active at stresses in the neighborhood of the proportional limit. The absence of permanent set upon loading associated itself with the absence of secondary creep at the lower temperatures, 700°F and 800°F. At the higher temperatures, 900°F and 1000°F, the absence of permanent set upon loading did not associate itself with the absence of secondary creep because secondary creep was in evidence at these temperatures. These tests did not show a clear association between primary creep, the loading conditions and the presence or absence of secondary creep.

EFFECT OF STAINLESS STEEL ALLOY CHANGE ON CREEP STABILITY

In order to inquire into circumstances arising out of incremental and decremental loading tests with Armco PH 15-7 Mo, Condition RH 950 stainless steel which suggested association between the proportional limit stress and creep initiation stress, the associations of work hardening attendent to stressing in excess of the proportional limit with creep initiation and the stability of creep, once it was initiated, were examined in a series of tests made with Allegheny Ludlum AM 355, Condition SCT stainless steel. These tests incorporated a change in material within the alloy class of stainless steels to broaden the field of generalization.

In preparation for creep tests, stress-strain tests were made in a 60,000 pound capacity Olsen Electromatic universal testing machine equipped with autographic load-deflection recorders, an automatic strain rate control and ASTM Class B extensometers. Figure 76 shows the composite stress-strain diagram derived from five individual tests with Allegheny Ludlum AM-355, Condition SCT stainless steel at 700°F., and a strain rate of 0.005 in per in per min. The 80.6 ksi proportional limit, the 111.2 ksi stress required to produce 0.1 percent permanent set and the 146.3 ksi yield stress for use in creep testing were estimated with the aid of this diagram.

Figures 77 and 78 show outcomes of creep tests run at 80.6 ksi, the proportional limit stress, at 700°F for 100 hours. Negligible creep asserted itself in these tests. Figures 79 and 80 show outcomes of creep tests run at 111.2 ksi, that stress required to produce 0.1 percent permanent set, at 700°F for 100 hours. In the initial 70 to 75 hours of these tests negligible creep appeared. After this period creep was evidenced and progressed at a rate of about 6×10^{-7} in per hr or 1×10^{-8} in per min. Figures 81 and 82 show outcomes of creep tests run at 146.3 ksi, the yield strength, at 700°F for 100 hours. In the first test negligible creep asserted itself. In the second test creep asserted itself after 70 hours and then proceeded at a rate of 5×10^{-6} in per hr or 8.3×10^{-7} in per min.

Figures 83 and 84 show outcomes of creep tests run at 80.6 ksi stress and 700°F. for 100 hours after initial prestressing at 111.2 ksi stress. Creep action was negligible during the first 60 hours of these tests. During the last 40 hours of test, creep initiated and progressed at a rate of about 6.8×10^{-6} in per hr or 1.1×10^{-7} in per min. In comparison with the outcome of tests run at 80.6 ksi in the absence of prestress (Figures 77 and 78), these tests showed an effect from prestress which resulted in a delay in creep initiation.

Figures 85 and 86 show outcomes of creep tests run at 80.6 ksi stress and 700°F for 100 hours after initial prestressing at 146.3 ksi stress. These outcomes did not indicate a clear tendency for prestressing to supress creep action early in test. Retesting did not shed additional light on the matter because the random test outcome persisted.

Figures 87 and 88 show outcomes of creep test run at 111.2 ksi stress and 700°F for 100 hours after initial prestressing at 146.3 ksi stress. These tests showed a tendency for initial creep followed by an arrest in creep action to occur. The time of creep initiation varied extensively.

Those tests which were run in the absence of prestress indicate that creep can start at the time a load is applied, as is the usual connotation, or at some time after load application. The tests at hand do not directly relate creep initiation time to creep stress. The similarity of the times, regardless of stress, at which creep started in these tests hints at the possibility of the activity of a time dependent mechanism such as aging entering into play.

The stabilizing value of prestressing prior to introducing creep was not borne out by those tests wherein prestressing was employed. Prestressing at the lower stress levels tended to promote some stability of comparatively short duration. Prestressing at the higher stress levels was conducive to initial creep action followed by an interval of creep stability. The tests were not of sufficient duration to indicate the permanence of this state of stability.

EFFECT OF BASE METAL CHANGE ON CREEP STABILITY

The effect of change in base metal upon creep initiation was looked into by a series of tests replicating those made in connection with the Allegheny Ludlum AM-355 stainless steel. In the present test series, tension tests with Rene 41 alloy preceded creep testing. The tension tests were run at 1600°F, 1400°F, and 1300°F. These temperatures were chosen

above, at and below the 1400°F precipitation hardening temperature so that the hardening effect could be reckoned into outcomes. The stress strain curves resulting from several tests at each temperature are summarized in Figure 89.

The stress strain curve representing the typical 1600°F behavior of the Rene 41 nickel base alloy in Figure 89 illustrates a condition wherein maximum stress and concurrent plastic flow initiation were attained at a low value of strain. This condition is considered indicative of circumstances conducive to plastic flow rather than those opposing it. Conditions such as these arise largely because of the temperature present.

The usual effect of increasing temperature is to compress full range stress-strain curves into shapes which are "skewed" to the left. The interpretation applied to such curve shapes is that they indicate conditions where plastic flow dominates the deformation process and thus indicate conditions conducive to rapid creep.

The stress strain curve which represents the typical behavior of the Rene 41 nickel base alloy at 1400°F also is shown in Figure 89. This curve illustrates conditions wherein "early" compression effects resulting from high temperature are not in evidence as they were at 1600°F. This curve is not "skewed." At 1400°F plastic flow was not in evidence at 1.5 percent strain. It was clearly evidenced at about 0.5 percent strain at 1600°F. Accordingly, 1400°F was taken as a temperature at which moderate creep at fairly high stress levels might be anticipated.

Initial creep tests at 1400°F were run at a stress of 79 ksi. This stress was taken to be the proportional limit of the Rene 41 alloy at 1400°F and was obtained from extrapolations of the plastic stress strain curve to 1×10^{-7} strain. At 1400°F and 79 ksi stress brittle fracture occurred in 18 to 42 minutes. This indicated that precipitation hardening activity was present and dominated conditions prevalent during test. For this reason testing at the 1400°F temperature was discontinued in favor of testing at 1300°F, a temperature of 100°F removed from the aging temperature used in preparing the test material.

Those creep tests which were run with the Rene 41 alloy at 1300°F were run at the proportional limit stress at 1×10^{-7} plastic strain, 73.5 ksi, the stress required to produce 0.1% strain, 120 ksi, and the yield stress, 123 ksi. Figures 90 and 91 show the outcome of the tests run at 73.5 ksi. The test shown in Figure 90 terminated in rupture at one of the extensometer attachment points and that shown in Figure 92 terminated in failure on the spot welds attaching doubler pieces to the connection areas of the specimen. This indicated that the material was extremely sensitive to "notch" effects, whether mechanical or metallurgical, in the 0.025 in thickness tested. This indicated that the heat treatment was at fault and required revision although it was a producer recommended schedule aimed for optimum "short time" strength. Figure 90 and 91 data also indicated that in this material creep initiation was not associated with the proportional limit, since a creep rate of 2.67×10^{-5} per hour was observed at the proportional limit stress. Both of the tests shown in Figure 92 were run at a stress of 120 ksi and resulted in fracture. In both cases fracture occurred at an extensometer attachment point. These test outcomes show increase in creep activity

resulting from relatively minor work hardening arising from introduction of 0.1 percent permanent set into the material. Figure 93 shows the outcome of creep tests run under a stress of 123 ksi. The creep curves shown in Figure 93 resemble those of Figure 92 but tend to rise at a greater rate. Comparisons of the increment in the initial permanent set with the creep stress increments of 69.5 and 3 ksi used in these tests indicated the predominating influence of creep stress in relation to initial plastic strain in governing the progress of creep once it is underway.

Figure 94 shows the outcome of creep tests run with Rene 41 at 1300°F and a stress of 73.5 ksi, subsequent to prestressing at 120 ksi. Comparison of the Figure 94 curve with that shown in Figure 91 is shown by the dashed line drawn in Figure 91. Figure 95 shows the outcome of creep tests run with Rene 41 at 1300°F and a stress of 73.5 ksi subsequent to prestressing at 123 ksi. The shorter of the two tests failed at an extensometer attachment and was considered more representative of conditions prevalent in the presence of a notch than creep. The longer test failed at the connection doublers and was believed representative of the creep action present. This curve is shown in Figure 91 by the broken line drawn in it. The comparisons shown in Figure 91 point in the direction that the role of prestress prior to creep action is to govern the amount of initial deformation observed and that its influence on creep at a stress under the prestress level is minor. The progress of creep appeared to depend chiefly on the stress acting at the time creep was in progress.

Figure 96 shows the outcome of tests run at 1300°F and a stress of 120 ksi after prestressing at 123 ksi. Comparison of the curves shown in Figure 96 with those shown in Figure 92 is given by the dashed lines drawn into Figure 92. This comparison does not confirm that discussed in the preceding paragraph. In the case of material prestressed at 123 ksi and creep tested at 120 ksi its behavior varied markedly from that displayed when creep testing was done at 120 ksi in the absence of prestress. In the present instance the prestress appeared to accelerate creep action and exerted comparatively little effect upon the initial strain observed. The effect of the prestress upon the initial strain may be rationalized on the basis of the 3 ksi stress difference between the creep stress and the prestress. The wide differences observed in creep behavior, (1) where creep progressed at a comparatively low stress level subsequent to prestressing in comparison with that observed (2) where creep progressed at comparatively high stress level subsequent to prestressing, did not offer a simple rationalization for the observed differences in creep behavior.

EFFECT OF A "NON-HARDENING" MATERIAL ON CREEP STABILITY

The effect of change from a precipitation hardening to a non-precipitation hardening material with respect to creep initiation was looked into by a series of tests replicating those made in connection with the Allegheny Ludlum AM-355 stainless steel. In the present series of tests, tension tests with the HS-25 alloy preceded creep tests. The tension tests were run at 1800°F and 1600°F. These temperatures were chosen to represent an area of design interest where environmental conditions suggest a region of choice between super-

alloys and refractory metals. The stress strain curves resulting from several tests at each temperature are summarized in Figure 97.

The stress strain curve representing the typical 1800°F behavior of the HS-25 alloy in Figure 97 illustrates again a condition where maximum stress and concurrent plastic flow initiation are attained at a low value of strain. The condition is conducive to plastic flow rather than opposing it. Conditions such as these arise largely because of the temperature prevailing. The usual effect of increasing temperature to compress full range stress strain curves into shapes which "skew" to the left is evidenced in this curve.

The 1600°F stress strain curve of Figure 97 represents the typical behavior of the HS-25 cobalt base alloy at this temperature. This curve illustrates conditions wherein "early" compression effects resulting from high temperature are not in evidence as they were at 1800°F because this curve is not "skewed." At 1600°F plastic flow as evidenced by passage of the stress-strain curve through a maximum stress was not in evidence out to 1.5 percent strain. Plastic flow however was evidenced at about 0.15 percent strain at 1800°F. Accordingly, 1600°F was taken as a temperature at which moderate creep at fairly high stress levels might be anticipated.

Initial creep tests at 1600°F were run at a stress of 23 ksi. This stress was taken to be the proportional limit of the HS-25 alloy at 1600°F and was obtained from extrapolations of the plastic stress strain curve to 1×10^{-5} strain. Figure 98 shows the outcome of the creep tests run at 23 ksi and 1600°F. The creep rates of 6.8×10^{-3} and 5.5×10^{-3} strain per minute showed absence of creep arrest at the proportional limit chosen. To examine the choice of proportional limit more closely the plastic strain curve was extrapolated an additional order of magnitude to arrive at a new value of 18.5 ksi at 1×10^{-6} strain. Figure 99 shows the outcome of creep tests run at this stress at 1600°F. In these tests the creep rates were reduced to 6.25×10^{-3} strain per hour or 1.04×10^{-4} per minute. This reduction in strain rate amounted to somewhat more than one order of magnitude, a circumstance that roughly fitted in with the single order extension in proportional limit extrapolation.

The foregoing tests indicated a lack of correlation between the proportional limit exhibited by the HS-25 alloy and its creep initiation stress. This outcome contrasted sharply with those observed with the two precipitation hardened stainless steels, Armco PH 15-7 Mo, Condition RH 950 and Allegheny Ludlum AM 355, Condition SCT, which showed strong inclinations to correlate with respect to their proportional limits and creep initiation stresses. The outcome of the present series of tests coincide with vendor information (Haynes Alloy No. 25, Haynes Stellite Company, Kokomo, Indiana, September, 1960) which show the proportional limit for HS-25 at 1600°F to be 25.7 ksi.

In view of the pronounced tendency for the HS-25 alloy to creep appreciably at relatively low "proportional" limit stresses, Haynes' creep data were examined with reference to the time required to produce 0.2 percent total elongation at a stress of 10 ksi. These data show that at 1500°, 1600° and 1700°F. a 0.2 percent total elongation is attained in 12, 2.5 and

2 hours respectively at 10 ksi stress. They also show that at 1500°, 1600° and 1700°F. a 1.0 percent total elongation is attained in 800, 400 and 250 hours respectively. Because of both the low stress level and the short times indicated for attainment of significant deformation at temperatures of design interest in airframe construction, the utility of an essentially plastic material, such as this, in primary airframe structure appears to be questionable in the absence of positive assurance that time, temperature and stress limitations imposed by the material cannot be exceeded in service.

SUMMARY AND CONCLUSIONS

1. Incremental and decremental loading tests demonstrate the ability of high stresses to work harden metal at elevated temperature. This results in the establishment of a new high proportional limit at the expense of introducing plastic deformation. Work hardening causes metals to behave in an elastic manner after the work hardening is done. Work hardening does not serve to arrest creep action.

2. The stress at which creep initiated in Armco PH 15-7 Mo, Condition RH 950 and Allegheny Ludlum AM 355, Condition SCT stainless steels was associated with their proportional limits at elevated temperature. The creep initiation stress of the Rene 41 nickel base alloy and the HS 25 cobalt base alloy did not associate itself with their elevated temperature proportional limits.

3. The stabilizing value of prestressing prior to introducing creep was not borne out by tests wherein prestressing was employed. Prestressing at stresses slightly in excess of proportional limit stresses promoted stability of short duration. Prestressing at stresses considerably above the proportional limit was conducive to early creep action followed by a period of stability. These tests indicated that the onset of creep was not bound to the event of stress application but could occur at times subsequent to that of stress application.

4. Tests with the Rene 41 nickel base alloy indicated that metallurgical factors, such as strain aging, can control metal reactions in creep environments. Early strain aging failures in the neighborhood of the aging heat treatment temperature were associated with spot welds and possible mechanical notches.

5. The non-hardenable HS-25 cobalt base alloy tended to creep readily at stresses and temperatures of design interest. The inability of this alloy to accommodate creep stresses of design interest was observed.

6. The foregoing test outcomes did not lead to creep prediction method. They did suggest the possible utility of creep-rupture test data and its study in non-dimensional terms as an approach toward a creep prediction method.

REFERENCES

1. Cottrell, A. H., "Theoretical Structural Metallurgy," St. Mary's Press, Inc., New York, 1955.

2. Shanley, F. R., "Strength of Materials," McGraw-Hill Book Company, Inc., New York, 1957.

3. Morrison, J. D. and Kattus, J. R., "Tensile Properties of Aircraft - Structural Metals at Various Rates of Loading After Rapid Heating," W.A.D.C. Technical Report 59-199, Part 2, Wright Air Development Center, November 1956.

4. Giemza, C. J., "Experimentation, Analysis and Prediction for Environmental Creep," WADD Technical Report 60-777, Wright Air Development Division, November 1960.

5. Larson, F. R. and Miller, J., "A Time-Temperature Relationship for Rupture and Creep Stress," Transactions of American Society of Mechanical Engineers, Vol. 74, No. 5, pp 765 to 775, 1952.

6. Manson, S. S. and Hafred, A. M., "A Linear Time-Temperature Relation for Extrapolation of Creep and Stress-Rupture Data," N.A.C.A. Technical Note 2890, National Advisory Committee for Aeronautics, Washington D. C., March 1953.

TABLE 1 ELEMENT STIFFNESS MATRIX

Section	Area Sq. In.	Length In.	Stiffness A/L
	Element Sections Box II		
1-11-21-31	.117117	2.00	.0585585
2-12-22-32	.180683		.0903415
3-13-23-33	.180683		.0903415
4-14-24-34	.204966		.1024830
5-15-25-35	.131400		.0657000
6-16-26-36	.176400		.0882000
7-17-27-37	.334917		.1674585
8-18-28-38	.334917		.1674585
9-19-29-39	.334917		.1674585
10-20-30-40	.176400		.0882000
11-12-13-14-15	.176400		.088200
21-22-23-24-25	.176400		.088200
16-17-18-19-20	.266400		.133200
26-27-28-29-30	.266400		.133200
Diagonals			
Top Plate	.063640	2.828	.022500
Spars - Ribs	.063640		.022500
Bottom Plate	.127280		.075000
	Element Sections Box III		
1-11-21-31	.110280	2.00	.055140
2-12-22-32	.133450		.066725
3-13-23-33	.125770		.062885
4-14-24-34	.141130		.070565
5-15-25-35	.110280		.055140
6-16-26-36	.117780		.088890
7-17-27-37	.313486		.156734
8-18-28-38	.313486		.156734
9-19-29-39	.313486		.156734
10-20-30-40	.177780		.088890
11-12-13-14-15	.133780		.066890
21-22-23-24-25	.133780		.066890
16-17-18-19-20	.267780		.133870
26-27-28-29-30	.267780		.133870
Diagonals			
Top Plate	.031820	2.828	.011250
Spars - Ribs	.063640		.022500
Bottom Plate	.127280		.045000

TABLE 1 (CONT'D) ELEMENT STIFFNESS MATRIX

Element Stiffness Matrix Example

$$T = \begin{bmatrix} 1 \\ \\ -1 \end{bmatrix}, \quad T' = \begin{bmatrix} 1 & -1 \end{bmatrix}, \quad K = TST = \begin{bmatrix} 1 \\ \\ -1 \end{bmatrix} S \begin{bmatrix} 1 & -1 \end{bmatrix} = \begin{bmatrix} S & -S \\ \\ -S & S \end{bmatrix}$$

$$S = AE/L, \quad K = \begin{bmatrix} AE/L & -AE/L \\ \\ -AE/L & AE/L \end{bmatrix}$$

where

$$K\delta = F \quad \text{or} \quad \begin{bmatrix} AE/L & -AE/L \\ \\ -AE/L & AE/L \end{bmatrix} \begin{bmatrix} \delta_1 \\ \\ \delta_2 \end{bmatrix} = \begin{bmatrix} F_1 \\ \\ F_2 \end{bmatrix}$$

Ref. WADD TR 60-411 PART I.

TABLE 2 BOX STIFFNESS MATRIX - REPRESENTATION OF COLUMNS OF T_1

Line of Matrix	Degree of Freedom		Line of Matrix	Degree of Freedom	
	Node	Direction		Node	Direction
1	*	δ_x	34	20	X
2	*	δ_y	35	20	Y
3	*	δ_z	36	20	Z
4	*	θ_x	37	21	X
5	*	θ_y	38	21	Y
6	*	θ_z	39	21	Z
7	11	X	40	22	X
8	11	Y	41	22	Y
9	11	Z	42	22	Z
10	12	X	43	23	X
11	12	Y	44	23	Y
12	12	Z	45	23	Z
13	13	X	46	24	X
14	13	Y	47	24	Y
15	13	Z	48	24	Z
16	14	X	49	25	X
17	14	Y	50	25	Y
18	14	Z	51	25	Z
19	15	X	52	26	X
20	15	Y	53	26	Y
21	15	Z	54	26	Z
22	16	X	55	27	X
23	16	Y	56	27	Y
24	16	Z	57	27	Z
25	17	X	58	28	X
26	17	Y	59	28	Y
27	17	Z	60	28	Z
28	18	X	61	29	X
29	18	Y	62	29	Y
30	18	Z	63	29	Z
31	19	X	64	30	X
32	19	Y	65	30	Y
33	19	Z	66	30	Z

TABLE 2 (CONT'D) BOX STIFFNESS MATRIX - REPRESENTATION OF COLUMNS OF T_1

Note: Since the assembled stiffness matrix is too large to be conveniently displayed, only the method used to sum the various stiffnesses is given. The symmetrical transform matrix was used to relate the element stiffness to the structure as shown below.

$$S_{total} = T_1^T S_1 T_1 + T_2^T S_2 T_2$$

where S_1 = A diagonal matrix representing, G, the element stiffness acting parallel to the coordinate axis.

S_2 = A diagonal matrix representing the element stiffness acting at 45° to the coordinate axis

T_n = A matrix relating element stiffness to structure coordinates

T_n^T = The transpose of T_n

As an example, T_1 is given in Table 3. The meanings of the matrix rows and columns are shown in Tables 2 and 4.

TABLE 3 BOX STIFFNESS MATRIX - TRANSFORMATION MATRIX T_1

Locations for +1				Locations for -1			
Row	Column	Row	Column	Row	Column	Row	Column
1	1	27	16	1	7	22	33
1	5	28	19	2	10	23	36
2	1	29	22	3	13	24	37
2	5	30	25	4	16	25	40
3	1	31	28	5	19	26	43
3	5	32	31	6	5	27	46
4	1	33	34	6	22	28	49
4	5	34	38	7	5	29	52
5	1	35	41	7	25	30	55
5	5	36	44	8	5	31	58
6	1	37	47	8	28	32	61
7	1	38	50	9	5	33	64
8	1	39	56	9	31	34	41
9	1	40	59	10	5	35	44
10	1	41	62	10	34	36	47
11	8	42	39	11	11	37	50
12	11	43	42	12	14	38	56
13	14	44	45	13	17	39	59
14	17	45	48	14	20	40	62
15	23	46	51	15	26	41	64
16	26	47	37	16	29	42	54
17	29	48	40	17	32	43	57
18	32	49	43	18	35	44	60
19	9	50	46	19	24	45	63
20	12	51	49	20	27	46	66
21	15	52	52	21	30		
22	18	53	55				
23	21	54	58				
24	7	55	61				
25	10	56	64				
26	13						

Locations for +2		Locations for -2	
Row	Column	Row	Column
2	6	4	6
7	6	9	6

Locations for +4		Locations for -4	
Row	Column	Row	Column
1	6	5	6
6	6	10	6

Note: The rows shown in Table 3 represent the elements shown in Table 4

TABLE 4 BOX STIFFNESS MATRIX

Line	Element	Line	Element
1	1 - 11	33	20 - 30
2	2 - 12	34	21 - 22
3	3 - 13	35	22 - 23
4	4 - 14	36	23 - 24
5	5 - 15	37	24 - 25
6	6 - 16	38	26 - 27
7	7 - 17	39	27 - 28
8	8 - 18	40	28 - 29
9	9 - 19	41	29 - 30
10	10 - 20	42	21 - 26
11	11 - 12	43	22 - 27
12	12 - 13	44	23 - 28
13	13 - 14	45	24 - 29
14	14 - 15	46	25 - 30
15	16 - 17	47	21 - 31
16	17 - 18	48	22 - 32
17	18 - 19	49	23 - 33
18	19 - 20	50	24 - 34
19	11 - 16	51	25 - 35
20	12 - 17	52	26 - 36
21	13 - 18	53	27 - 37
22	14 - 19	54	28 - 38
23	15 - 20	55	29 - 39
24	11 - 21	56	30 - 40
25	12 - 22		
26	13 - 23		
27	14 - 24		
28	15 - 25		
29	16 - 26		
30	17 - 27		
31	18 - 28		
32	19 - 29		

Note: The elements shown in Table 4 are represented by the rows shown in Table 3.

TABLE 5 BOX DEFLECTIONS FOR UNIT LOADS

Node	Coordinate	Box II	
		$M_y = E$	$M_z = E$
δ_x	-	0.508269	0.017538
δ_y	-	0.056136	1.056010
δ_z	-	-7.532853	- .056135
θ_x	-	0	0
θ_y	-	2.510956	-0.018712
θ_z	-	0.018712	0.352004
11	X	2.063316	0.965520
11	Y	0.327047	0.523829
11	Z	-3.237859	-0.066981
12	X	2.045824	0.496506
12	Y	0.150728	0.460183
12	Z	-3.423945	-0.041352
13	X	2.017482	0.024237
13	Y	0.023305	0.438836
13	Z	-3.463701	-0.026109
14	X	1.994856	-0.447687
14	Y	-0.101953	0.457073
14	Z	-3.422422	-0.010163
15	X	1.963237	-0.916963
15	Y	-0.271659	0.516651
15	Z	-3.233437	0.018209
16	X	-1.286902	0.939569
16	Y	-0.123463	0.504852
16	Z	-3.203968	0.023059
17	X	-1.311702	0.467935
17	Y	-0.038058	0.461238
17	Z	-3.405421	-0.015520
18	X	-1.335338	-0.000760
18	Y	0.023786	-0.446730
18	Z	3.445357	-0.025438
19	X	-1.361722	-0.471481
19	Y	0.087075	0.461186
19	Z	-3.406597	-0.346980
20	X	-1.386876	-0.941186
20	Y	0.177134	0.505030
20	Z	-3.209001	-0.069707
21	X	1.030755	0.478746
21	Y	0.308355	0.171826
21	Z	-0.726908	-0.048270
22	X	1.010823	0.243752
22	Y	0.132016	0.108180
22	Z	-0.912995	-0.022640

TABLE 5 (CONT'D) BOX DEFLECTION FOR UNIT LOADS

Node	Coordinate	Box II	
		$M_y = E$	$M_z = E$
23	X	1.001741	0.012013
23	Y	0.004593	0.086833
23	Z	-0.952751	-0.007397
24	X	0.986943	-0.220071
24	Y	-0.120664	0.105070
24	Z	-0.911474	0.008549
25	X	-0.981138	-0.454803
25	Y	-0.290370	-0.164648
25	Z	-0.722409	0.036921
26	X	-0.640936	0.467273
26	Y	-0.142175	0.152849
26	Z	-0.693017	0.041770
27	X	-0.653560	0.232900
27	Y	-0.056770	0.109235
27	Z	-0.894470	0.003192
28	X	-0.667348	-0.000413
28	Y	0.005024	0.094727
28	Z	-0.934407	-0.006726
29	X	0.678381	-0.233701
29	Y	-0.068363	0.109183
29	Z	-0.895649	-0.015986
30	X	-0.690656	-0.468004
30	Y	0.158422	0.153027
30	Z	-0.698053	-0.050995

Node	Coordinate	Box III		
		$P_x = E$	$M_y = *$	$M_x = E$
δ_x	-	2.777896	0.001993	.003640
δ_y	-	0.010921	0.000021	1.103587
δ_z	-	-3.262118	-0.016588	-0.011596
θ_x	-	0	0	0
θ_y	-	1.087374	0.005529	0.003865
θ_z	-	0.003640	0.000007	0.367863
11	X	2.509006	0.005047	0.988937
11	Y	0.257506	0.000500	0.518446
11	Z	-1.537623	-0.007188	-0.066145
12	X	2.589704	0.005032	0.497521
12	Y	0.124161	0.000211	0.483204
12	Z	-1.525980	-0.007567	-0.013266

* $M_y = .001833E$

TABLE 5 (CONT'D) BOX DEFLECTION FOR UNIT LOADS

Node	Coordinate	Box III		
		$P_x = E$	$M_y = *$	$M_z = E$
13	X	2.584653	0.005017	0.005010
13	Y	0.004652	0.000009	0.470201
13	Z	-1.534964	-0.007650	-0.005369
14	X	2.579594	0.005013	-0.487398
14	Y	-0.114588	-0.000913	0.482769
14	Z	-1.525886	-0.007567	0.002637
15	X	2.570540	0.005009	-0.978911
15	Y	-0.247226	-0.000480	0.517460
15	Z	-1.536461	-0.007185	0.055878
16	X	1.132680	-0.002832	0.983503
16	Y	0.212090	-0.000444	0.561485
16	Z	-1.329112	-0.007026	0.047405
17	X	1.141050	-0.002362	0.494713
17	Y	0.097879	-0.000178	0.475238
17	Z	-1.387025	-0.007455	0.020887
18	X	1.134998	-0.002366	-0.000147
18	Y	0.004436	0.000019	0.448439
18	Z	-1.391281	-0.007536	-0.005175
19	X	1.131264	-0.002381	-0.495011
19	Y	-0.088746	0.000196	0.475254
19	Z	-1.387619	-0.007456	-0.031136
20	X	1.113213	-0.002370	-0.983804
20	Y	-0.200977	0.000465	0.561562
20	Z	-1.330189	-0.007028	-0.057119
21	X	1.289825	0.002504	0.480021
21	Y	0.253866	0.000493	0.150583
21	Z	-0.450251	-0.001658	-0.062280
22	X	1.282847	0.002504	0.245711
22	Y	0.120521	0.000204	0.115342
22	Z	-0.438608	-0.002038	-0.009400
23	X	1.280616	0.002505	0.002495
23	Y	-0.001012	0.000002	0.102339
23	Z	-0.447592	-0.002121	-0.001504
24	X	1.278395	-0.002495	-0.240822
24	Y	-0.118228	-0.000199	0.114907
24	Z	-0.438514	0.002038	0.006502
25	X	1.280168	0.002495	-0.485035
25	Y	-0.250866	-0.000487	0.149598
25	Z	-0.479090	-0.001656	0.059744

* $M_y = .001833E$

TABLE 5 (CONT'D) BOX DEFLECTION FOR UNIT LOADS

Node	Coordinate	Box III		
		P_x = E	M_y = *	M_z = E
26	X	0.572404	-0.001176	0.487724
26	Y	0.208450	-0.000451	0.193623
26	Z	-0.241740	-0.001997	0.051270
27	X	0.556753	-0.001160	0.240758
27	Y	0.094239	-0.000185	0.107376
27	Z	-0.299653	-0.001926	0.024752
28	X	0.555525	-0.001171	-0.000078
28	Y	0.000795	0.000002	0.080566
28	Z	-0.303909	-0.002006	-0.001310
29	X	0.551977	-0.001169	-0.240939
29	Y	-0.092116	0.000189	0.107392
29	Z	-0.300247	-0.001927	-0.027270
30	X	0.562749	0.001195	-0.487873
30	Y	-0.204618	0.458128	0.193700
30	Z	-0.242818	-0.001500	-0.053253

* M_y = .01833E

TABLE 6 PREDICTED ELASTIC STRAINS AND CURVATURES

Predicted Stress ksi	Load			M in. lbs	M | E in. lbs	M | E ÷ .001833
	Cell 1 lbs	Cell 2 lbs	Ave lbs			
1	2	3	4	5	6	7
65	3700	3640	3670	70731	.002818	1.538
85	4880	4760	4820	92894	.003701	2.019
105	6000	5870	5935	114383	.004557	2.486
125	7180	6990	7085	136547	.005397	2.944
130	7450	7270	7405	142714	.005685	3.102
135	7800	7550	7645	147918	.005893	3.215
140	8090	7830	7960	153411	.006112	3.334
145	8900	8110	8255	159096	.006339	3.458

Longitudinal Strain *					Transverse Strain *	
ϵ_1	ϵ_2	ϵ_3	ϵ_4	ϵ_5	ϵ_{T-1}	ϵ_{T-2}
8	9	10	11	12	13	14
.001956	.001943	.001932	.001936	.001940	.000222	.000155
.002569	.002553	.002537	.002592	.002548	.000291	.000203
.003163	.003143	.003122	.003130	.003147	.000358	.000252
.003745	.003722	.003698	.003707	.003716	.000424	.000298
.008946	.003921	.003896	.003905	.003914	.000446	.000314
.004090	.004064	.004039	.004048	.004058	.000463	.000324
.004241	.004214	.004188	.004198	.004208	.000480	.000337
.004400	.004372	.004344	.004355	.004364	.000498	.000349

Transverse Strain *		Curvature **				
ϵ_{T-3}	ϵ_{T-4}	C_1	C_2	C_3	C_4	C_5
15	16	17	18	19	20	21
.000155	.000222	.001488	.001343	.001309	.001343	.001488
.000203	.000291	.001955	.001762	.001721	.001762	.001955
.000252	.000358	.002407	.002170	.002118	.002170	.002407
.000298	.000424	.002850	.002571	.002509	.002571	.002850
.000314	.000446	.003002	.002708	.002642	.002708	.003002
.000324	.000463	.003113	.002807	.002740	.002807	.003113
.000337	.000480	.003227	.002911	.002841	.002911	.003227
.000349	.000498	.003448	.003019	.002947	.003019	.003348

TABLE 6 (CONT'D) PREDICTED ELASTIC STRAINS AND CURVATURES

Curvature C_T
22
-.000064
-.000084
-.000103
-.000122
-.000128
-.000134
-.000138
-.000143

* Where ϵ_1, ϵ_2, ϵ_3, ϵ_4 and ϵ_5 represent strain at Sections 11-12, 12-13, 13-14 and 14-15 respectively, and where

$$\epsilon_N = \frac{M|E}{.001883}\left[\delta_{(1+.5)} - \delta_{(1-.5)}\right]$$

** Where C_1, C_2, C_3, C_4, C_5 and C_T represent curvature at Sections 1-11-21-31, 2-12-22-32, 3-13-23-33, 4-14-24-34, 5-15-25-35 and 12-13-14 respectively, and where

$$C_N = \frac{M|E}{.001883}\left\{\frac{1}{8}\left[\delta_{(i+1.5)} - \delta_{(i+.5)} - \delta_{(i-.5)} + \delta_{(i-1.5)}\right]\right\}$$

TABLE 7 STRESS AND STRAIN REDISTRIBUTION FOR ϵ_c = .000100 IN./IN.

Strain in Box III Tensile Elements for Unit Loads P_x = 25,100,000 lbs				
Section	δ_x (1i)	δ_x (2i)	$\Delta\delta_x$	$1/L\ (\Delta\delta_x)$ (L = 2)
11-21	2.590006	1.289825	1.300181	0.650090
12-22	2.589704	1.282847	1.306857	0.653428
13-23	2.584653	1.280616	1.304037	0.652018
14-24	2.579594	1.278395	1.301199	0.650599
15-25	2.570540	1.280165	1.290372	0.645186
Section	δ_y (1i)	δ_y (2i)	$\Delta\delta_y$	$1/L\ (\Delta\delta_y)$ (L = 2)
11-12	0.257506	0.124161	0.133345	0.066672
12-13	0.124168	0.004652	0.119509	0.059755
13-14	0.004652	-0.114588	0.119240	0.059620
14-15	-0.114588	-0.247226	0.132638	0.066319
M_y = 46,000 lbs				
Section	δ_x (1i)	δ_x (2i)	$\Delta\delta_x$	$1/L\ (\Delta\delta_x)$ (L = 2)
11-21	0.005047	0.002504	0.002543	0.001272
12-22	0.005072	0.002504	0.002528	0.001264
13-23	0.005017	0.002505	0.002512	0.001256
14-24	0.005013	0.002495	0.002510	0.001259
15-25	0.005009	0.002485	0.002524	0.001262
Section	δ_y (1i)	δ_y (2i)	$\Delta\delta_y$	$1/L\ (\Delta\delta_y)$ (L = 2)
11-12	.000500	.000211	.000289	.000144
12-13	.000211	.000009	.000202	.000101
13-14	.000009	-.000192	.000201	.000101
14-15	.000192	-.000480	.000288	.000144

TABLE 7 (CONT'D) STRESS AND STRAIN REDISTRIBUTION FOR ϵ_c = .000100 IN. | IN.

M_z = 25,100,000 lbs

Section	δ_x (1i)	δ_x (2i)	$\Delta\delta_x$	$1 \mid L\ (\Delta\delta_x)$ (L = 2)
11-21	.988937	.490021	.489916	.249458
12-22	.497521	.245711	.251810	.125905
13-23	.005010	.002495	.002515	.001257
14-24	-.487398	-.240822	-.246576	-.123288
15-25	-.978911	-.485035	-.493876	-.246938

Section	δ_y (1i)	δ_y (2i)	$\Delta\delta_y$	$1 \mid L\ (\Delta\delta_y)$ (L = 2)
11-12	.518446	.483204	.035242	.017621
12-13	.483204	.470201	.013003	.006501
13-14	.470201	.482769	-.012568	-.006284
14-15	.482769	.517460	.034691	.017345

Note: $P = E\epsilon A$, $M_y = E\epsilon A\bar{Z}$, $M_z = E\epsilon A\bar{Z}$, where unit loads equal E or 25.1×10^6 lbs.

Creep Loads From .00100 In. | In. Strain In Spar Caps

Section	Area Sq. In.	P_x ($E\epsilon A$)	M_y ($E\epsilon \bar{Z}$)	M_z ($E\epsilon \bar{Y}$)
11-21	0.0465	116.72	113.10	423.09
11-22	↓	↓	↓	277.20
13-23				- 43.77
14-24				-277.20
15-25				-423.09

Creep Loads From .000100 In. | In. Strain In Cover Plates

Section	Area Sq. In.	P_x ($E\epsilon A$)	M_y ($E\epsilon \bar{Z}$)	M_z ($E\epsilon \bar{Y}$)
11-12-21-22	.062	155.62	158.03	466.86
12-13-22-23	↓	↓	↓	155.62
13-14-23-24				-155.62
14-15-24-25				-466.86

Total Strain can now be found by superposition of strains caused by unit loads as shown in the following example:

$$\epsilon_{11\text{-}12\ (creep)} = .000100$$

TABLE 7 (CONT'D) STRESS AND STRAIN REDISTRIBUTION FOR ϵ_c = .000100 IN.|IN.

$$\epsilon_{11\text{-}12} = \frac{116.72}{25100000}(0.650090) + \frac{113.10}{46000}(0.001272) + \frac{423.09}{25100000}(0.249458)$$

$$= 10.37 \times 10^{-6} \text{ In.|In.}$$

$$\epsilon_{11\text{-}12\,(\text{change})} = +\epsilon_c + \epsilon_{\text{redistribution}} = -100 + 10.371 = -89.629 \text{ In.|In.}$$

When the strains have been computed, the stresses can be found as shown in the following example:

$$\sigma_{x(\text{plate})} = E'(\epsilon_x + \upsilon\epsilon_y)$$

$$\sigma_{y(\text{plate})} = E'(\epsilon_y + \upsilon\epsilon_x)$$

$$\sigma_{x(\text{cap})} = E\,\epsilon_x$$

where $E = E|1 - \upsilon^2$

Element	Strain In Spar Caps ($\times 10^{-6}$)				
	11-21	12-22	13-23	14-24	15-25
11-21	10.371	8.23	6.156	4.058	1.956
12-22	8.921	7.551	6.149	4.774	3.391
13-23	5.731	5.941	6.133	6.351	6.549
14-24	3.411	4.771	6.121	7.498	8.845
15-25	1.961	4.039	6.114	8.214	10.280
11-21-12-22	13.040	10.735	8.381	6.066	3.743
12-22-13-23	9.947	9.174	8.365	7.595	6.805
13-23-14-24	6.853	7.612	8.351	9.123	9.687
14-24-15-25	3.760	6.051	8.335	10.652	12.929

Element	"X" Strain In Plate ($\times 10^{6}$)			
	11-21-12-22	12-22-13-23	13-23-14-24	14-24-15-25
11-21	9.327	7.220	5.107	3.007
12-22	8.236	6.850	5.461	4.082
13-23	5.836	6.027	6.232	6.450
14-24	4.091	5.446	6.809	8.171
15-25	3.000	5.076	7.164	9.247
11-21-12-22	11.888	9.558	7.223	4.904
12-22-13-23	9.560	8.769	7.980	7.200
13-23-14-24	7.232	7.981	8.737	9.495
14-24-15-25	4.905	7.193	9.493	11.790

TABLE 7 (CONT'D) STRESS AND STRAIN REDISTRIBUTION FOR ϵ_c = .00100 IN./IN.

Element	"Y" Strain In Plate (x 10^6)			
	11-21-12-22	12-22-13-23	13-23-14-24	14-24-15-25
11-21	1.256	0.842	0.626	0.665
12-22	1.153	0.804	0.663	0.765
13-23	0.929	0.721	0.743	0.987
14-24	0.765	0.660	0.801	1.149
15-25	0.662	0.622	0.838	1.249
11-21-12-22	1.253	0.844	0.594	0.566
12-22-13-23	1.017	0.757	0.677	0.798
13-23-14-24	0.799	0.677	0.757	1.014
14-24-15-25	0.563	0.590	0.840	1.246

Elastic Strain Redistribution

Spar Caps			Plate - "X" Direction		
Matrix Row	Matrix Column	Strain x 10^6	Matrix Row	Matrix Column	Strain x 10^6
11-21	11-21	-89.629	11-21-12-22	11-21-12-22	-88.112
12-22	12-22	-92.449	12-22-13-23	12-22-13-23	-91.231
13-23	13-23	-93.669	13-23-14-24	13-23-14-24	-91.263
14-24	14-24	-92.502	14-24-15-25	14-24-15-25	-88.210
15-25	15-25	-89.720			

Element	Stress In Spar Caps, psi				
	σ_{11-21}	σ_{12-22}	σ_{13-23}	σ_{14-24}	σ_{15-25}
11-21	-2250	207	155	102	49
12-22	224	-2320	154	120	85
13-23	144	149	-2351	109	164
14-24	86	120	154	-2322	222
15-25	49	101	153	206	-2252
11-21-12-22	327	269	210	152	94
12-22-13-23	250	230	210	191	171
13-23-14-24	170	190	210	229	248
14-24-15-25	94	152	209	267	325

TABLE 7 (CONT'D) STRESS AND STRAIN REDISTRIBUTION FOR ϵ_c = .000100 IN./IN.

Element	"X" Stress In Plates, psi			
	σ_x (1)	σ_x (2)	σ_x (3)	σ_x (4)
11-21	251	196	138	79
12-22	221	185	148	108
13-23	156	163	169	173
14-24	108	148	184	220
15-25	79	137	196	249
11-21-12-22	-2500	262	198	133
12-22-13-23	260	-2584	220	195
13-23-14-24	196	219	-2574	258
14-24-15-25	133	197	260	-2500
Element	"Y" Stress In Plates, psi			
	σ_y (1)	σ_y (2)	σ_y (3)	σ_y (4)
11-21	52	44	30	10
12-22	47	41	32	16
13-23	29	36	38	33
14-24	16	32	41	45
15-25	9	30	43	52
11-21-12-22	-864	66	51	30
12-22-13-23	61	-877	56	45
13-23-14-24	45	56	-877	60
14-24-15-25	30	51	65	-864

TABLE 8 LOAD SPECTRUM - PREDICTED AND FINAL - BOX I, II AND III

Box I			Box II		
Predicted		Test	Predicted		Test
Stress Ksi	Hold Time Min	Hold Time Min	Stress Ksi	Hold Time Min	Hold Time Min
80	5	5.21	65	2	1.87
100	5	5.05	85	2	1.20
120	5	5.16	105	2	2.67
140	5	1.18	125	10	4.94
145	10	Failed	135	10	Failed
150	10		140	10	
155	10		145	10	
160	10				

Box III			
Predicted			Test
Stress		Hold Time Min	Hold Time Min
Max Ksi	Ave Ksi		
65	52.7	3	3.20
85	68.9	3	3.21
105	85.0	3	2.66
125	101.3	10	9.33
130	105.2	10	6.93
135	109.3	10	6.40
140	113.3	10	9.05
145	117.4	15	15.85

TABLE 9 TEMPERATURES FOR DISCREET LOAD LEVELS - BOX III

Predicted Stress Ksi	Thermocouple									
	1	2	3	4	5	6	7	8	9	10
65	*	795° F	710° F	800° F	812° F	785° F	765° F	775° F	798° F	765° F
85	*	↓	715	800	812	785	765	775	802	765
105	*		715	800	812	785	765	772	802	764
125	*		722	798	812	785	769	771	805	763
130	*		723	798	813	785	769	771	805	768
135	*		723	798	814	784	769	770	807	768
140	*		723	798	813	783	769	770	809	768
145	*	↓	725	797	809	783	770	770	808	767

Predicted Stress Ksi	Thermocouple									
	11	12	13	14	15	16	17	18	19	20
65	768° F	790° F	786° F	802° F	790° F	785° F	802° F	785° F	*	802° F
85	↓	792	786	↓	↓	785	↓	↓	*	802
105		792	786			785			*	801
125		802	790			784			*	801
130		802	790			783			*	800
135		806	790			782			*	800
140		810	790			782			*	800
145	↓	813	790	↓	↓	782	↓	↓	*	800

* Thermocouple Failure

TABLE 10 PREDICTED CREEP STRAIN, BOX II AND III

Predicted Creep Strains - Box II						
Time At Load Min	Load Ksi	Strain Due To Creep At Load				
		Section				
		11-21	12-22	13-23	14-24	15-25
0	125	.000750	.000360	.000190	.000160	.000580
5	125	.000300	.000200	.000130	.000160	.000300

Predicted Creep Strains - Box III					
Plate (1)	Elastic Strain At 125 Ksi Load		Elastic Stress At 125 Ksi Load Psi (2)		Equivalent Uniaxial Stress - Psi (3)
	ϵ_x	ϵ_y	σ_x Psi	σ_y Psi	σ_o Psi
1	.003734	.000424	108984	24894	98915
2	.003710	.000298	109547	28488	98445
3	.003702	.000298	109319	28412	98244
4	.003711	.000424	108302	24266	98718

Notes: (1) Plates 1, 2, 3, and 4 occur at Sections 11-12-21-22, 12-13-22-23, 13-14-23-24 and 14-15-24-25 respectively.

(2) where $\sigma_x = (E/1 - \upsilon^2)(\epsilon_x + \upsilon\epsilon_y)$

$\sigma_y = (E/1 - \upsilon^2)(\epsilon_T + \upsilon\epsilon_x)$

(3) where $\sigma_o = \left(\sigma_x^2 - \sigma_x \sigma_y + \sigma_y^2 + 3\tau_{xy}\right)^{1/2}$

TABLE 11 STRAIN REDISTRIBUTION IN BOX III

Strain Redistribution						
Element *	Axial Strain	Strain Redistribution Due to Creep Strain Indicated in Spar Cap Element				
		Creep Strain				
		.000143	.000141	.000136	.000135	.000139
		Spar Cap Element				
		11 - 21	12 - 22	13 - 23	14 - 24	15 - 25
		Strain x 10^6				
11-21	.003745	15	12	8	5	3
12-22	.003722	12	11	8	6	6
13-23	.003698	9	9	8	8	9
14-24	.003707	6	7	8	10	11
15-25	.003716	3	5	8	12	14
1-L	.003734	13	12	8	6	4
2-L	.003710	10	10	8	7	7
3-L	.003702	7	8	8	9	10
4-L	.003711	4	7	9	11	13
1-T	-.000424	2	2	1	1	1
2-T	-.000298	1	1	1	1	1
3-T	-.000298	1	1	1	1	1
4-T	-.000424	1	1	1	2	2

* Where 1, 2, 3 and 4 represent sections 11-21 - 12-22, 12-22 - 13-23, 13-23 - 14-24, 14-24 - 15-25, and, L and T represent the axial and transverse directions respectively.

Element *	Axial Strain	Strain Redistribution Due To Strain Indicated In Plate Element				Total Strain
		Creep Strain				
		.000185	.000181	.000179	.000185	
		Plate Element **				
		A	B	C	D	
		Strain x 10^6				
11-21	.003745	24	18	12	7	.003849
12-22	.003722	20	17	14	11	.003827
13-23	.003698	16	15	15	15	.003802
14-24	.003707	11	14	16	20	.003810
15-25	.003716	7	12	18	24	.003819
1-L	.003734	27	17	13	9	.003838
2-L	.003710	18	16	14	13	.003813
3-L	.003702	13	14	16	18	.003815
4-L	.003711	9	13	17	22	.003816

TABLE 11 (CONT'D) STRAIN REDISTRIBUTION IN BOX III

Element*	Axial Strain	Strain Redistribution Due To Strain Indicated In Rate Element				Total Strain
		Creep Strain				
		.000185	000181	.000179	.000185	
		Plate Element **				
		A	B	C	D	
		Strain x 10^6				
1-T	-.000424	2	1	1	1	-.000436
2-T	-.000298	1	1	1	1	-.000307
3-T	-.000298	1	1	1	1	-.000307
4-T	-.000424	1	1	1	1	-.000436

* Where 1, 2, 3 and 4 represent sections 11-21 - 12-22, 12-22 - 13-23, 13-23 - 14-24, 14-24 - 15-25, and, L and T represent axial and transverse directions respectively.

** Where A, B, C and D represent sections 11-21 - 12-22, 12-22 - 13-23, 13-23 - 14-24, and 14-24 - 15-25 respectively

TABLE 12 STRESS REDISTRIBUTION IN BOX III

Element *	Trial Stress psi	Spar Cap Stress Redistribution **				
		A	B	C	D	E
		P.S.I.				
11-21	93529	-1699	160	99	60	36
12-22	93038	156	-1659	103	84	74
13-23	92512	117	110	-1633	108	112
14-24	92664	77	86	75	-1625	151
15-25	92850	37	61	113	155	-1655
1	97479	190	158	108	76	58
2	97103	148	132	112	104	100
3	96591	104	106	117	129	144
4	97331	60	77	119	154	193

Element *	Trial Stress psi	Plate Stress Redistribution **				Redistributed Stress psi***
		F	G	H	K	
		P.S.I.				
11-21	93529	343	255	170	97	93529
12-22	93038	282	235	190	157	93038
13-23	92512	220	214	210	216	92510
14-24	92664	160	195	229	276	92664
15-25	92850	99	174	248	336	92850
1	97479	-2625	265	196	138	97479
2	97103	275	-2636	219	204	97103
3	96591	208	224	-2574	269	96951
4	97331	140	199	258	-2588	97331

* Where 1, 2, 3 and 4 represent elements 11-21-12-22, 12-22-13-23, 13-23-14-24 and 14-24-15-25 respectively.

** Where A through K represent the creep strains giving rise to stress redistribution as follows:

$$A = .5\epsilon_{c(11-21)} = .0000755$$

$$B = .5\epsilon_{c(12-22)} = .0000715$$

$$C = .5\epsilon_{c(13-23)} = .0000690$$

$$D = .5\epsilon_{c(14-24)} = .0000700$$

$$E = .5\epsilon_{c(15-25)} = .0000735$$

TABLE 12 (CONT'D) STRESS REDISTRIBUTION IN BOX III

** (Continued)

$$F = .5\epsilon_{c(11\text{-}21\text{-}12\text{-}22)} = .000105$$

$$G = .5\epsilon_{c(12\text{-}22\text{-}13\text{-}23)} = .000102$$

$$H = .5\epsilon_{c(13\text{-}23\text{-}14\text{-}24)} = .000100$$

$$K = .5\epsilon_{c(14\text{-}24\text{-}15\text{-}25)} = .0001035$$

*** Trial 2

Note: The columns of stress redistribution given above represent factors times lines of Table 5, for example

$\Delta\sigma_{11\text{-}21}$ (Due to .000755 in/in creep strain in element 11-21) $= \frac{.0000755}{.000100}(-2250) = -1699$ psi

TABLE 13 STRESS REDISTRIBUTION
IN BOX III DUE TO CREEP

Element *	Trial Stress psi	Spar Cap Stress Redistribution Due To Change Of Creep **				
		A	B	C	D	E
11-21	93529	90	-2	-1	-2	-2
12-22	93038	-8	23	-1	-3	-4
13-23	92512	-6	-2	23	-4	-6
14-24	92664	-4	-1	-1	58	-8
15-25	92850	-2	-1	-2	-6	-23
1	97479	-10	-2	-2	-3	-3
2	97103	-8	-2	-2	-4	-5
3	96591	-6	-1	-2	-5	-8
4	97331	-3	-1	-2	-6	-10

Element *	Trial Stress psi	Plate Stress Redistribution Due To Change Of Creep **			
		A	B	C	D
11-21	93529	-33	-21	-13	-8
12-22	93038	-27	-20	-14	-13
13-23	92512	-21	-18	-16	-18
14-24	92664	-15	-16	-17	-23
15-25	92850	-9	-14	-19	-28
1	97479	250	-22	-15	-11
2	97103	-26	220	-16	-17
3	96591	-20	-19	193	-22
4	97331	-13	-17	-19	212

* Where 1, 2, 3 and 4 represent sections 11-21-12-22, 12-22-13-23, 13-23-14-24 and 14-24-15-25, respectively.

** psi

TABLE 14 SUMMATION OF STRESS AND STRAIN REDISTRIBUTION IN BOX III

Element *	Trial Stress psi	Final Stress psi	Uniaxial Creep Strain**
11-21	93529	93537	.000143
12-22	93038	92971	.000141
13-23	92512	92492	.000136
14-24	92664	92637	.000135
15-25	92850	92792	.000139
1	97479	97661	.000190
2	97103	97243	.000187
3	96591	97061	.000185
4	97331	97471	.000190

Directional Creep in Plates

Plate* Element	$\frac{1}{\sigma_o}\left(\sigma_x - \frac{\sigma_y}{2}\right)$	$\frac{1}{\sigma_o}\left(\sigma_y - \frac{\sigma_y}{2}\right)$	$\Delta\epsilon_{c_o}$	$\Delta\epsilon_{x_c}^{***}$	$\Delta\epsilon_{y_c}^{***}$
1	.976	-.299	.000190	.000185	-.000057
2	.968	-.267	.000187	.000181	-.000050
3	.968	-.267	.000185	.000179	-.000050
4	.962	-.299	.000190	.000185	-.000057

* Where 1, 2, 3 and 4 represent elements 11-21-12-22, 12-22-13-23, 13-23-14-24 and 14-24-15-25 respectively

** Uniaxial creep strain equals sum of trial creep strains

*** $$\Delta\epsilon_{x_c} = \frac{\sigma_x - \frac{\sigma_y}{2}}{\sigma_o}\ \Delta\epsilon_{c_o}$$

$$\Delta\epsilon_{y_c} = \frac{\sigma_y - \frac{\sigma_x}{2}}{\sigma_o}\ \Delta\epsilon_{c_o}$$

TABLE 15 PREDICTED CREEP CURVATURE, BOX III

P_x = 25100000 lb.					
Section	δ(i-1.5)	δ_z(i-.5)	δ_z(i+.5)	δ_z(i+1.5)	Curvature
11-21	-3.262118	-1.537623	-0.450251	0	0.159281
12-22	↓	-0.525980	-0.438608	↓	0.162191
13-23		-1.534964	-0.447592		0.159945
14-24		-1.525866	-0.438514		0.162215
15-25		-1.536461	-0.449090		0.159571
M_y = 46000 in. lb.					
Section	δ_z(i-1.5)	δ_z(i-.5)	δ_z(i+.5)	δ_z(i+1.5)	Curvature
11-21	-0.016588	-0.007188	-0.001658	0	0.000968
12-22	↓	-0.007567	-0.002038	↓	0.000873
13-23		-0.007650	-0.002121		0.000852
14-24		-0.007567	-0.002038		0.000873
15-25		-0.007185	-0.001656		0.000968
M_z = 25100000 lb.					
Section	δ_z(i-1.5)	δ_z(i-.5)	δ_z(i+.5)	δ_z(i+1.5)	Curvature
11-21	-0.011596	-0.066145	-0.062280	0	-0.014603
12-22	↓	-0.013266	-0.009400	↓	-0.001384
13-23		-0.005369	-0.001504		-0.000590
14-24		0.002637	0.006502		-0.002590
15-25		0.055878	0.059704		-0.015897

TABLE 15 (CONT'D) PREDICTED CREEP CURVATURE, BOX III

Unit Strain in Element	Curvature* In Element Due To 0.000100 Strain In Elements x 10^6				
	11-21	12-22	13-23	14-24	15-25
Caps					
11-21	2.852	2.874	2.850	2.949	3.414
12-22	2.960	2.885	2.846	2.928	3.297
13-23	3.096	2.898	2.839	2.905	3.149
14-24	3.282	2.915	2.832	2.872	2.945
15-25	3.390	2.926	2.828	2.852	2.828
Plates**					
1	4.014	3.980	3.930	4.053	4.611
2	4.222	3.997	3.923	4.021	4.414
3	4.404	4.013	3.915	3.989	4.216
4	4.585	4.030	3.908	3.957	4.019

* Where curvature is found by superposition as in Table 7, for example

$$\frac{116.72}{25.1 \times 10^6}(1.59281) + \frac{113.10}{46000}(.000968) + \frac{463.09}{25.1 \times 10^6}(-0.04603) = 2.852 \times 10^{-6}$$

** Plates 1, 2, 3 and 4 occur at sections 11-12-21-22, 12-13-22-23, 13-14-23-24 and 14-15-24-25 respectively

TABLE 15 (CONT'D) PREDICTED CREEP CURVATURE, BOX III

	Creep Strain In Spar Cap Elements				
Element	11-21 .000143	12-22 .000141	13-23 .000136	14-24 .000135	15-25 .000139
	Curvature In Elements x 10^6				
11-21	4.1	4.2	4.2	4.4	4.7
12-22	4.1	4.1	3.9	3.9	4.1
13-23	4.1	4.0	3.9	3.8	3.9
14-24	4.2	4.1	4.0	3.9	4.0
15-25	4.9	4.6	4.3	4.0	3.9

	Creep Strain In Plate Element			
Element	11-12-21-22 .000185	12-13-22-23 .000181	13-14-23-24 .000179	14-15-24-25 .000185
	Curvature In Elements x 10^6			
11-21	7.4	7.6	8.0	8.3
12-22	7.4	7.2	7.3	7.3
13-23	7.3	7.1	7.1	7.1
14-24	7.5	7.3	7.2	7.2
15-25	8.5	8.0	7.6	7.3

Element	Curvature Without Creep	Curvature With Creep
11-21	.002850	.002903
12-22	.002571	.002620
13-23	.002509	.002557
14-24	.002571	.002620
15-25	.002850	.002903

TABLE 16 DEFLECTIONS AND CURVATURES, BOX II

Mean Stress Ksi	Dial Gage Deflections					
	Gage Number					
	1	2	3	4	5	6
65	.0115	.0479	.0887	.1306	.1309	.0882
85	.0164	.0626	.1142	.1717	.1692	.1137
105	.0215	.0781	.1423	.2158	.2157	.1411
125	.0271	.0975	.1758	.2739	.2722	.1723

Mean Stress Ksi	Dial Gage Deflections					
	Gage Number					
	7	8	9	10	11	12
65	.0469	.0091	.0122	.0393	.0857	.1383
85	.0612	.0139	.0176	.0527	.1116	.1897
105	.0772	.0205	.0234	.0684	.1395	.2428
125	.0950	.0268	.0300	.0868	.1708	.3501

In determination of curvature, let

$$W = A + B\left(\frac{x}{L}\right) + C\left(\frac{x}{L}\right)^2 + D\left(\frac{x}{L}\right)^3$$

and by differentiating twice

$$\text{Curvature} = \frac{\partial^2 W}{\partial x^2} = \frac{2C}{L^2} + \frac{6Dx}{L^3}$$

where

$$C = W_1 - 5/2\, W_2 + 2\, W_3 - 1/2\, W_4$$

$$D = 1/6\,(W_4 - W_1) + 1/2\,(W_2 - W_3)$$

and

W, W_1, W_2, W_3, W_4 = vertical deflection

A, B, C, D = coefficients of polynomial

x = distance from fixed edge

L = total length

TABLE 16 (CONT'D) DEFLECTIONS AND CURVATURES, BOX II

Mean Stress Ksi	Power Series Expansion Coefficient					
	C			D		
	1-2-3-4	5-6-7-8	9-10-11-12	1-2-3-4	5-6-7-8	9-10-11-12
65	.003850	.002800	.016200	-.000550	-.000350	-.002183
85	.002450	.003700	.014200	.000083	-.000367	-.000767
105	.002950	.001850	.010000	.000283	.000583	.002017
125	-.002000	.001800	.002050	.001983	.001250	.003462

Mean Stress Ksi	Curvature		
	1-2-3-4	5-6-7-8	9-10-11-12
65	.000688	.000613	.003128
85	.001038	.001024	.005374
105	.002112	.002237	.000358
125	.003462	.004253	.009688

TABLE 17 DEFLECTIONS AND CURVATURES, BOX III

Load	Dial Gage Deflection Indications, Gage Number 1	2	3	4	5	6
Tare	.0129	.0406	.0713	.1081	.1035	.0691
1	.0172	.0540	.0945	.1437	.1397	.0962
Tare	.0176	.0517	.0865	.1289	.1267	-
2	.0222	.0680	.1204	.1821	.1774	-
Tare	.0229	.0590	.0983	.1456	.1428	.0969
3-1	.0286	.0838	.1487	.2250	.2191	-
Tare	.0277	.0672	.1113	.1632	.1603	-
3-2	.0296	.0854	.1512	.2280	.2218	.1475
3-3	.0304	.0871	.1534	.2313	.2253	.1499
Tare	.0281	.0658	.1096	.1605	.1567	-
4-1	.0323	.0913	.1607	.2418	.2358	.1570
4-2	.0327	.0931	.1628	.2443	.2385	.1591
Tare	.0310	.0372	.1186	.1727	.1695	-
5-1	.0343	.0962	.1689	.2535	.2471	.1650
5-2	.0353	.0978	.1707	.2562	.2496	.1671
Tare	.0323	.0761	.1246	.1809	.1775	-
6-1	.0373	.1019	.1772	.2665	.2596	.1740
6-2	.0382	.1033	.1797	.2701	.2635	.1765
Tare	.0320	.0724	.1203	.1750	.1696	-
7-1	.0400	.1077	.1864	.2805	.2734	.1833
7-2	.0410	.1102	.1905	.2858	.2789	.1872
Tare	.0372	.0830	.1350	.1954	.1913	-
Zero	.0251	.0441	.0578	.0761	.0748	.0572

Load	Dial Gage Deflection Indications, Gage Number 7	8	9	10	11	12
Tare	.0371	.0101	.0090	.0345	.0663	.1032
1	.0500	.0141	.0120	.0468	.0895	.1386
Tare	.0479	.0142	.0128	.0460	.0823	.1257
2	.0635	.0187	.0167	.0598	.1137	.1766
Tare	.0546	.0194	.0176	.0522	.0937	.1416
3-1	.0794	.0244	.0219	.0738	.1400	.2160
Tare	.0628	.0249	.0223	.0605	.1071	.1591
3-2	.0810	.0252	.0238	.0763	.1439	.2209
3-3	.0328	.0265	.0247	.0781	.1467	.2245
Tare	.0619	.0257	.0229	.0588	.1048	.1568
4-1	.0869	.0285	.0266	.0820	.1526	.2346
4-2	.0881	.0285	.0270	.0831	.1547	.2377

TABLE 17 (CONT'D) DEFLECTIONS AND CURVATURES, BOX III

Load	Dial Gage Deflection Indications					
	Gage Number					
	7	8	9	10	11	12
Tare	.0680	.0286	.0253	.0651	.1150	.1680
5-1	.0917	.0301	.0286	.0868	.1593	.2456
5-2	.0930	.0308	.0308	.0880	.1615	.2492
Tare	.0717	.0308	.0277	.0692	.1204	.1762
6-1	.0968	.0323	.0307	.0919	.1678	.2584
6-2	.0986	.0334	.0320	.0937	.1719	.2632
Tare	.0692	.0310	.0274	.0660	.1145	.2702
7-1	.1026	.0351	.0332	.0973	.1789	.2724
7-2	.1052	.0359	.0346	.1002	.1830	.2791
Tare	.0778	.0349	.0313	.0571	.1292	.1897
Zero	.0388	.0245	.0228	.0380	.0547	.0751

Note: Throughout Tables 17, 19 and 20 Tare, 1, 2, 3, 4, 5, 6 and 7 loads represent 65, 85, 105, 125, 130, 135, 140 and 145 Ksi respectively. -1, -2 and -3 indicate load application sequence.

Load	Curvature *						
	Longitudinal			Transverse			
	A	B	C	D	E	F	G
Tare	.001150	.001033	.001425	.000425	.000225	-.000100	.001075
1	.001550	.001492	.001787	.000250	.000200	-.002100	.000725
Tare	.001037	.001490	.001783	.000500	.000525	-	.000300
2	.001988	.002025	.002475	.000375	.000200	-	.000975
Tare	.001400	.001338	.002030	.000425	.000500	-.000450	.000400
3-1	.002638	.002475	.003012	.000425	.000300	-	.000700
Tare	.001550	.001810	.001725	.000100	.000525	-	.000425
3-2	.002625	.002313	.003063	.000750	.000075	.000025	.001325
3-3	.002650	.002388	.003050	.000525	.000100	.000075	.001300
Tare	.001650	.001865	.002020	-.000100	.000200	-	.000975
4-1	.002763	.002550	.003333	.000475	.000125	.000175	.001200
4-2	.002637	.002475	.003370	.000675	0	-.000175	.001250
Tare	.001488	.001890	.001673	-.000225	.000575	-.000450	.000725
5-1	.002838	.002563	.003513	.000675	-.000100	.000500	.001225
5-2	.002875	.002538	.003813	.001125	.000050	-	.001550
Tare	.001563	.001950	.001718	-.000400	.000375	-.000750	.000525
6-1	.003088	.002638	.003675	.000700	.000050	-.000350	.001425
6-2	.003163	.002725	.003693	.000850	-.000050	-	.001575

TABLE 17 (CONT'D) DEFLECTIONS AND CURVATURES, BOX III

	Curvature *						
	Longitudinal			Transverse			
Load	A	B	C	D	E	F	G
Tare	.001788	.002000	.002138	-.000650	0	-	.001500
7-1	.003300	.002825	.003675	.000750	-.000050	-.000325	.001525
7-2	.003263	.002800	.003813	.000950	0	-.000225	.001775
Tare	.001825	.002310	.002088	-.000325	.000625	-	.000625
Zero	.000088	.000412	.000650	-.000275	.001125	-.000475	.000400

	1	8	9
	2	7	10
	3	6	11
	4	5	12

Gage Location
(Schematic)

Note

Longitudinal Curvature = $1/8\ (W_{i-1.5} - W_{i-.5} - W_{i+.5} + W_{i+1.5})$

Transverse Curvature = $1/4\ (W_{i-1} - 2\,W_{i+1})$

Longitudinal Curvature (W_{i+5} not recorded) = $t\ (W_{i-1.5} - 3\,W_{i+.5} + 2\,W_{i+1.5})$

* Where A, B, C, D, E, F and G represent Sections 1-2-3-4, 5-6-7-8, 9-10-11-12, 1-8-9, 2-7-10, 3-6-11 and 4-5-12 respectively.

TABLE 18 STRAIN COMPARISON, BOX II

Load *	Total Strain					
	Gage 1			Gage 3		
	Test	Predicted	Error	Test	Predicted	Error
Tare	.002400	None	-	.002500	None	-
1	.003130	None	-	.003300	None	-
2	.003880	None	-	.004050	None	-
3	.005150	.005170	0.4	.005050	.005130	1.6
3	.005410	.005370	-0.7	.005230	.005300	1.3
3	.005700	-	-	.005420	-	-

Load *	Total Strain			State of Box
	Gage 5			
	Test	Predicted	Error	
Tare	.002750	None	-	Undamaged
1	.003600	None	-	Undamaged
2	.004450	None	-	Undamaged
3	.005650	.005470	-3.2	Undamaged
3	.005690	.005700	-4.4	Rivet Failed
3	.005500	-	-	Box Failed

Load *	Strain Due To Creep					
	Gage 1		Gage 3		Gage 5	
	Test	Predicted	Test	Predicted	Test	Predicted
Tare	0	None	0	None	0	None
1	0	None	0	None	0	None
2	0	None	0	None	0	None
3	.000550	.000320	.000200	.000140	.000320	.000420
3	.000750	.000530	.000380	.000300	.000640	.000650
3	.001070	-	.000580	-	.000150	-

* Where Tare, 1, 2, and 3 represent 65, 85, 105 and 125 Ksi loads respectively.

TABLE 19 STRAIN COMPARISON, BOX III

Load	Total Strain					
	Gage 1			Gage 2		
	Test	Predicted	Error	Test	Predicted	Error
Tare	.001750	.001950	11.4	.002200	.001943	-11.7
1	.002220	.002561	9.6	.003000	.002553	-14.9
2	.002650	.003153	18.9	.003700	.003143	-15.1
3	.003300	.003733	13.1	.004650	.003722	-19.9
3	.003550	.003838	8.1	.004910	.003827	-22.1
4	.003720	.004040	8.3	.005180	.004026	-22.3
4	.003800	.004182	10.0	.005240	.004167	-22.4
5	.003900	.004324	10.9	.005450	.004310	-20.9
5	.003950	.004530	14.7	.005550	.004515	-18.6
6	.004120	.004681	13.6	.005700	.004665	-18.1
6	.004290	.004908	14.4	.005820	.004891	-16.0
7	.004520	.005066	12.3	.006000	.005049	-15.8
7	.004700	.005408	15.0	.006130	.005389	-12.1

Load	Total Strain					
	Gage 3			Gage 4		
	Test	Predicted	Error	Test	Predicted	Error
Tare	.003020	.001937	-35.9	.001880	.001932	2.8
1	.004080	.002545	-37.6	.002550	.002537	1.5
2	.005080	.003173	-37.9	.003720	.003122	- 4.5
3	.006300	.003710	-41.1	.004200	.003698	-12.0
3	.006860	.003813	-44.4	.004270	.003802	-11.0
4	.007220	.004014	-44.4	.005000	.004002	-20.0
4	.007380	.004153	-43.7	.005300	.004141	-21.8
5	.007560	.004294	-43.3	.005620	.004282	-24.1
5	.007820	.004499	-42.5	.005880	.004489	-23.6
6	.008110	.004678	-42.6	.006150	.004635	-24.6
6	.008140	.004873	-40.2	.006580	.004860	-26.2
7	.008800	.005030	-42.8	.006880	.005016	-27.1
7	.009220	.005368	-41.8	.007550	.005363	-29.1

TABLE 19 (CONT'D) STRAIN COMPARISON, BOX III

Load	Total Strain					
	Gage 5			Gage 6		
	Test	Predicted	Error	Test	Predicted	Error
Tare	.001750	.001932	1.0	.002400	.001934	-19.4
1	.002300	.002537	1.0	.003250	.002540	-21.8
2	.003140	.003122	- 0.6	.004100	.003127	-23.7
3	.004150	.003698	-10.7	.004900	.003702	-24.5
3	.004500	.003802	-15.6	.005300	.003805	-28.2
4	.004730	.004002	-15.4	.005500	.004005	-27.3
4	.004900	.004141	-15.5	.005640	.004143	-26.6
5	.005100	.004282	-16.0	.005900	.004286	-27.4
5	.005300	.004489	-15.3	.006000	.004491	-25.1
6	.005530	.004635	-16.2	.006200	.004635	-25.2
6	.005870	.004680	-17.2	.006530	.004680	-25.9
7	.006200	.005016	-19.2	.006850	.005021	-26.7
7	.006620	.005353	-19.3	.007200	.005359	-25.6

Load	Total Strain					
	Gage 7			Gage 8		
	Test	Predicted	Error	Test	Predicted	Error
Tare	.002050	.001936	- 5.6	.001840	.001938	5.4
1	.002790	.002542	- 8.9	.001700	.002545	49.7
2	.003500	.003131	-10.5	.002100	.003134	49.2
3	.004300	.003707	-14.0	.002600	.003172	42.8
3	.004430	.003810	-14.0	.002660	.003816	43.5
4	.004620	.004008	-13.2	.002800	.004014	43.4
4	.004700	.004148	-11.7	.002800	.004154	48.3
5	.004900	.004291	-12.4	.002900	.004927	48.1
5	.004990	.004496	-10.0	.003000	.004503	50.0
6	.005280	.004637	-12.2	.003180	.004563	45.0
6	.005500	.004863	-11.6	.003280	.004880	48.8
7	.005750	.005029	-12.5	.003290	.005037	53.0
7	.006050	.005368	-10.4	.003560	.005377	51.1

TABLE 20 CURVATURE COMPARISON, BOX III

Load	Curvature		
	Test	Predicted	Error
	Dial Gages 1-2-3-4		
Tare	.001138	.001343	+18.0
1	.001558	.001762	+13.7
2	.001988	.002170	+ 9.2
3	.002638	.002571	- 2.5
3	.002650	.002622	+ 1.1
4	.002763	.002759	- 0.1
4	.002637	.002829	+ 7.3
5	.002838	.002930	+ 3.5
5	.002875	.003033	+ 5.4
6	.003088	.003136	+ 1.6
6	.003163	.003249	+ 2.7
7	.003300	.003359	+ 1.8
7	.003263	.003529	+ 8.2
	Dial Gages 5-6-7-8		
Tare	.001033	.001309	+26.7
1	.001492	.001721	+15.3
2	.002025	.002118	+ 4.6
3	.002475	.002509	+ 1.4
3	.002398	.002560	+ 7.2
4	.002550	.002693	+ 3.9
4	.002475	.002763	+11.6
5	.002563	.002861	+11.7
5	.002538	.002963	+16.7
6	.002638	.003065	+16.2
6	.002725	.003168	+16.2
7	.002825	.003281	+16.1
7	.002800	.003450	+23.2
	Dial Gages 9-10-11-12		
Tare	.001425	.001348	- 5.8
1	.001787	.001762	- 1.4
2	.002475	.002710	-12.3
3	.003012	.002571	-14.7
3	.003050	.002622	-14.0
4	.003325	.002759	-17.0
4	.003363	.002829	-15.9
5	.003513	.002929	-16.6
5	.003813	.003032	-20.5
6	.003675	.003135	-14.7
6	.003700	.003249	-12.1
7	.003675	.003356	- 8.7
7	.003813	.003526	- 7.5

TABLE 21 EMPIRICAL CREEP POWER LAW EXPRESSIONS FOR 7075-T6 ALUMINUM ALLOY (1)

Temperature					
200° F		250° F		300° F	
Stress ksi	Kt^N (2)	Stress ksi	Kt^N (2)	Stress ksi	Kt^N (2)
54	$.0000407\ t^{.416}$	49	$.000062\ t^{.483}$	44	$.000120\ t^{.524}$
56	$.0000585\ t^{.416}$	50	$.000074\ t^{.483}$	45	$.000155\ t^{.524}$
58	$.0000835\ t^{.416}$	51	$.000091\ t^{.483}$	46	$.000178\ t^{.524}$
60	$.0001180\ t^{.416}$	52	$.000114\ t^{.483}$	47	$.000224\ t^{.524}$
62	$.0001676\ t^{.416}$	53	$.000134\ t^{.483}$	48	$.000264\ t^{.524}$
64	$.0002550\ t^{.416}$	54	$.000158\ t^{.483}$	49	$.000322\ t^{.524}$
		55	$.000192\ t^{.483}$	50	$.000382\ t^{.524}$

Temperature			
350° F		400° F	
Stress	Kt^N	Stress	Kt^N
35	$.000091\ t^{.598}$	20	$.0000273\ t^{.635}$
36	$.000110\ t^{.598}$	22	$.0000398\ t^{.635}$
37	$.000138\ t^{.598}$	24	$.0000580\ t^{.635}$
38	$.000162\ t^{.598}$	26	$.0000850\ t^{.633}$
39	$.000198\ t^{.598}$	28	$.0001180\ t^{.633}$
40	$.000235\ t^{.598}$		

(1) WADD TR 60-777, Figures 17 to 21 inclusive, data used.

TABLE 22 COMPARISON OF PERMANENT SETS * - INCREMENTAL LOADING CONDITION

Temperature °F	Yield Strength ksi	Permanent Set From Loading to Maximum Stress Percent Strain	Creep Set From Beginning of Second To End of Fifth Loading Cycle Percent Strain
700	110.0	0.75	0.30
700	87.5	0.48	0.12
900	86.0	0.34	0.30
900	67.5	0.31	0.40
1000	46.2	0.08	0.35
1000	37.5	0.08	0.50

* From work hardening occurring during loading and from creep in ARMCO PH 15-7 Mo condition RH 950 steel as a result of repeated applications of incremental loading cycles.

TABLE 23 COMPARISON OF PERMANENT SETS * - DECREMENTAL LOADING CONDITION

Temperature °F	Total Deformation Percent Strain	Creep Set From Beginning of Second To End of Fifth Loading Cycle Percent Strain	Permanent Set From Loading to Maximum Stress ** Percent Strain
700	1.20	0.55	.05
700	1.45	0.70	.03
800	1.10	0.81	.025
800	1.57	0.98	.03
900	0.97	0.38	.03
900	0.06	0.39	.015
1000	0.47	0.10	.10
1000	0.40	0.15	.035

* From work hardening occurring during loading and from creep in ARMCO PH 15-7 Mo condition RH 950 steel as a result of repeated applications of decremental loading cycles

** 182 ksi at 700° F, 175 ksi at 800° F, 135 ksi at 900° F and 77 ksi at 1000° F

TABLE 24 COMPARISON OF PERMANENT SETS * - DECREMENTAL LOADING CONDITION

Maximum Stress ** ksi	Total Deformation Percent Strain	Permanent Set From Loading to Maximum Stress Percent Strain	Creep Set From Beginning of Second to End of Fifth Loading Cycle Percent Strain
182	1.20	.55	.05
182	1.45	.70	.03
185	1.40	.75	.07
185	1.62	1.05	.13
188	1.35	.75	.02
188	1.38	.67	.08
191	1.40	.73	.17
191	1.60	.93	.05

* From work hardening occurring during loading and from creep in ARMCO PH 15-7 Mo condition RH 950 steel as a result of repeated applications of decremental loading cycles

** At 700° F

TABLE 25 CREEP TEST DATA * SUMMARY

Temperature °F	Stress ksi	Loading		Primary Creep Deformation %	Secondary Creep Rate in/min
		Total Deformation %	Permanent Set %		
700	105	1.08	nil	0.18	nil
700	105	1.18	nil	0.10	nil
700	112.5	1.18	nil	0.08	nil
700	112.5	1.30	nil	nil	nil
700	180	2.15	0.18	0.11	2.0×10^{-5}
800	80	0.88	nil	nil	nil
800	80	0.85	nil	nil	nil
800	86.5	0.92	nil	nil	nil
800	86.5	0.90	nil	nil	nil
800	148.5	2.10	0.18	0.20	nil
900	75	0.91	nil	0.10	6.7×10^{-6}
900	75	0.91	nil	0.10	1.0×10^{-5}
900	79	0.91	nil	0.11	1.6×10^{-5}
900	79	0.88	nil	0.11	nil
900	127.5	1.70	0.10	0.40	2.0×10^{-5}
1000	35	0.30	nil	0.10	1.3×10^{-5}
1000	35	0.30	nil	0.10	1.3×10^{-5}
1000	39	0.32	nil	0.20	0.8×10^{-5}
1000	39	0.35	nil	0.20	1.6×10^{-5}

* "Standard" creep tests with ARMCO PH 15-7 Mo condition RH 960 stainless steel at constant stress and constant temperature

TABLE 26 STRESSES ARISING FROM CREEP STRAIN INCREMENTS

Creep Strain Percent	Stress - PSI		
	σ_1/σ_{ave}	σ_2	σ_3
0.00	157555	78772	52517
	156908		
0.01	156262	78126	52086
	155615		
0.02	154619	77480	51655
	154323		
0.03	153676	76834	51224
	153030		
0.04	152383	76188	50793
	151737		
0.05	151090	75542	50362
	147858		
0.10	144625	73212	

Reference: Armco Precipitation Hardening Stainless Steels Technical Data Manual PH 15-7 Mo Flat-Rolled 2B-6-2, 3/1/58

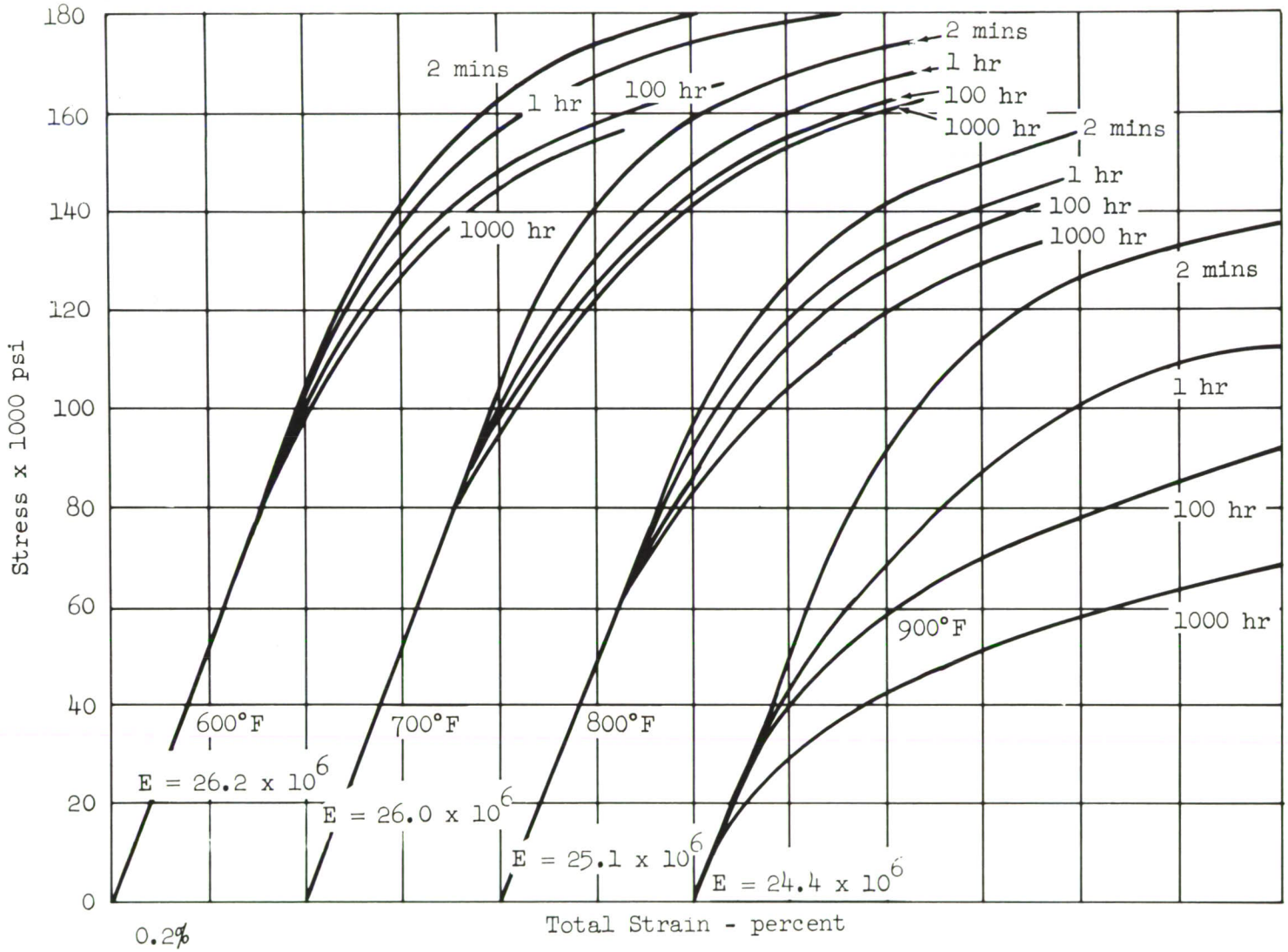


Figure 1. Tensile Stress Strain Time Curves for .050 Inch Thick Armco PH 15-7 Mo, Condition RH 950 Steel

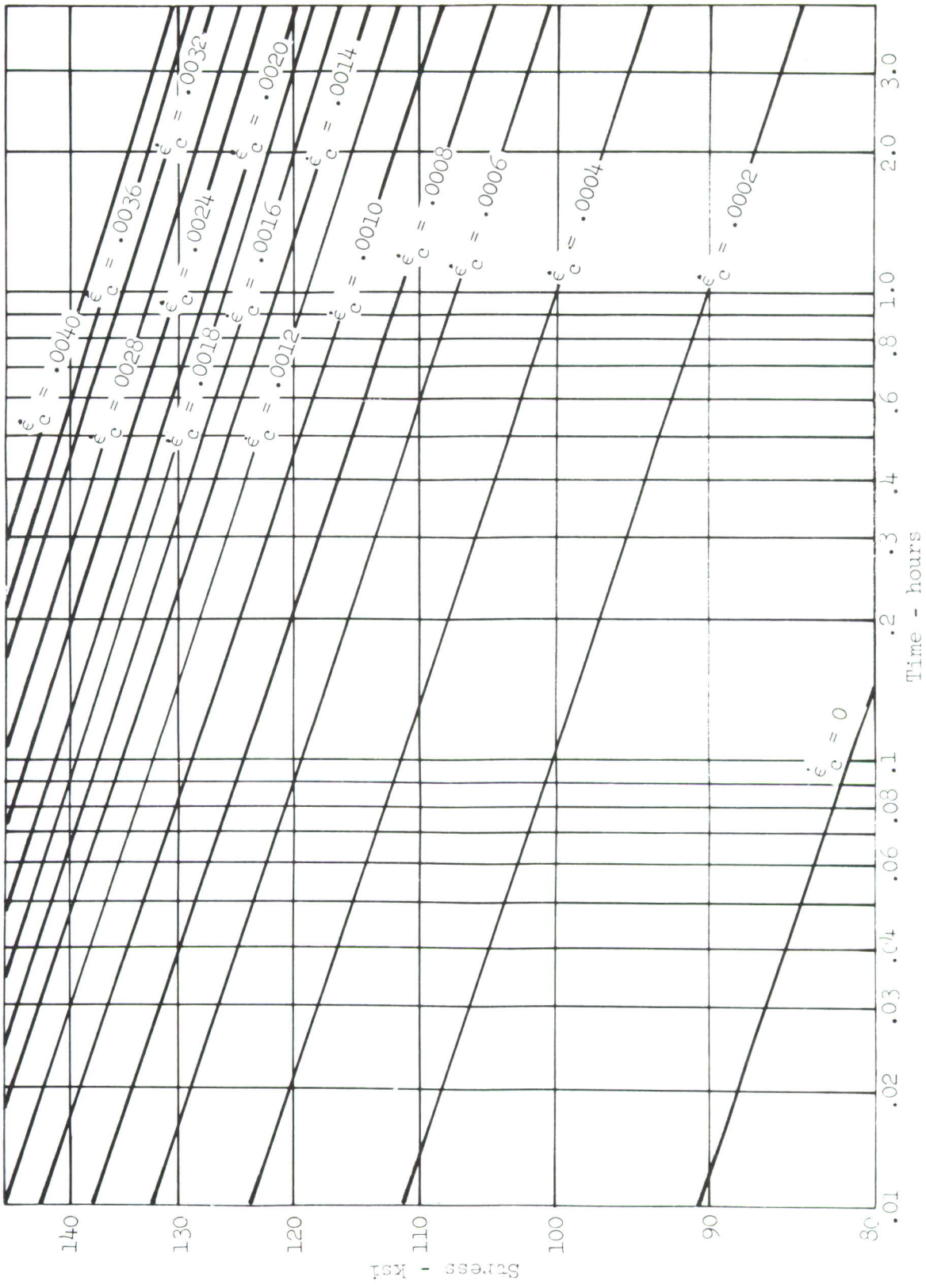


Figure 2. Tensile Stress Strain Time Curves (log-log) .050 Inch Thick Armco PH 15-7 Mo, Condition RH 950 Steel

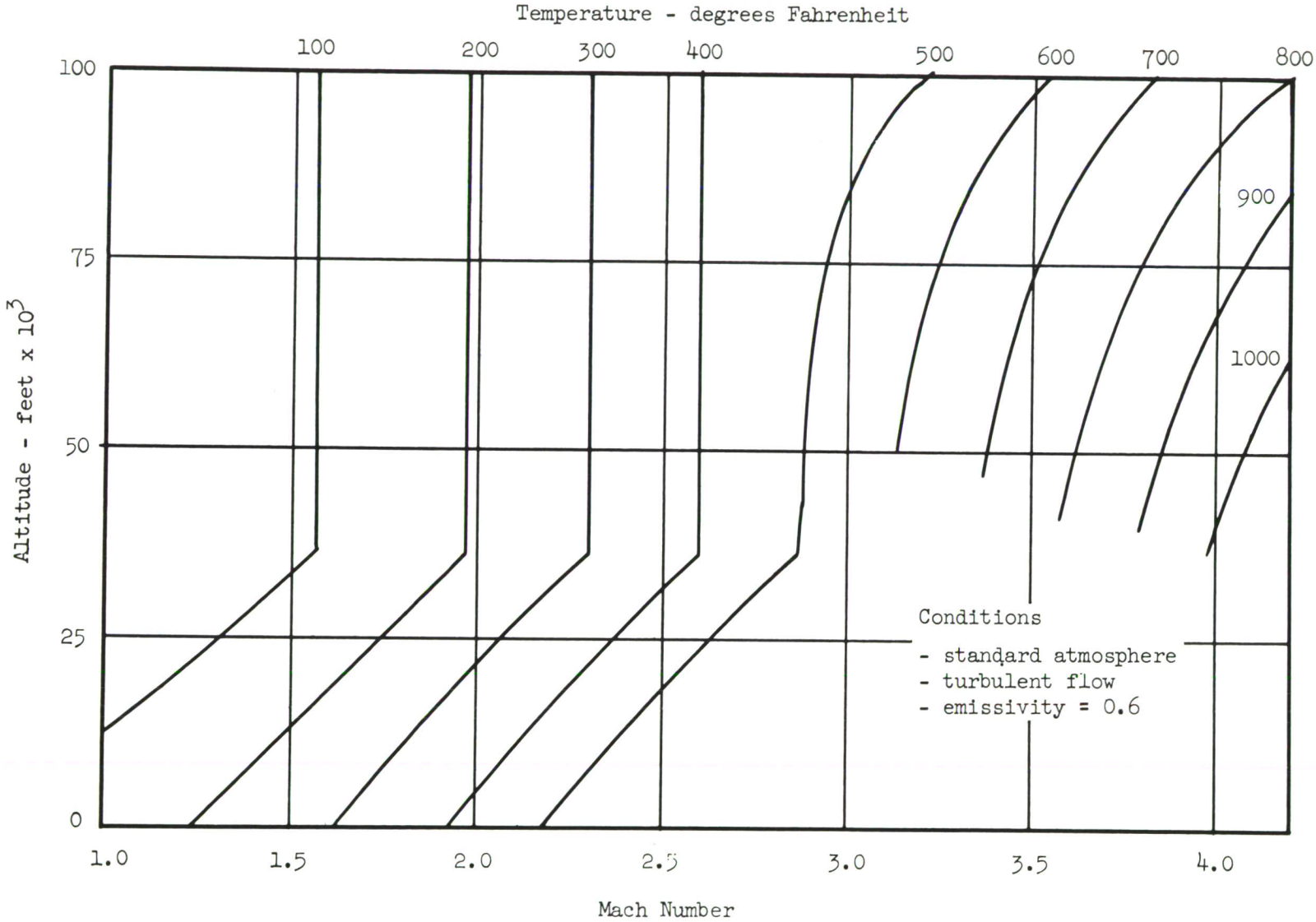


Figure 3. Temperature - Mach Number Speed Data

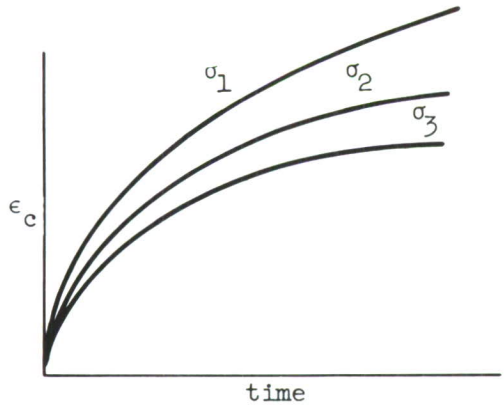


Figure 4a. Creep strain versus time for constant values of stress

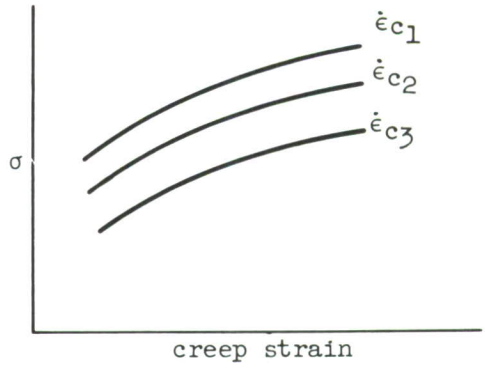


Figure 4b. Stress versus creep strain for different values of strain rate

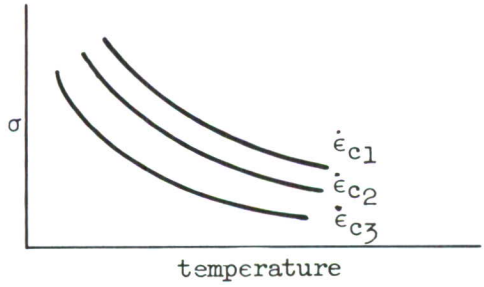


Figure 4c. Stress versus temperature for constant values of creep rate

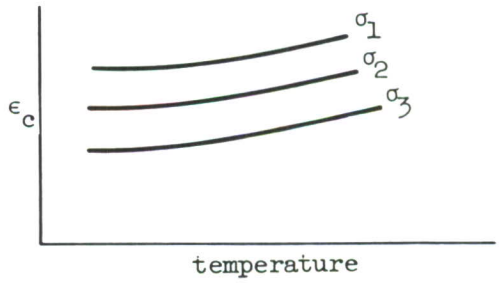


Figure 4d. Creep strain versus temperature for constant values of stress

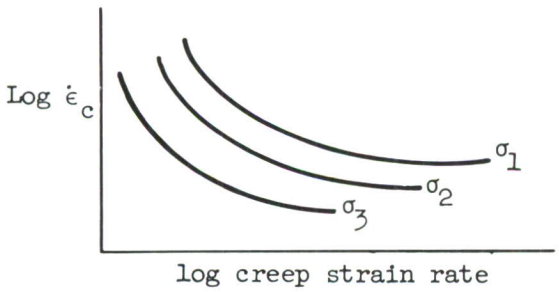


Figure 4e. Log creep strain versus log creep strain rate for constant discrete values of stress

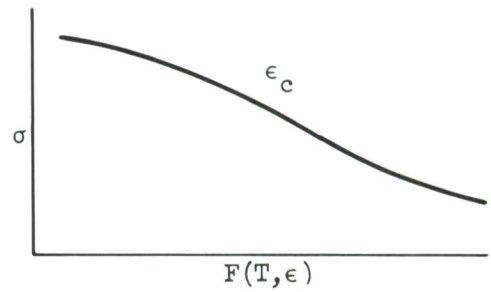


Figure 4f. Stress versus compound function of temperature such as Larson-Miller or Manson-Haferd parameter

Figure 4. Methods for Presenting Creep Data

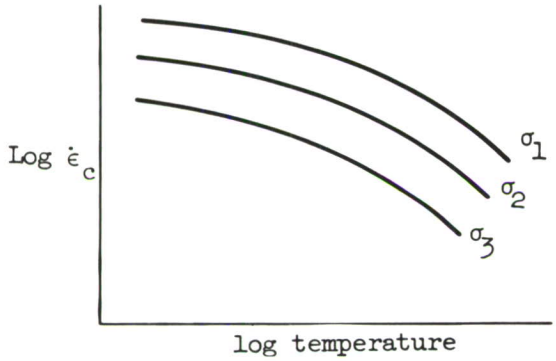


Figure 4g. Log temperature versus log creep rate for constant discrete values of stress

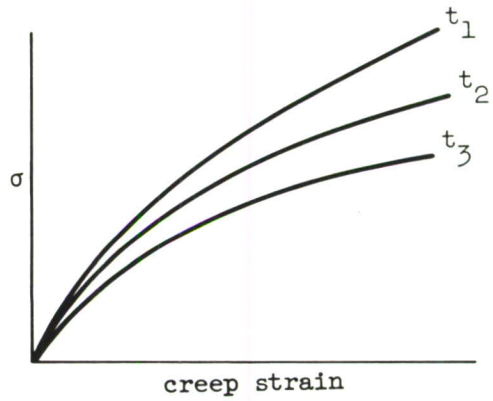


Figure 4h. Stress versus creep strain for different values of time

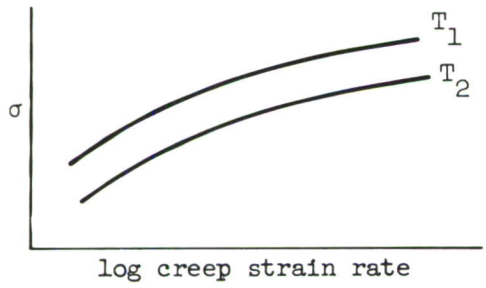


Figure 4j. Stress versus log creep strain rate for different values of temperature

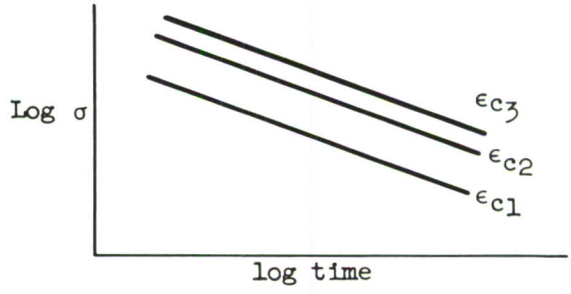
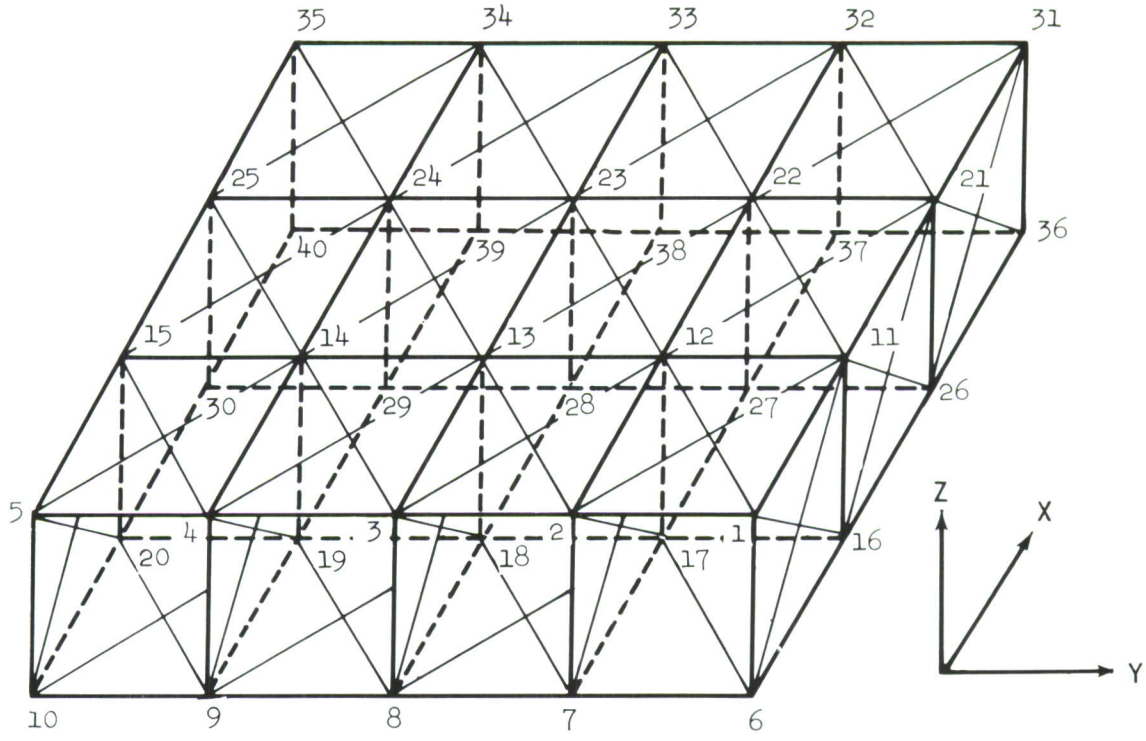
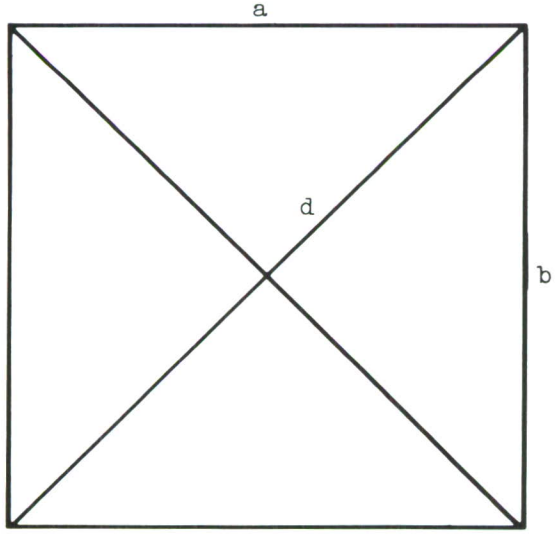


Figure 4k. Log stress versus log time for constant values of creep strain

Figure 4. Methods for Presenting Creep Data (Continued)





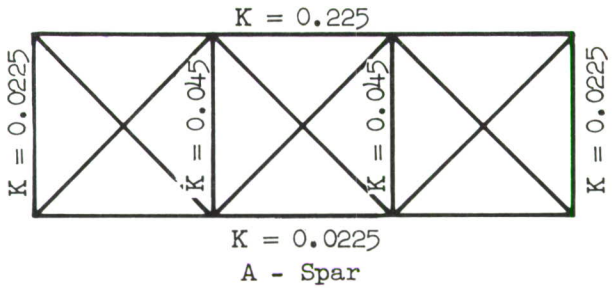
Areas

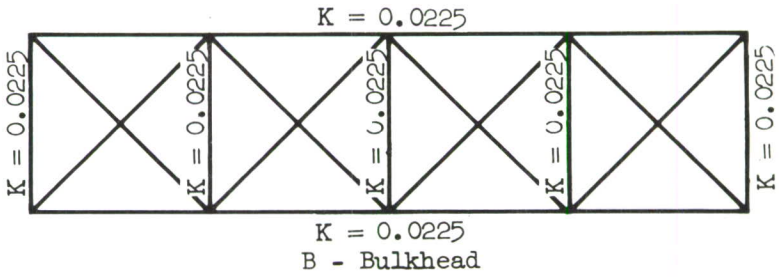
$$A_d = \frac{3(a^2 + b^2)^{3/2}}{16\ ab}\ t$$

$$A_b = \frac{3}{16}(3 - (b/a)^2)bt$$

$$A_a = \frac{3}{16}(3 - (a/b)^2)bt$$

Figure 5. Test Box Idealization - General





Note: all spar diagonals, K = 0.0225
all bulkhead diagonals, K = 0.0225

Figure 6. Test Box Idealization - Spars and Bulkheads - Box II and III

Figure 7. Test Box Idealization - Plate Surfaces - Box II

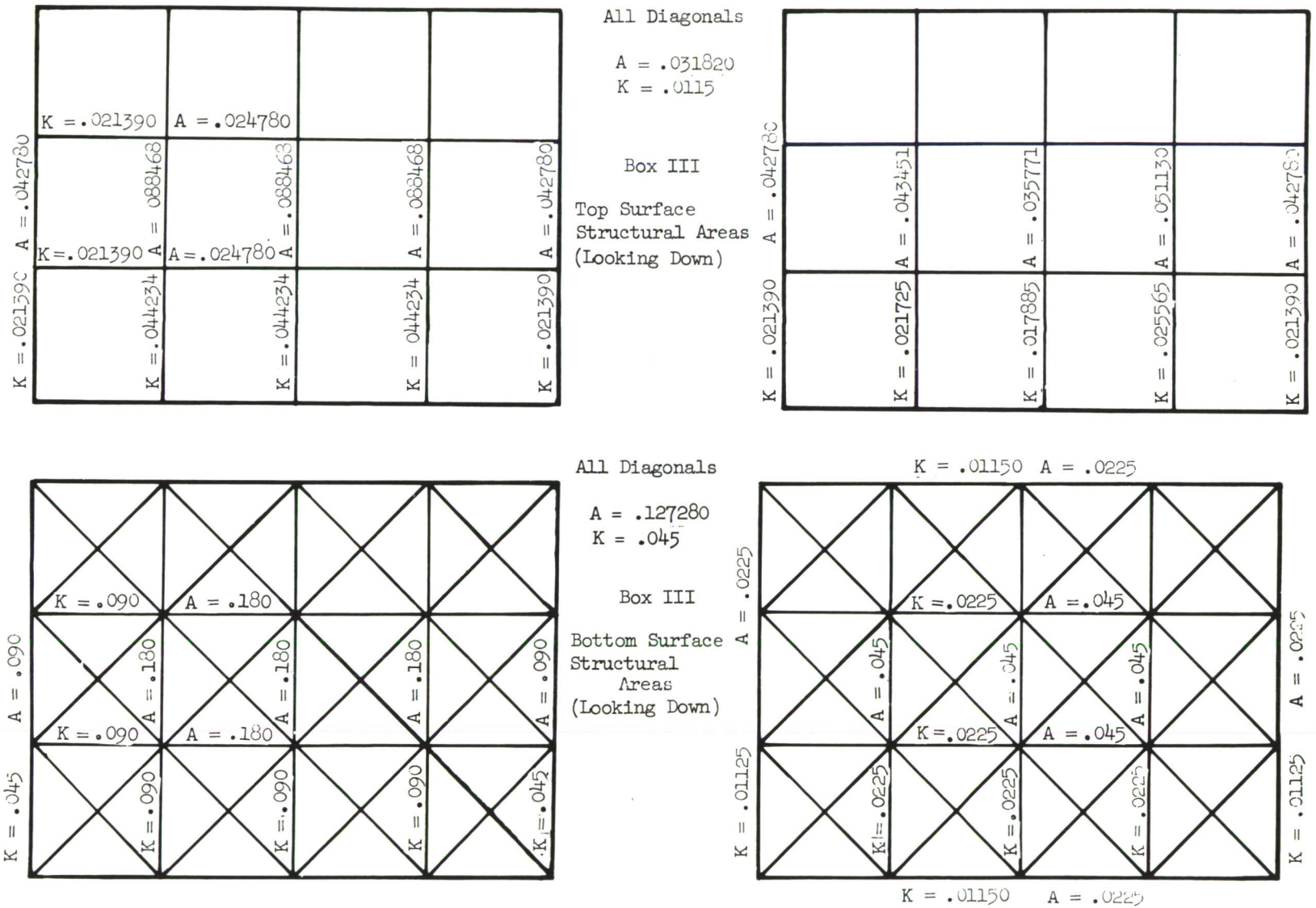


Figure 8. Test Box Idealization - Plate Surfaces - Box III

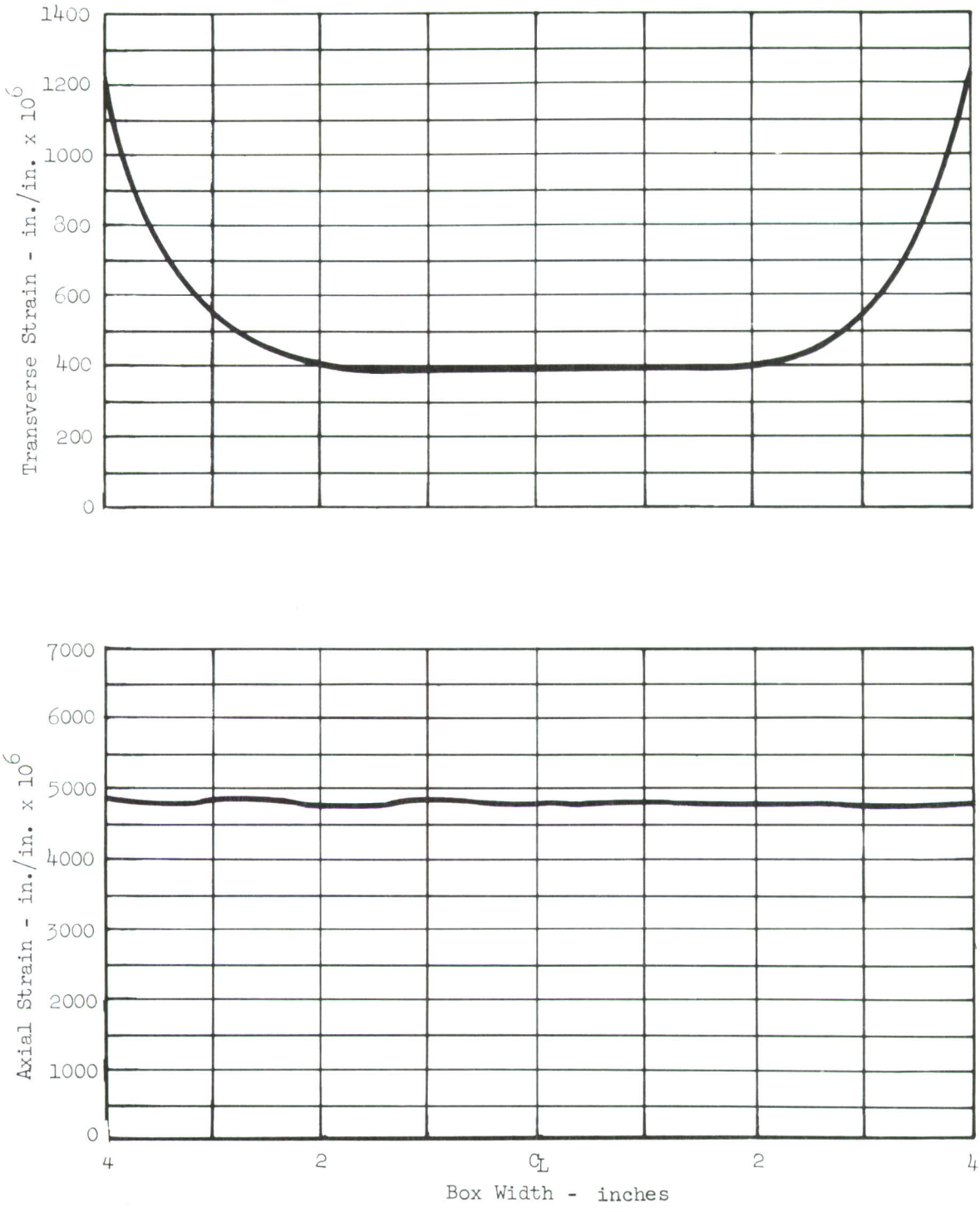


Figure 9. Predicted Elastic Strains in Box II Cover Plates

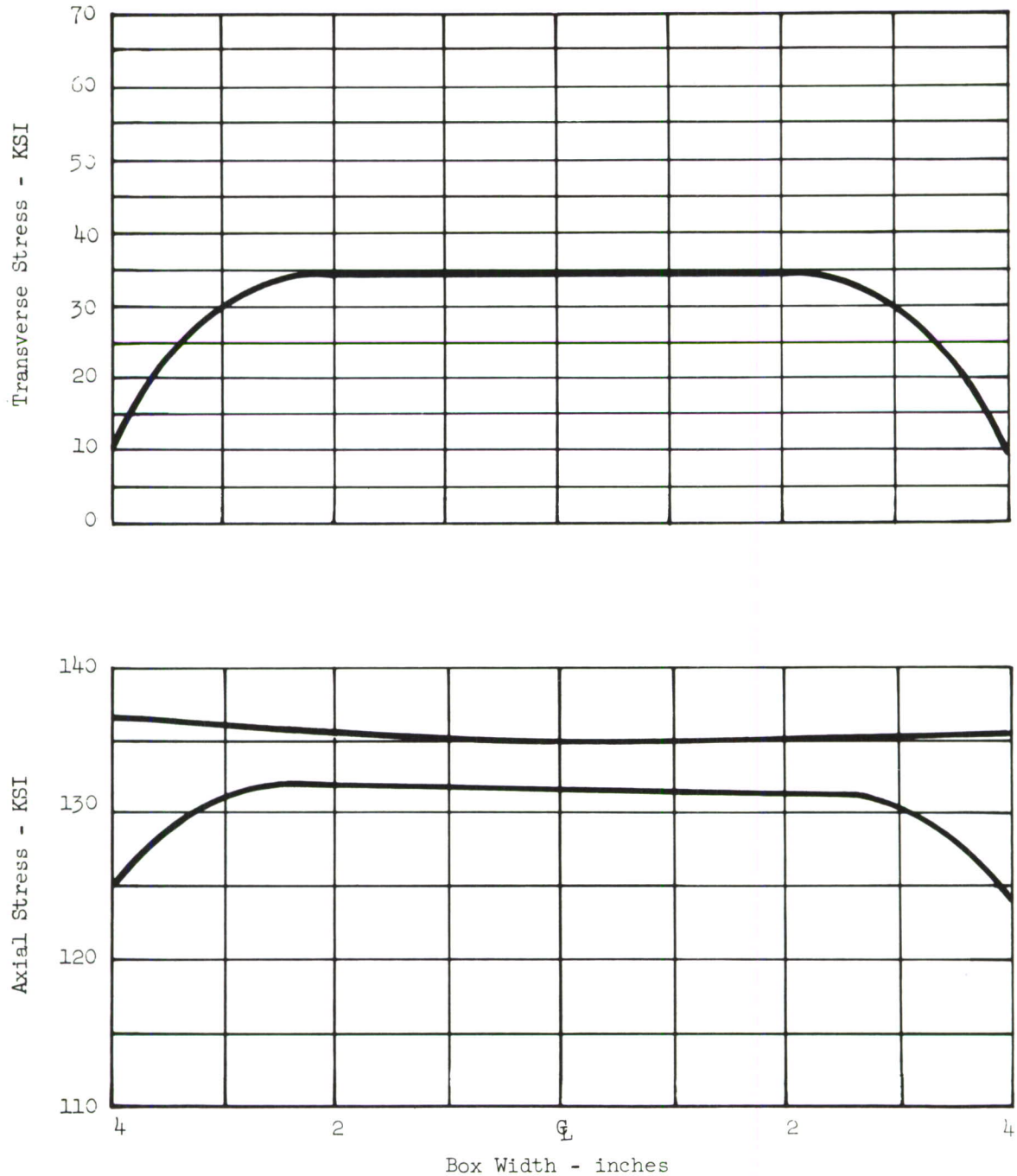


Figure 10. Predicted Elastic Stresses in Box II Cover Plates

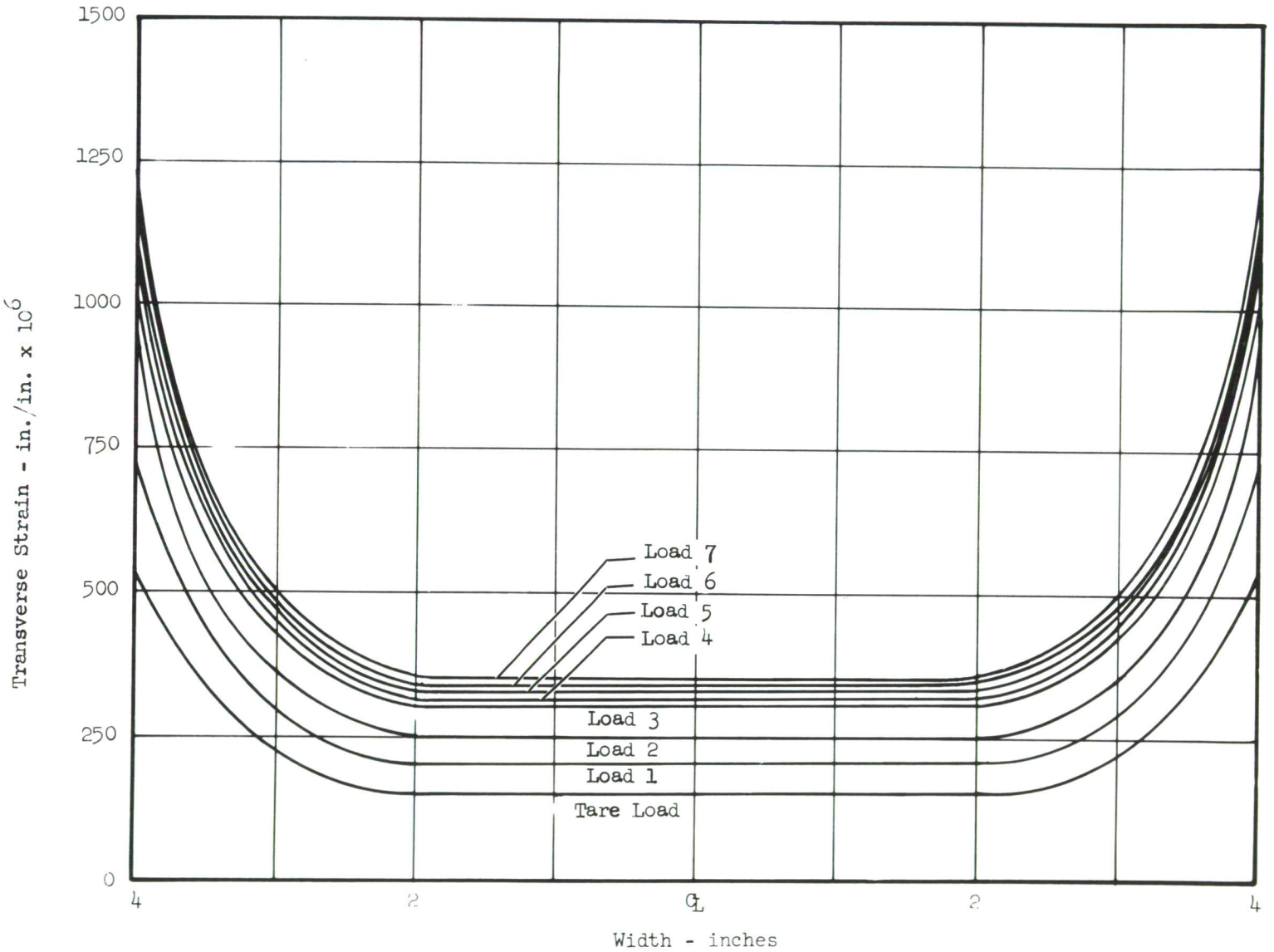


Figure 11. Predicted Elastic Strains in Box III Cover Plates

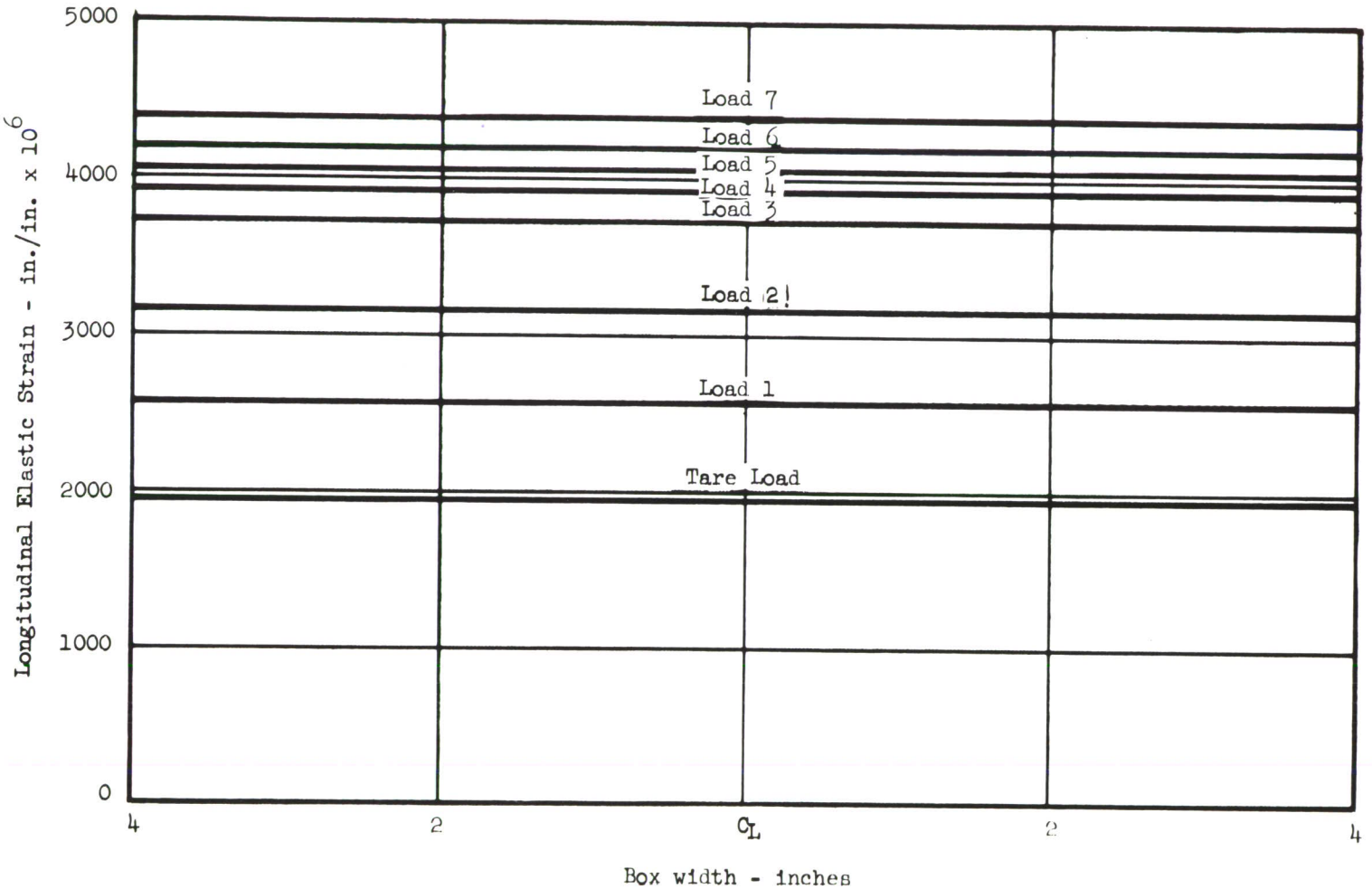


Figure 12. Predicted Elastic Strains in Box III Cover Plates

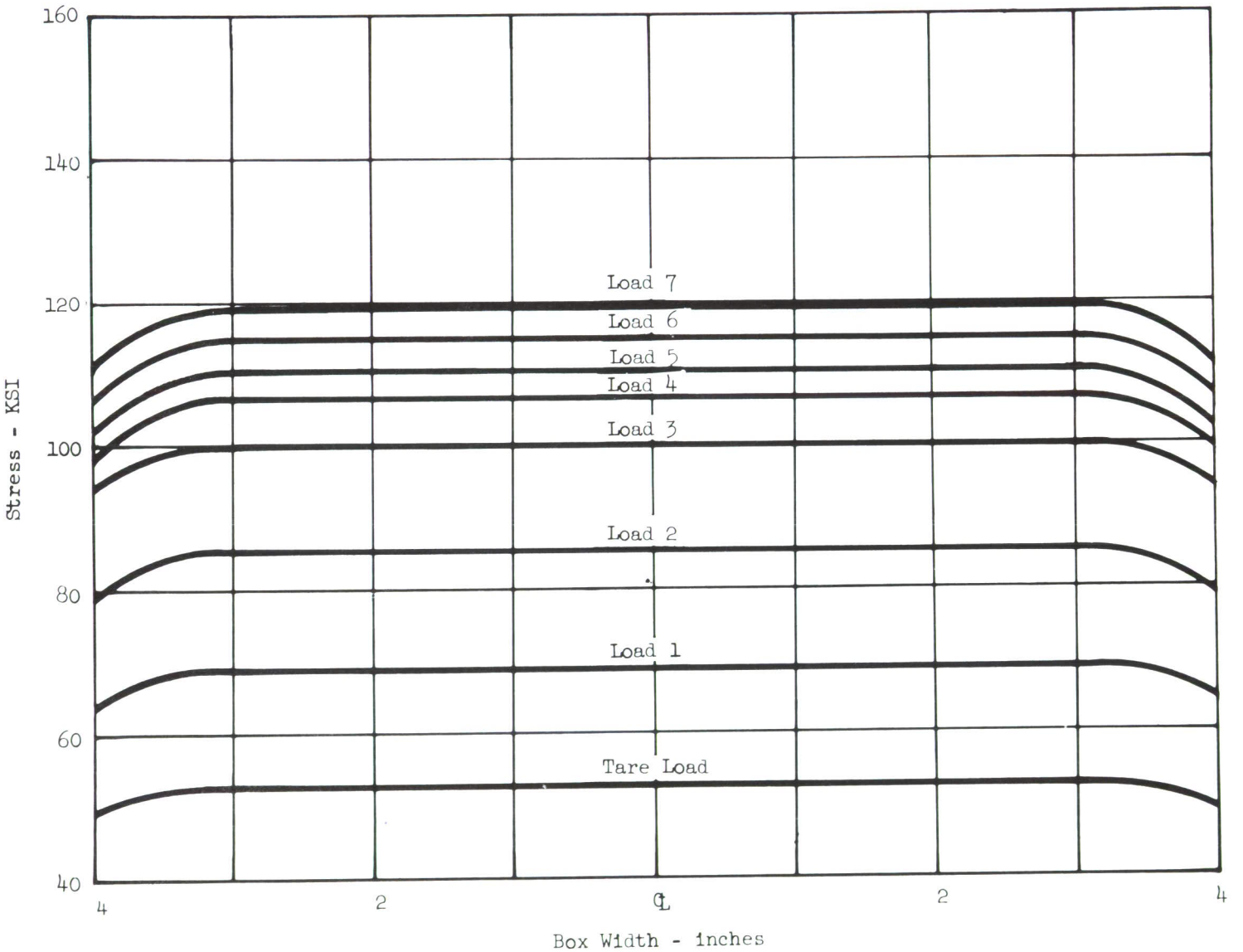


Figure 13. Predicted Elastic Stresses in Box III Cover Plates

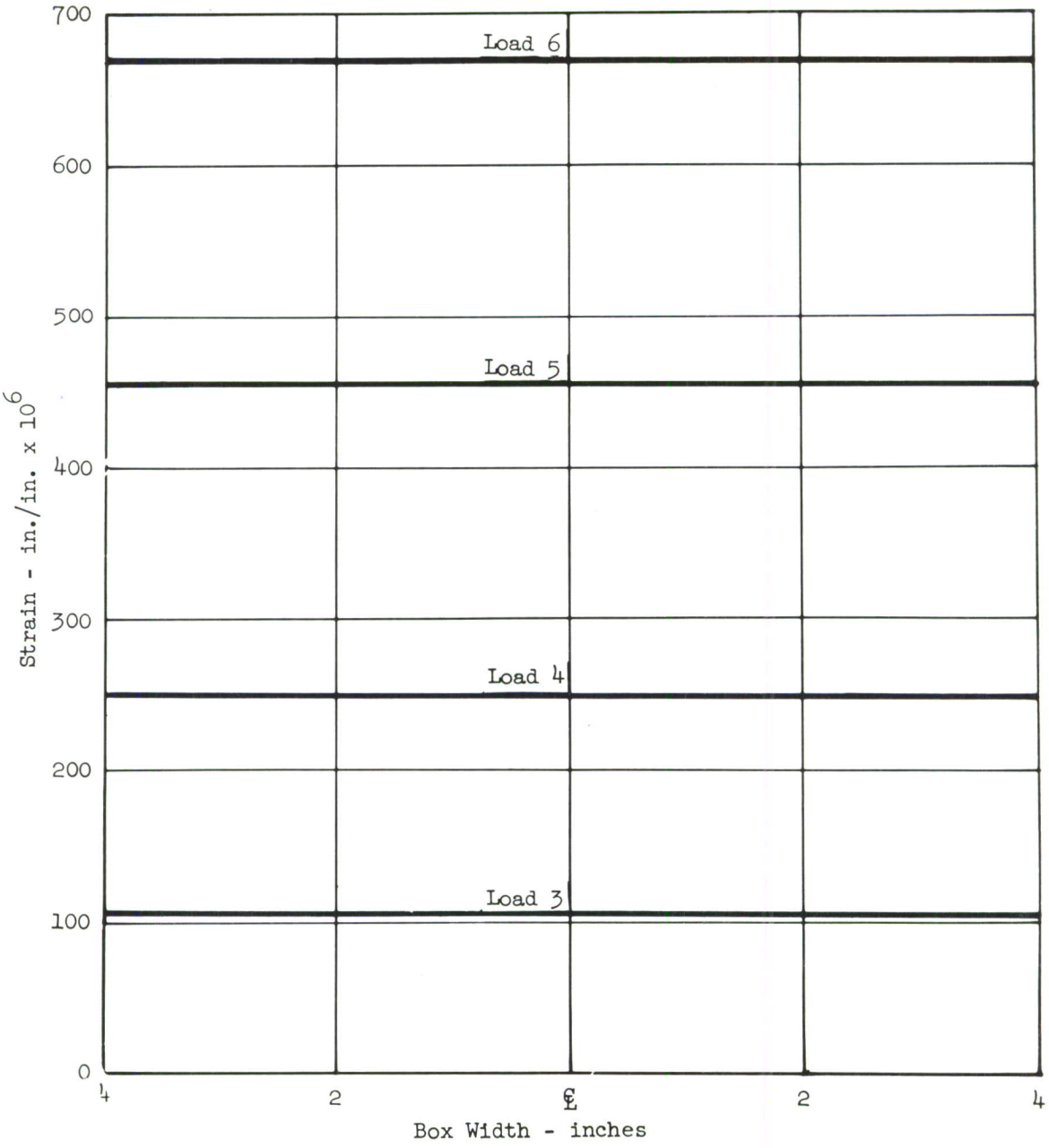
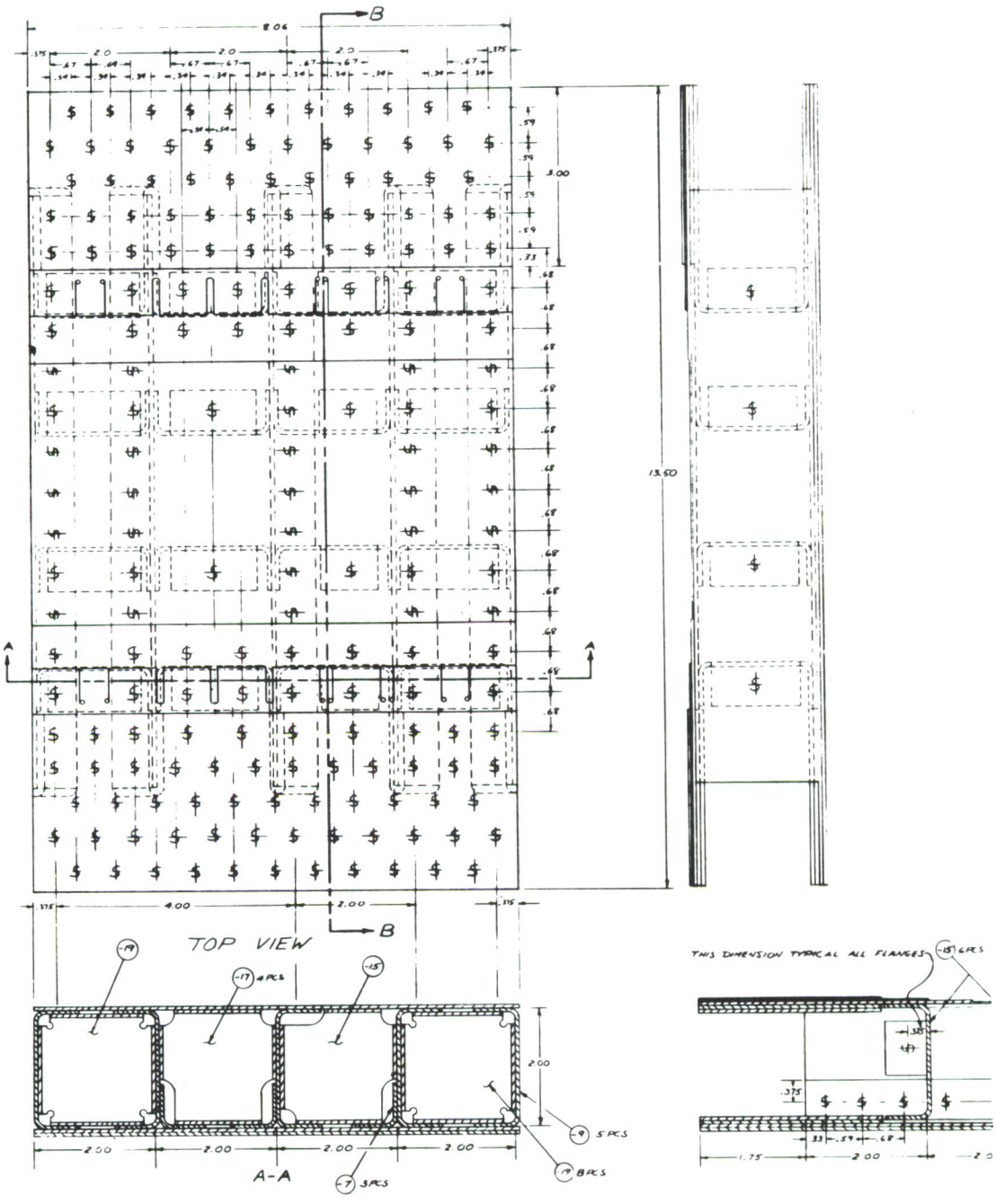
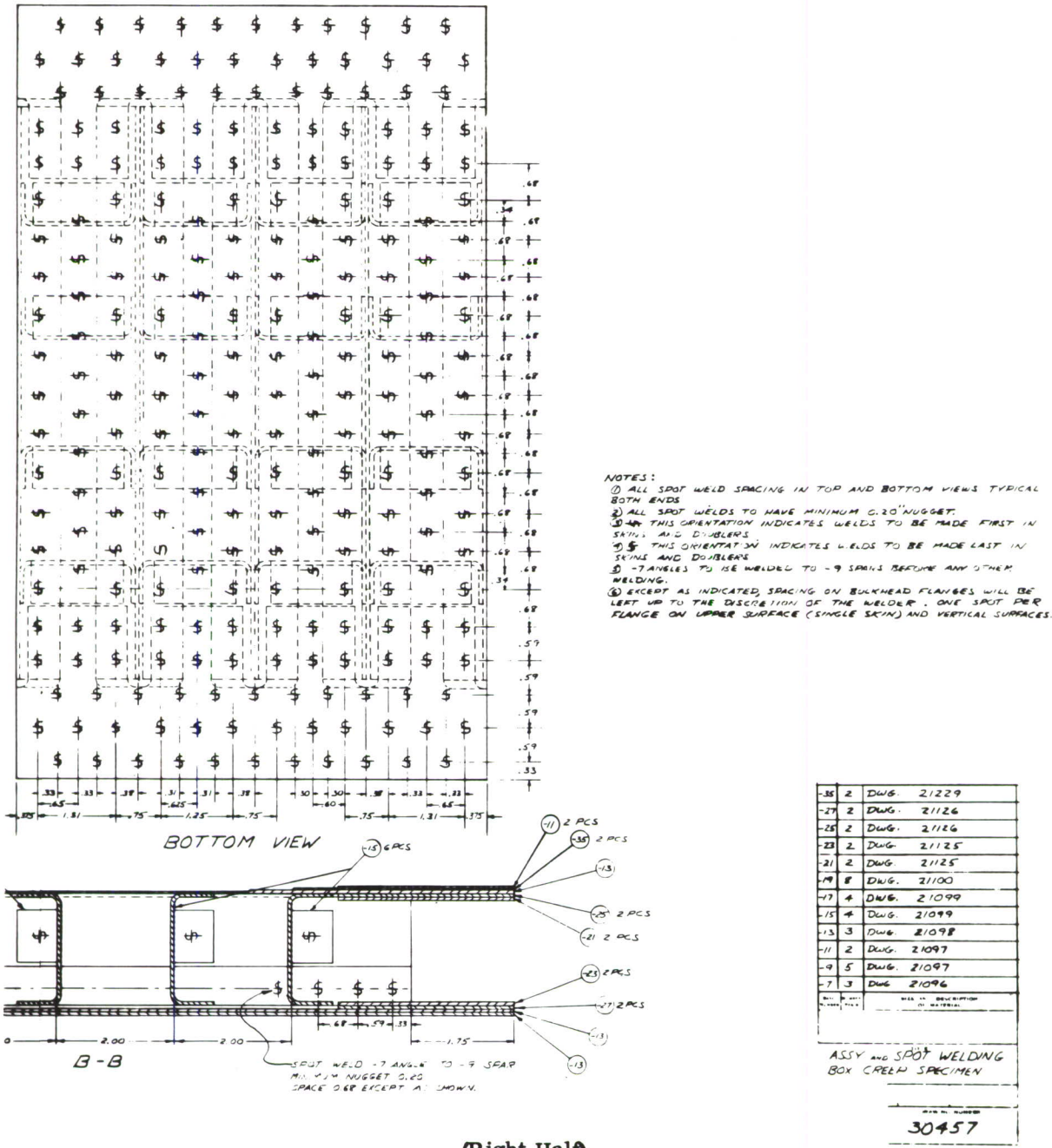


Figure 14. Predicted Creep Strain in Lower Cover Plate of Box III



(Left Half)

Figure 15. Fabrication Drawing for Test Box



(Right Half)

Figure 15. Fabrication Drawing for Test Box

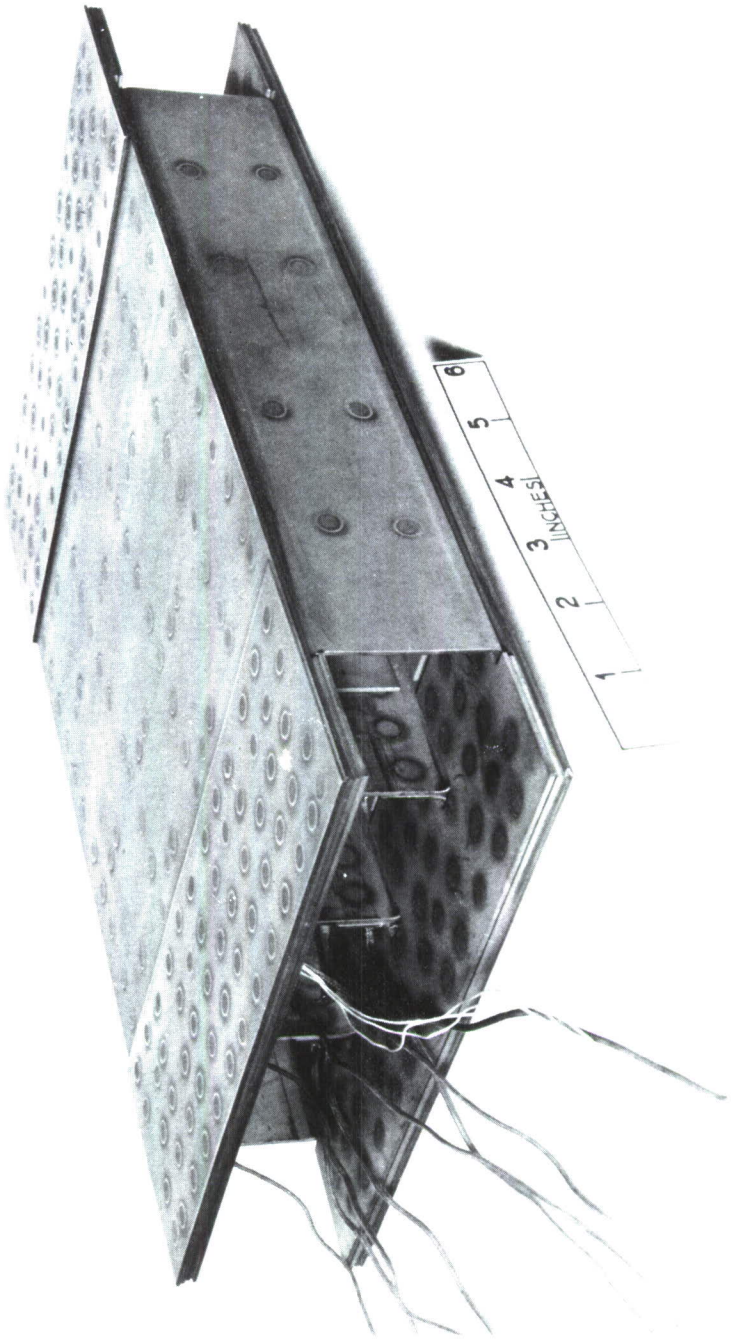


Figure 16. Test Box

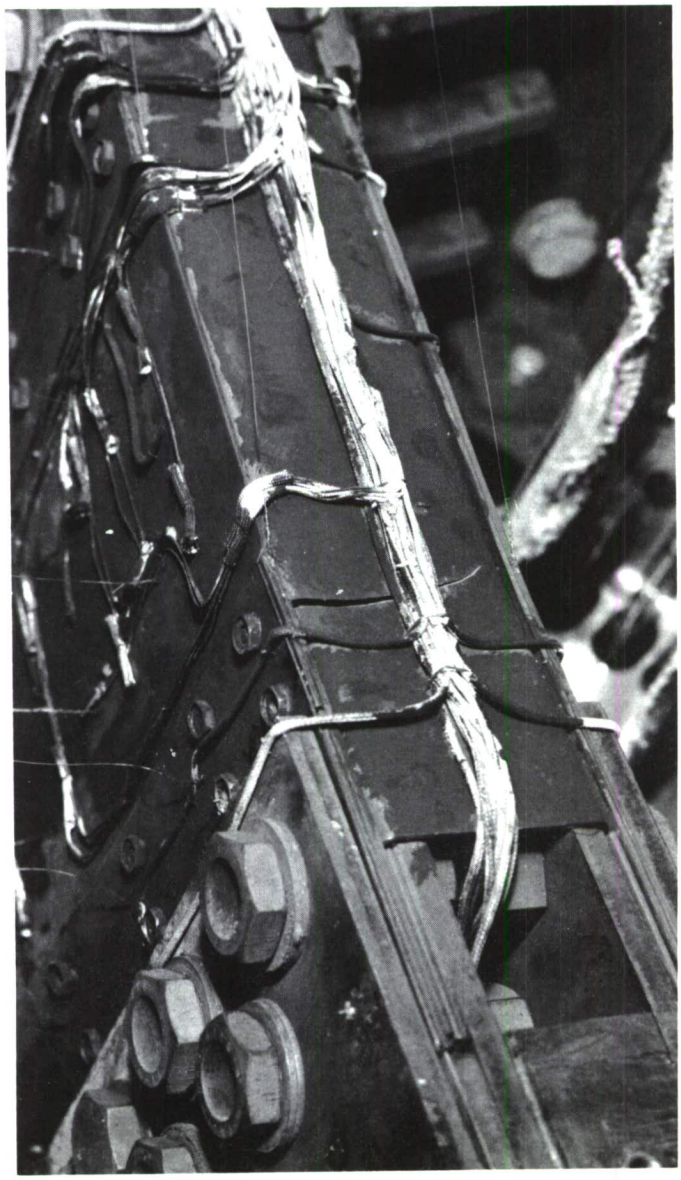


Figure 17. Test Box Failure - Box II

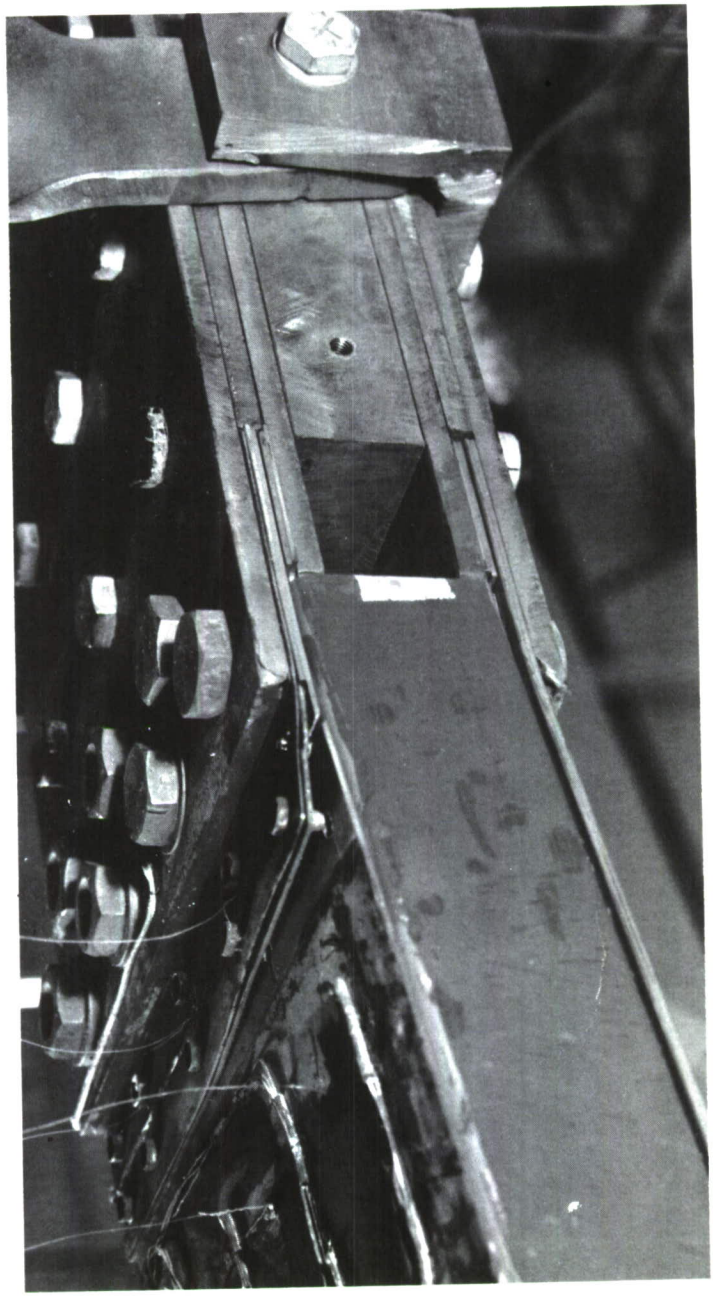


Figure 18. Test Box Failure - Box III

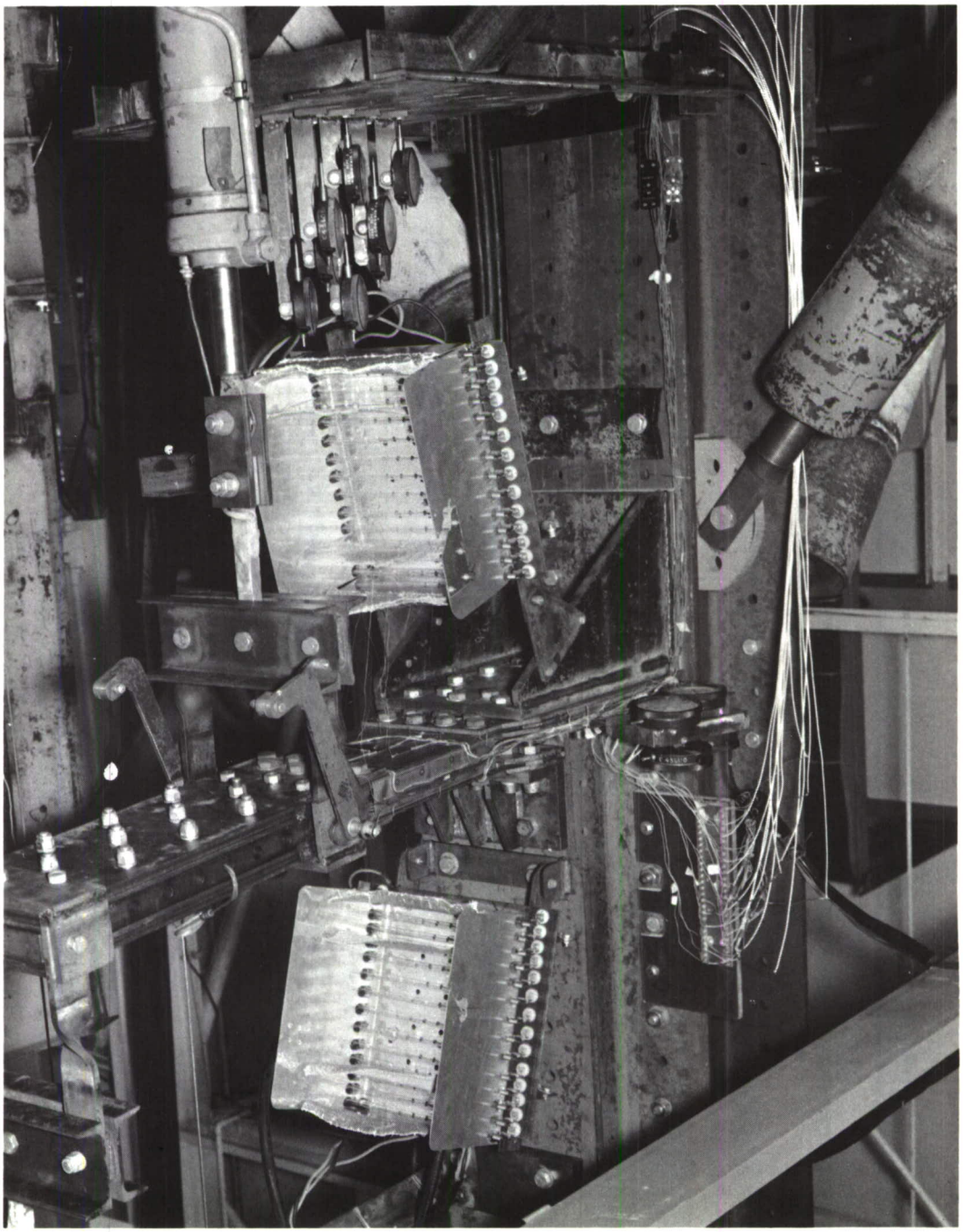


Figure 19. Test Box Installation

Note: Numbers without prefixes indicate thermocouple locations:
prefixed numbers indicate strain gage locations.
instrumentation shown looking toward box

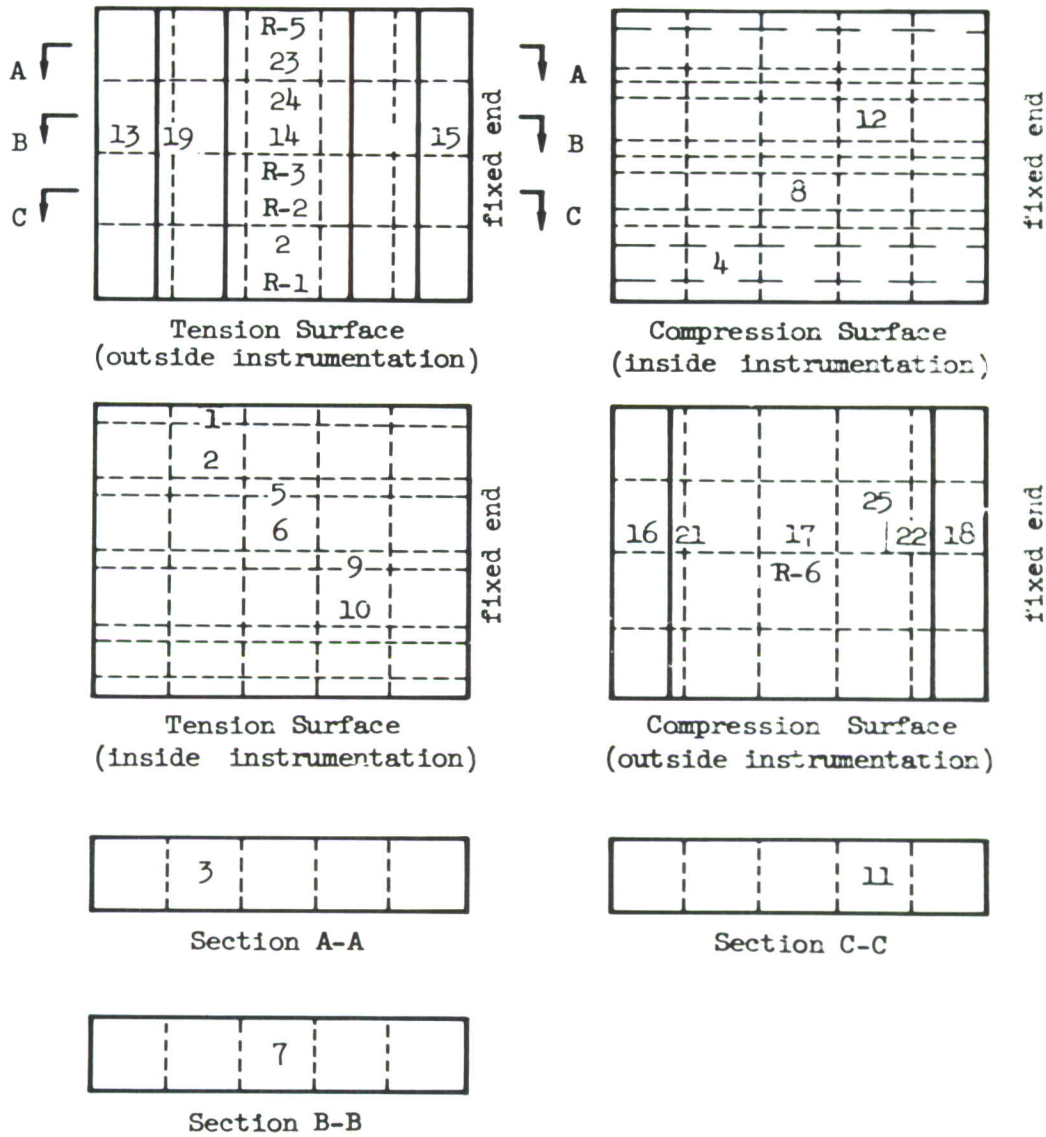


Figure 20. Test Temperatures - Box II

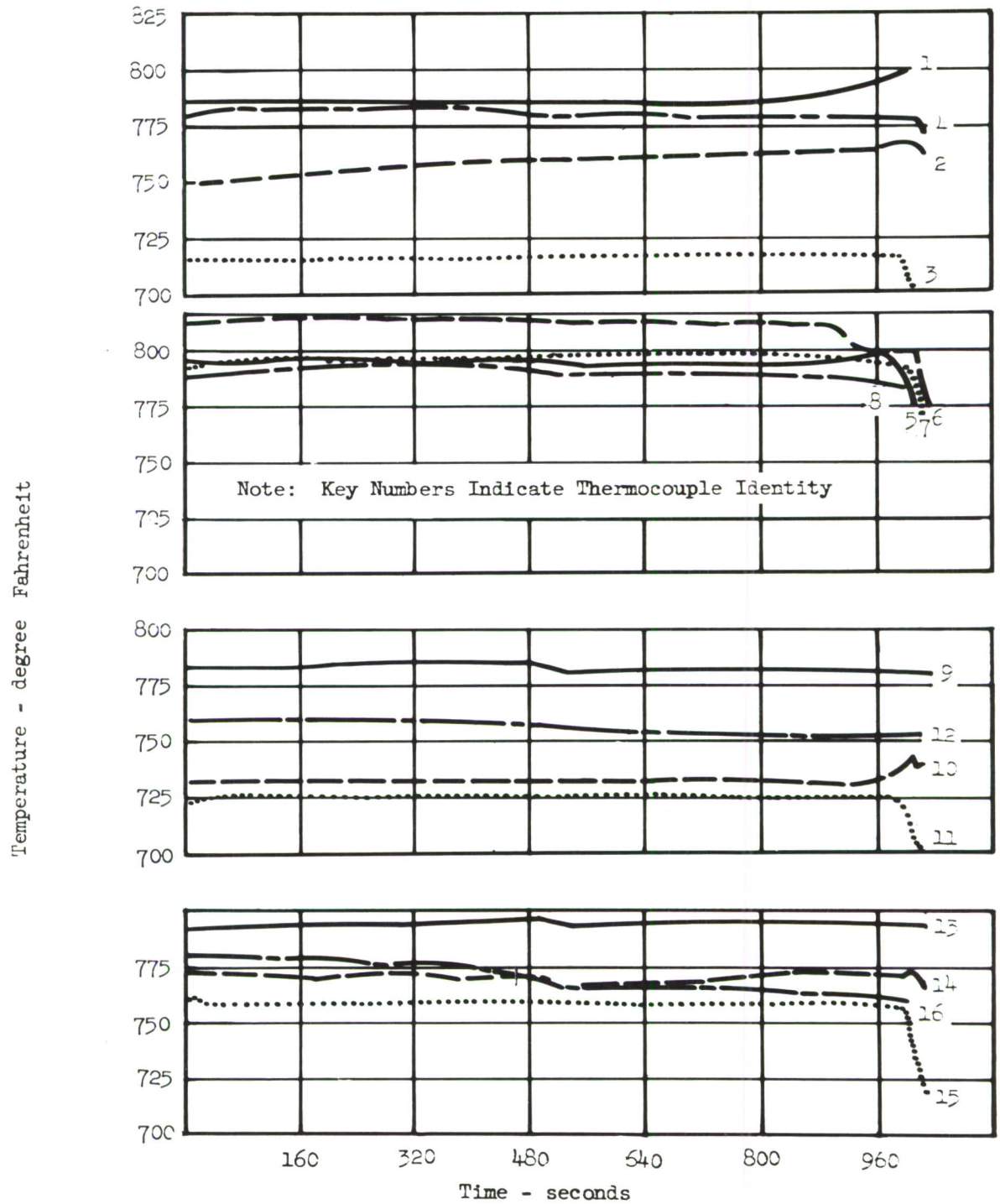


Figure 20. Test Temperatures - Box II (Continued)

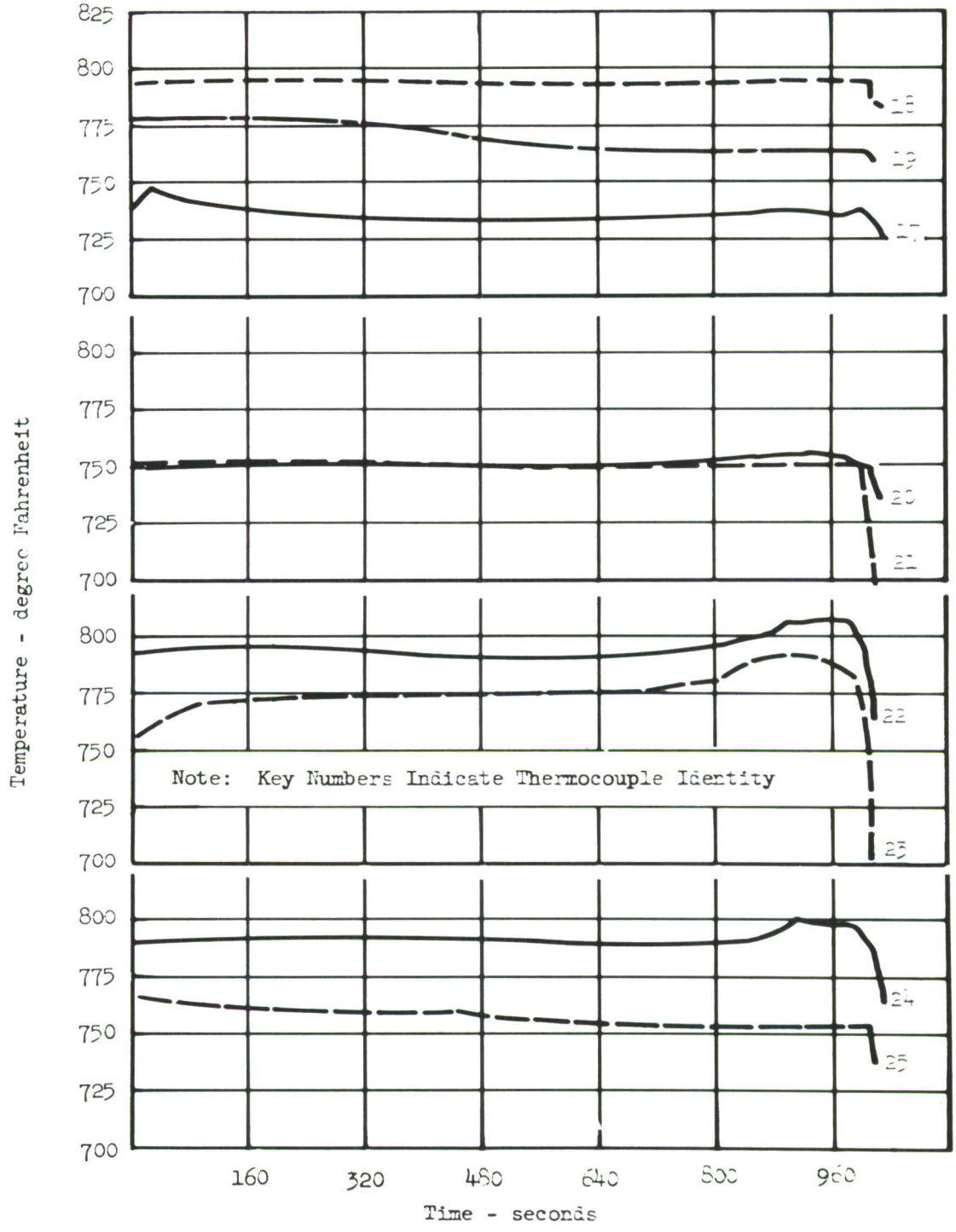


Figure 20. Test Temperatures - Box II (Continued)

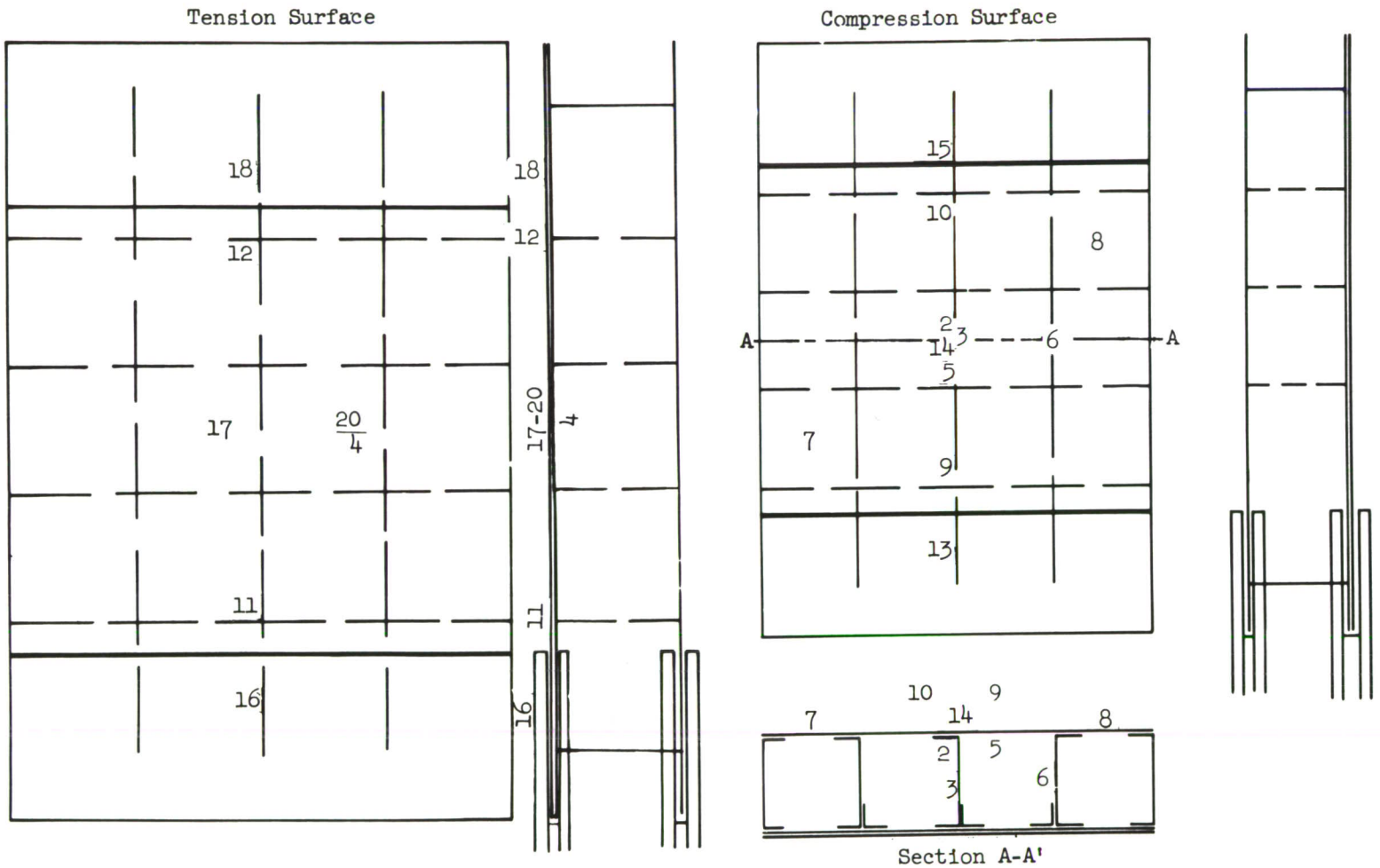


Figure 21. Thermocouple Locations - Box III

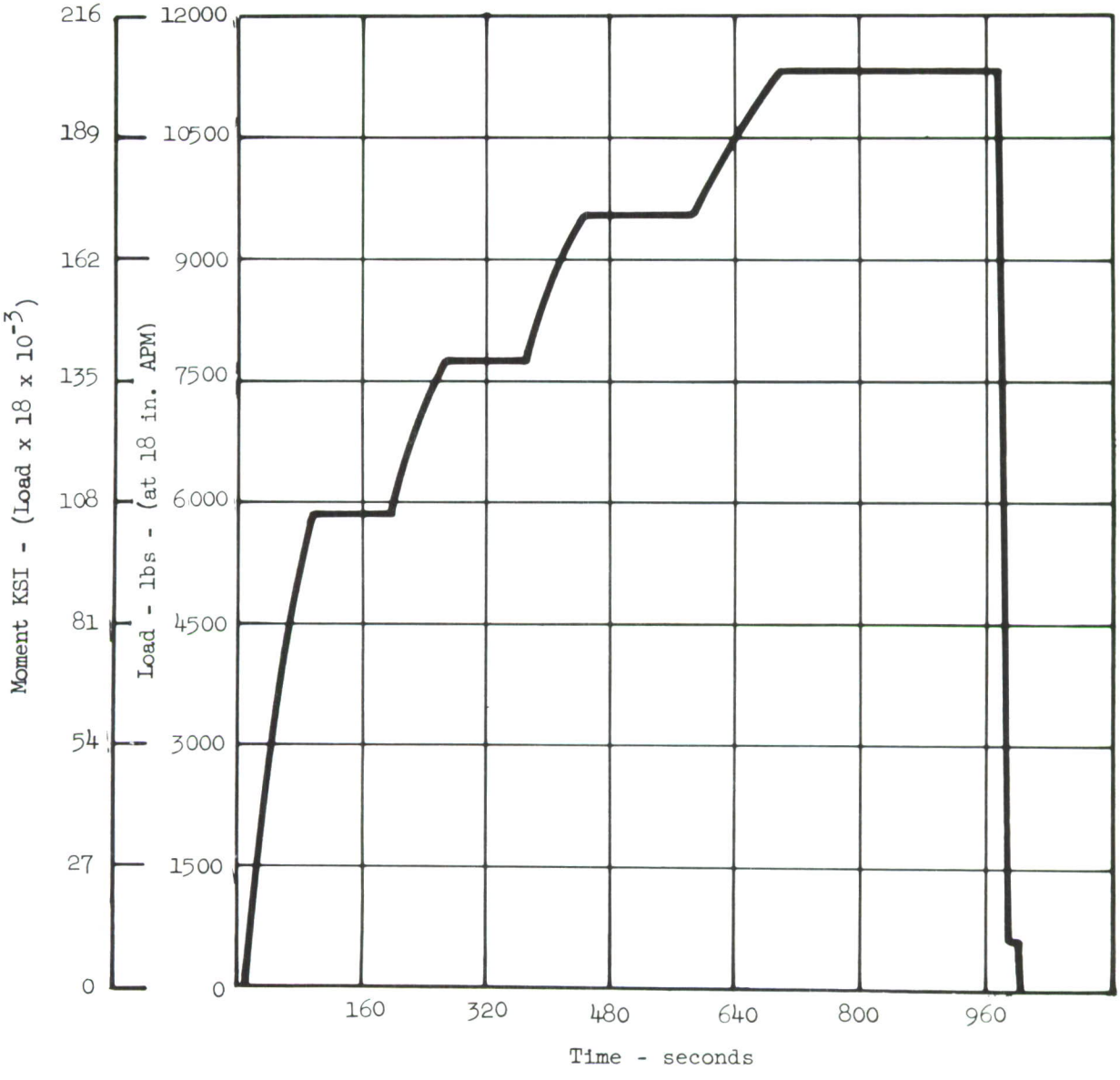


Figure 22. Test Load Spectrum - Box II

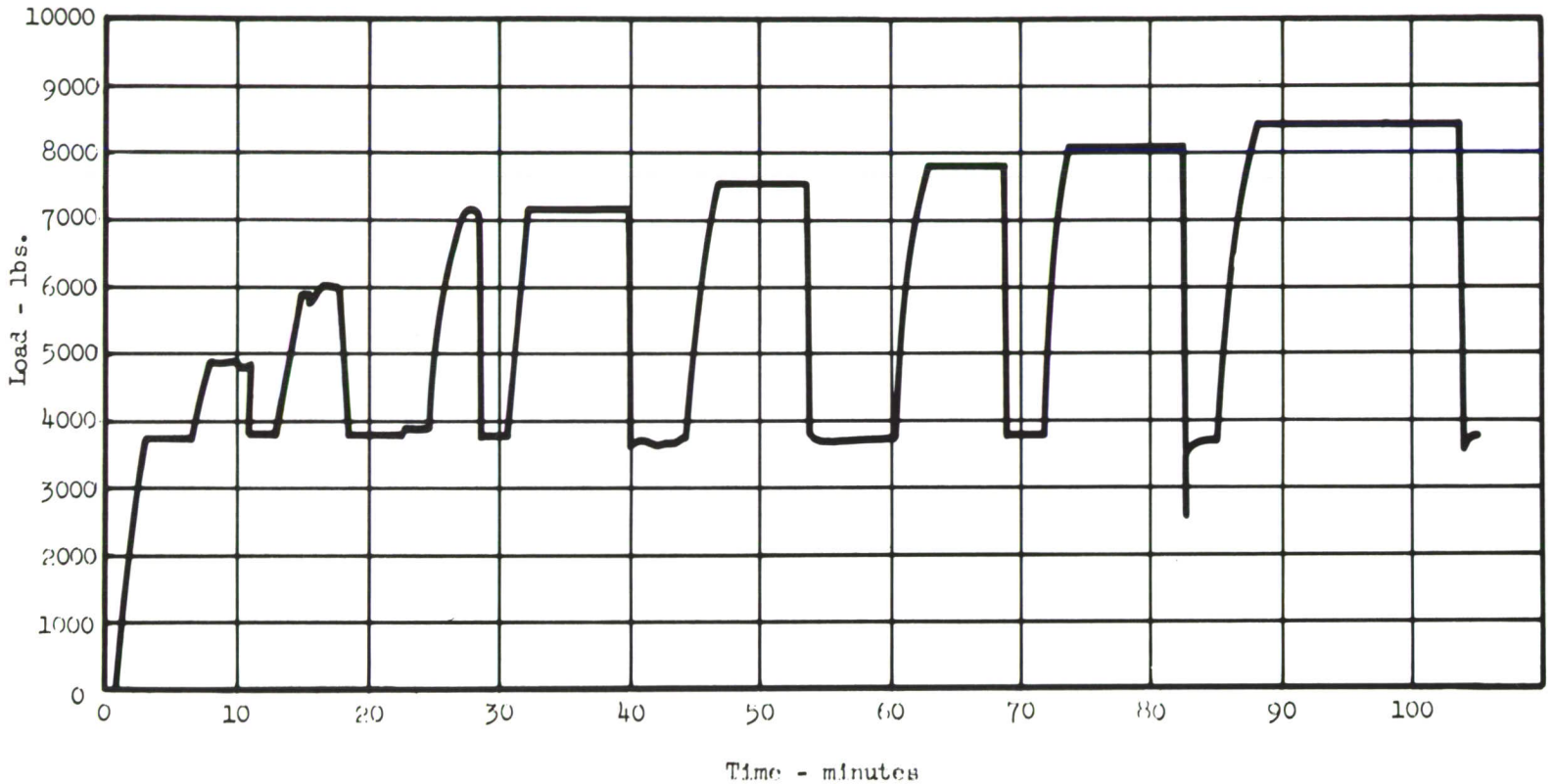


Figure 23. Test Load Spectrum - Box III

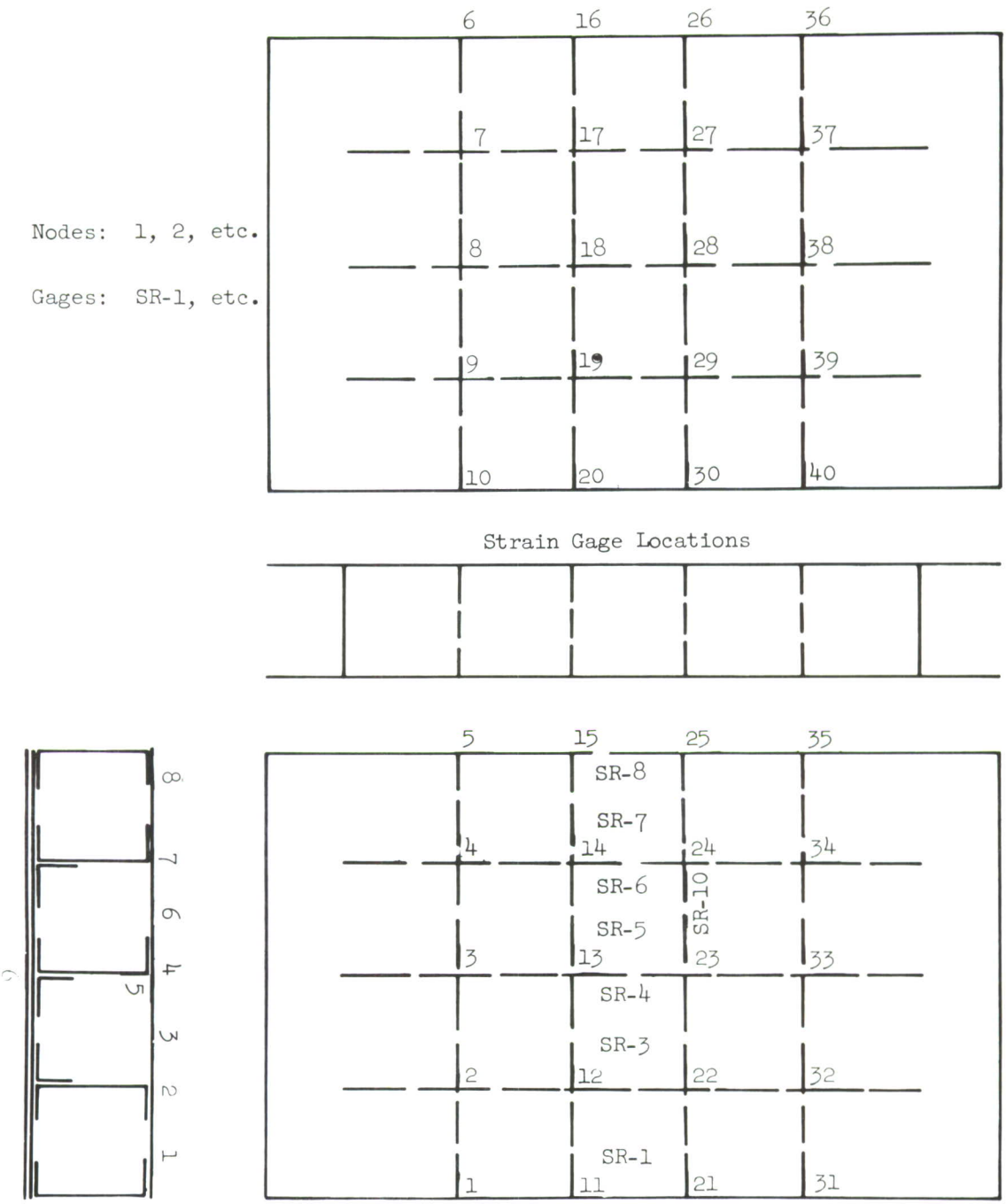


Figure 24. Strain Gage and Node Locations - Box III

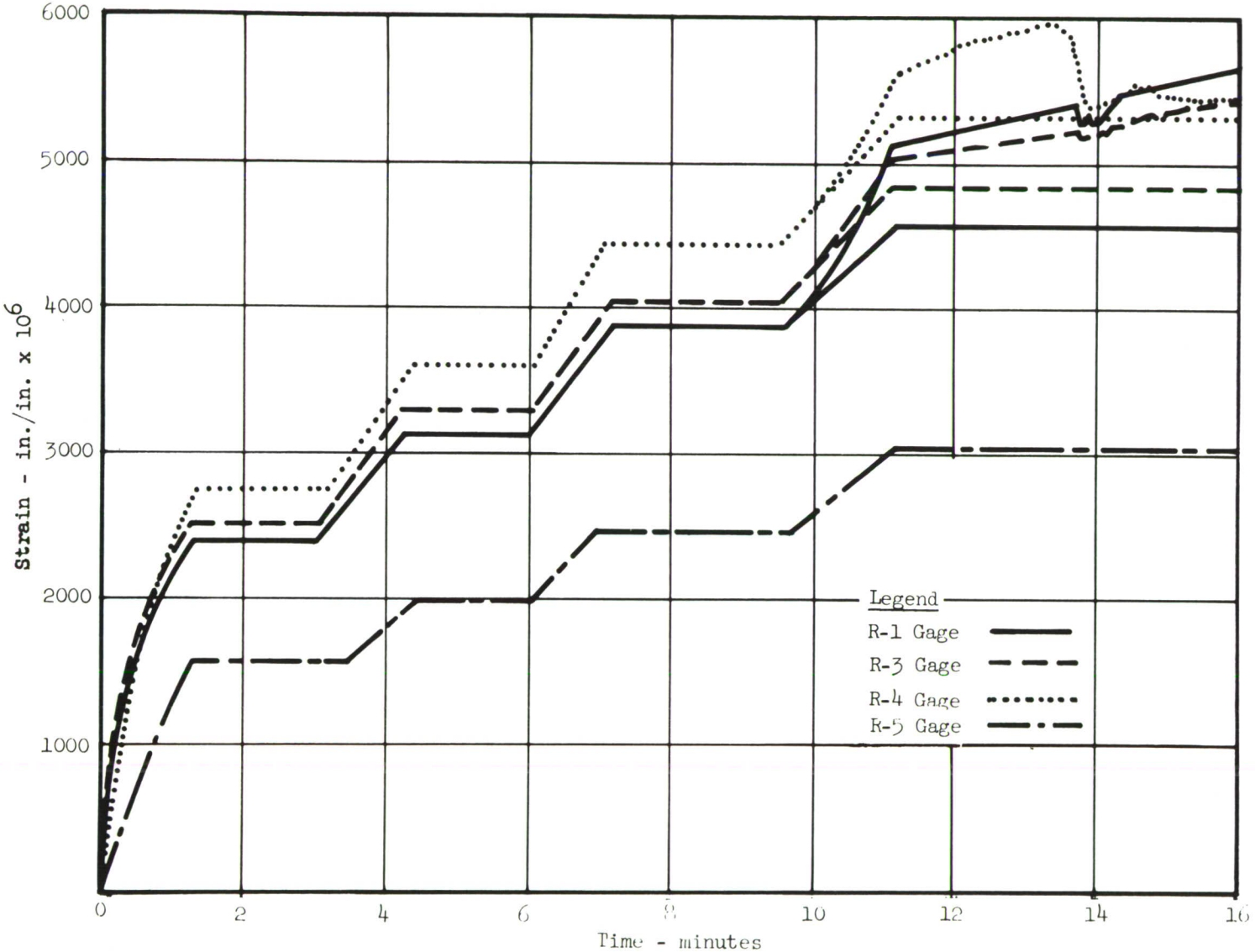


Figure 25. Test Strains, Box II

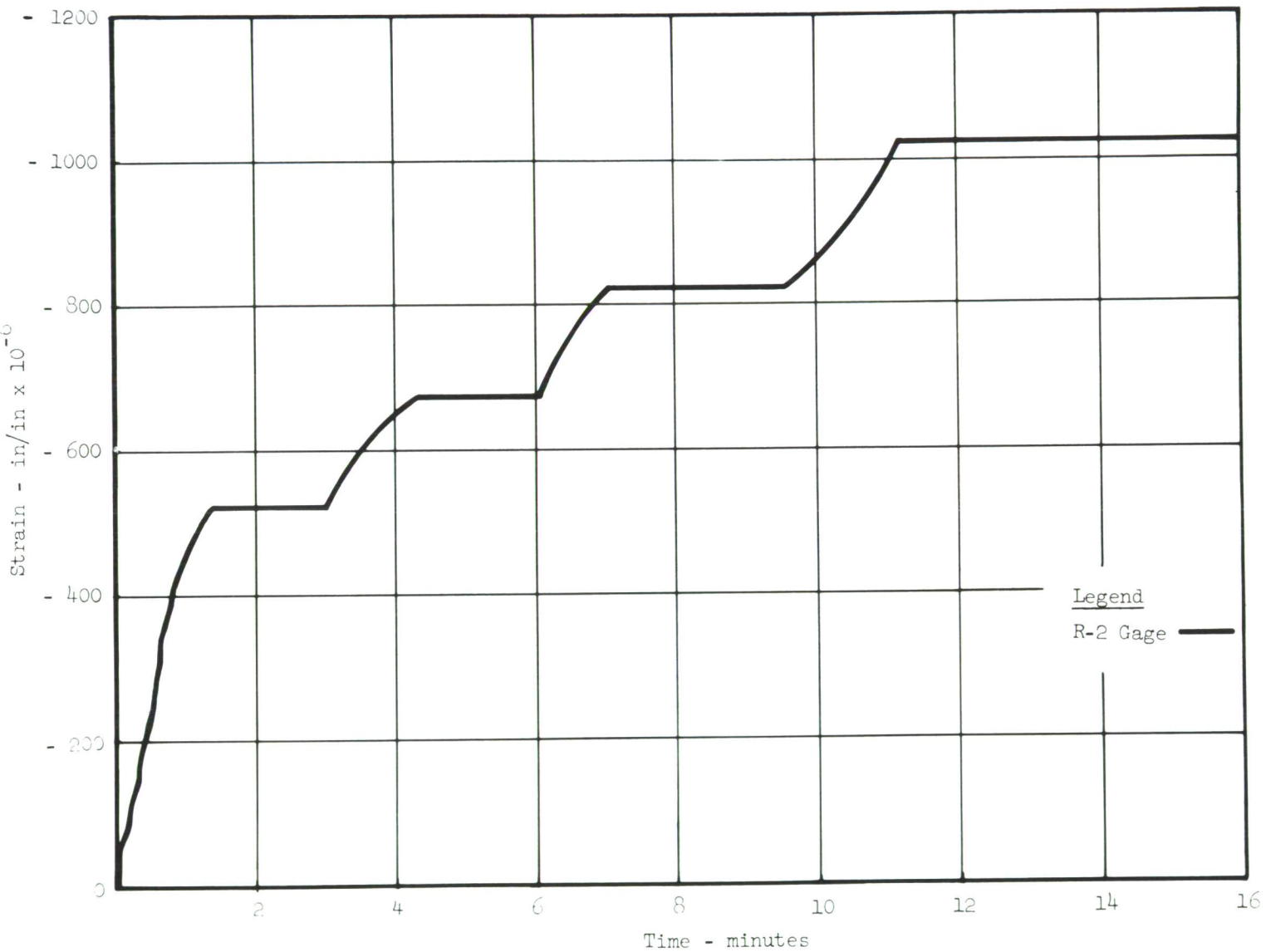


Figure 25. Test Strains, Box II (Continued)

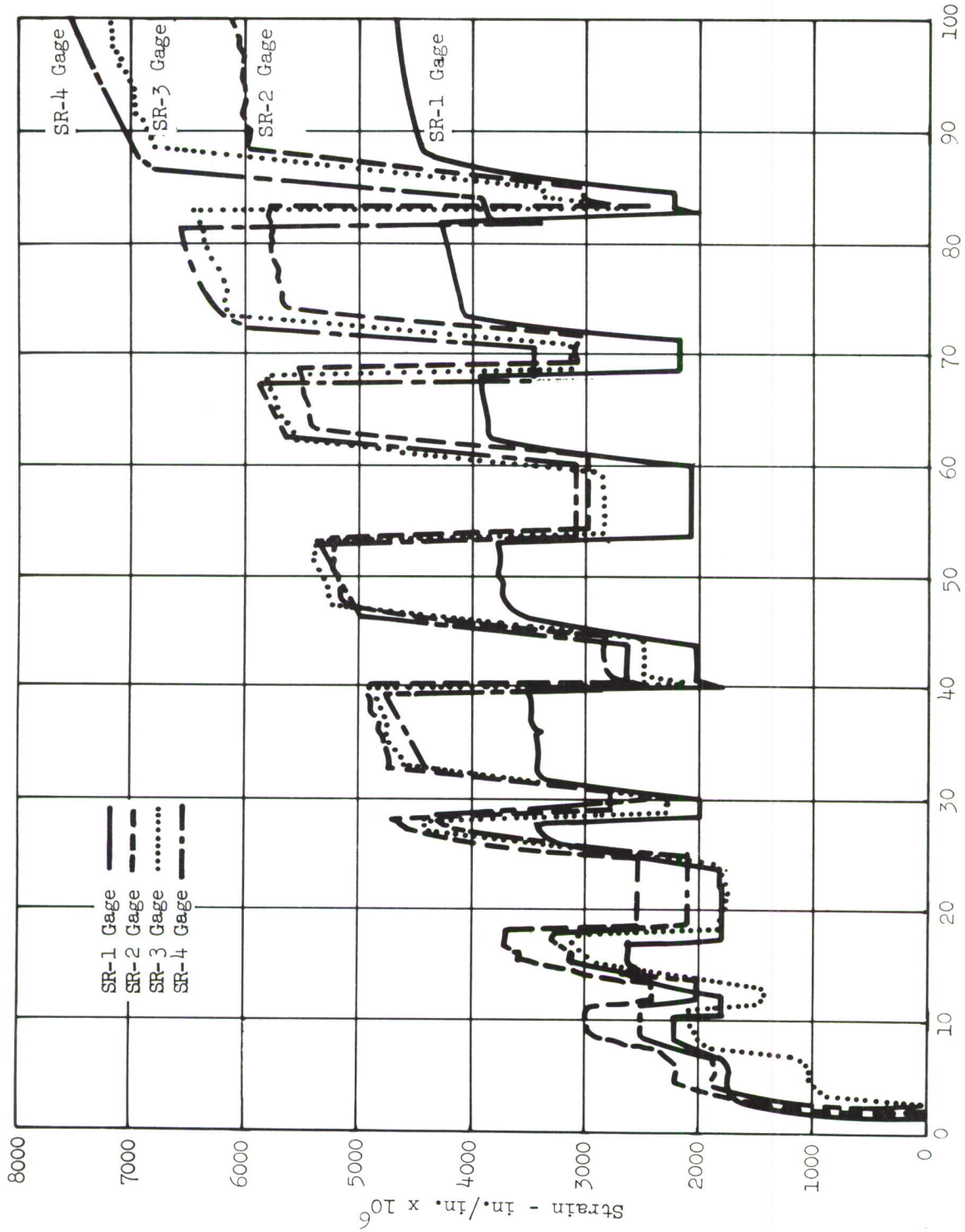


Figure 26. Test Strains - Box III

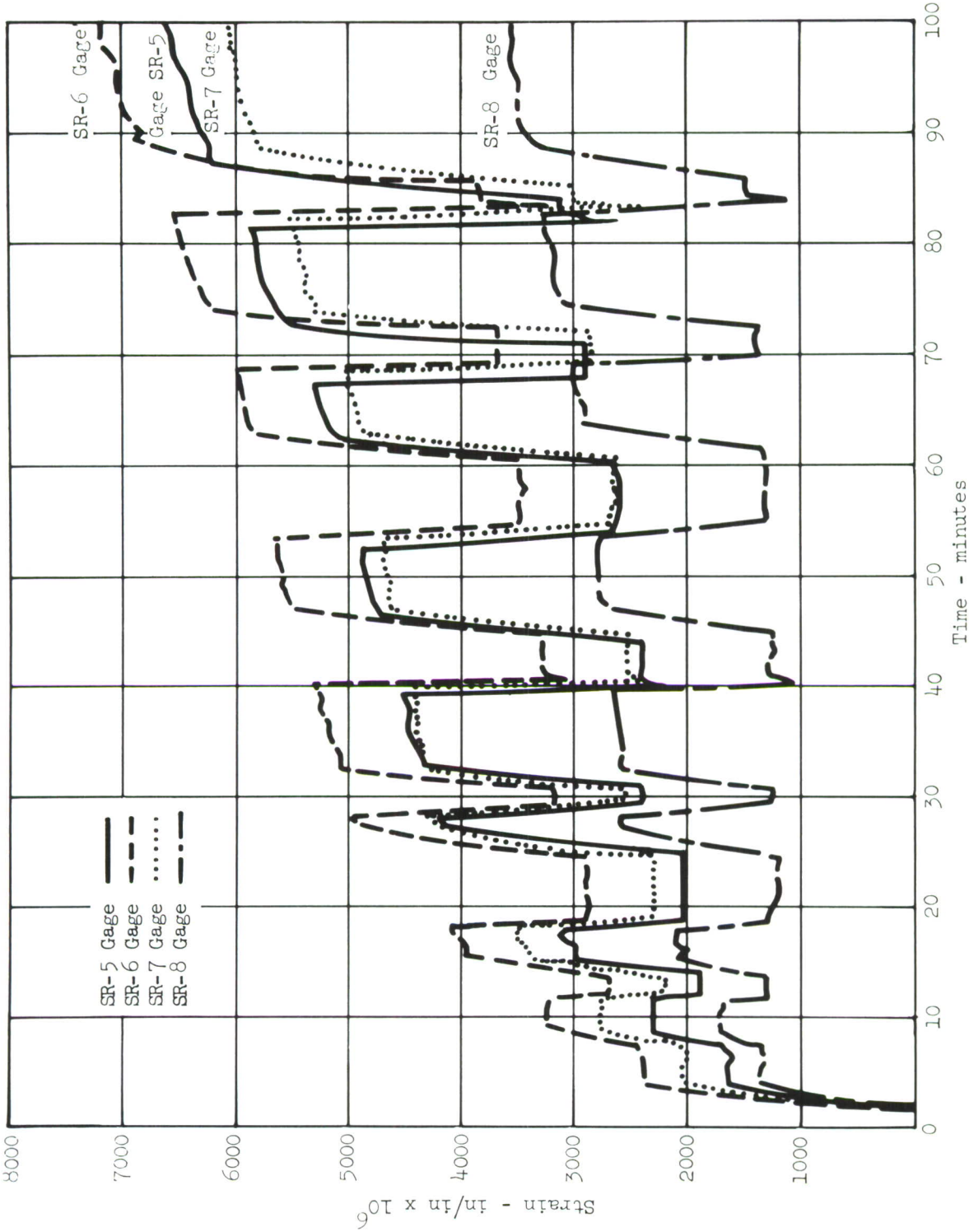


Figure 26. Test Strains - Box III (Continued)

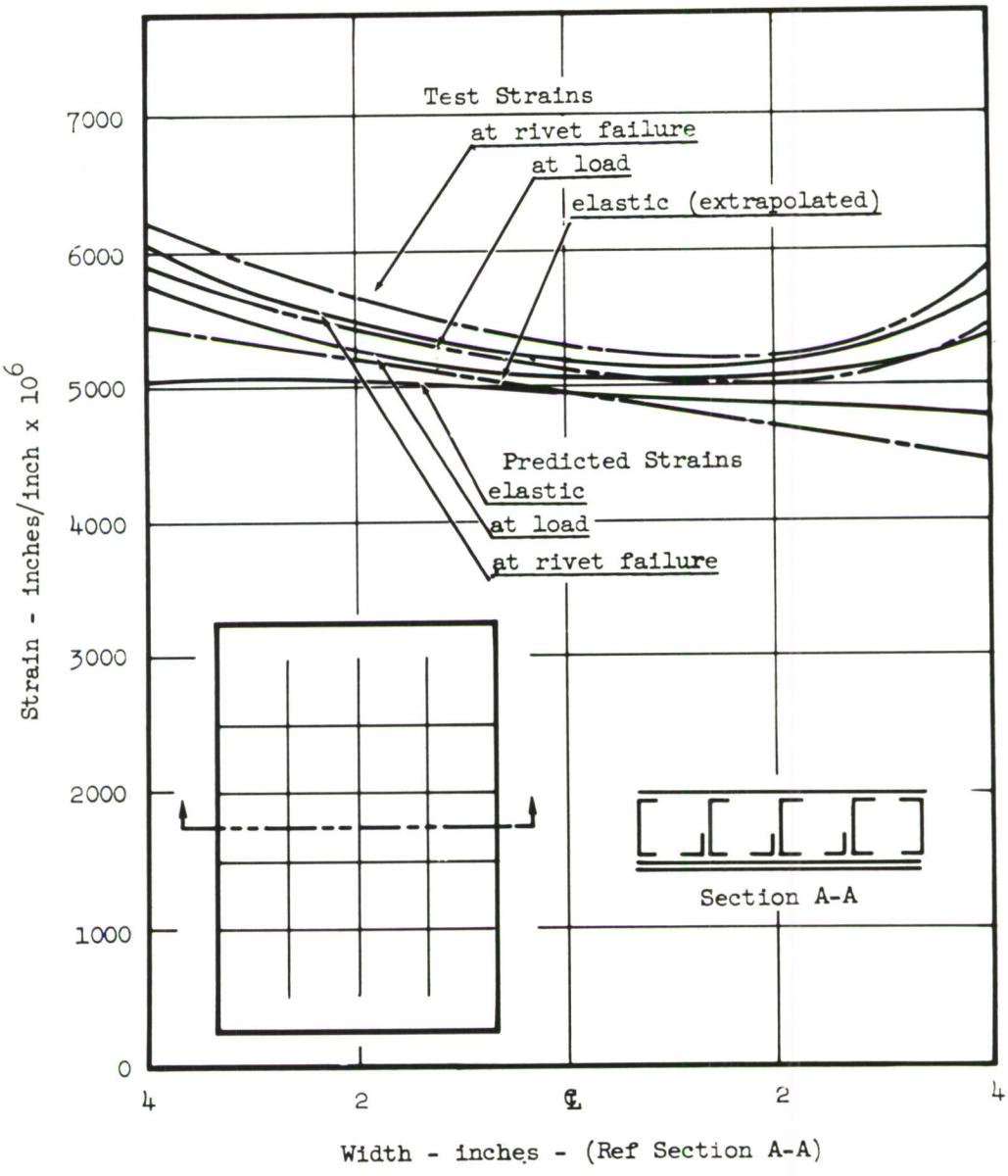


Figure 27. Strain Comparison - Box II Tension Surface

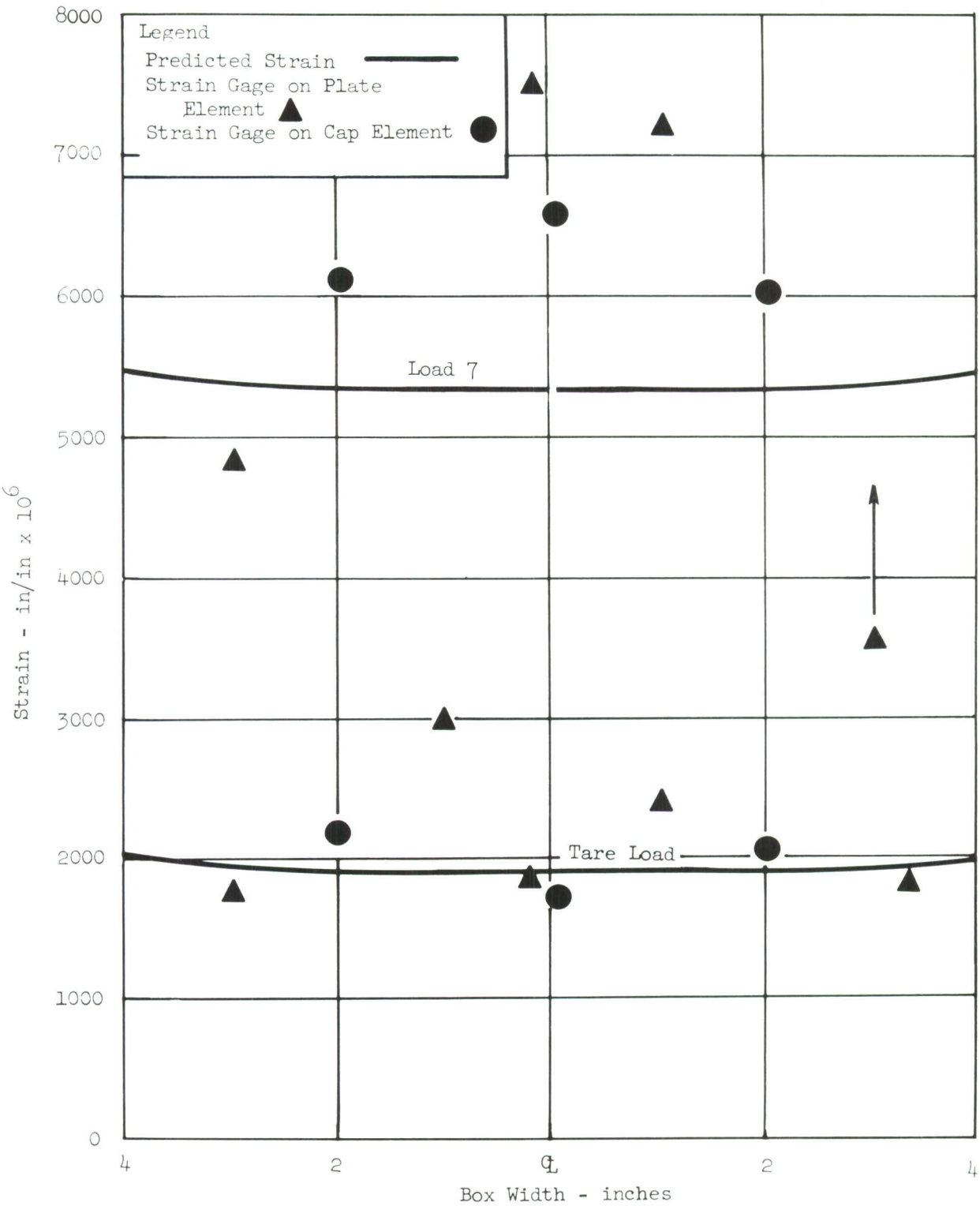


Figure 28. Strain Comparison - Box III

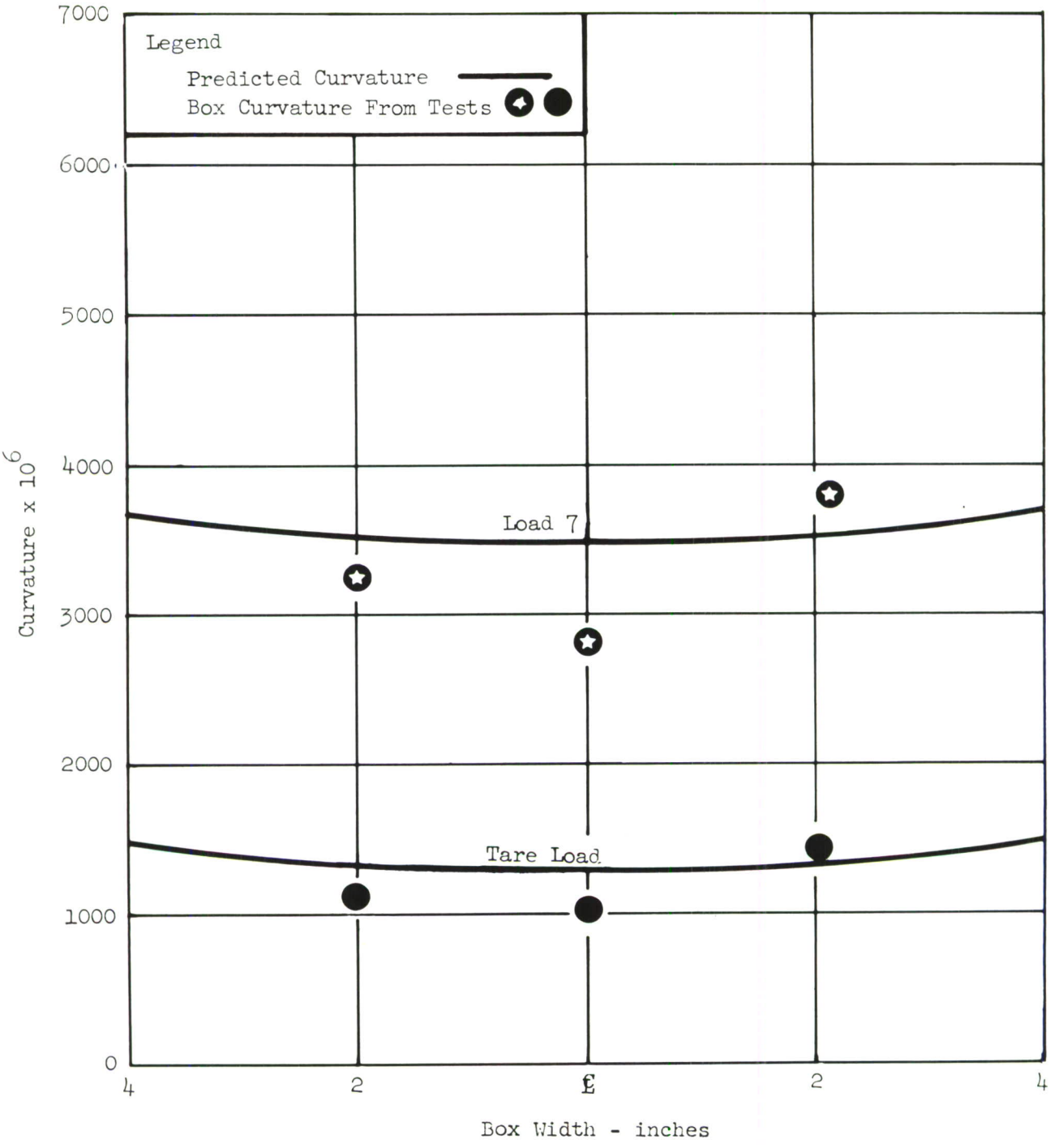


Figure 29. Curvature Comparison - Box III

Legend

AB - Elastic Deformation Under Load

BC - Plastic Deformation Under Load

AC - Total Deformation Under Load

OD - Permanent Set After Loading

DE - Elastic Spring-Back During Load Release

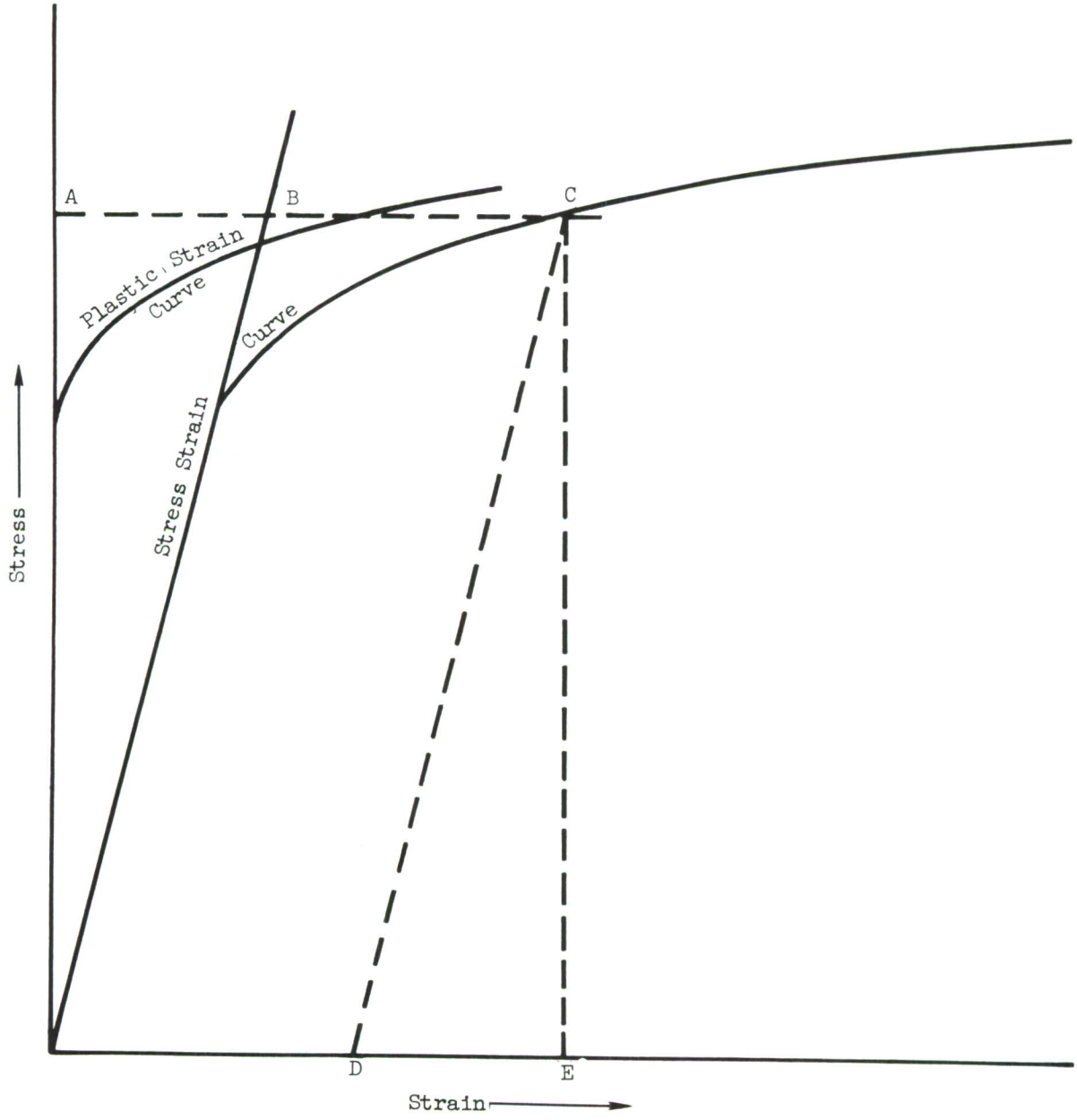


Figure 30. Schematic Stress Strain Curve with Derived Plastic Strain Curve

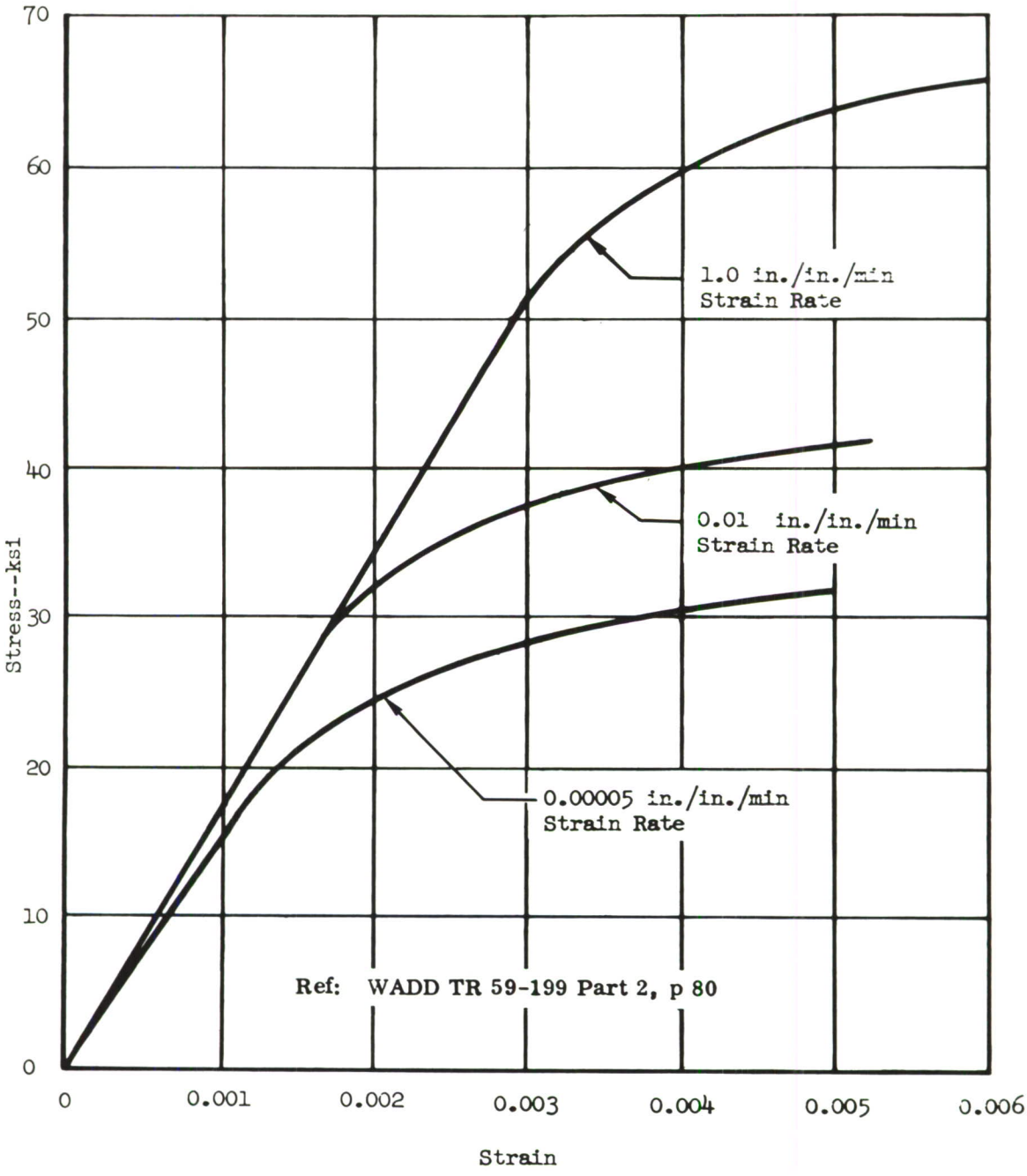


Figure 31. Stress Strain Curves for Armco 17-7 PH Condition TH 1050 Stainless Steel at Various Strain Rates at 1200°F

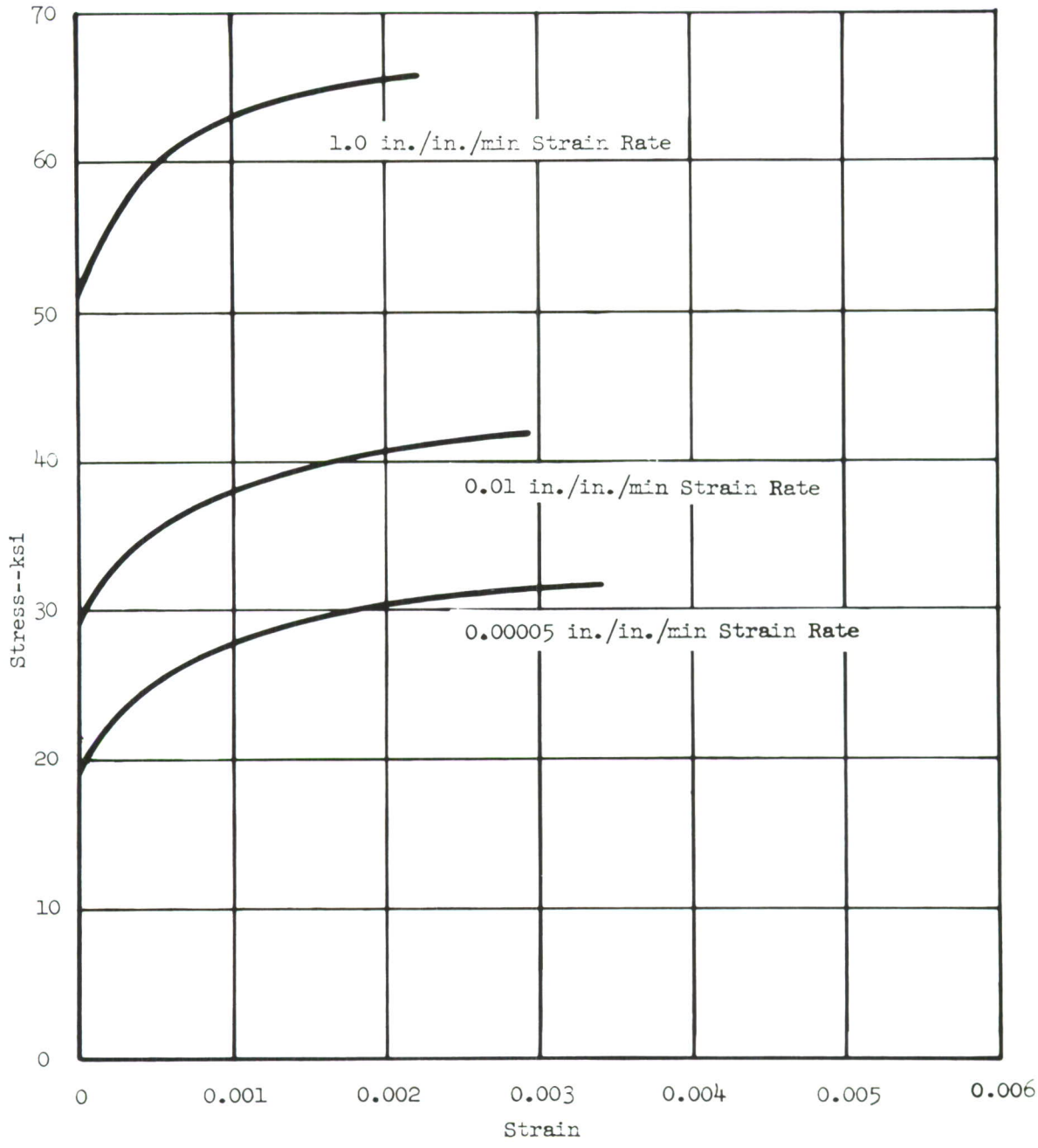


Figure 32. Plastic Stress Strain Curves for Armco 17-7 PH Condition TH 1050 Stainless Steel at Various Strain Rates at 1200°F

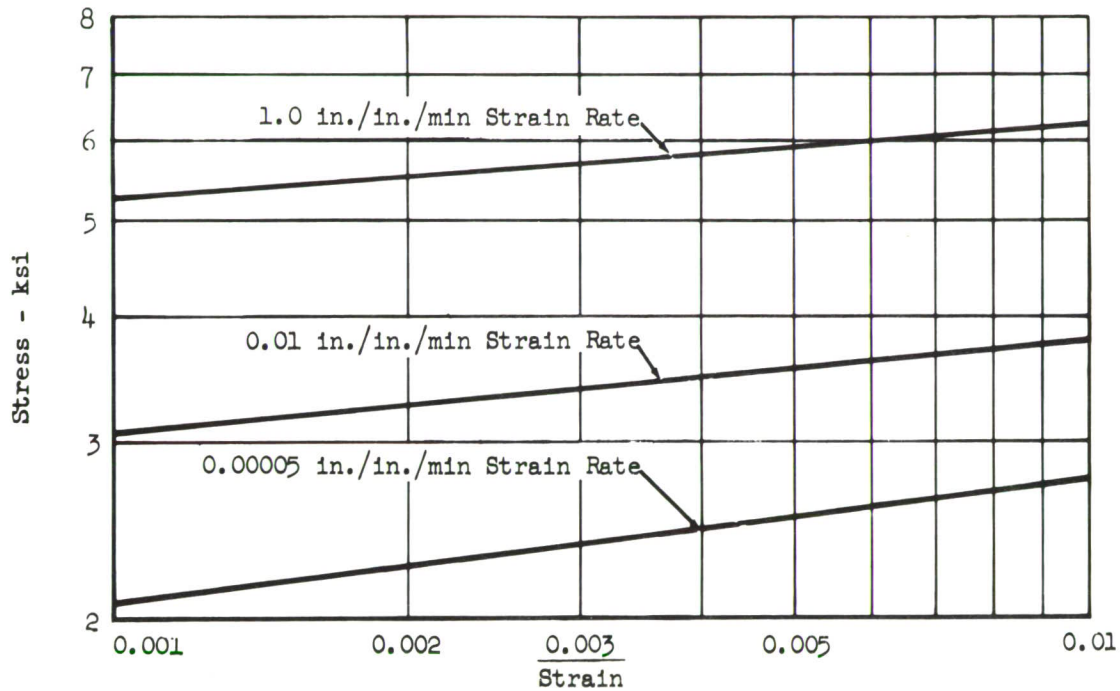


Figure 33. Plastic Stress Strain Curves for Armco 17-7 PH Stainless Steel at Various Strain Rates at 1200°F

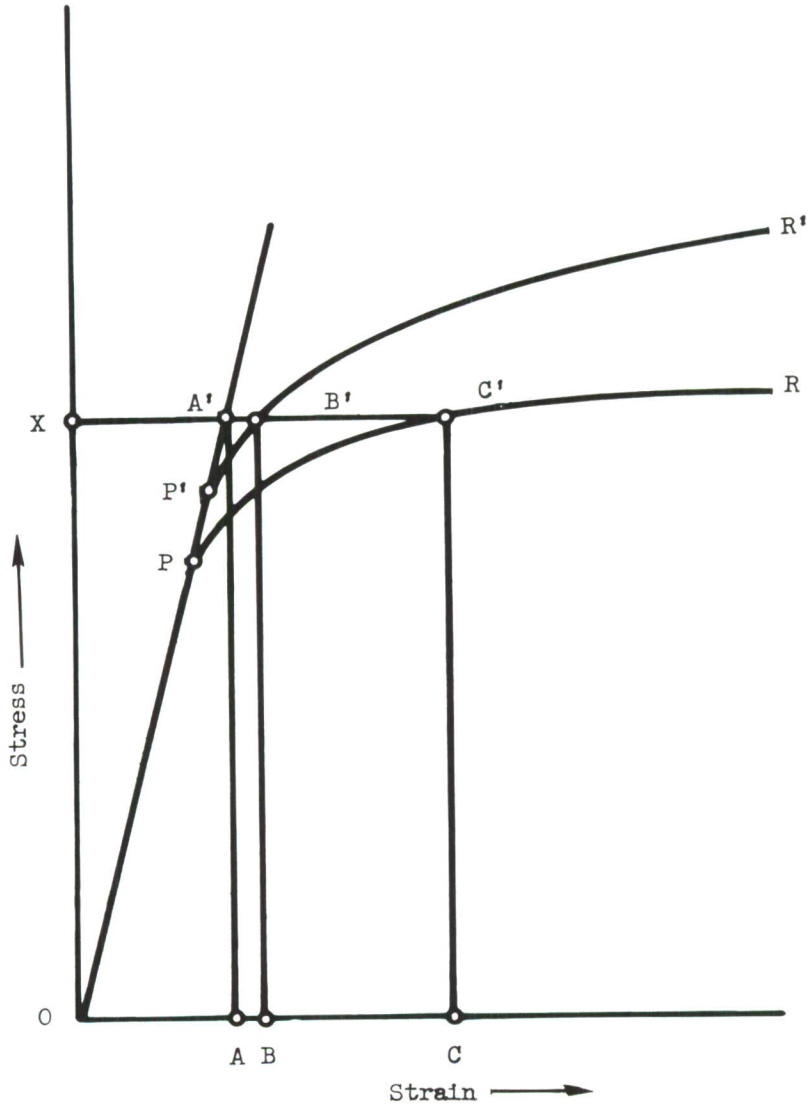


Figure 34. Schematic Stress Strain Curves Resulting from Load Applications at Different Strain Rates

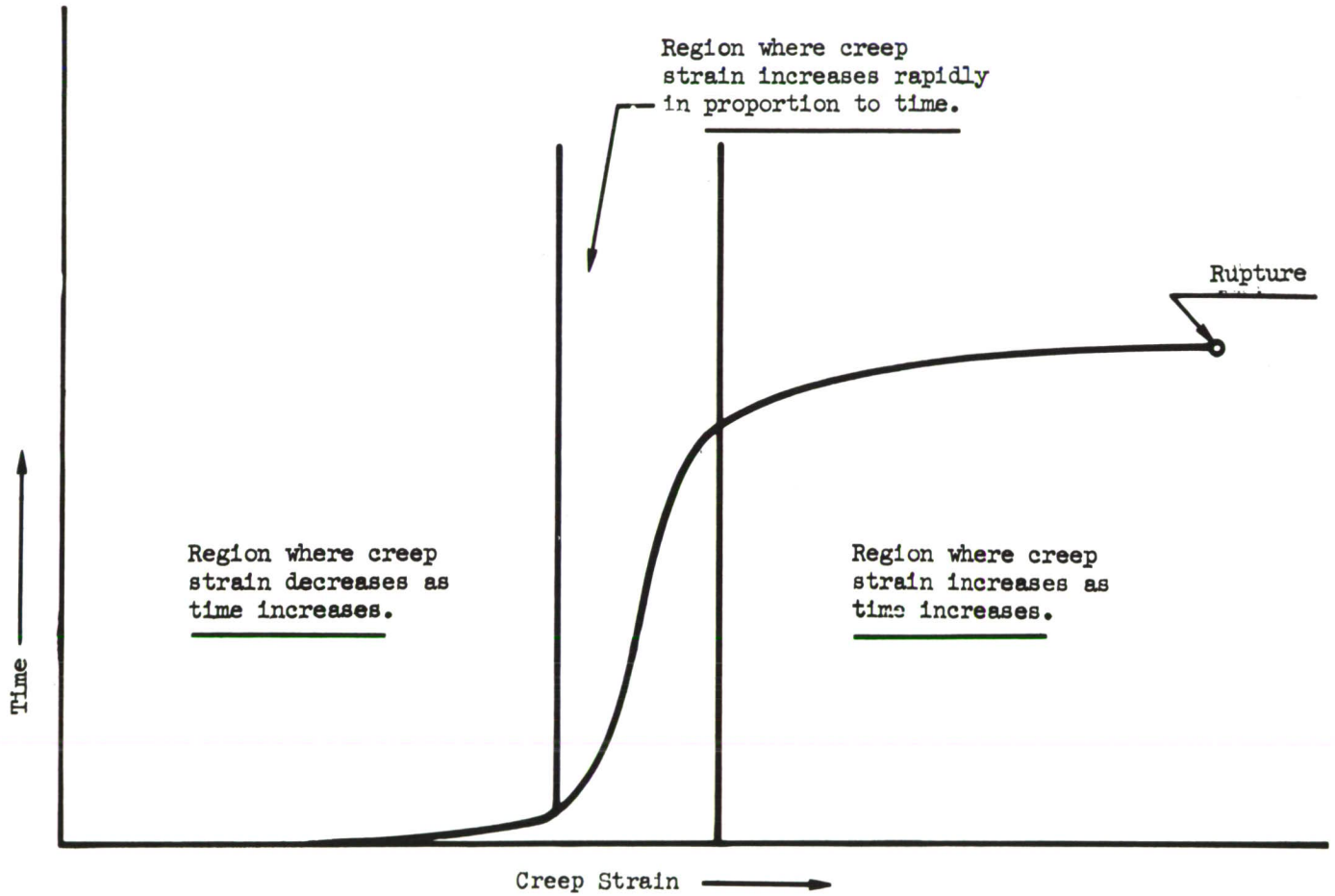


Figure 35. Schematic Creep Time versus Creep Strain Plot

Figure 36. Schematic Rupture Time Fraction versus Creep Strain Plot

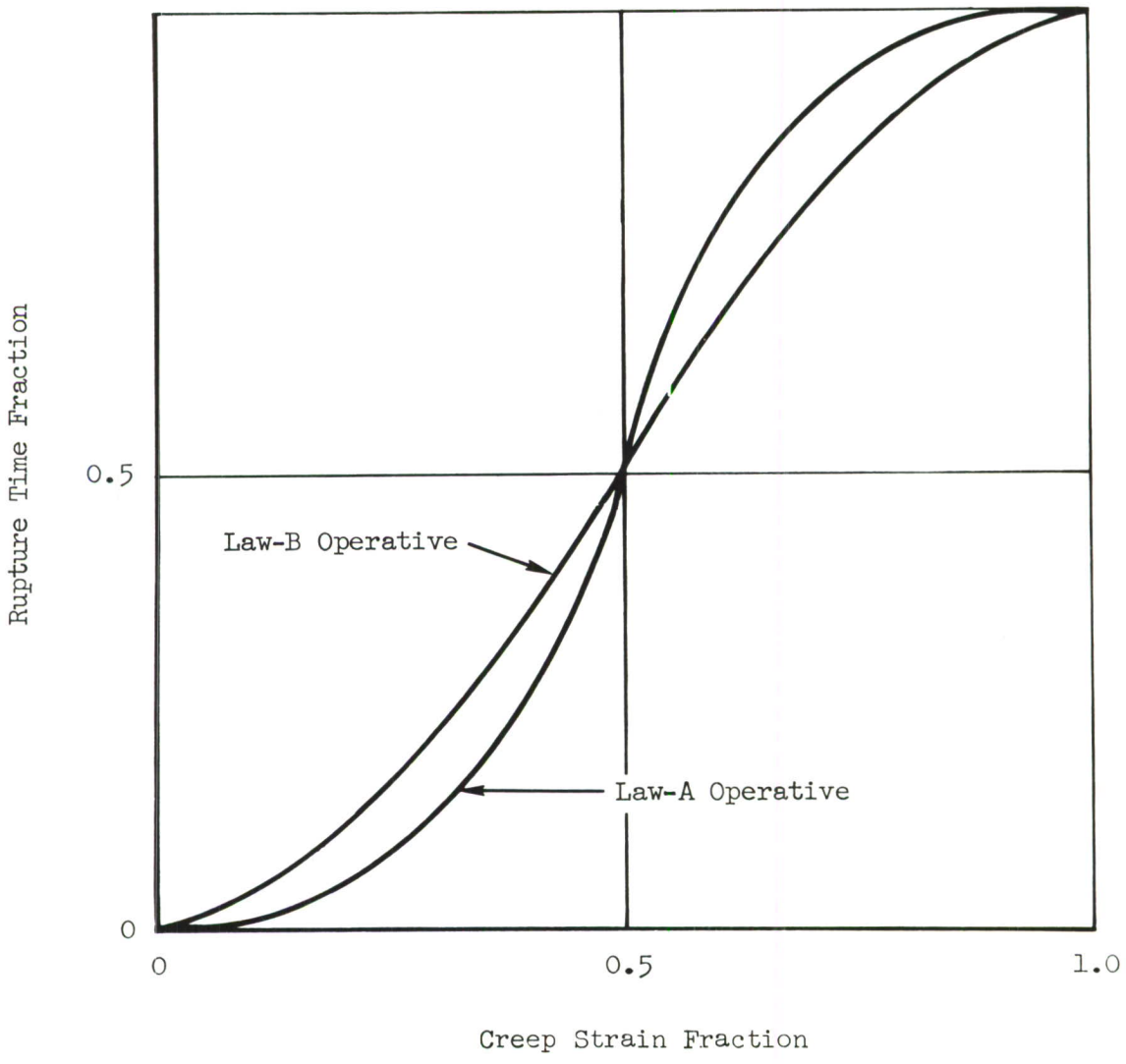


Figure 37. Non-Dimensional Creep Curves (Schematic)

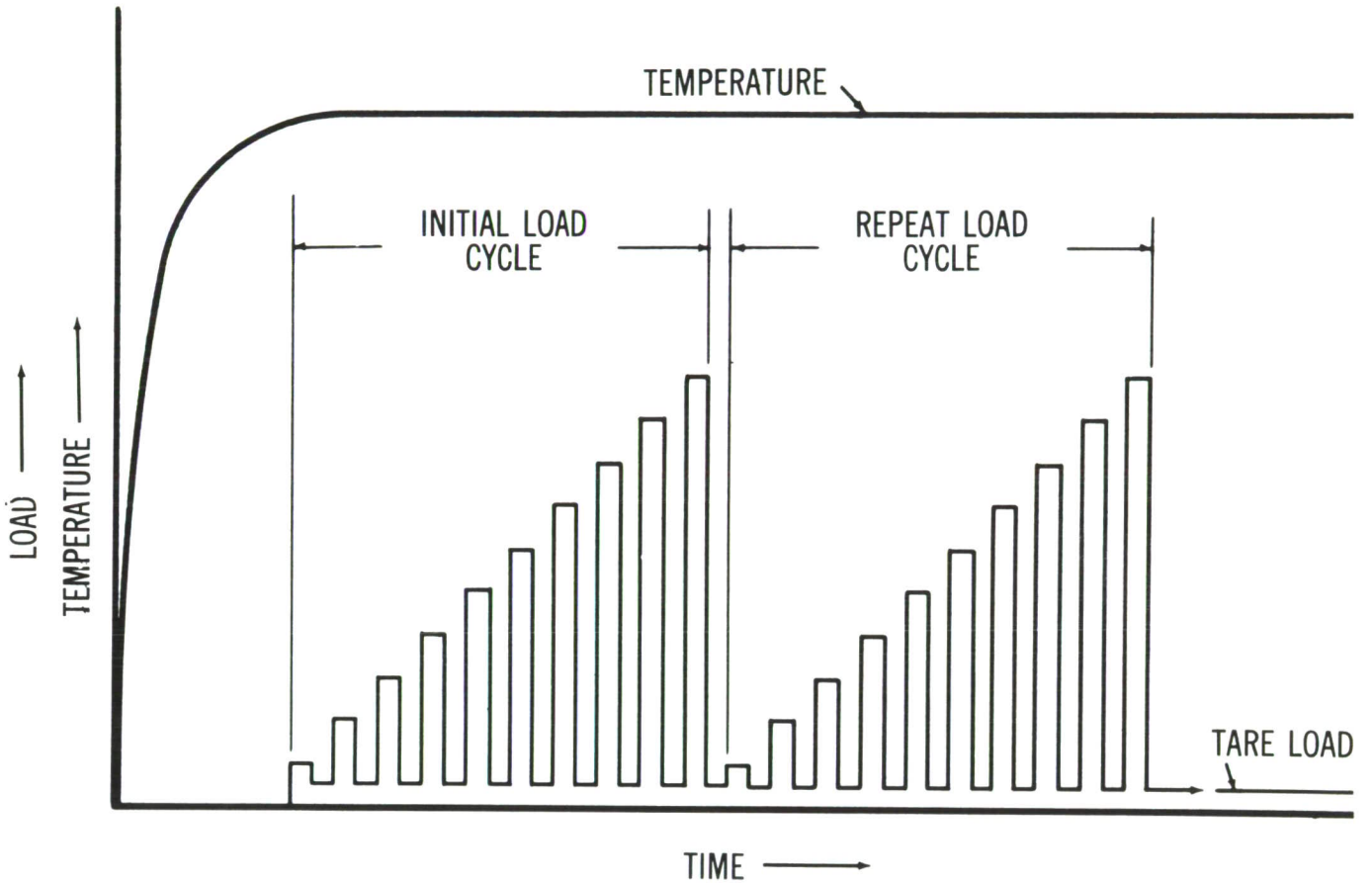


Figure 38. Program for Incremental Loading Test (Schematic)

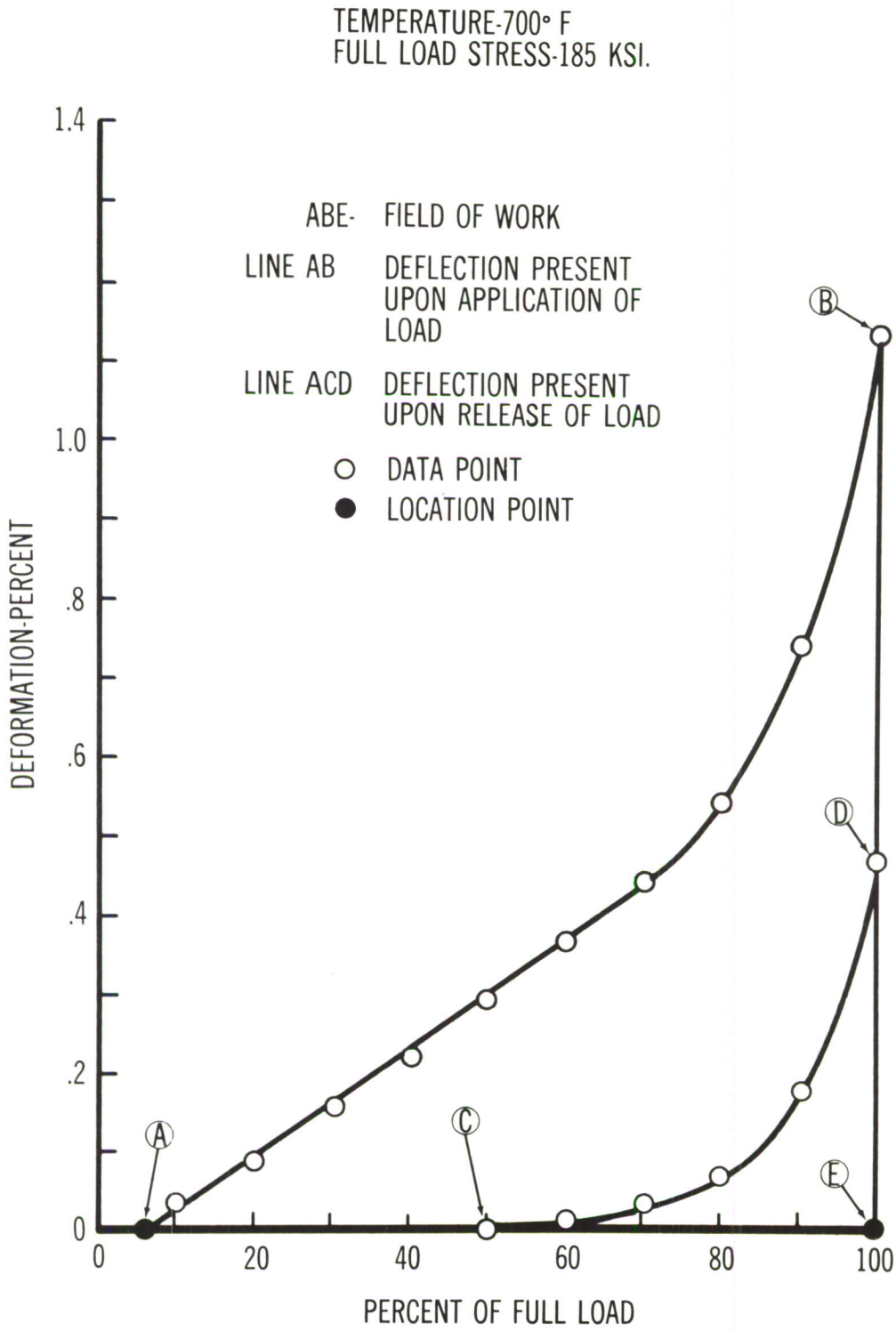


Figure 39. Typical Deformation Activity upon Incremental Loading Armco PH 15-7 Mo at Elevated Temperature

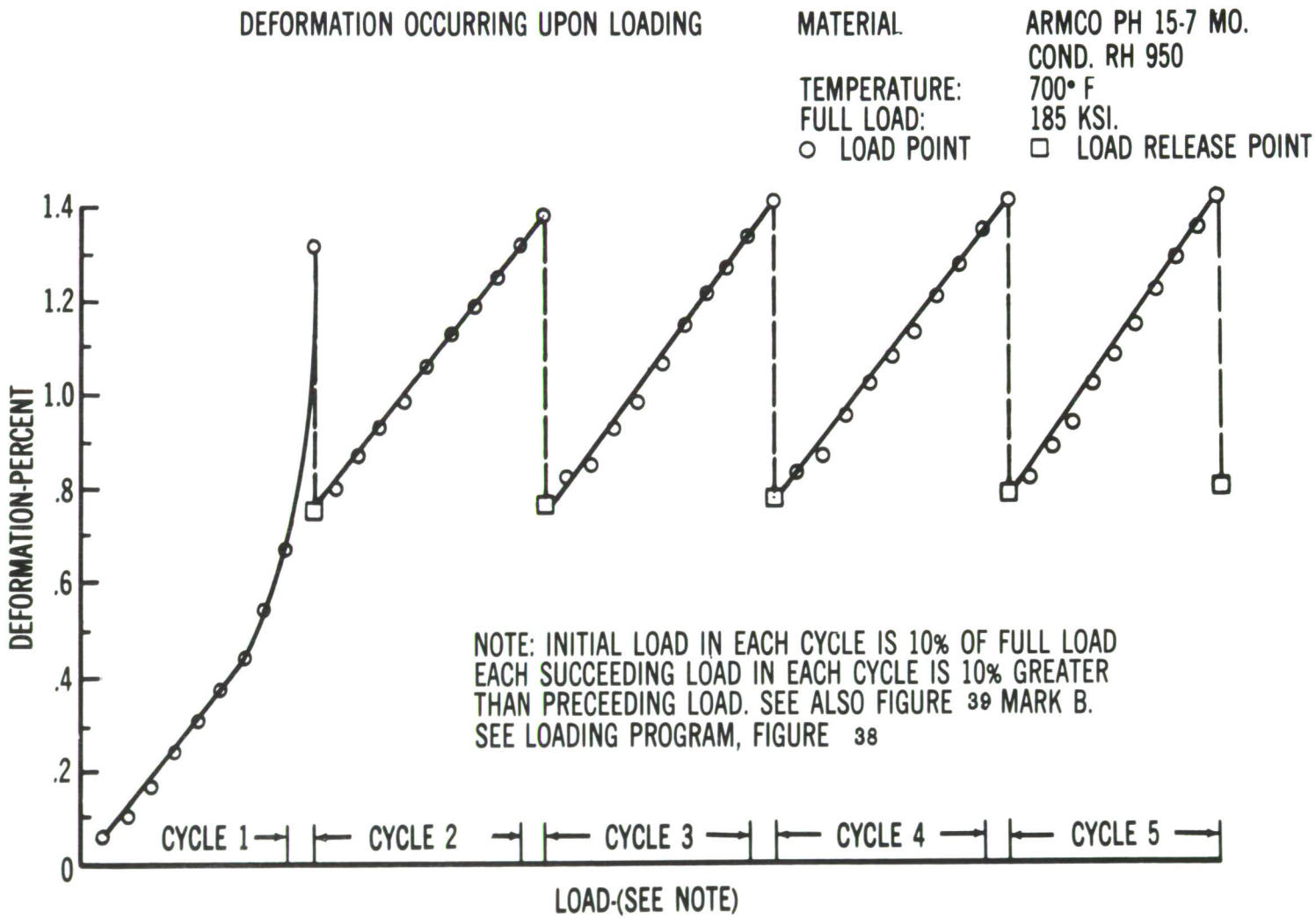


Figure 40. Time-Deformation Data, Incremental Loading Armco PH 15-7 Mo.

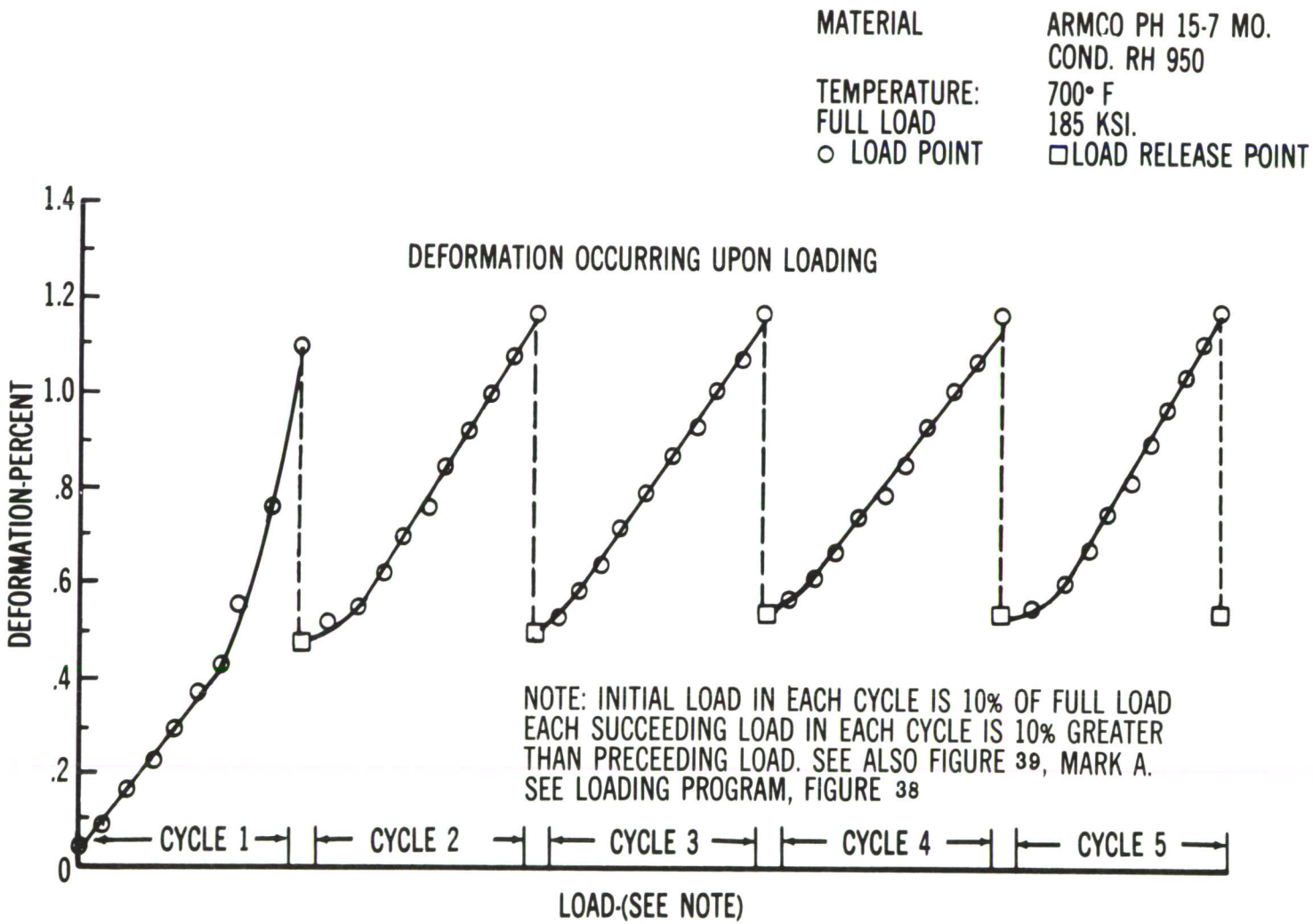
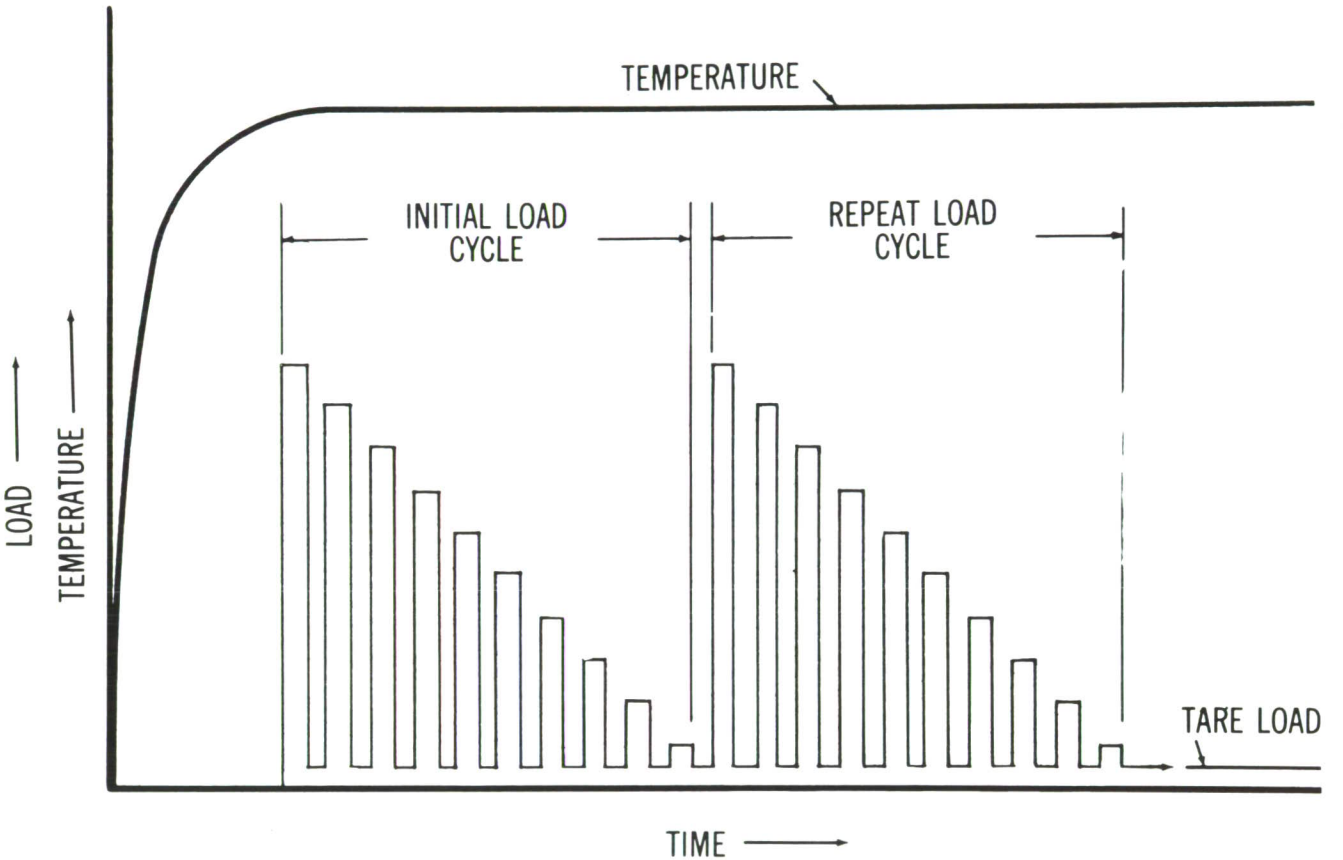


Figure 41. Time-Deformation Data, Armco PH 15-7 Mo, Incremental Loading.



CONDITION OF TEST: CONSTANT TEMPERATURE AND INTERRUPTED INCREMENTAL TRANSIENT LOAD CYCLE SEQUENCE

Figure 42. Program for Decremental Loading Test.

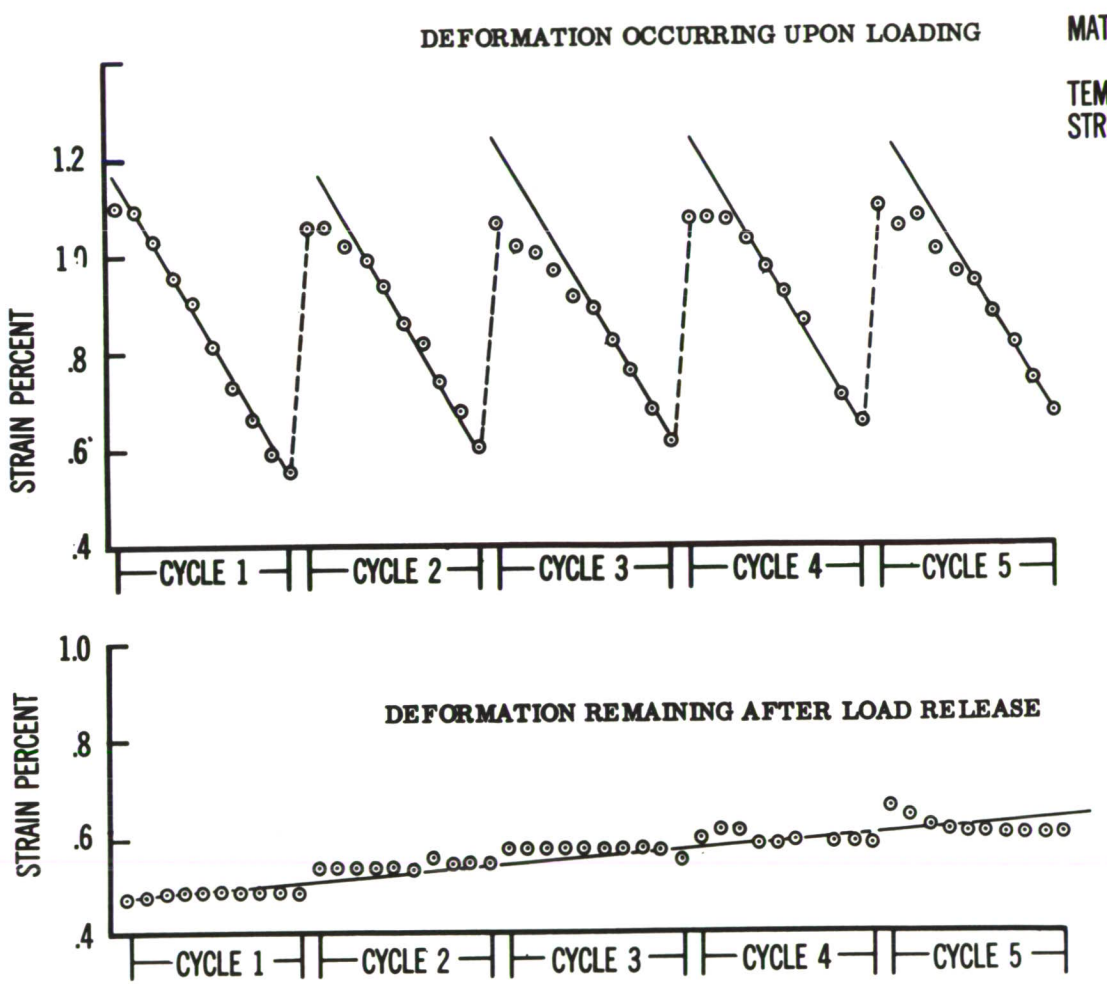


Figure 43. Time-Deformation Data, Decremental Loading Armco PH 15-7 Mo, 700°F,

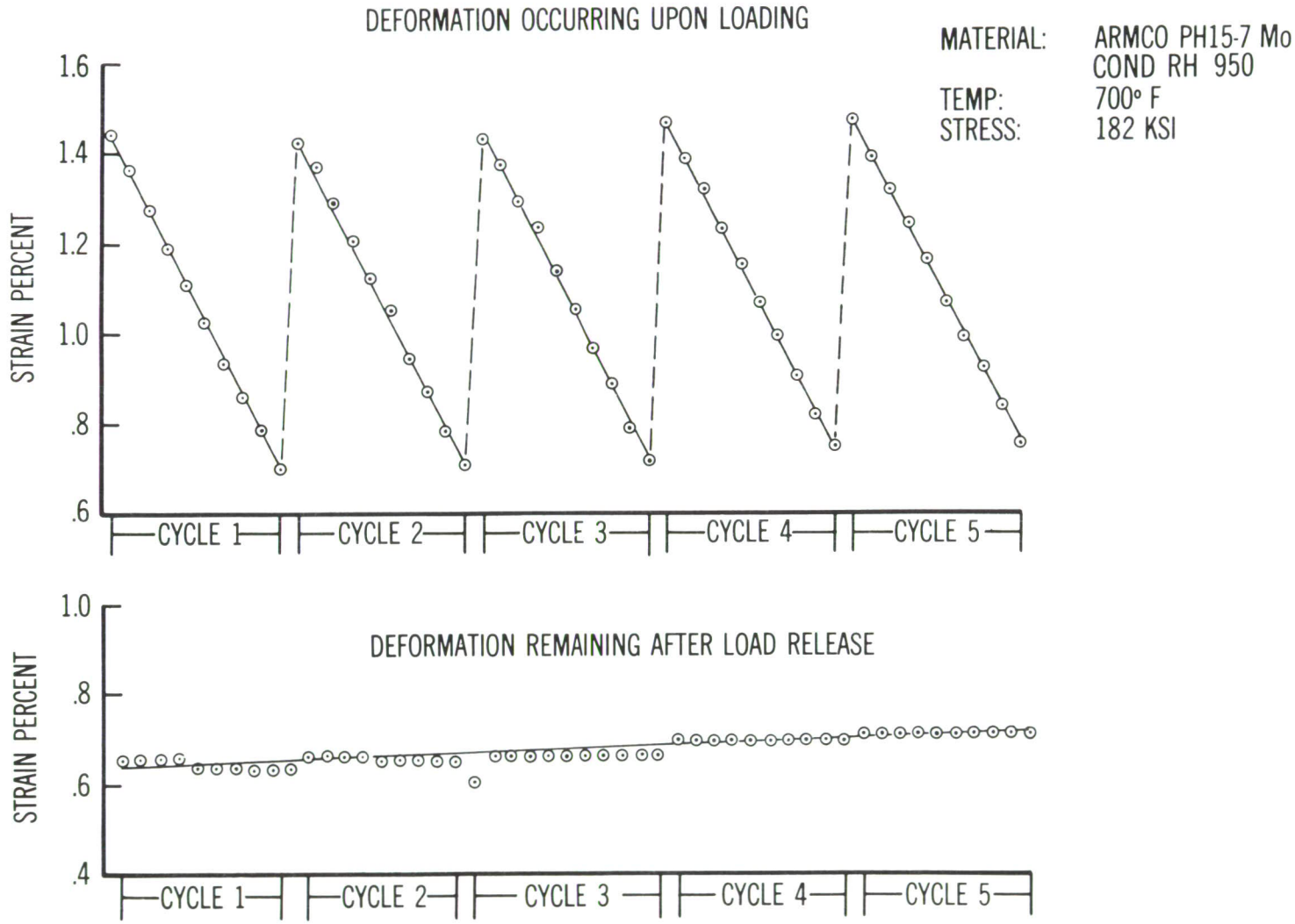


Figure 44. Time-Deformation Data, Decremental Loading Armco PH 15-7 Mo, 700°F.

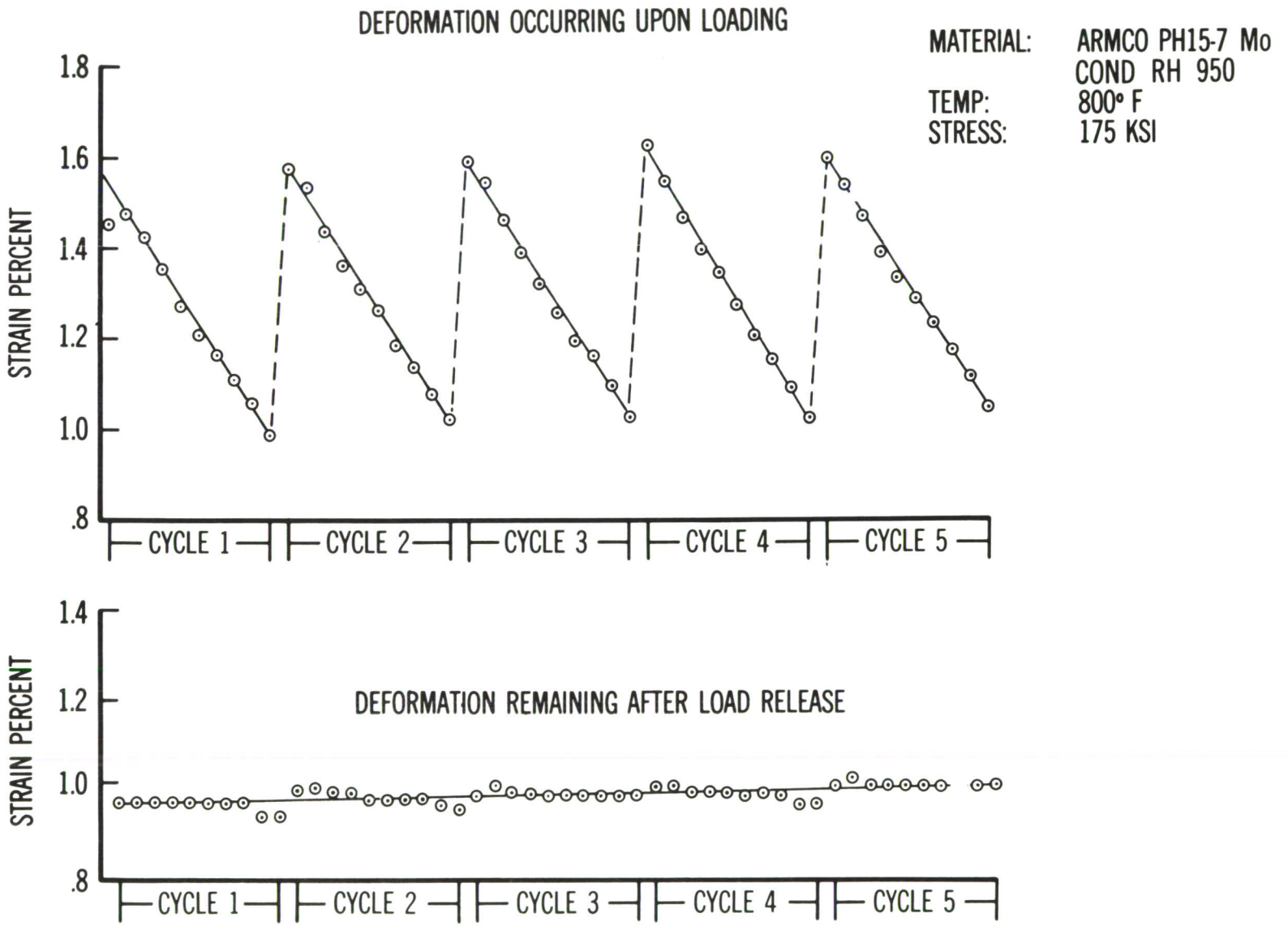


Figure 45. Time-Deformation Data, Decremental Loading Armco PH 15-7 Mo, 800°F.

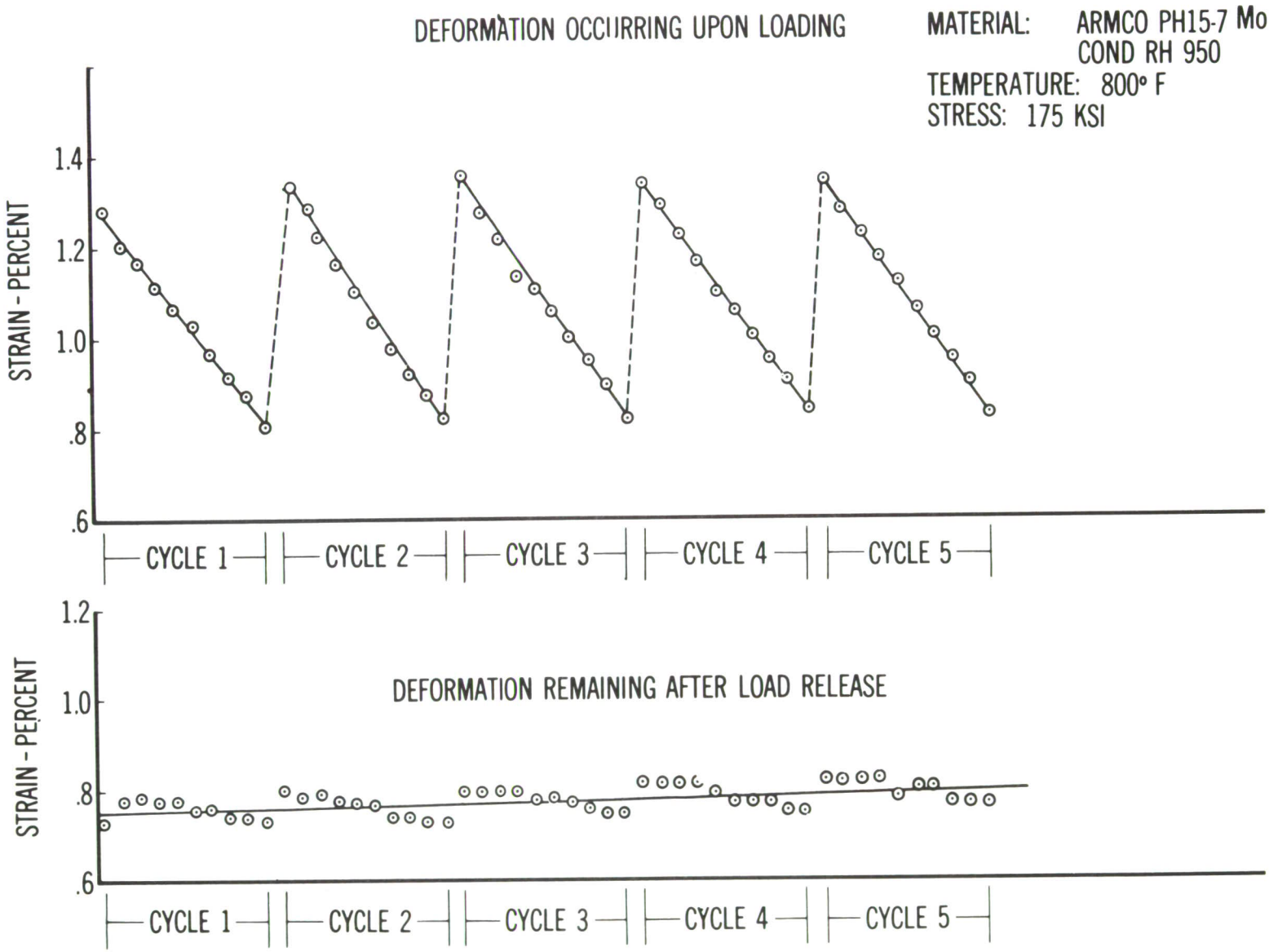


Figure 46. Time-Deformation Data, Decremental Loading Armco PH 15-7 Mo, 800°F.

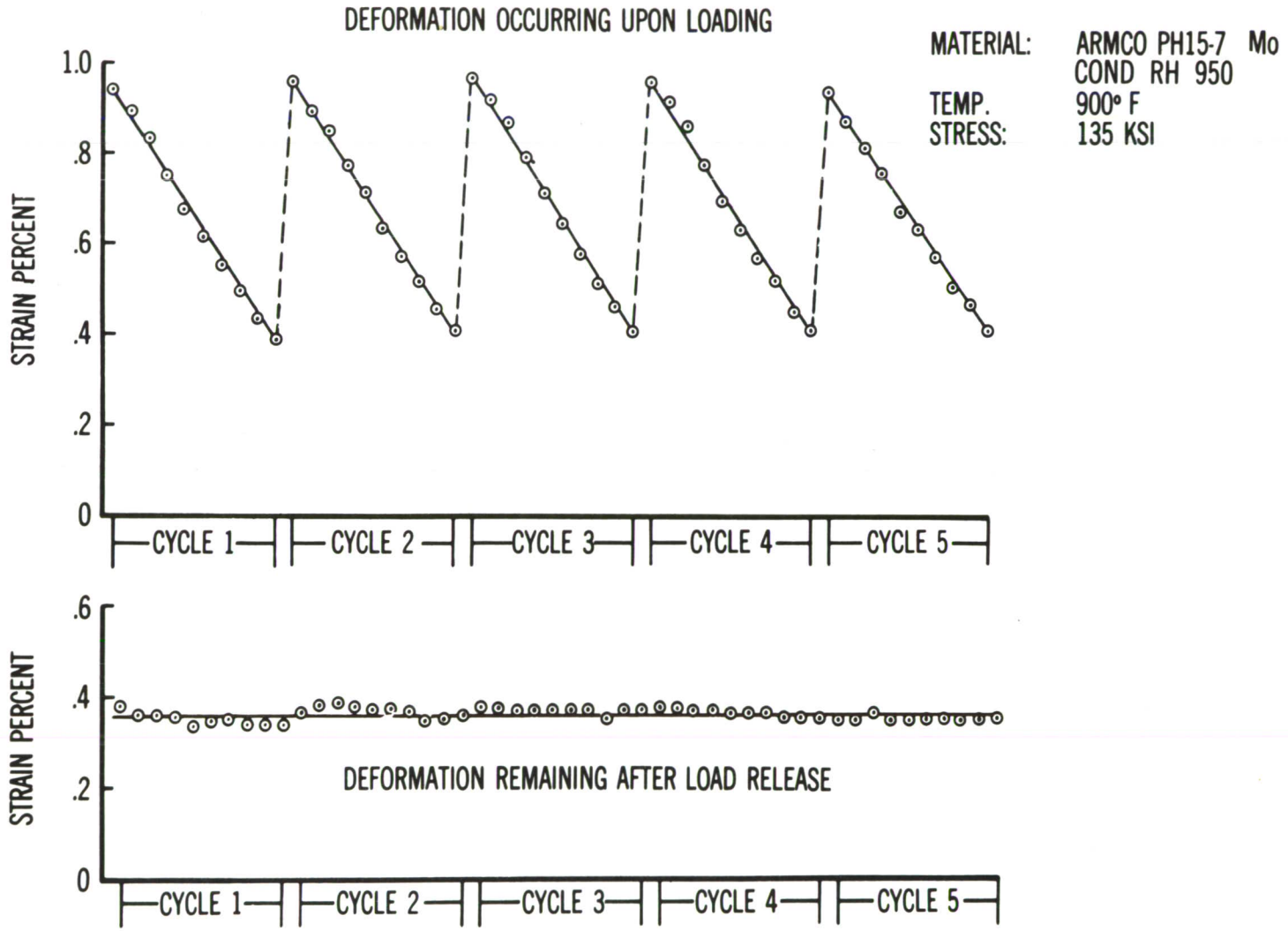


Figure 47. Time-Deformation Data, Decremental Loading Armco PH 15-7 Mo, 900°F.

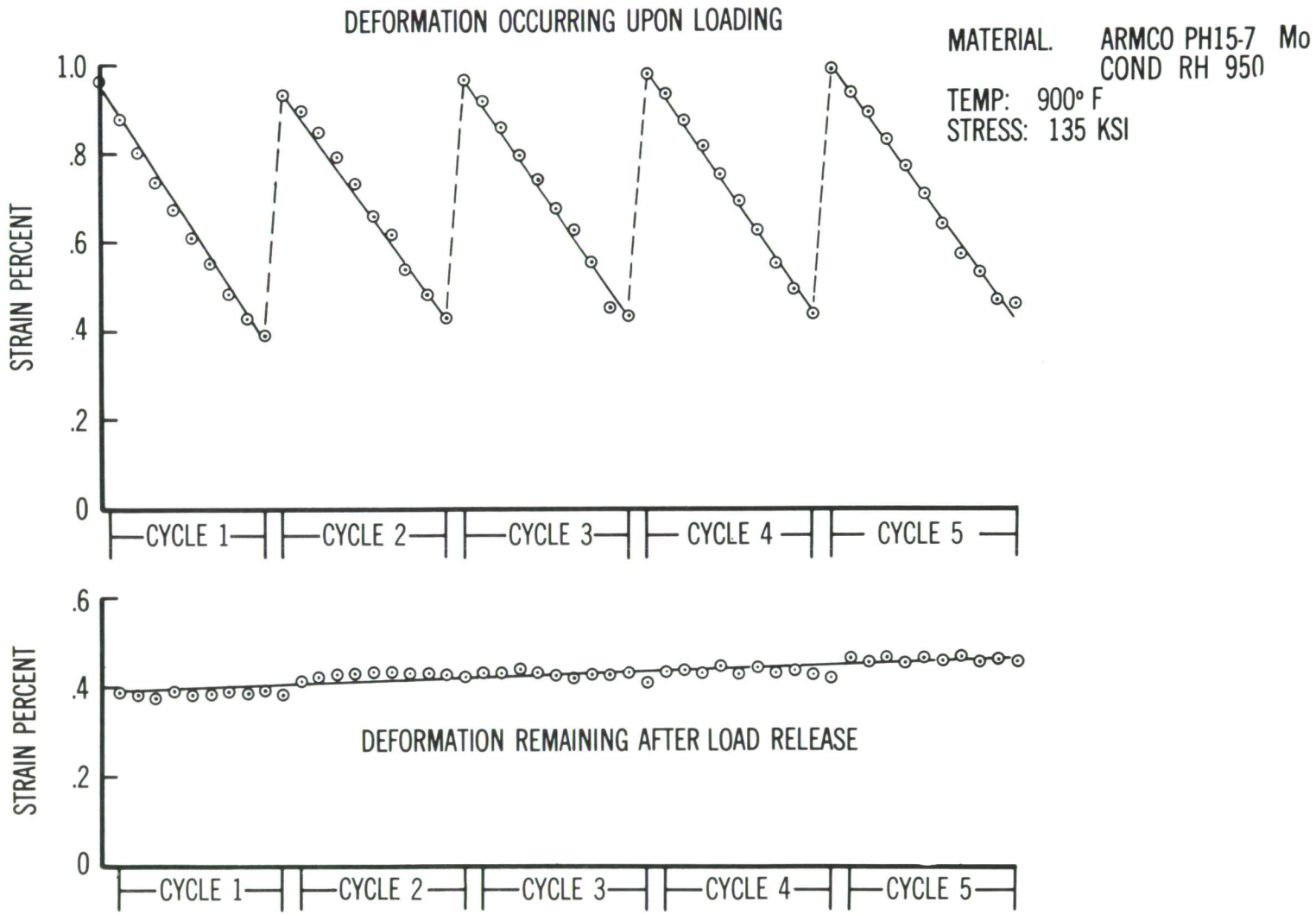


Figure 48. Time-Deformation Data, Decremental Loading Armco PH 15-7 Mo, 900°F.

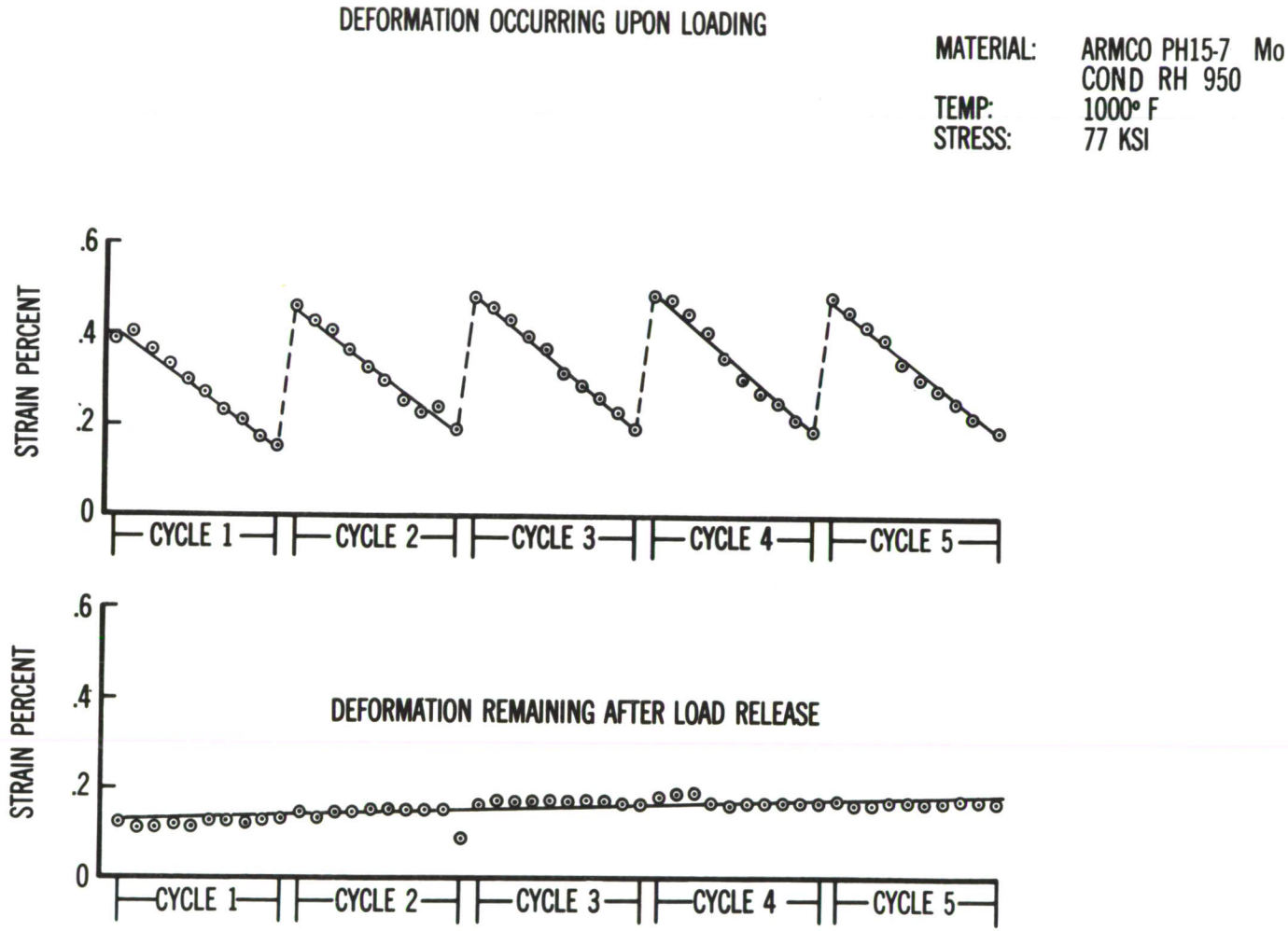


Figure 49. Time-Deformation Data, Decremental Loading Armco PH 15-7 Mo, 1000°F

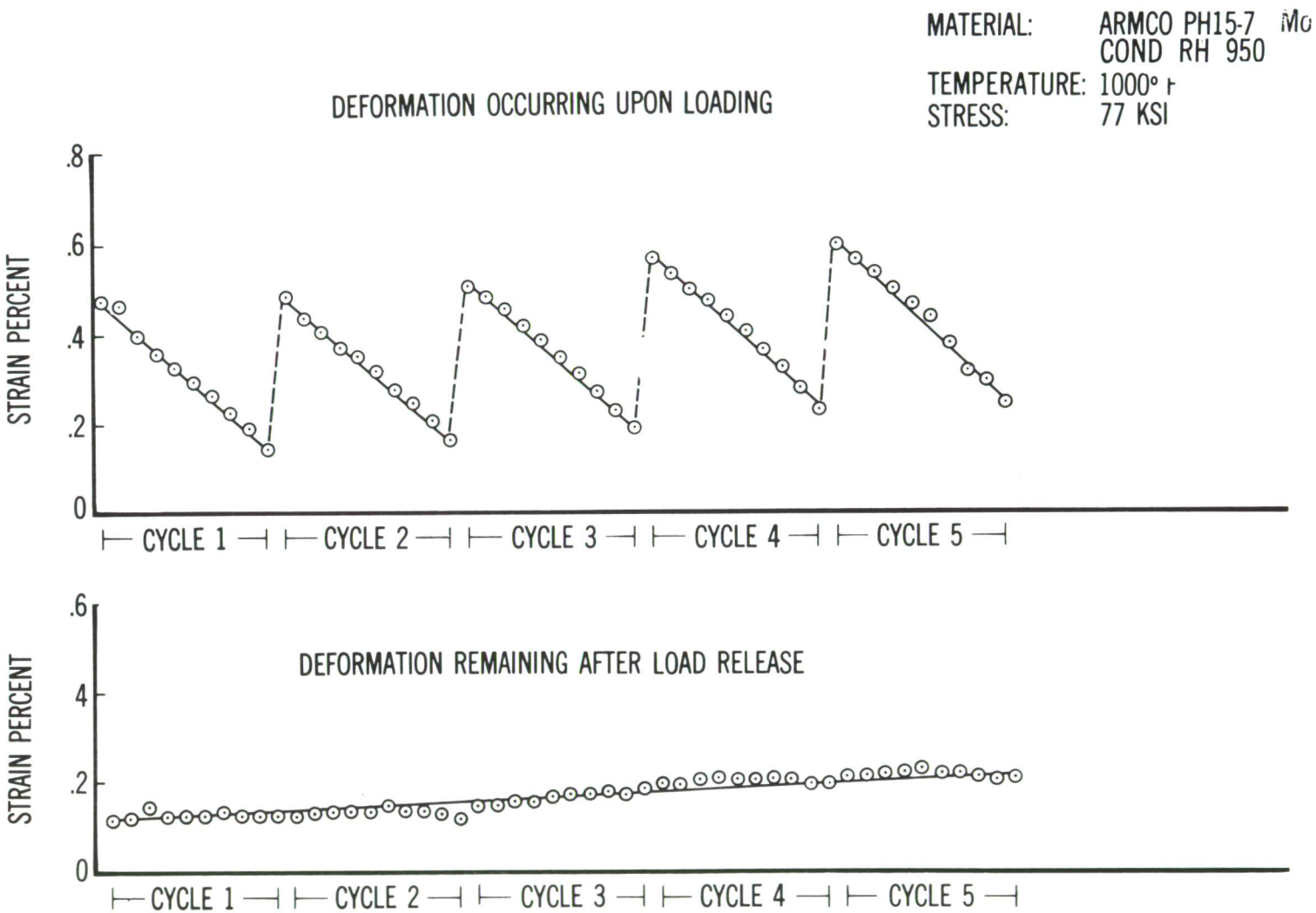


Figure 50. Time-Deformation Data, Decremental Loading Armco PH 15-7 Mo, 1000°F.

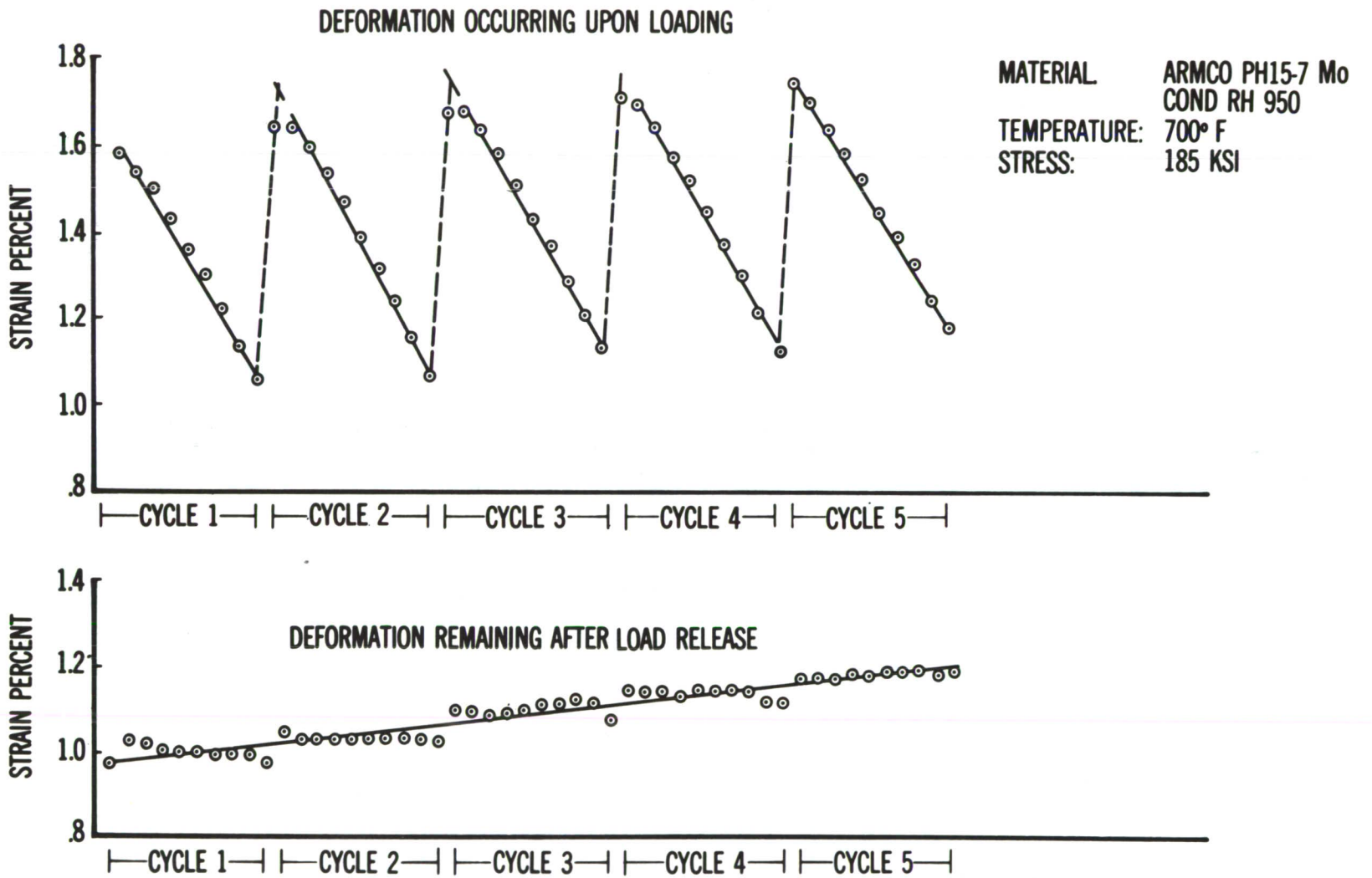


Figure 51. Time-Deformation Data, Decremental Loading Armco PH 15-7 Mo, 185 KSI.

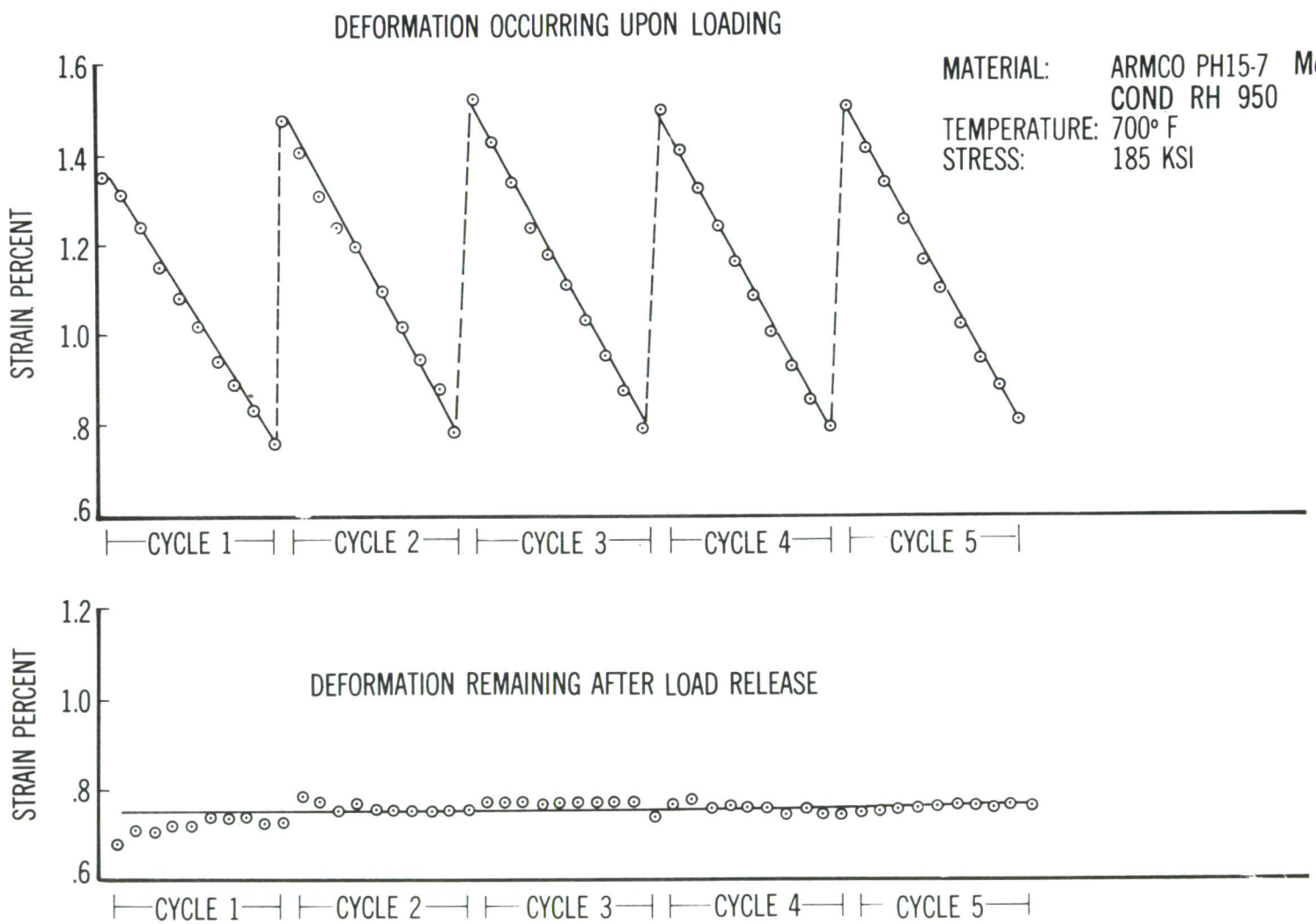


Figure 52. Time-Deformation Data, Decremental Loading Armco PH 15-7 Mo, 185 KSI.

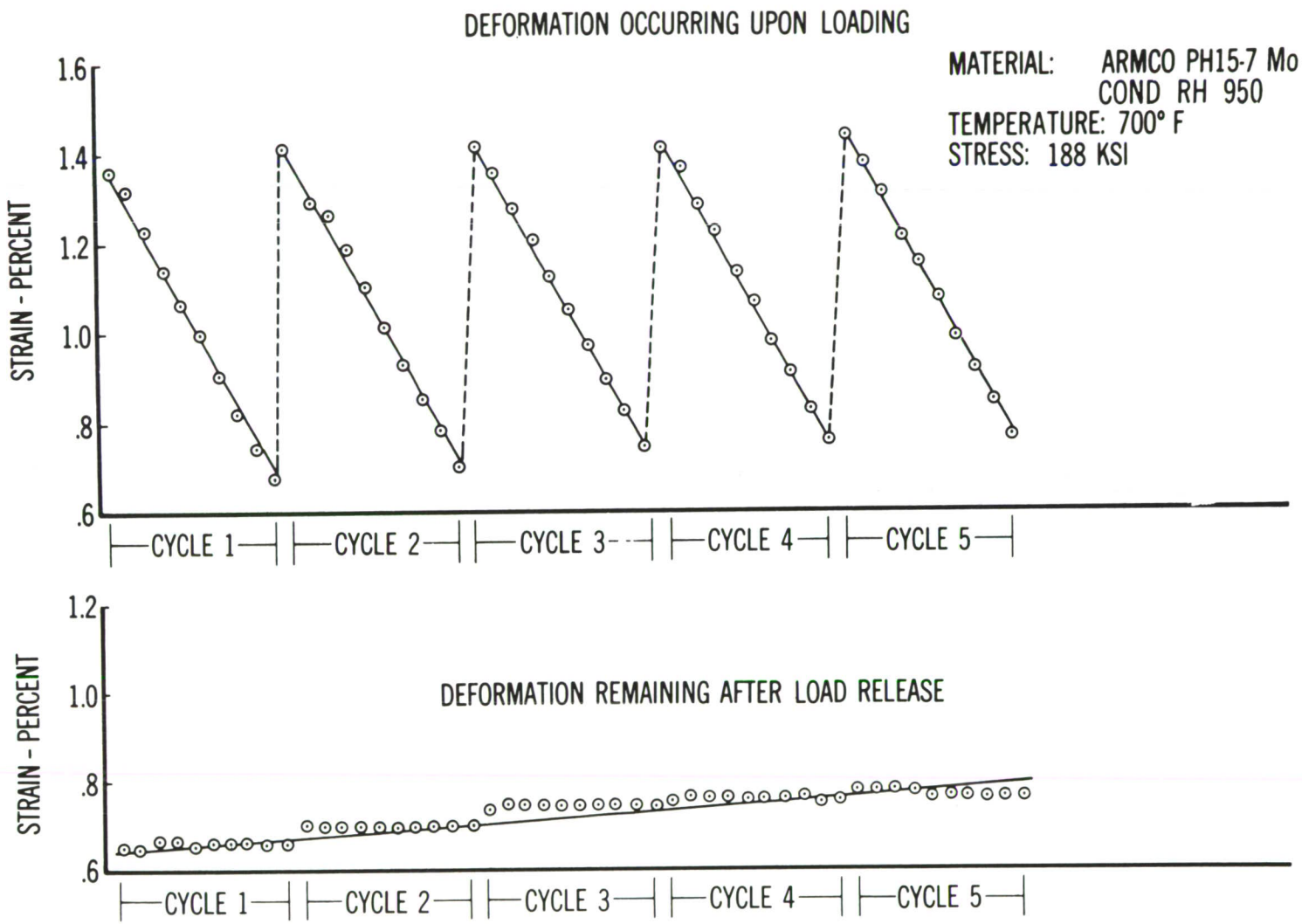


Figure 53. Time-Deformation Data, Decremental Loading Armco PH 15-7 Mo, 188 KSI.

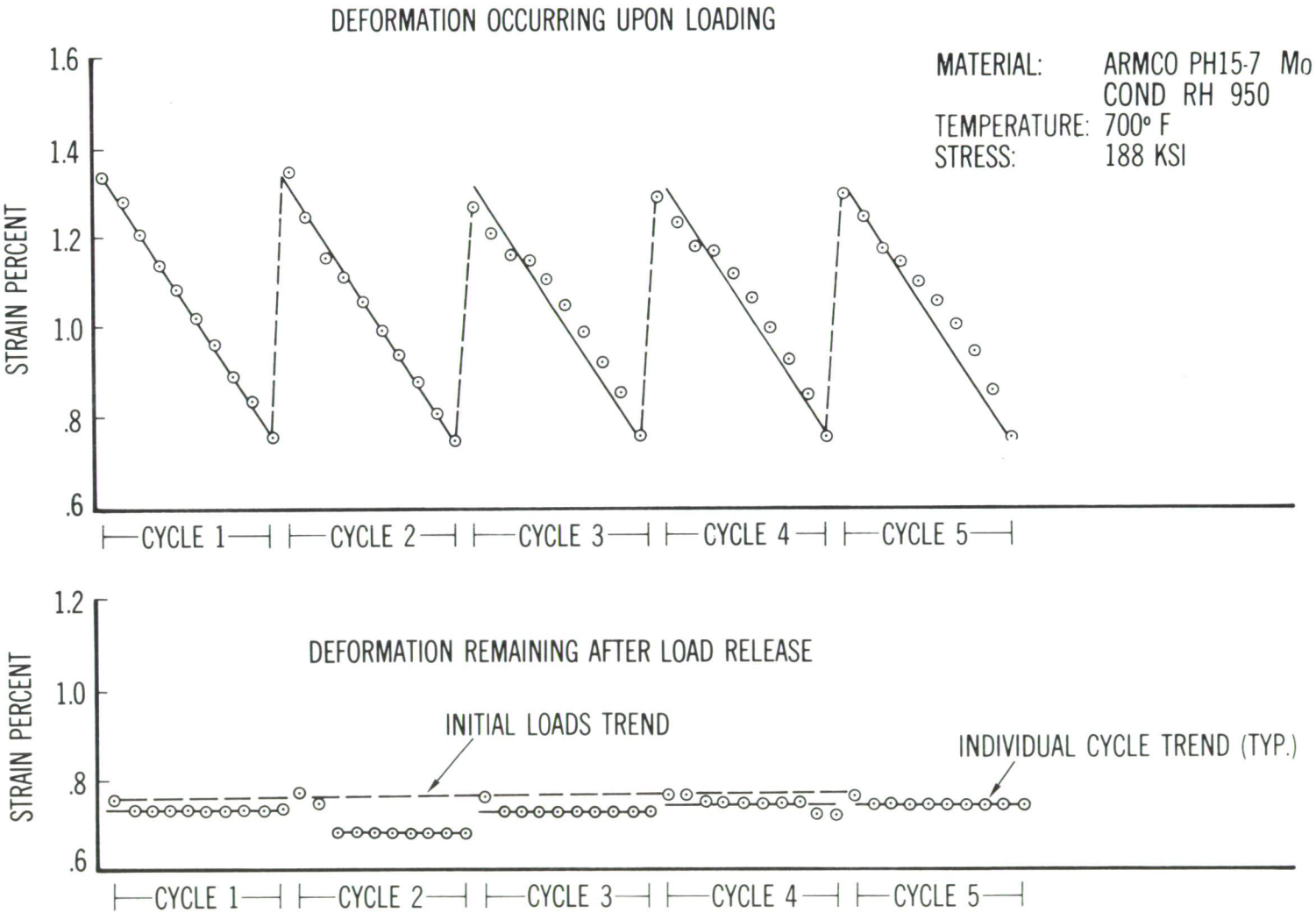


Figure 54. Time-Deformation Data, Decremental Loading Armco PH 15-7 Mo, 188 KSI.

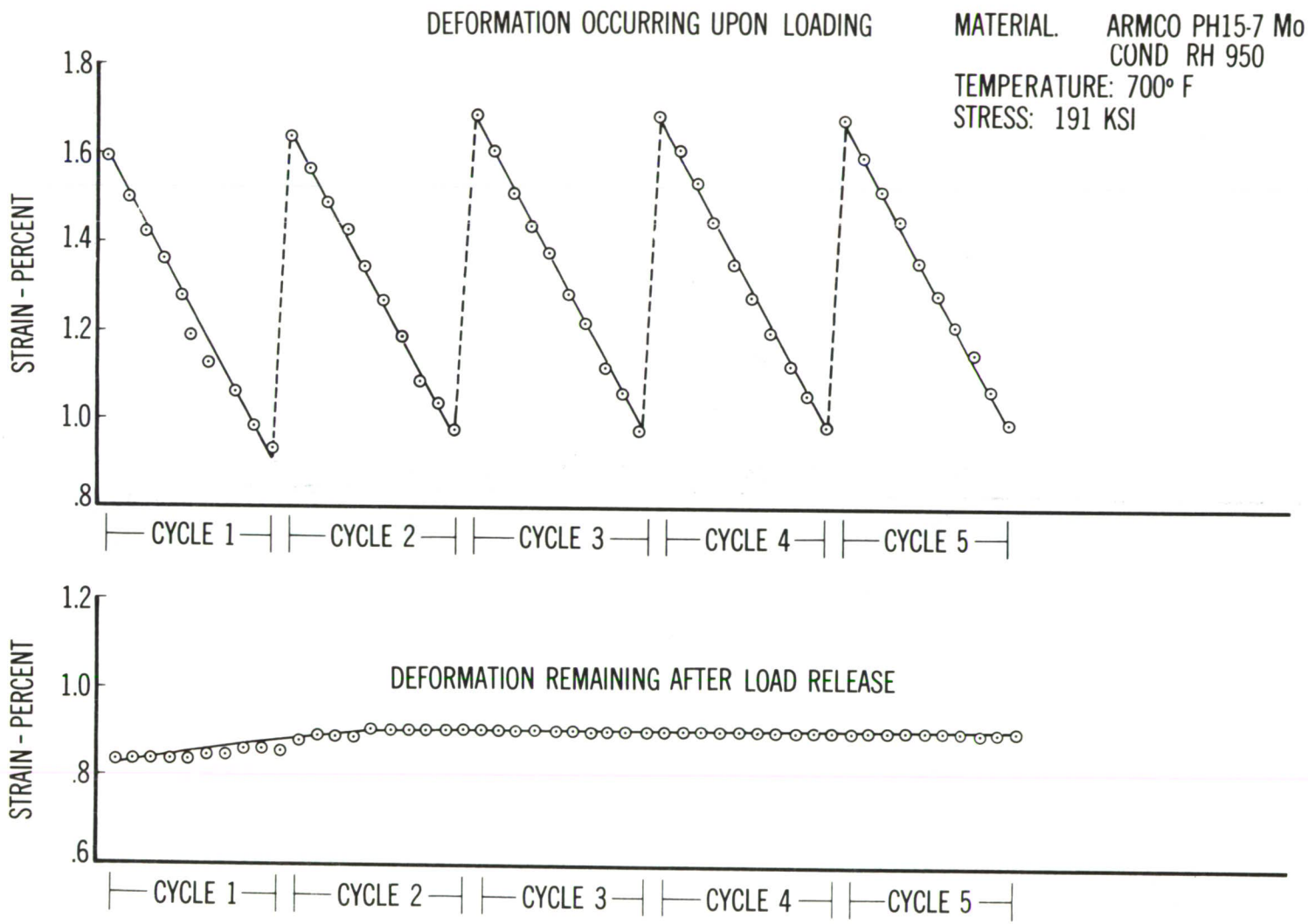


Figure 55 Time Deformation Data, Decremental Loading Armco PH 15-7 Mo, 191 KSI.

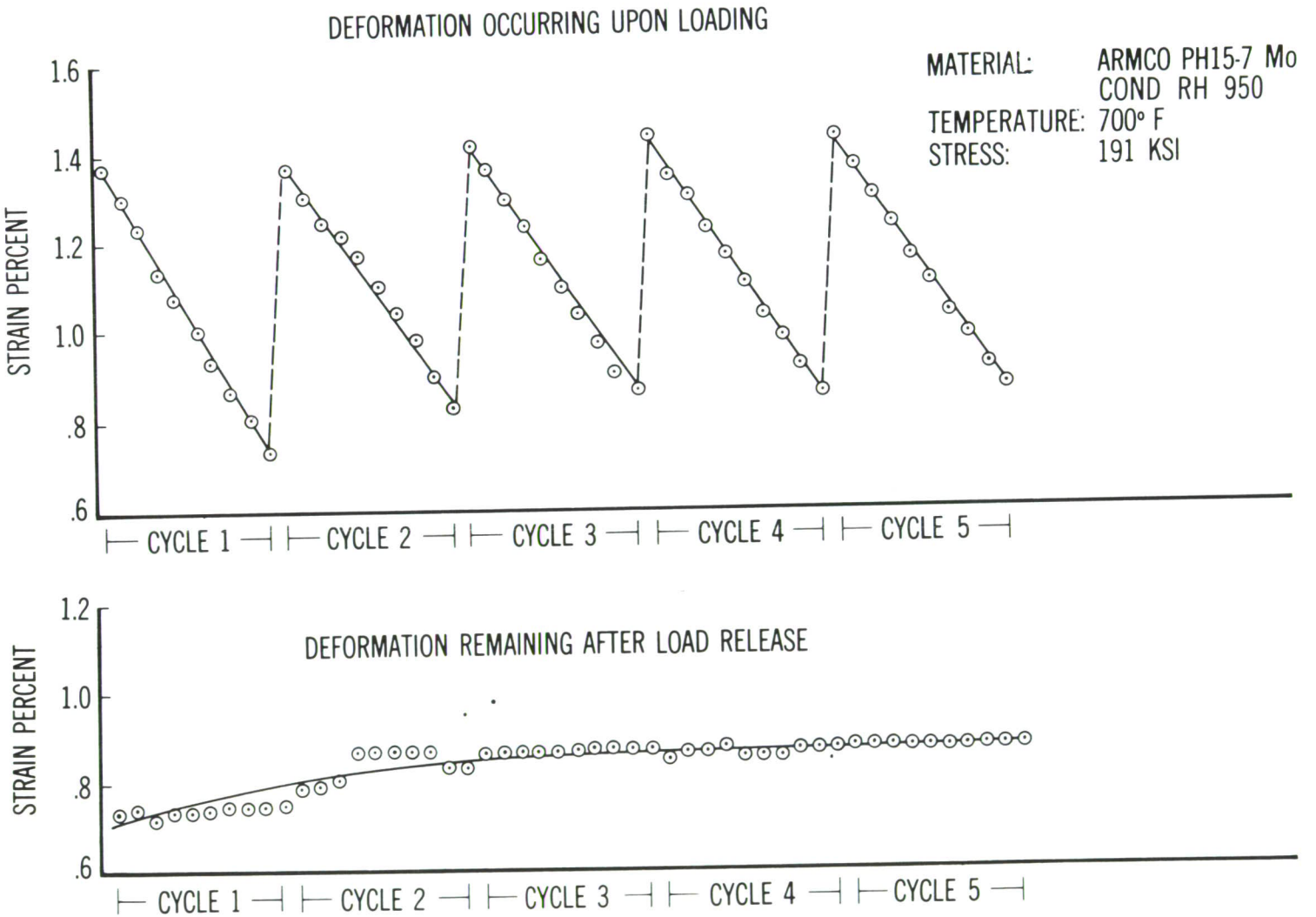
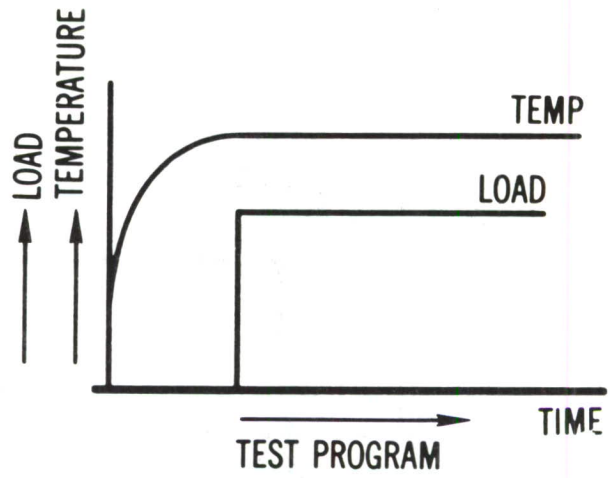


Figure 56. Time-Deformation Data, Decremental Loading Armco PH 15-7 Mo, 191 KSI.



MATERIAL: ARMCO PH 15-7 Mo COND RH 950
TEMPERATURE: 700° F
LOAD: 105 KSI.

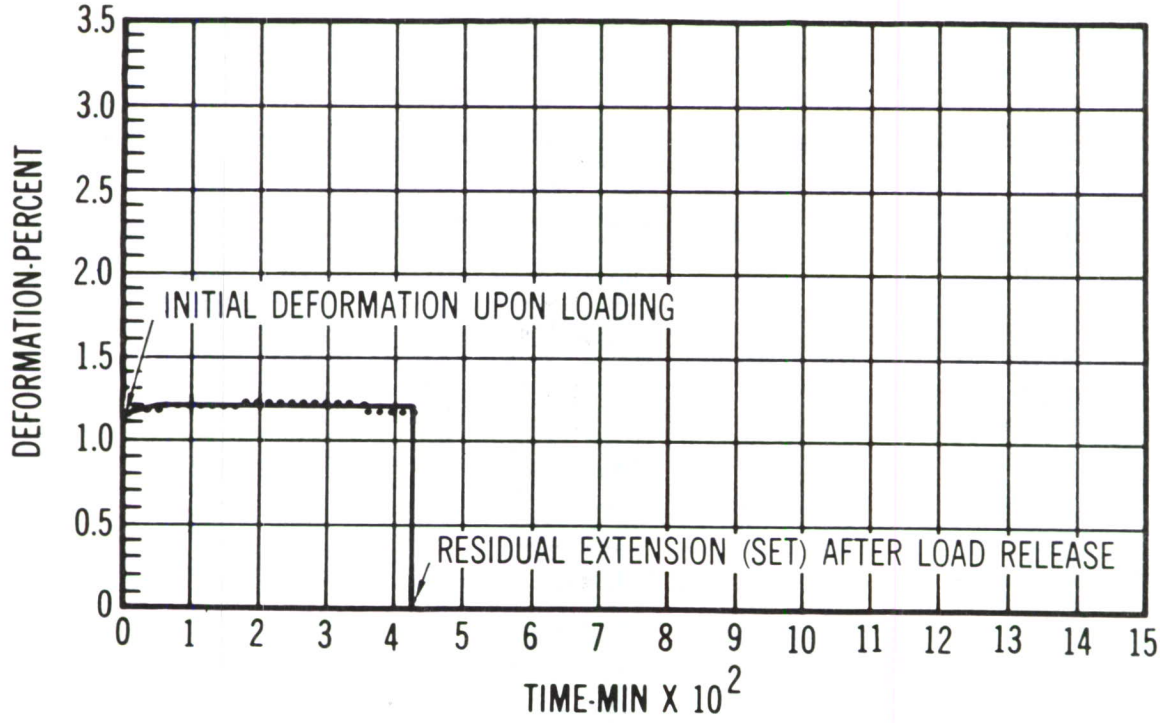
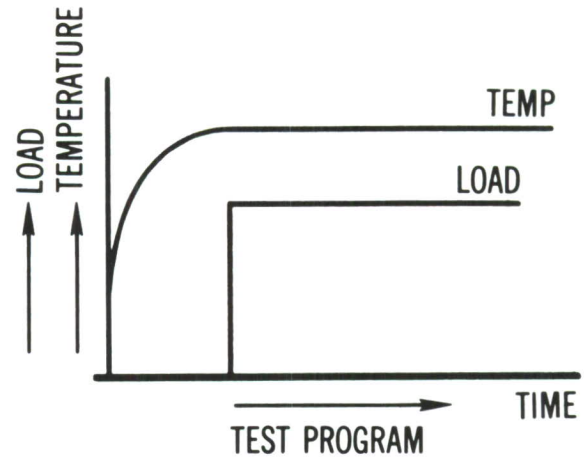


Figure 57. Time-Deformation Data, "Standard" Creep Test Armco PH 15-7 Mo, 700°F.



MATERIAL: ARMCO PH 15-7 Mo COND RH 950
TEMPERATURE: 700° F
LOAD: 105 KSI.

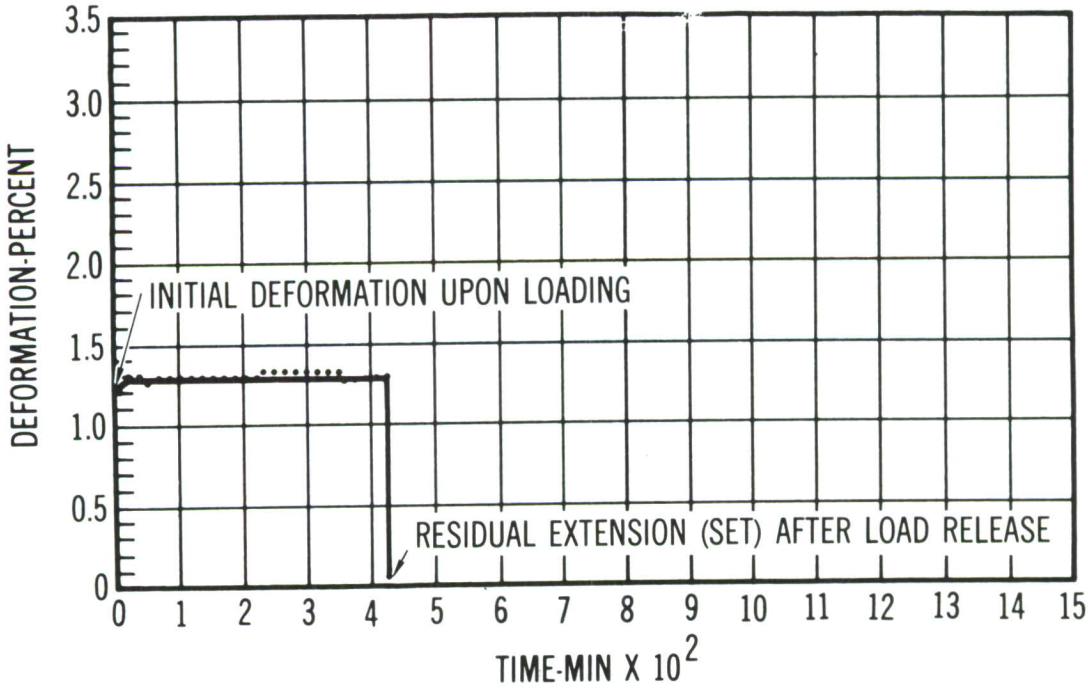
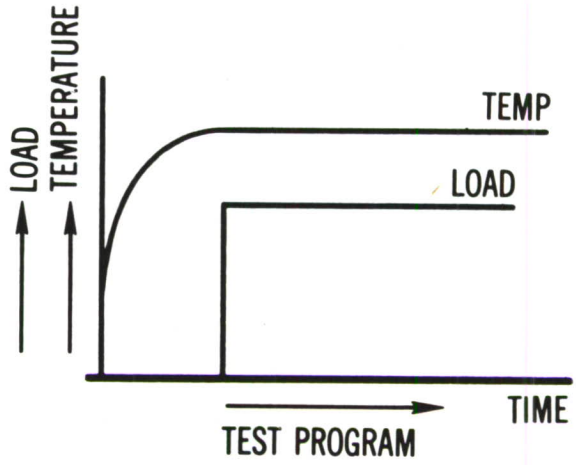


Figure 58. Time-Deformation Data, "Standard" Creep Test Armco PH 15-7 Mo, 700°F.



MATERIAL: ARMCO PH 15-7 Mo COND RH 950
TEMPERATURE: 700° F
LOAD: 112.5 KSI

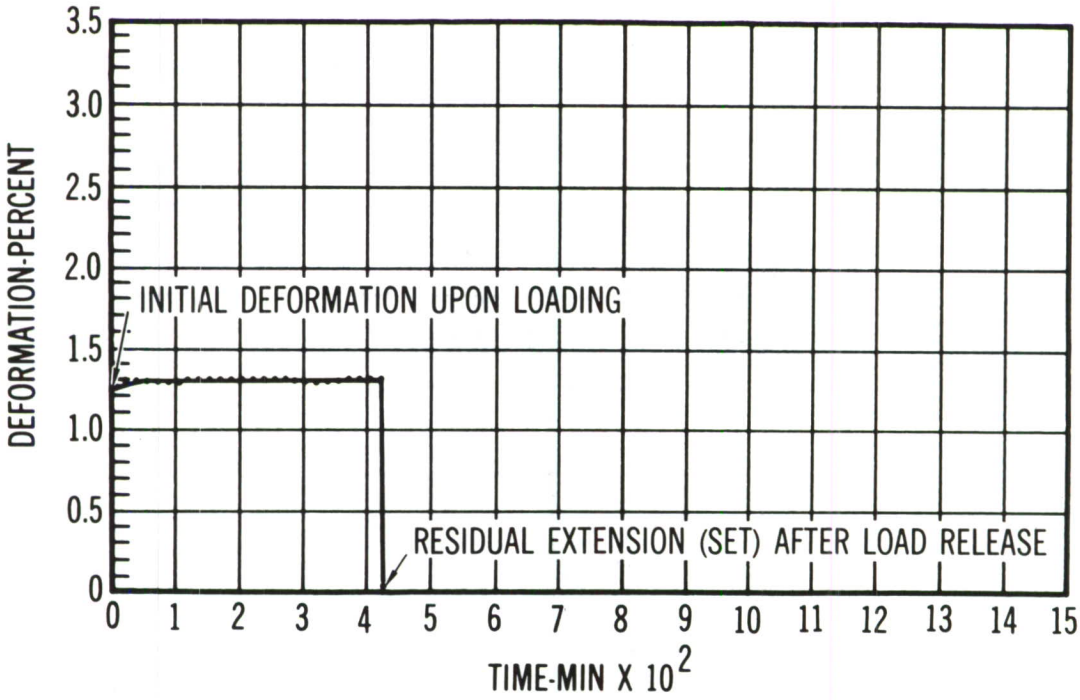
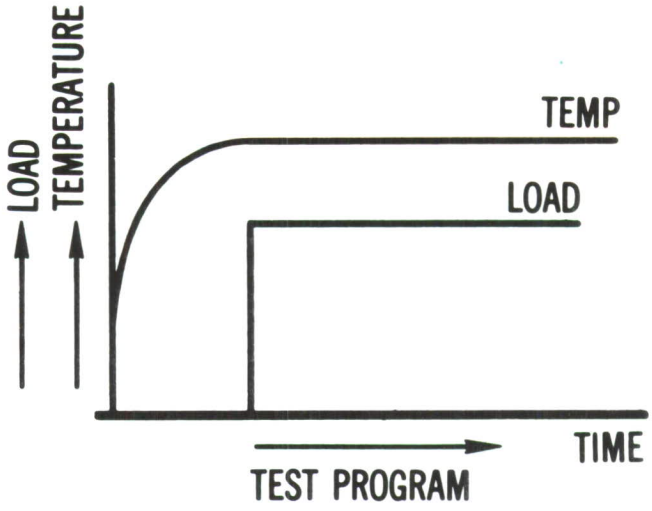


Figure 59. Time-Deformation Data, "Standard" Creep Test Armco PH 15-7 Mo, 700°F.



MATERIAL: ARMCO PH 15-7 Mo COND RH 950
TEMPERATURE: 700° F
LOAD: 112.5 KSI

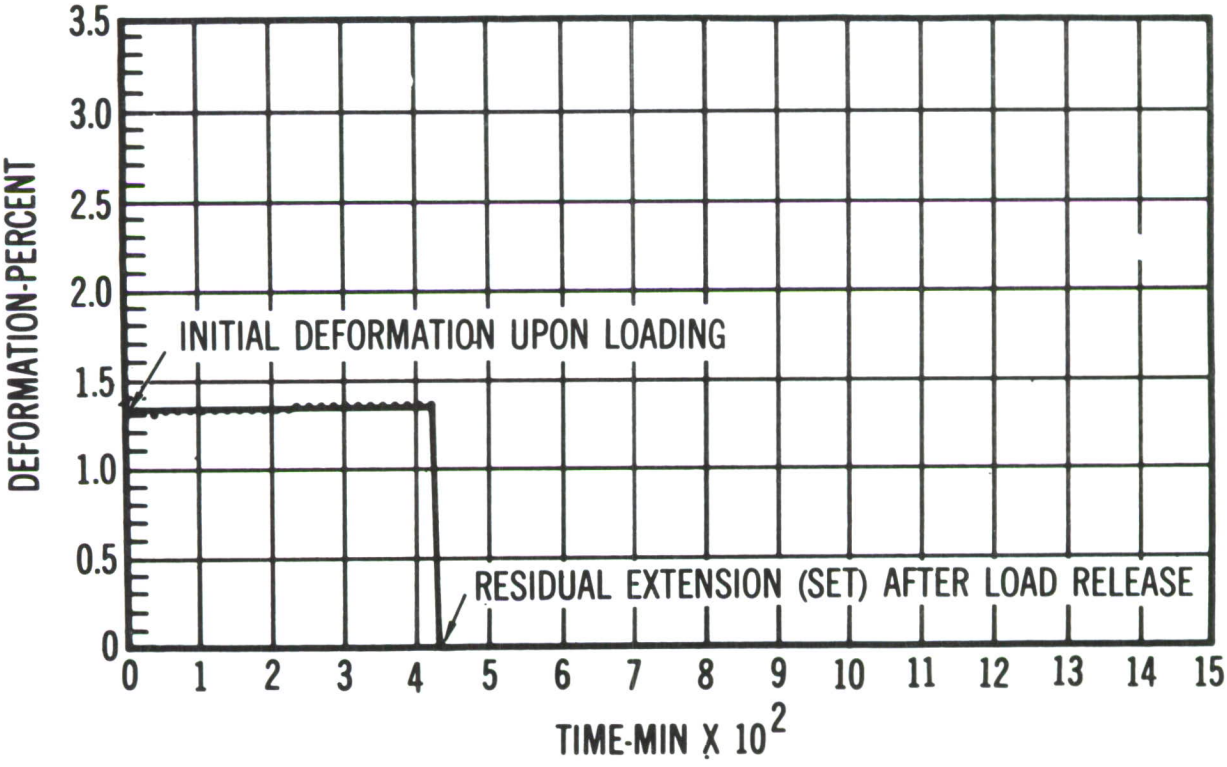
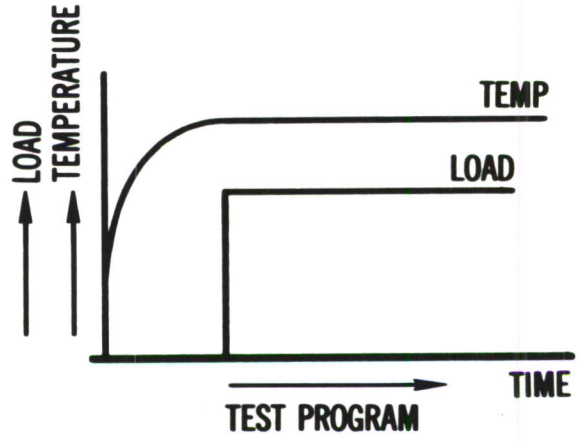


Figure 60. Time-Deformation Data, "Standard" Creep Test Armco PH 15-7 Mo, 700°F.



MATERIAL: ARMCO PH 15-7 Mo COND RH 950
TEMPERATURE: 700° F
LOAD: 180 KSI.

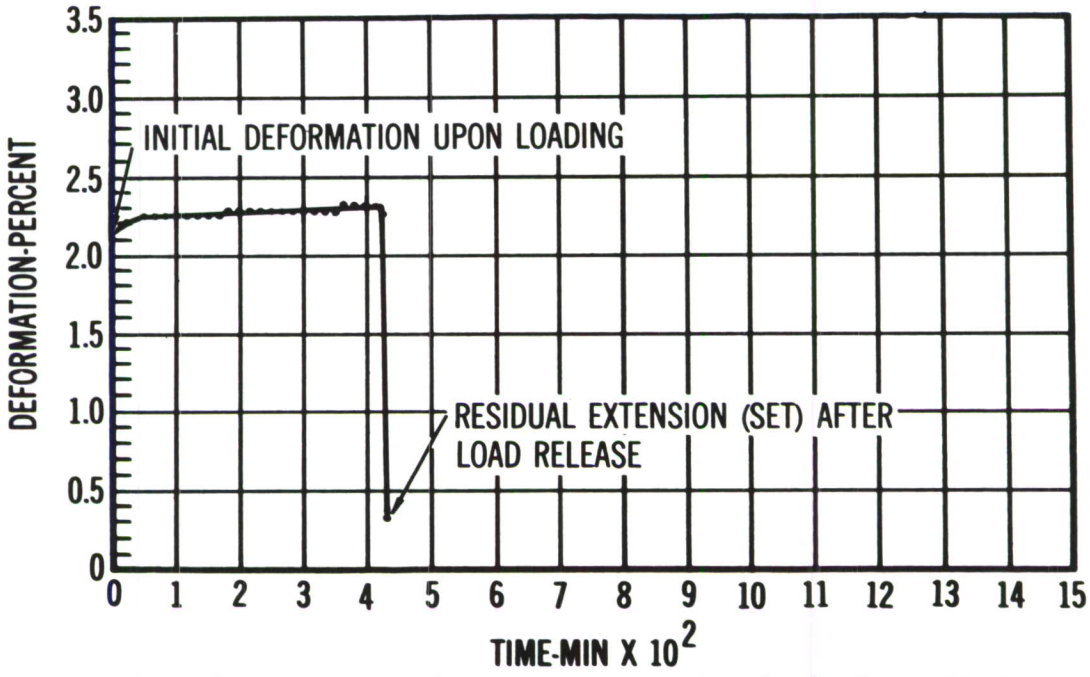
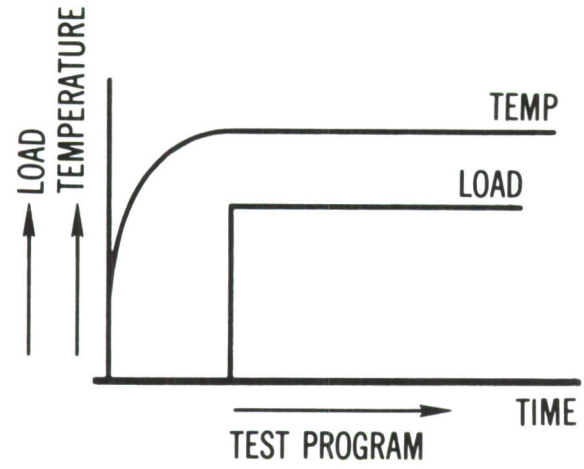


Figure 61. Time-Deformation Data, "Standard" Creep Test Armco PH 15-7 Mo, 700°F.



MATERIAL: ARMCO PH 15-7 Mo COND RH 950
TEMPERATURE: 800° F
LOAD: 80 KSI.

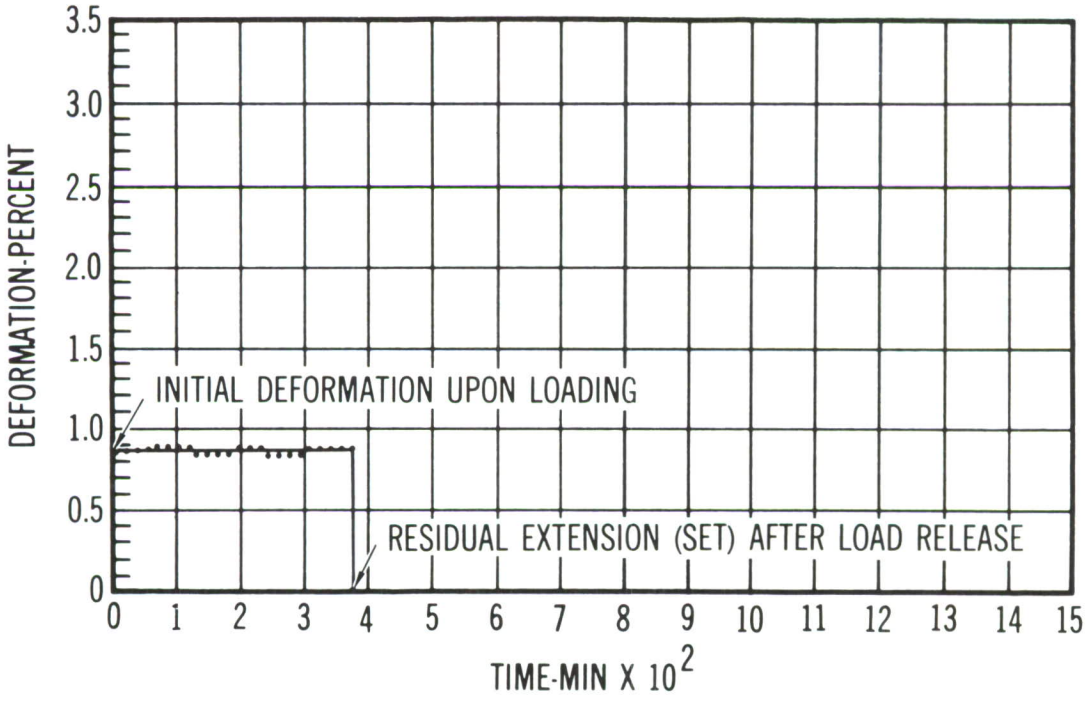
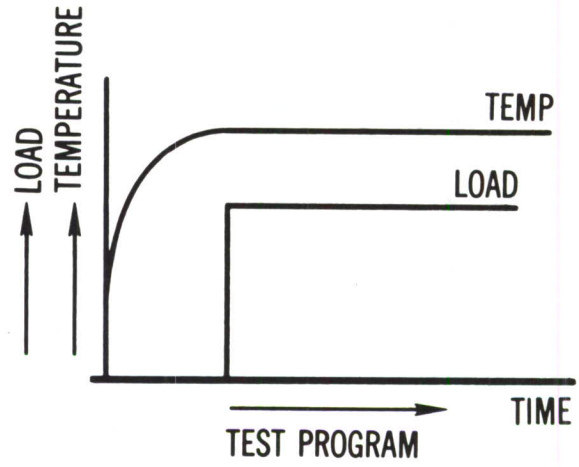


Figure 62. Time-Deformation Data, "Standard" Creep Test Armco PH 15-7 Mo, 800°F.



MATERIAL: ARMCO PH 15-7 Mo COND RH 950
TEMPERATURE: 800° F
LOAD: 80 KSI.

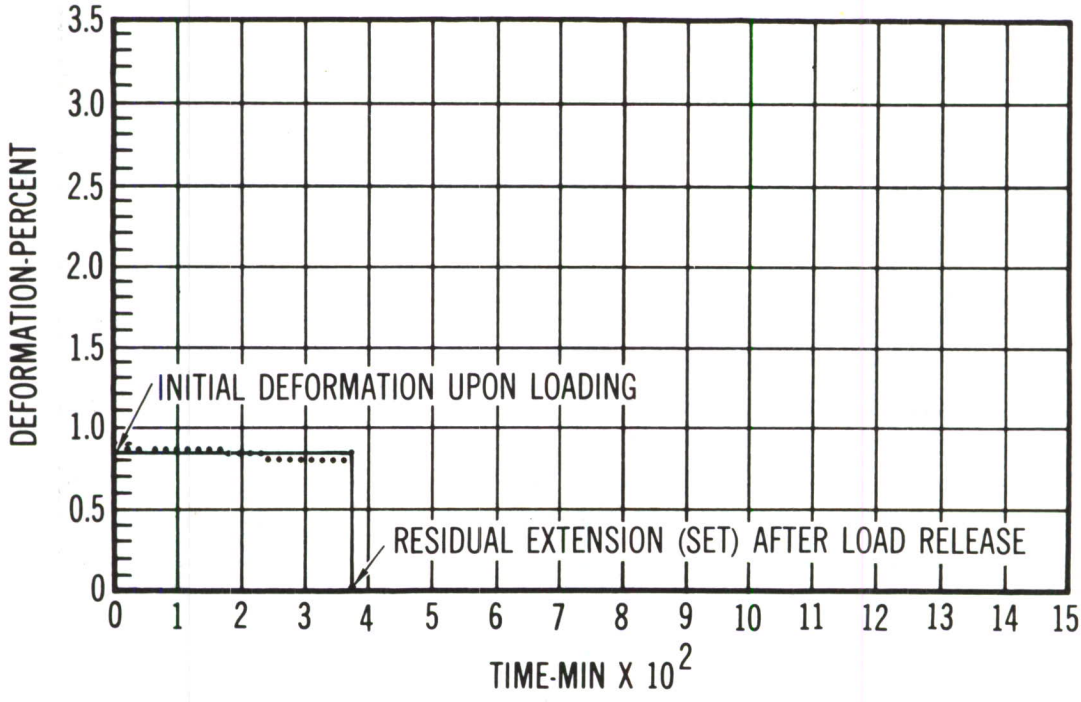
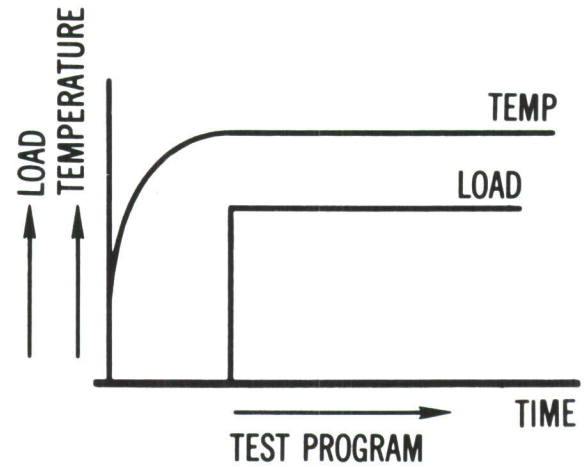


Figure 63. Time-Deformation Data, "Standard" Creep Test Armco PH 15-7 Mo, 800°F.



MATERIAL: ARMCO PH 15-7 Mo COND RH 950
TEMPERATURE: 800° F
LOAD: 86.5 KSI

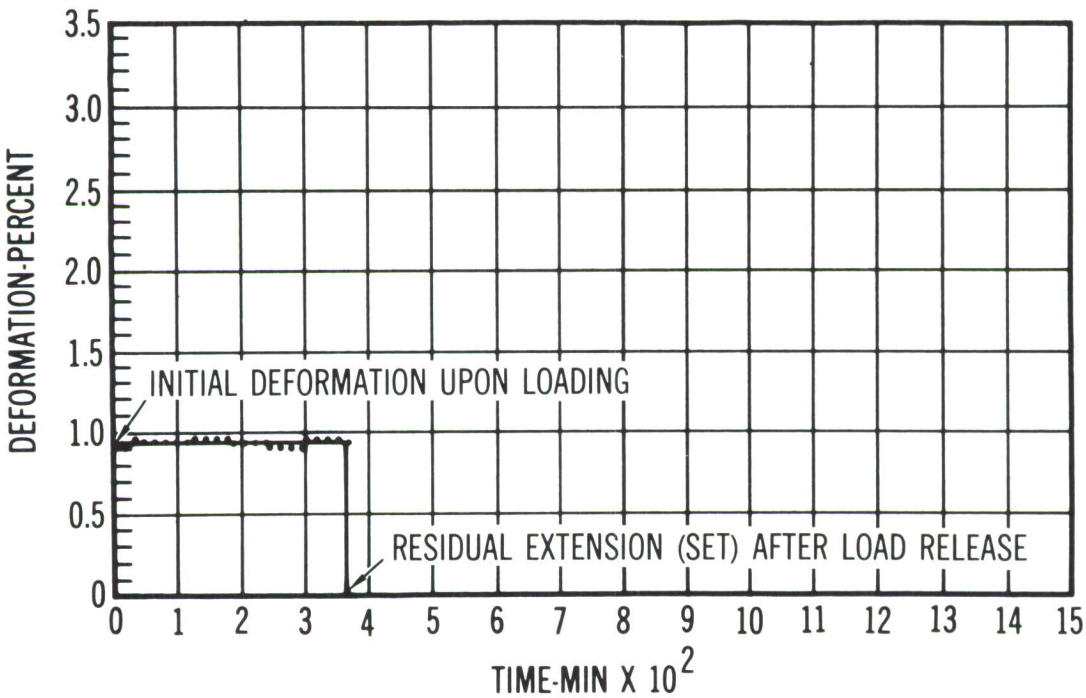
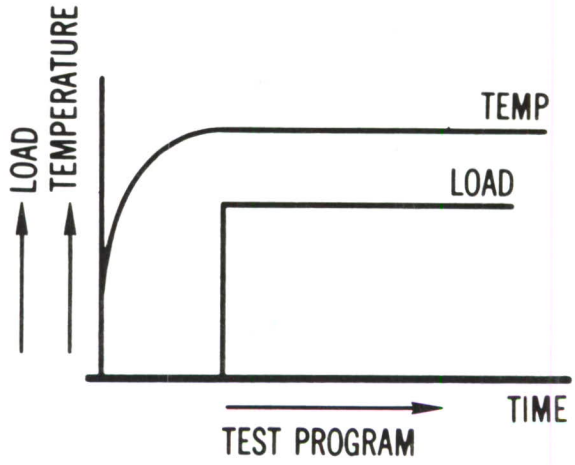


Figure 64. Time-Deformation Data, "Standard" Creep Test Armco PH 15-7 Mo, 800°F.



MATERIAL: ARMCO PH 15-7 Mo COND RH 950
TEMPERATURE: 800° F
LOAD: 86.5 KSI

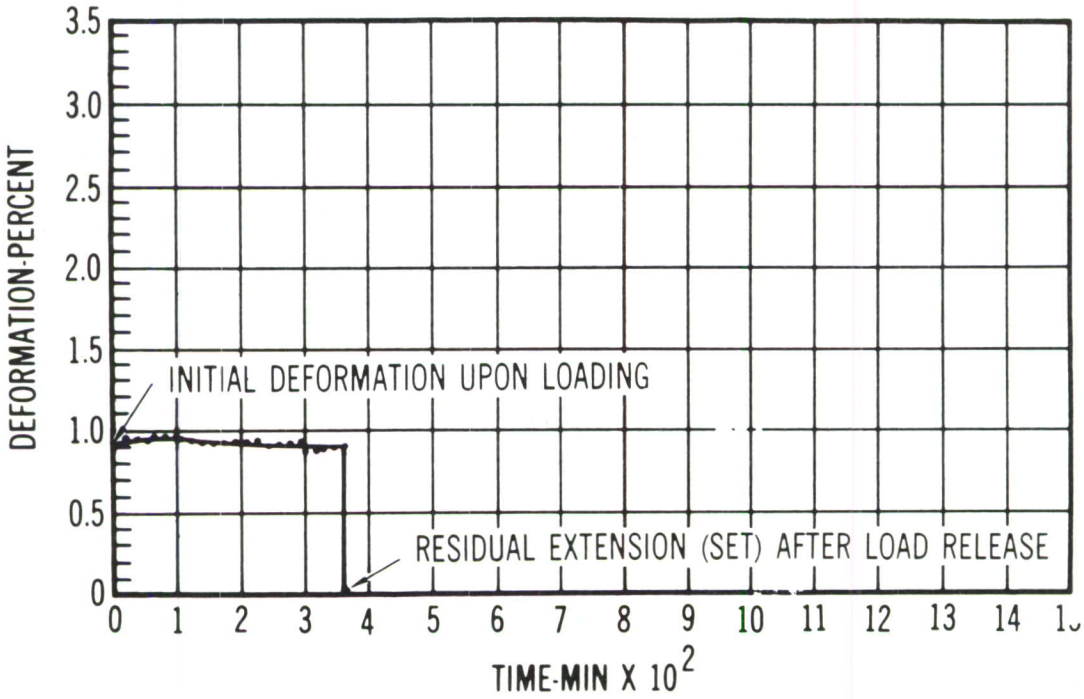
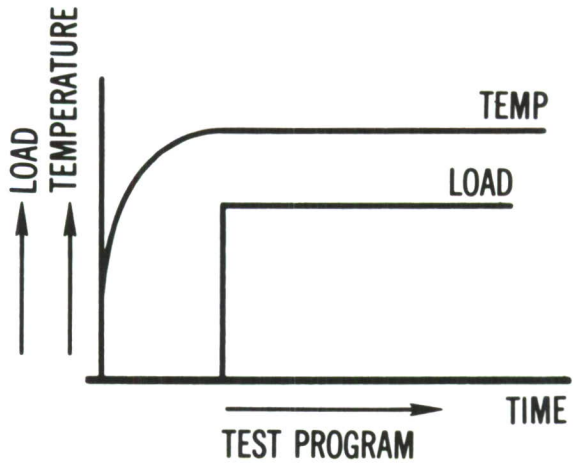


Figure 65. Time-Deformation Data, "Standard" Creep Test Armco PH 15-7 Mo, 800°F.



MATERIAL: ARMCO PH 15-7 Mo COND RH 950
TEMPERATURE: 800° F
LOAD: 148.5 KSI

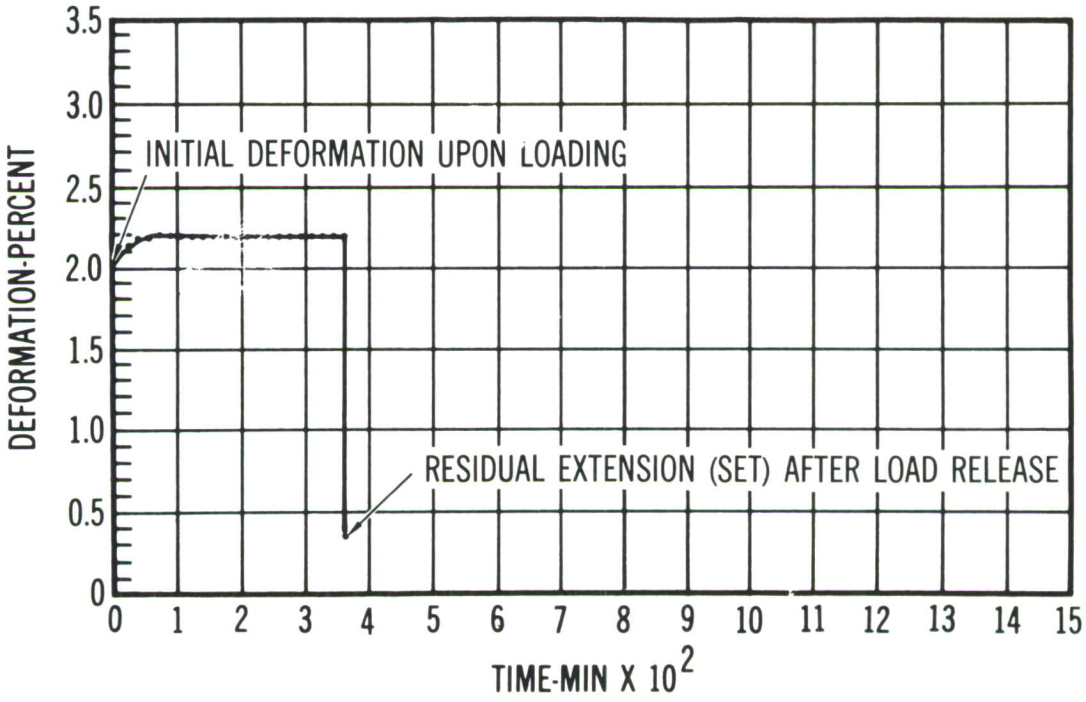
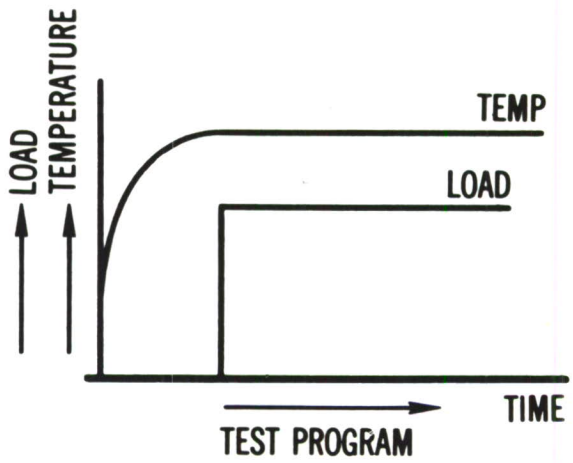


Figure 66. Time-Deformation Data, "Standard" Creep Test Armco PH 15-7 Mo, 800°F.



MATERIAL: ARMCO PH 15-7 Mo COND RH 950
TEMPERATURE: 900° F
LOAD: 75 KSI

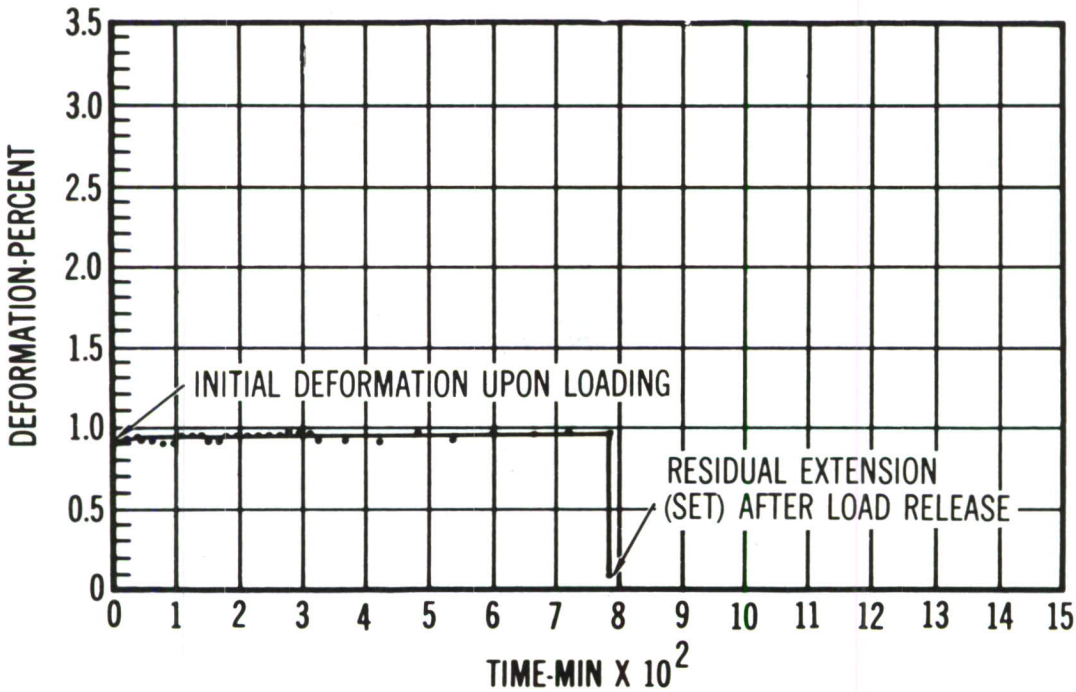
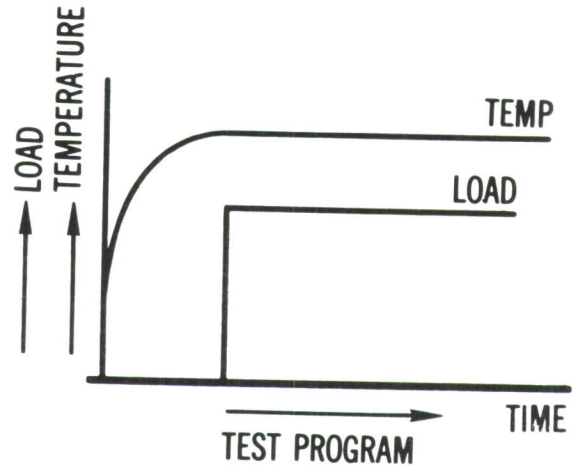


Figure 67. Time-Deformation Data, "Standard" Creep Test Armco PH 15-7 Mo, 900°F.



MATERIAL: ARMCO PH 15-7 Mo COND RH 950
TEMPERATURE: 900° F
LOAD: 75 KSI

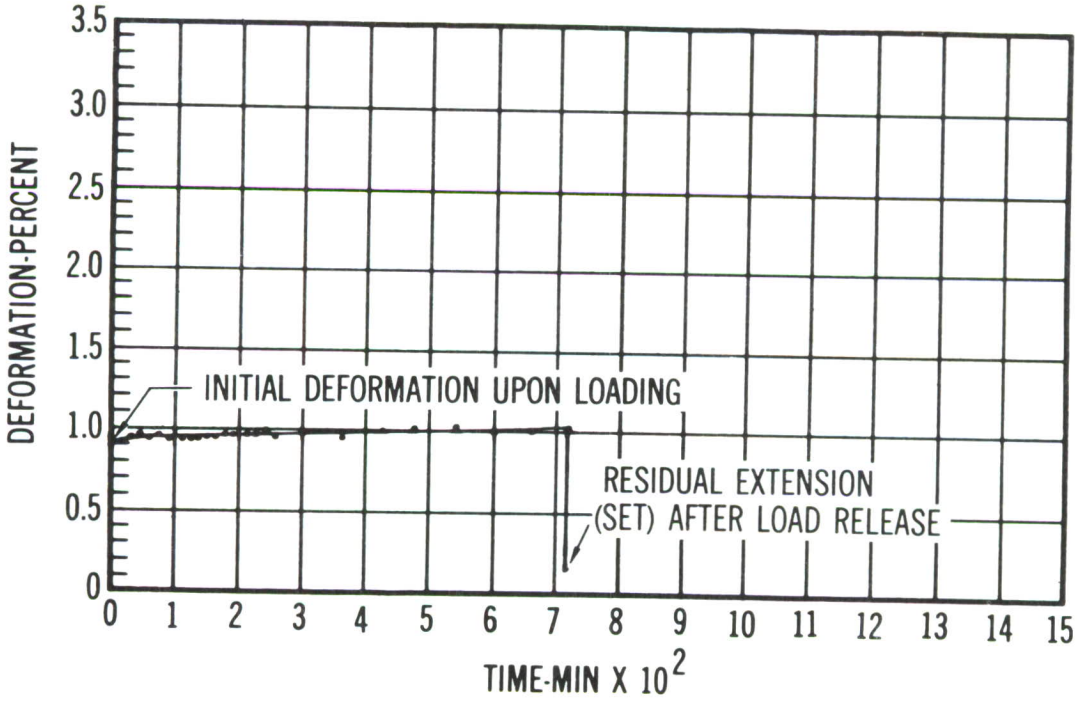
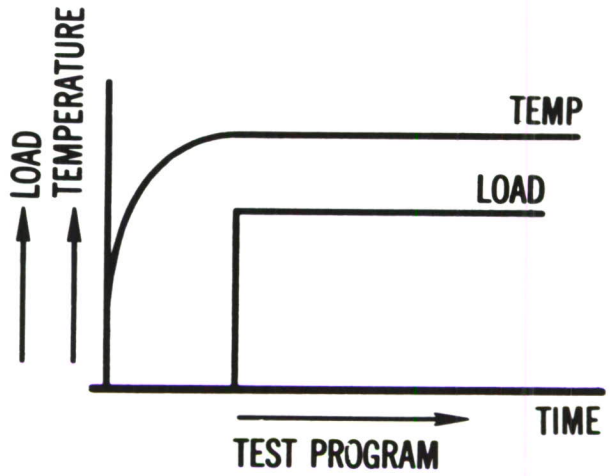


Figure 68. Time-Deformation Data, "Standard" Creep Test Armco PH 15-7 Mo, 900°F.



MATERIAL: ARMCO PH 15-7 Mo COND RH 950
TEMPERATURE: 900° F
LOAD: 79 KSI

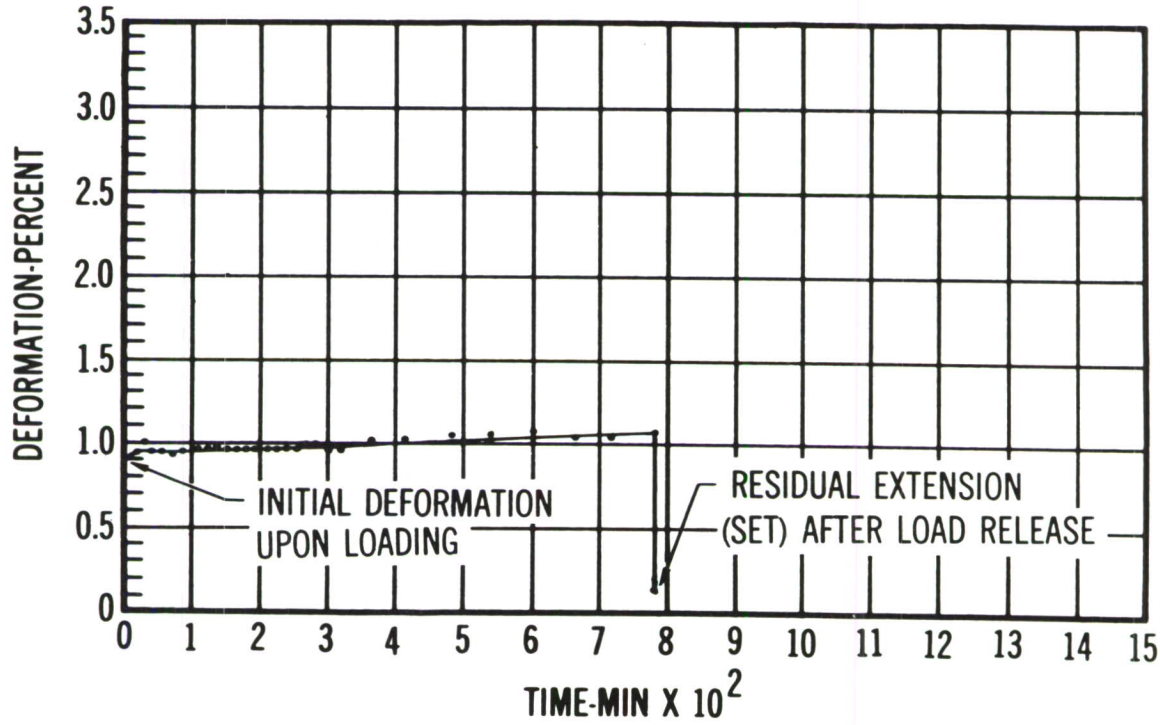
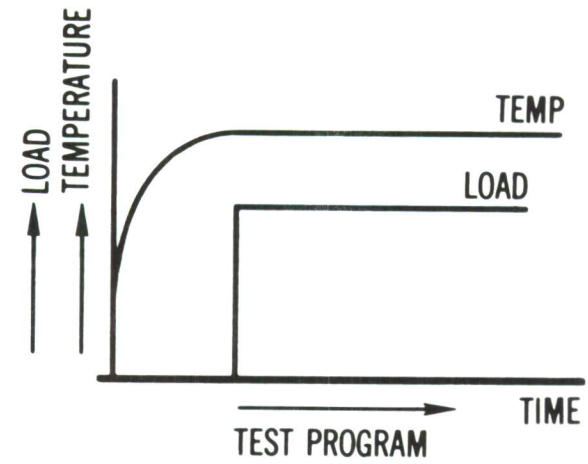


Figure 69. Time-Deformation Data, "Standard" Creep Test Armco PH 15-7 Mo, 900°F.



MATERIAL: ARMCO PH 15-7 Mo COND RH 950
TEMPERATURE: 900° F
LOAD: 79 KSI

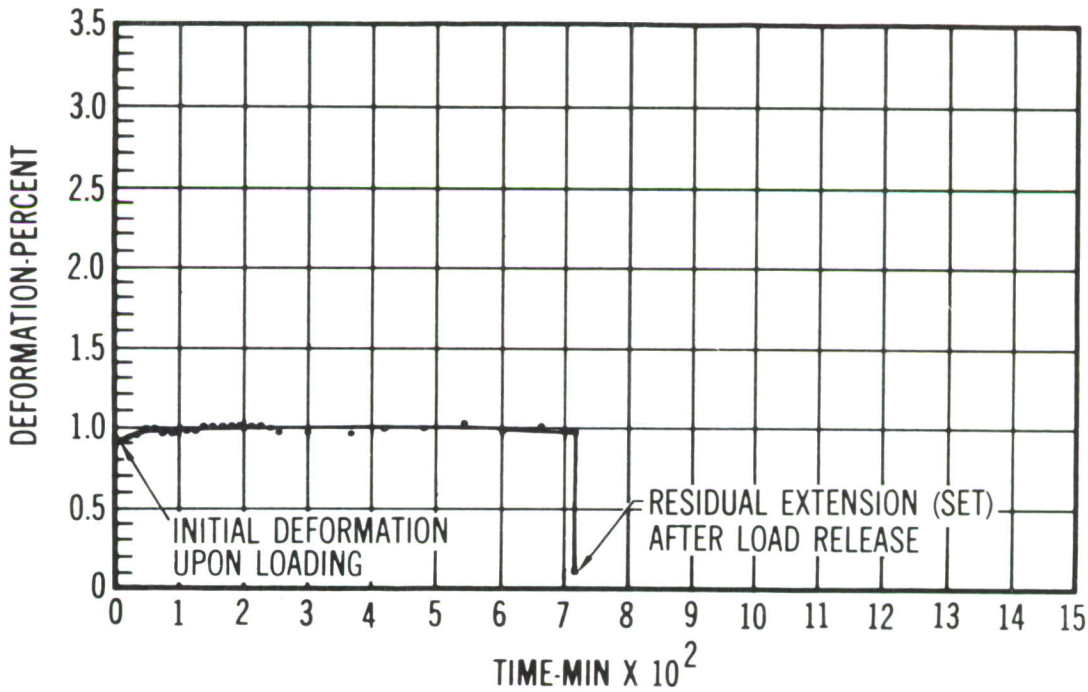
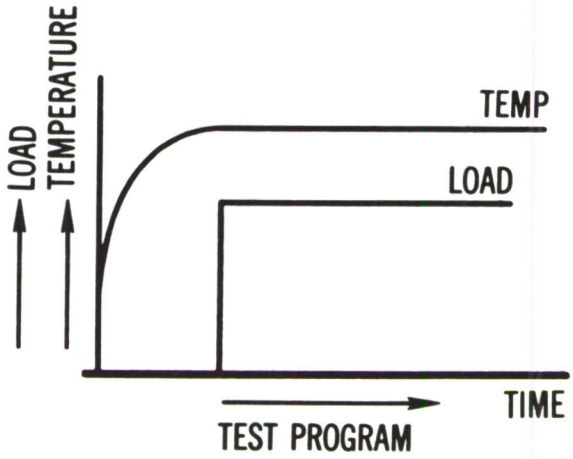


Figure 70. Time-Deformation Data, "Standard" Creep Test Armco PH 15-7 Mo, 900°F.



MATERIAL: ARMCO PH 15-7 Mo COND RH 950
TEMPERATURE: 900° F
LOAD: 127.5 KSI

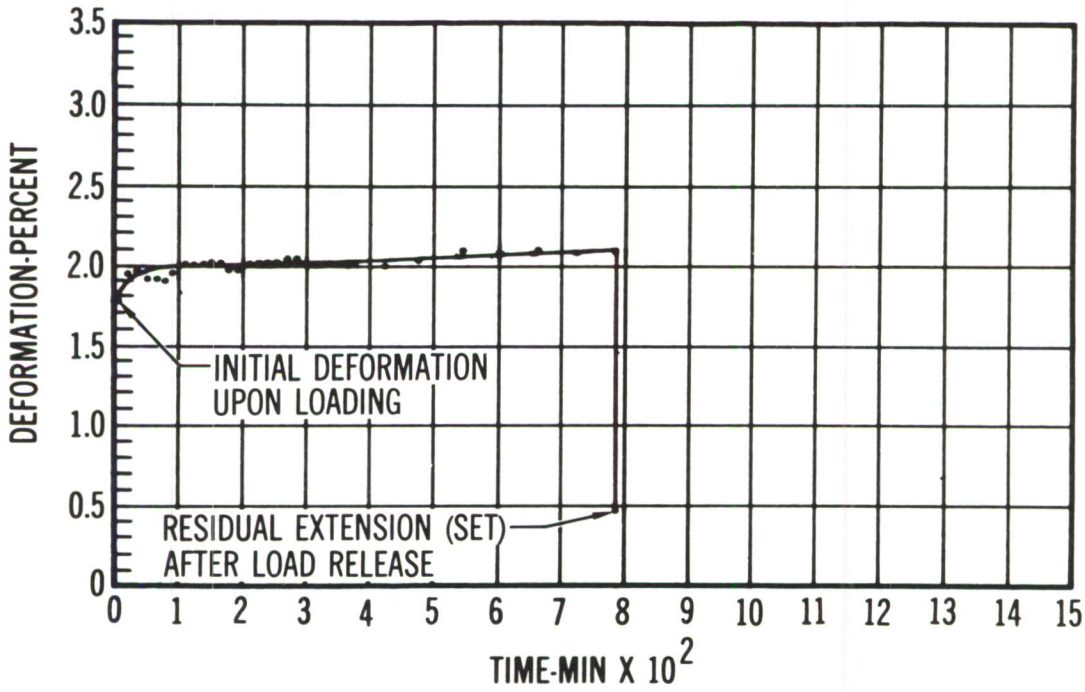
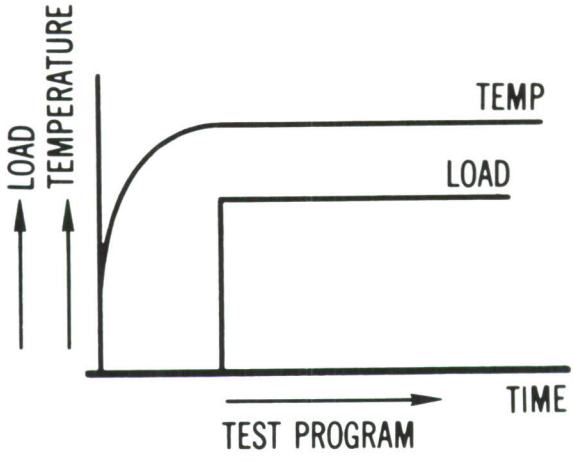


Figure 71. Time-Deformation Data, "Standard" Creep Test Armco PH 15-7 Mo, 900°F.



MATERIAL: ARMCO PH 15-7 Mo COND RH 950
TEMPERATURE: 1000° F
LOAD: 35 KSI

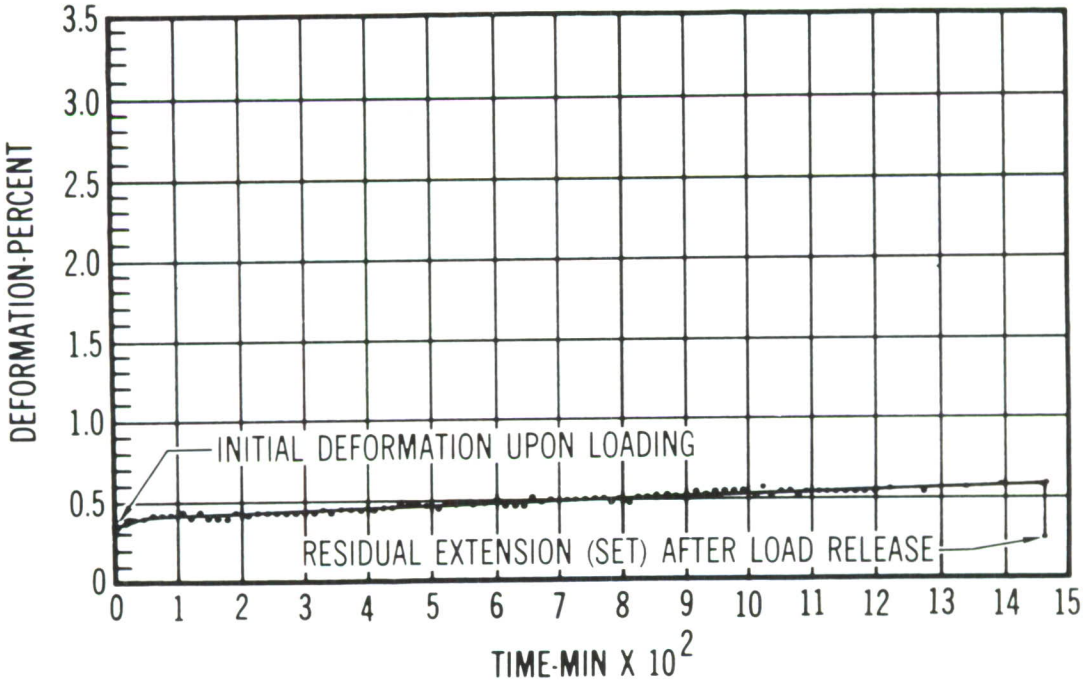
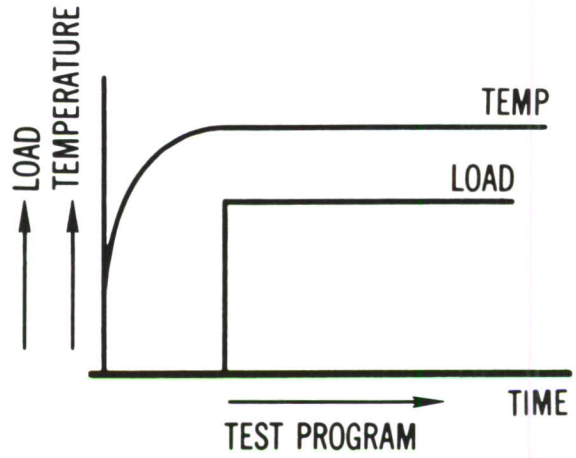


Figure 72. Time-Deformation Data, "Standard" Creep Test Armco PH 15-7 Mo, 1000°F.



MATERIAL: ARMCO PH 15-7 Mo COND RH 950
TEMPERATURE: 1000° F
LOAD: 35 KSI

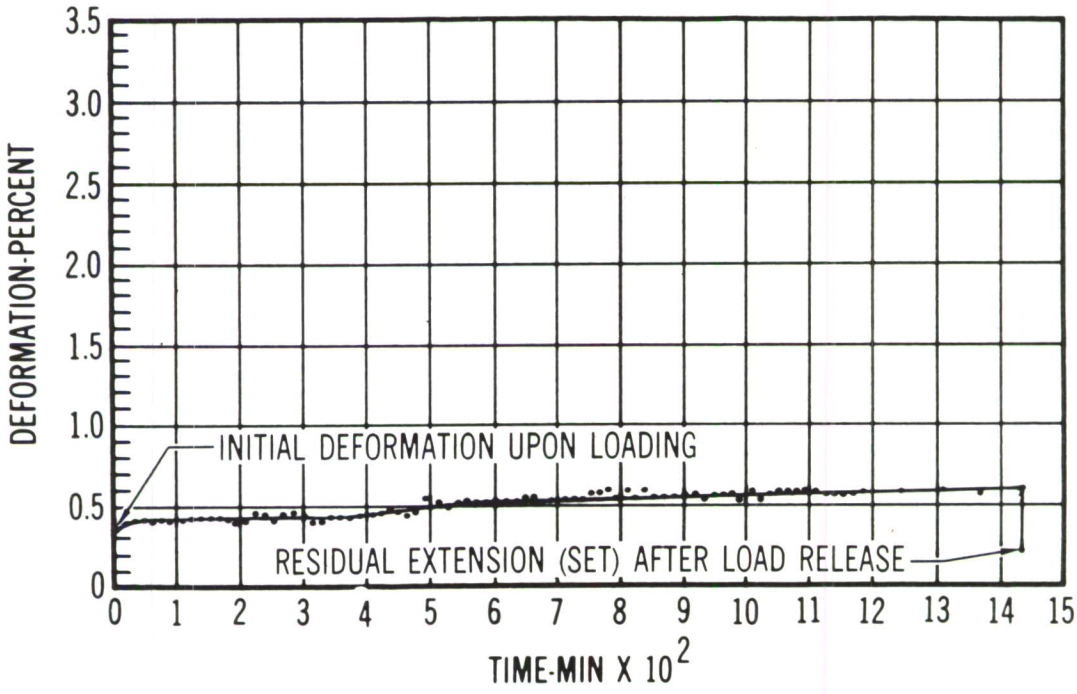
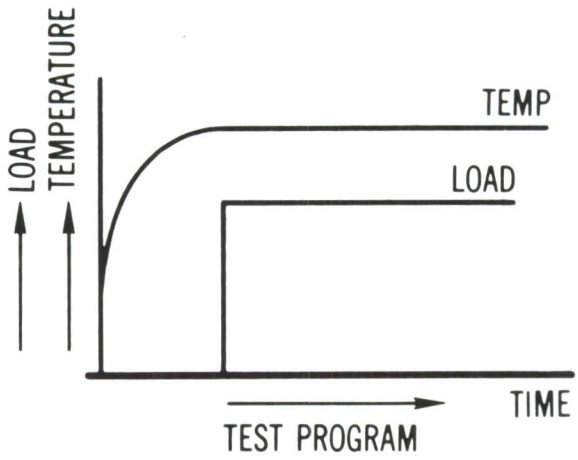


Figure 73. Time-Deformation Data, "Standard" Creep Test Armco PH 15-7 Mo, 1000°F.



MATERIAL. ARMCO PH 15-7 Mo COND RH 950
TEMPERATURE: 1000° F
LOAD: 39 KSI.

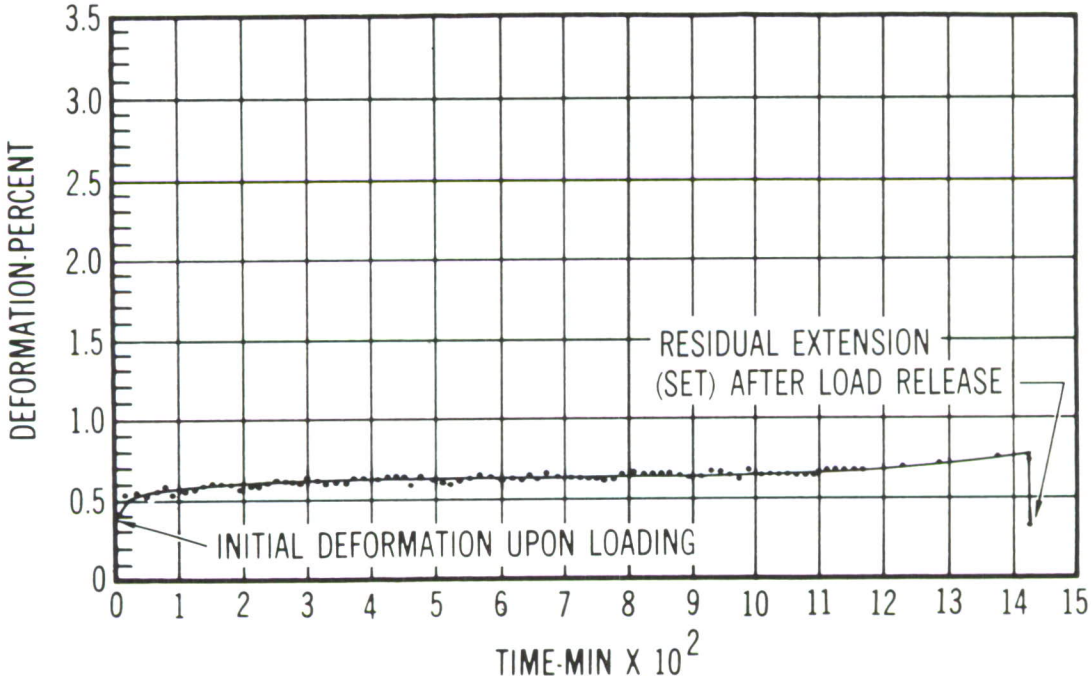
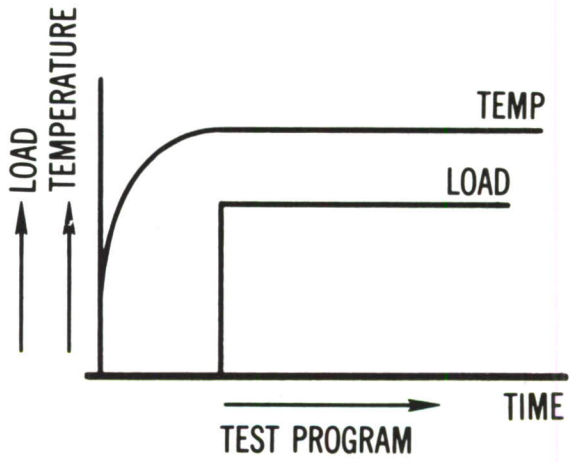


Figure 74. Time-Deformation Data. "Standard" Creep Test Armco PH 15-7 Mo, 1000°F.



MATERIAL: ARMCO PH 15-7 Mo COND RH 950
TEMPERATURE: 1000° F
LOAD: 39 KSI

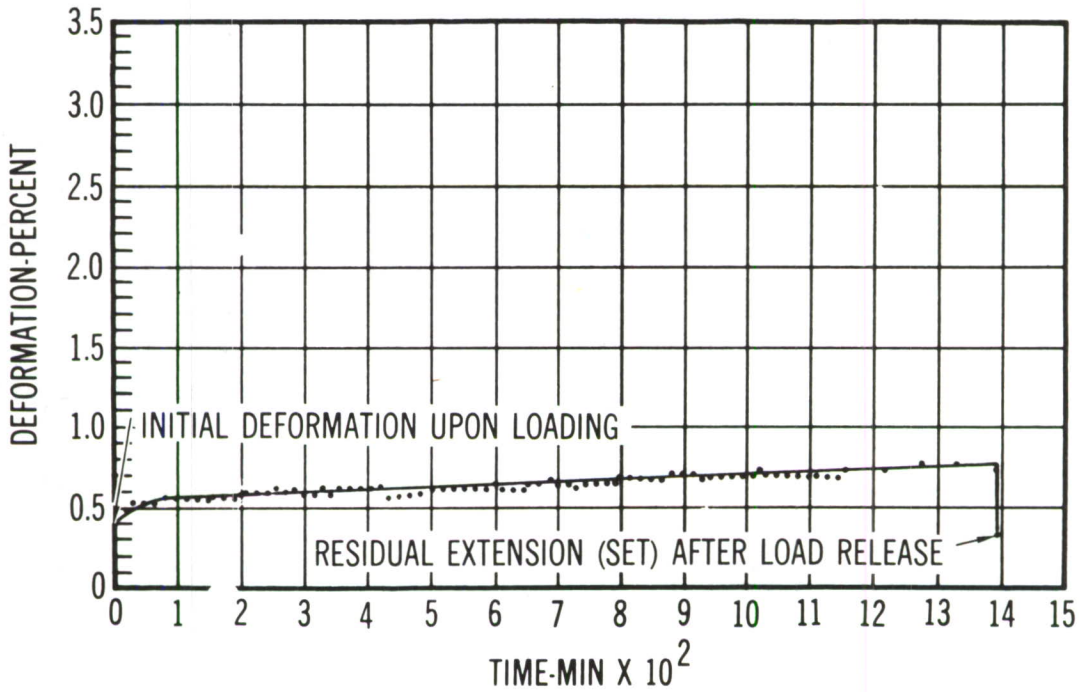


Figure 75. Time-Deformation Data, "Standard" Creep Test Armco PH 15-7 Mo, 1000°F.

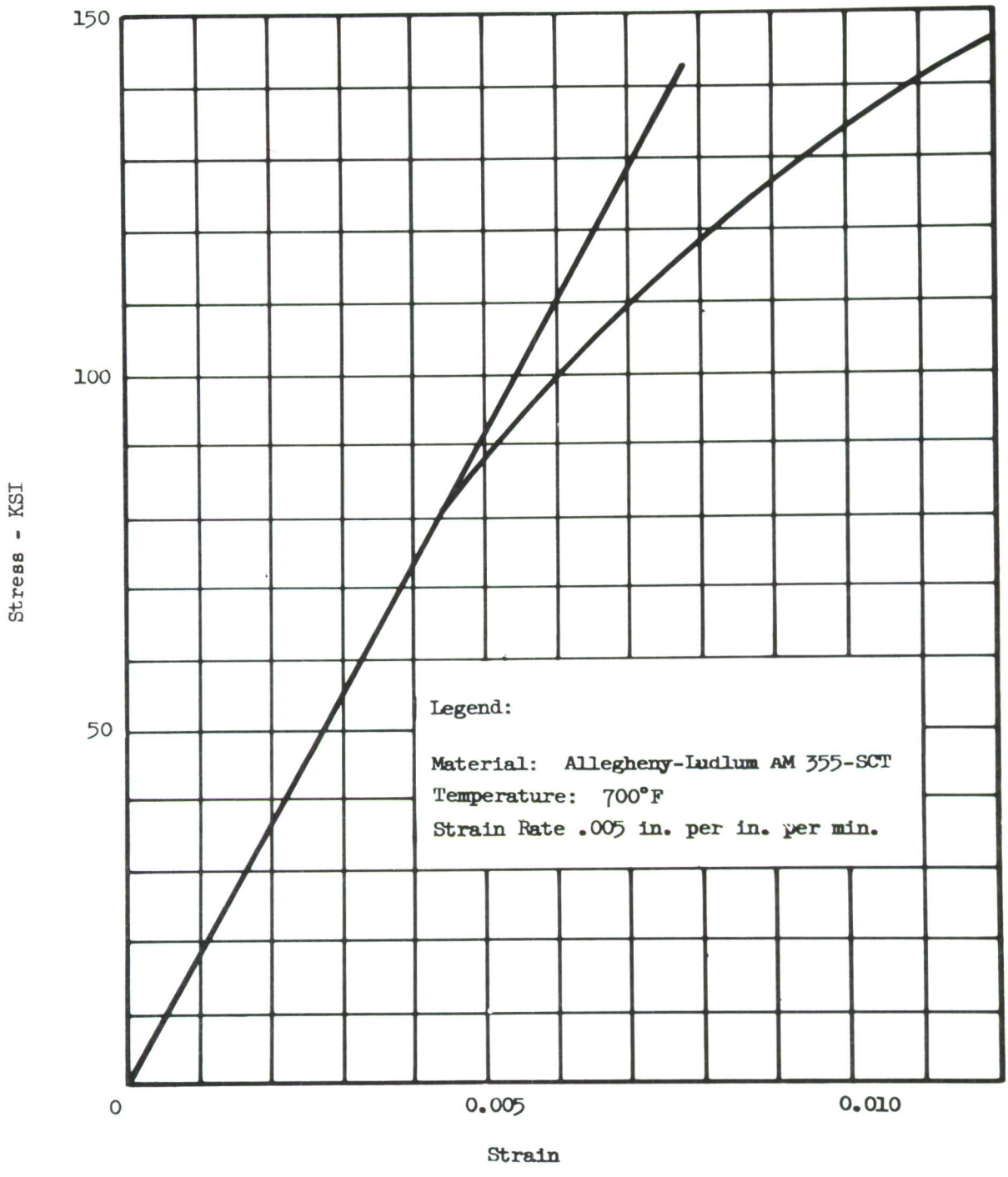


Figure 76. Stress Strain Diagram, Allegheny Ludlum AM 355, Condition SCT Stainless Steel, 700°F

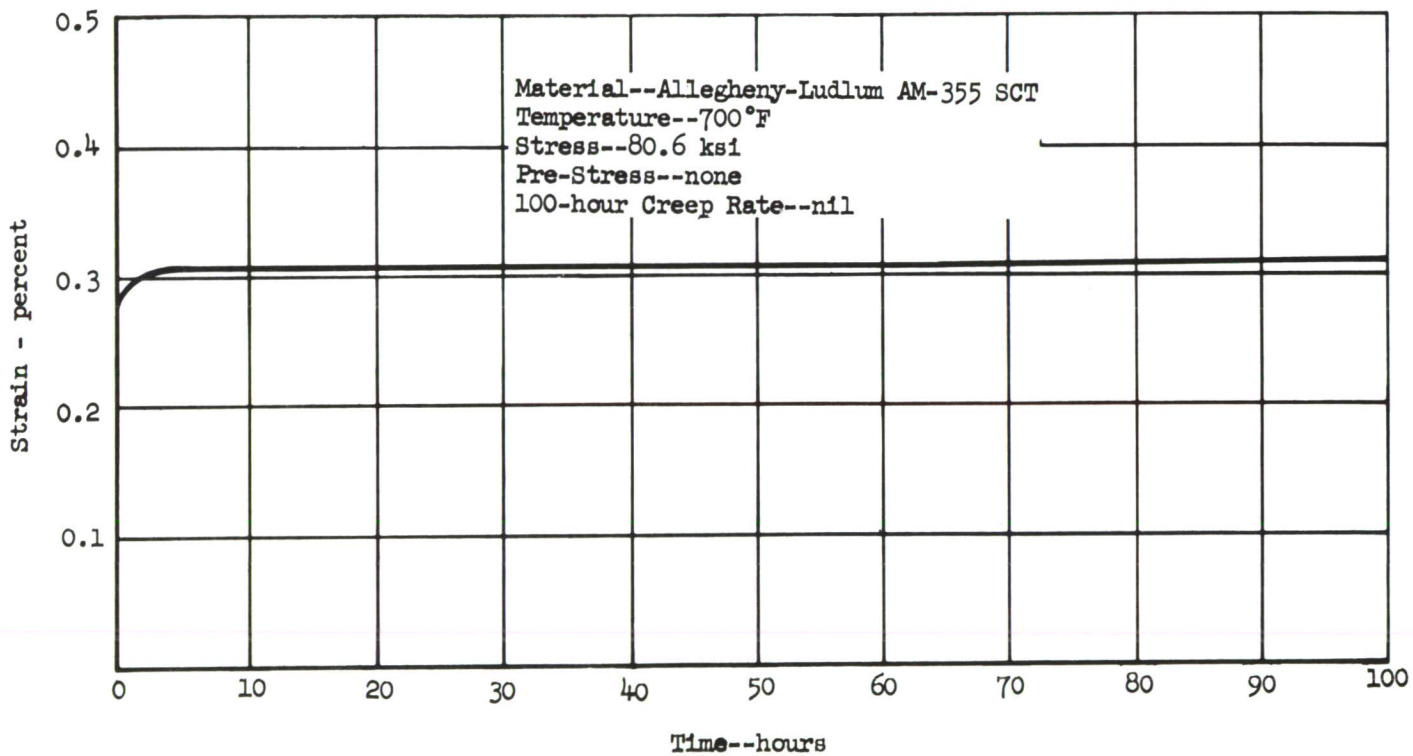


Figure 77. Creep Curve, Allegheny Ludlum AM 355, Condition SCT Stainless Steel

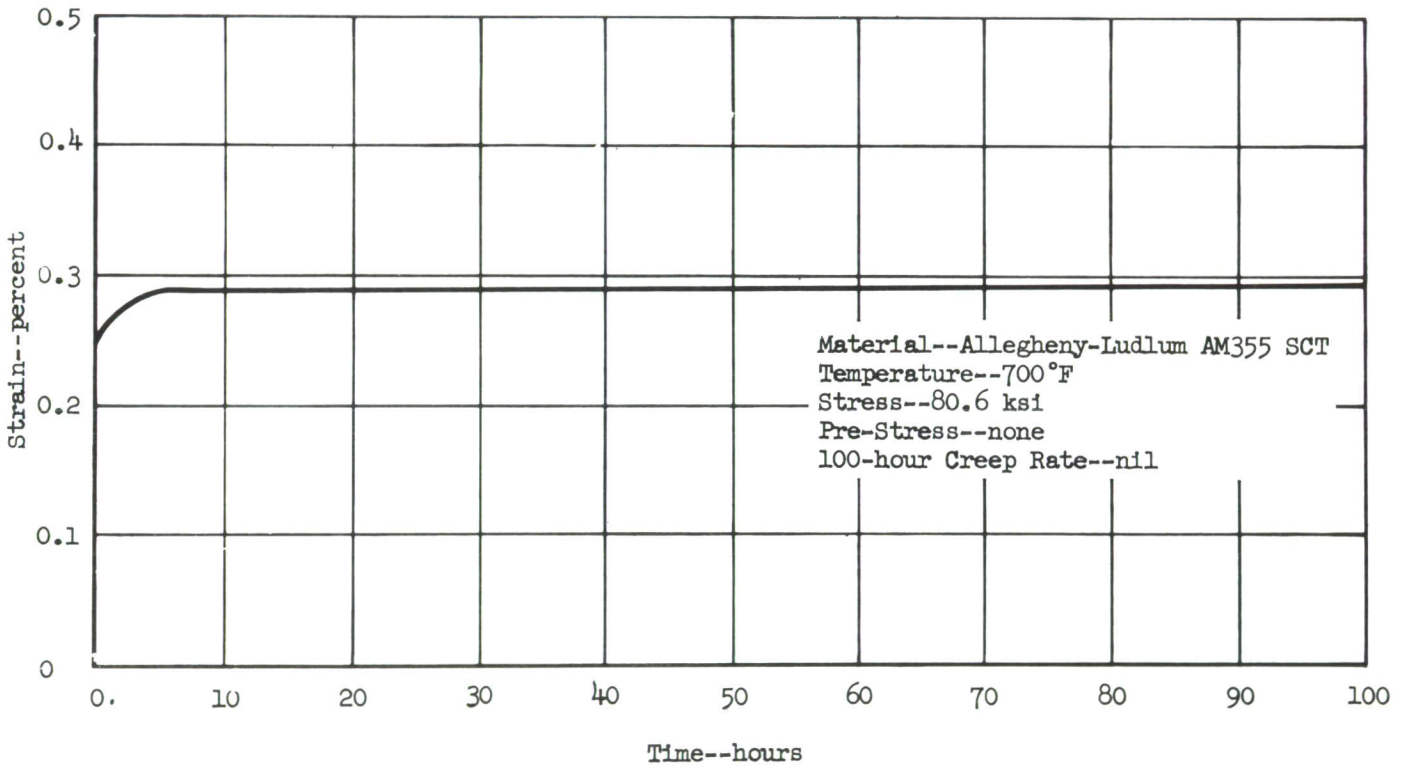


Figure 78. Creep Curve, Allegheny Ludlum AM 355, Condition SCT Stainless Steel

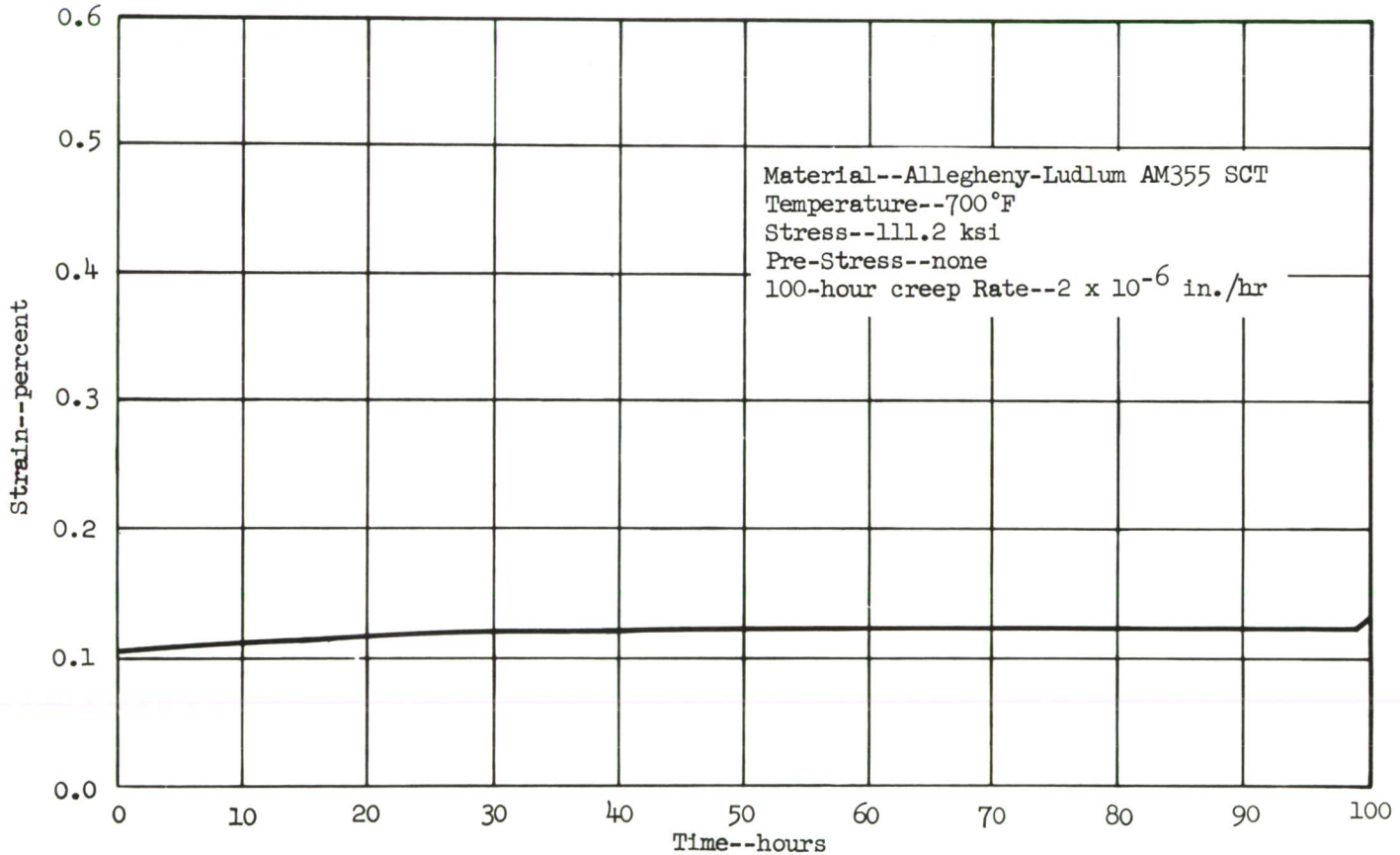


Figure 79. Creep Curve, Allegheny Ludlum AM 355, Condition SCT Stainless Steel

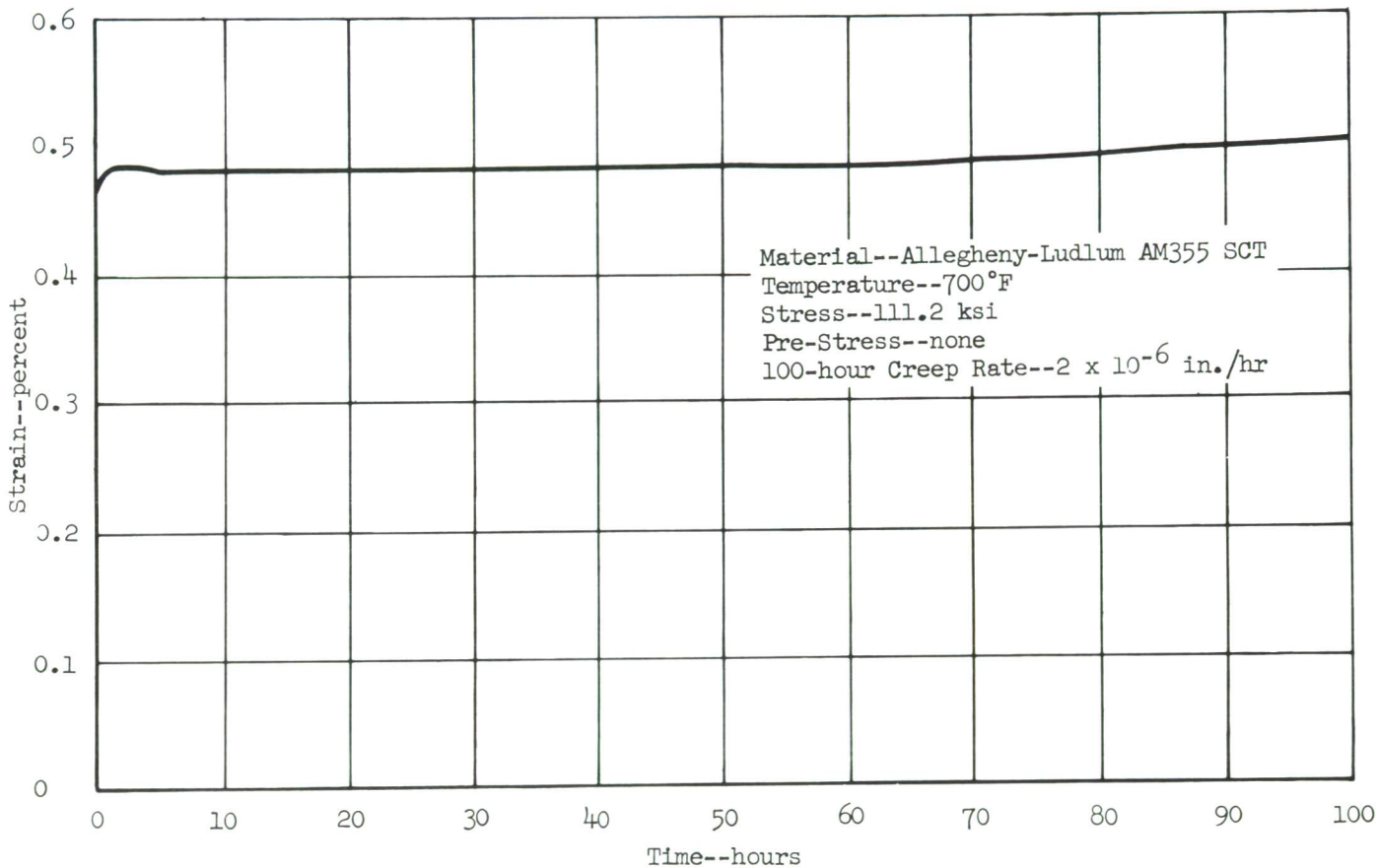


Figure 80. Creep Curve, Allegheny Ludlum AM 355, Condition SCT Stainless Steel

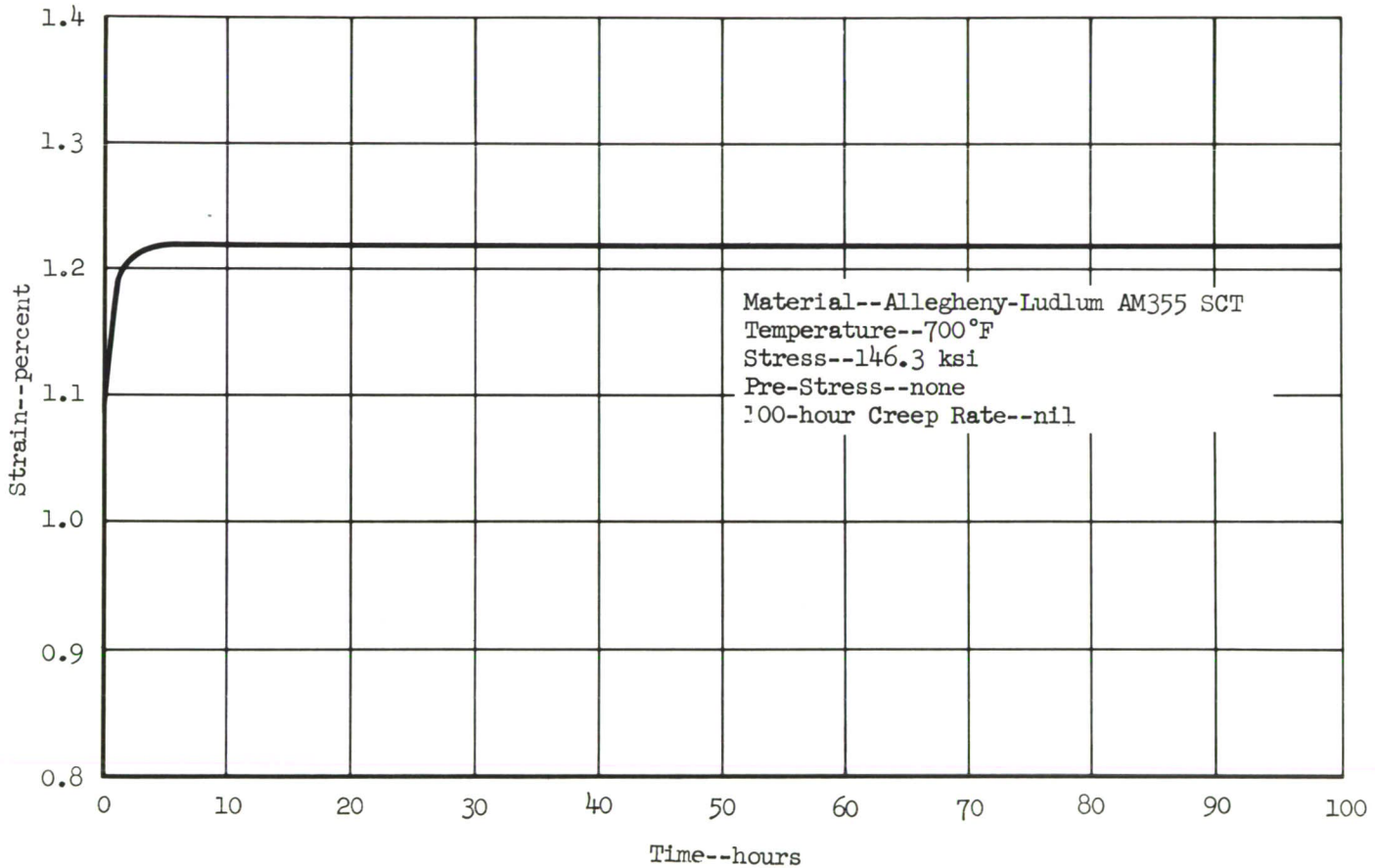


Figure 81. Creep Curve, Allegheny Ludlum AM 355, Condition SCT Stainless Steel

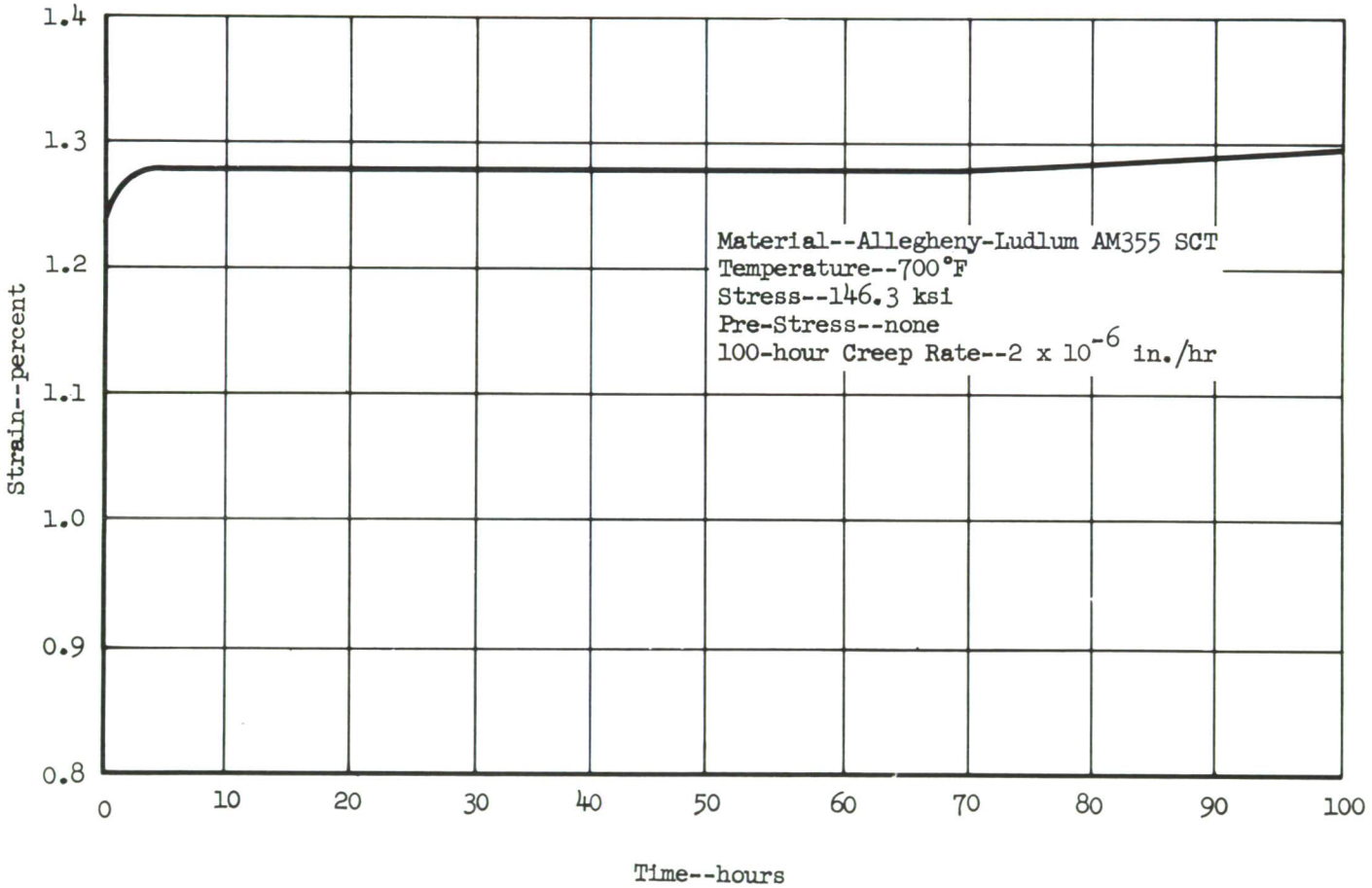


Figure 82. Creep Curve, Allegheny Ludlum AM 355, Condition SCT Stainless Steel

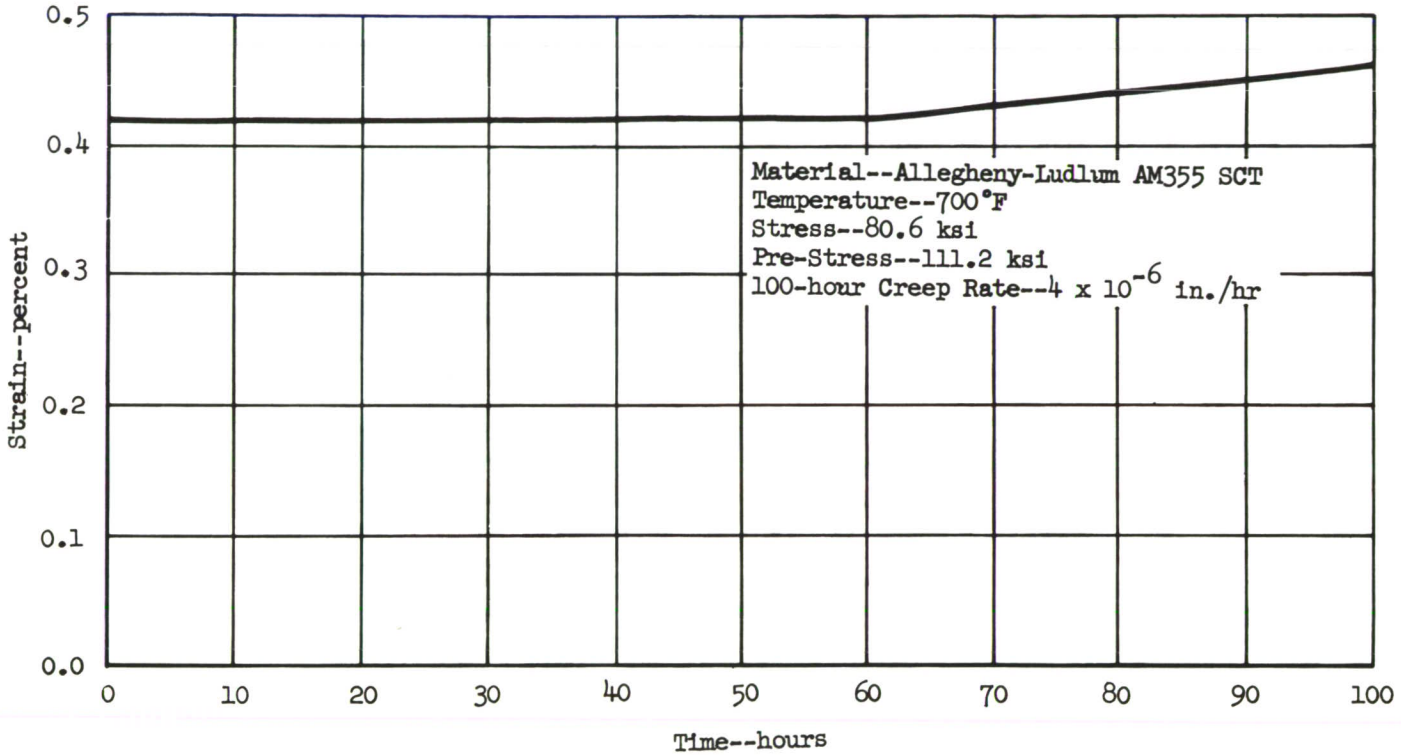


Figure 83. Creep Curve, Allegheny Ludlum AM 355, Condition SCT Stainless Steel

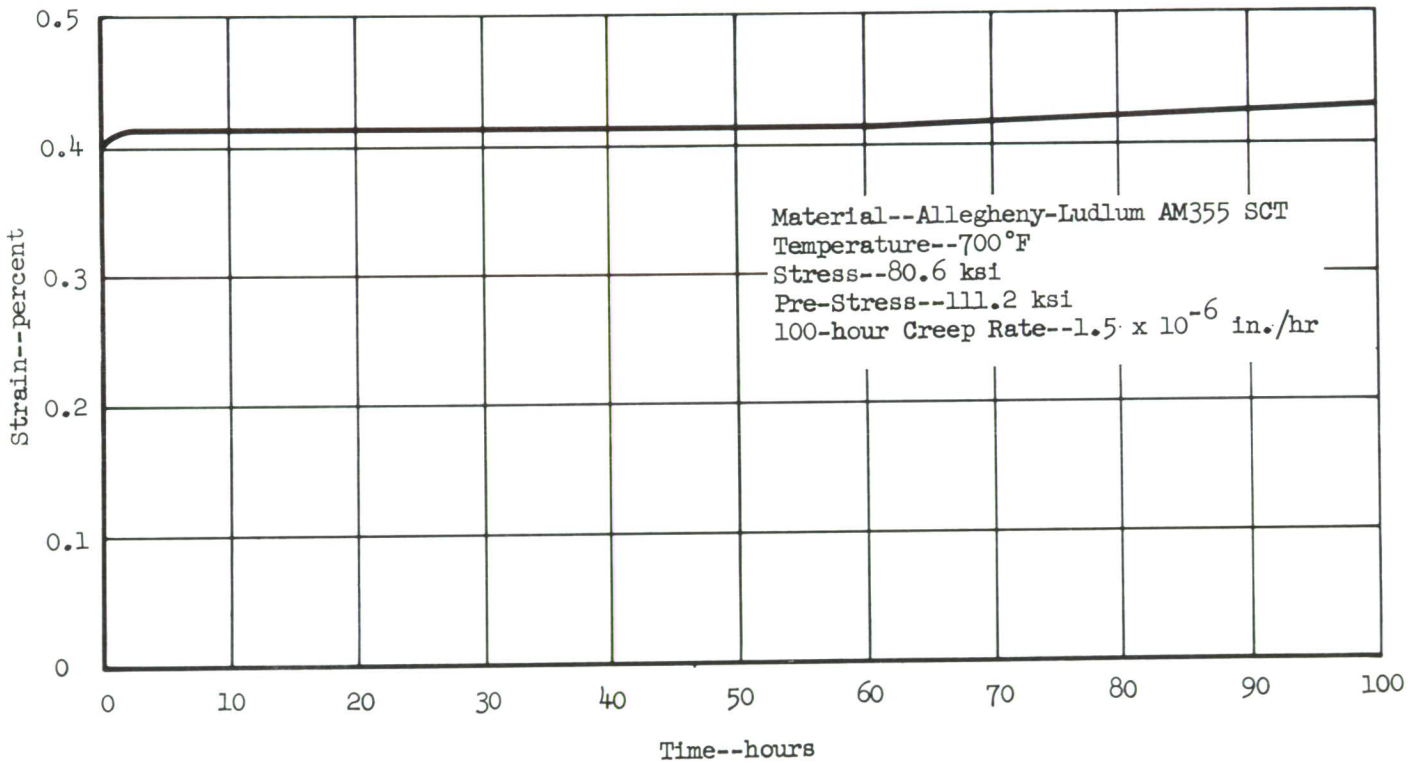


Figure 84. Creep Curve, Allegheny Ludlum AM 355, Condition SCT Stainless Steel

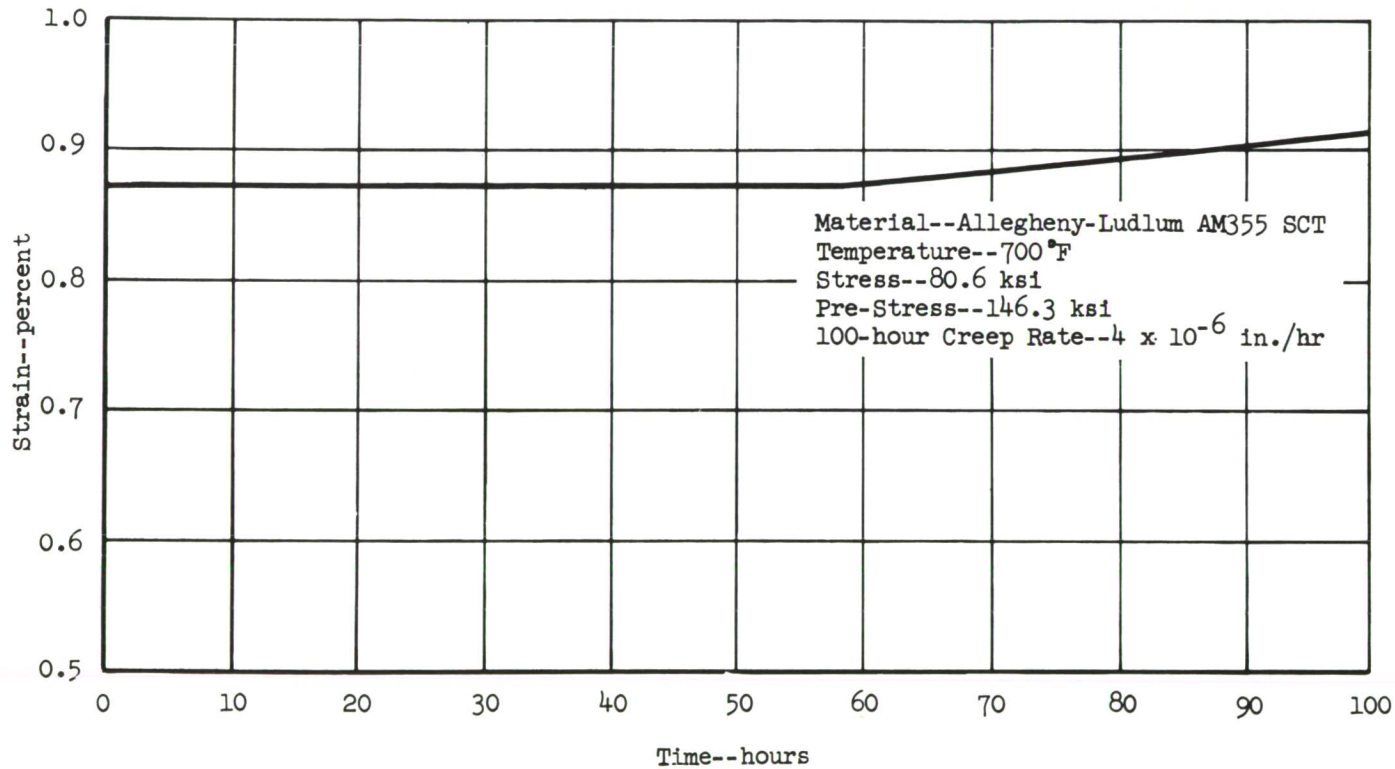


Figure 85. Creep Curve, Allegheny Ludlum AM 355,Condition SCT Stainless Steel

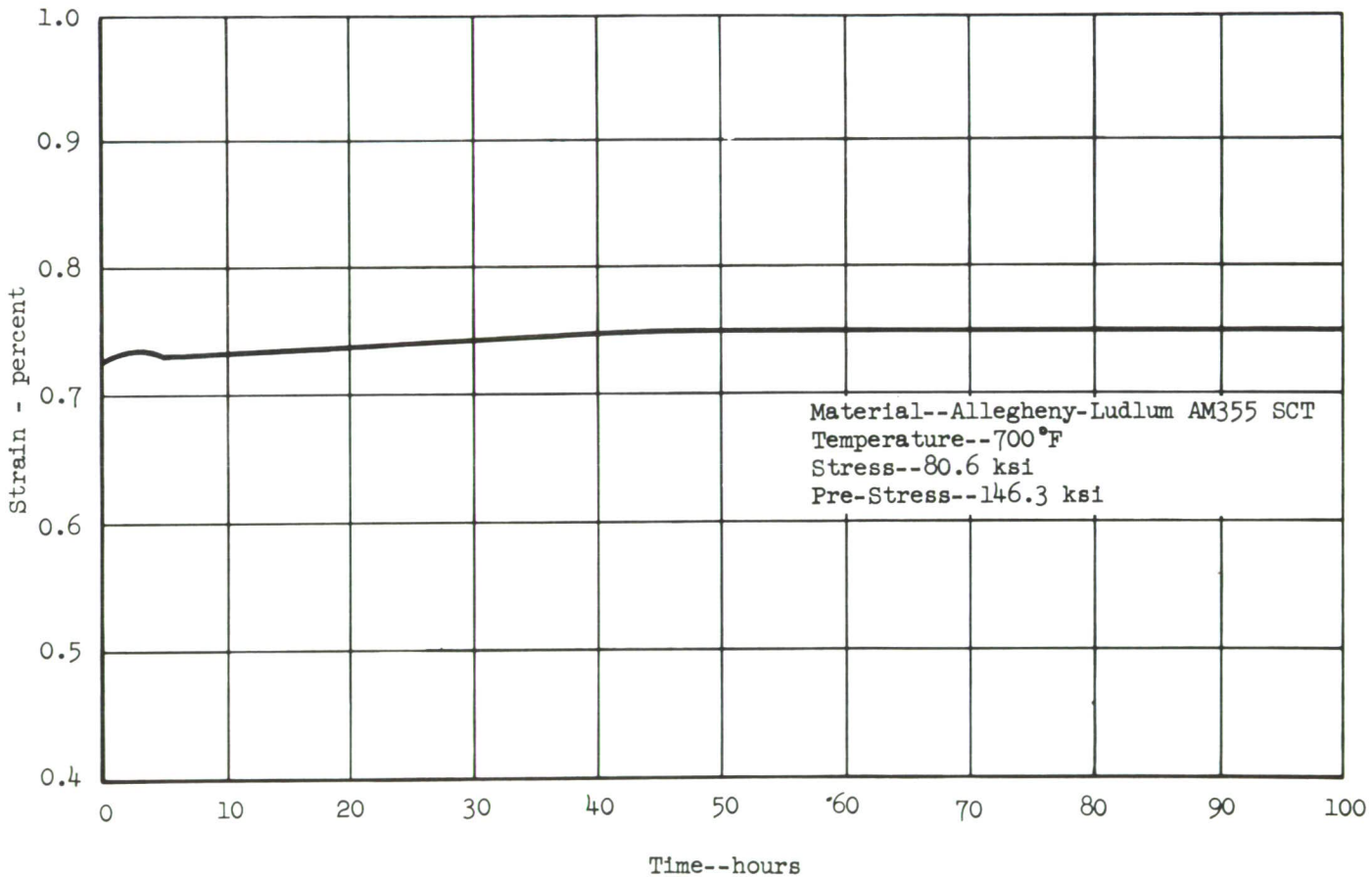


Figure 86. Creep Curve, Allegheny Ludlum AM 355, Condition SCT Stainless Steel

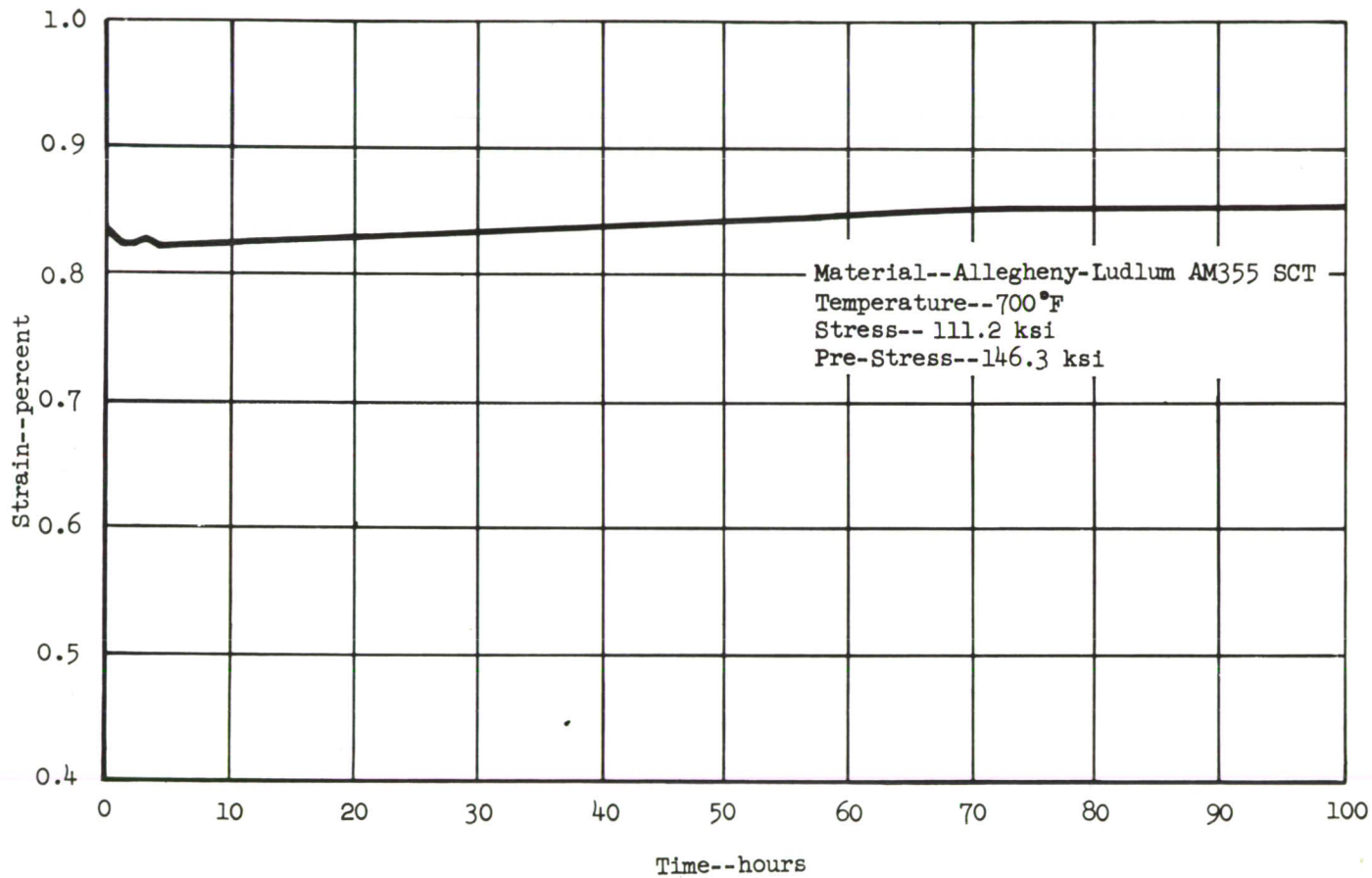


Figure 87. Creep Curve, Allegheny Ludlum AM 355, Condition SCT Stainless Steel

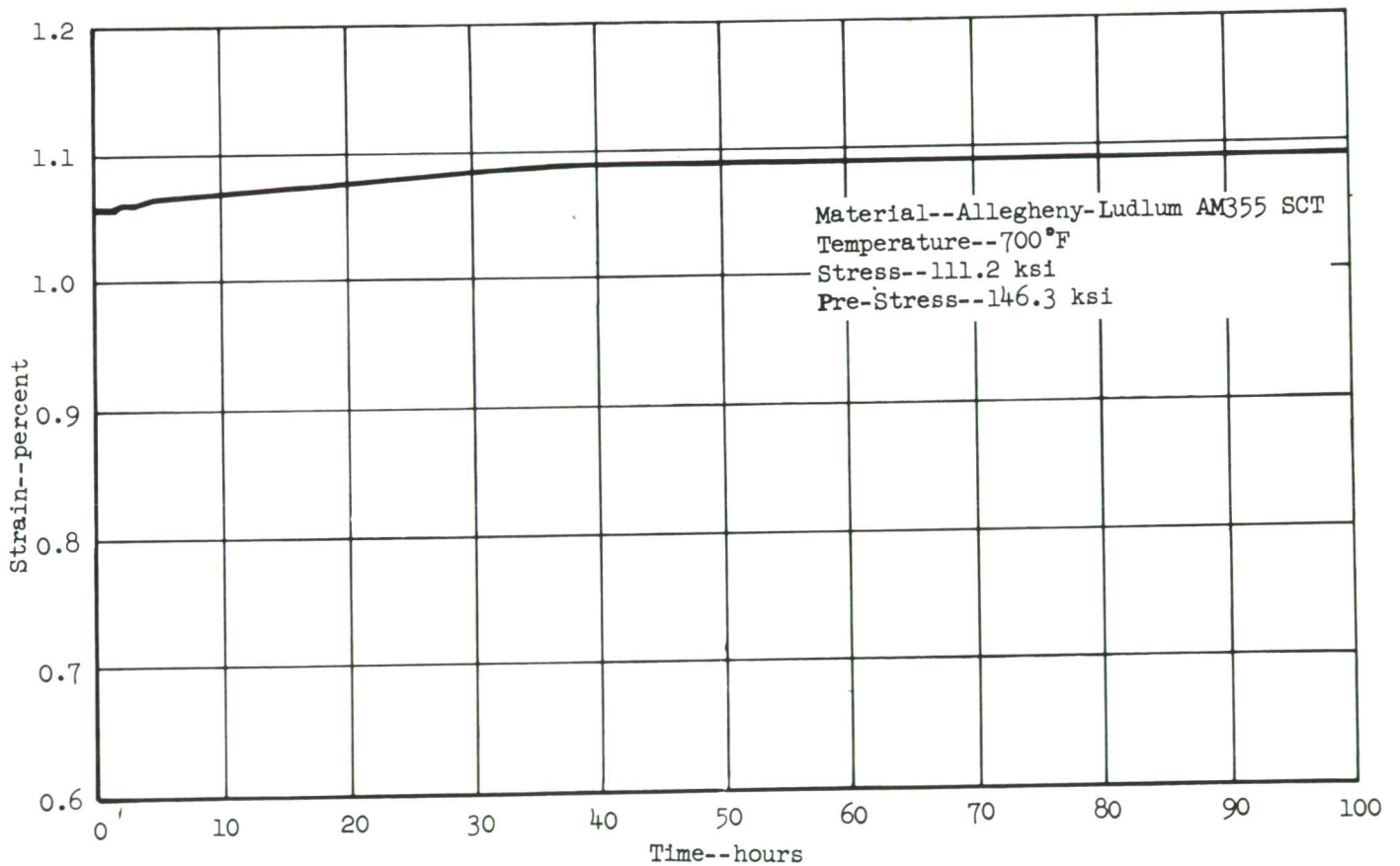


Figure 88. Creep Curve, Allegheny Ludlum AM 355, Condition SCT Stainless Steel

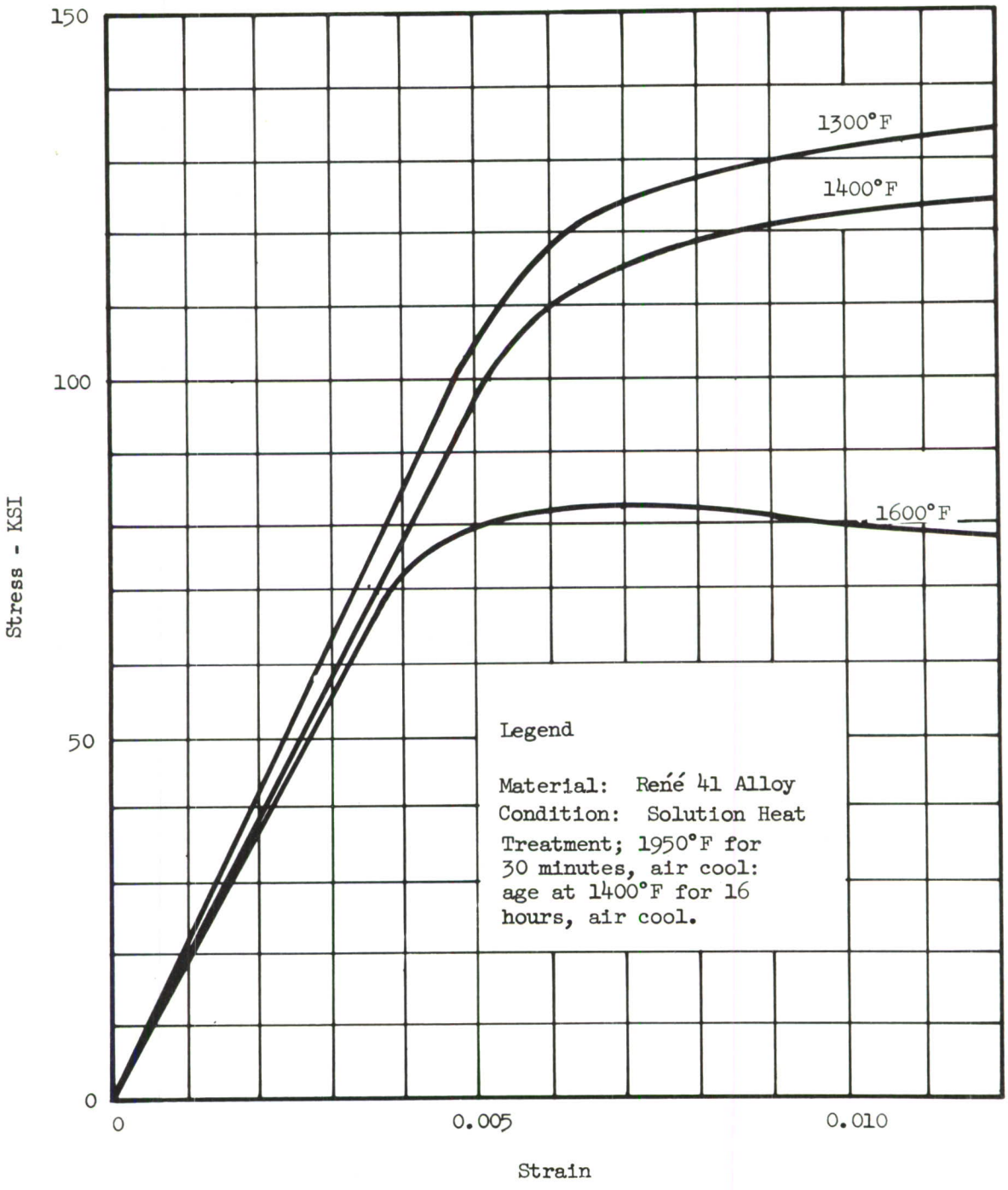


Figure 89. Stress Strain Curves, Rene 41 Alloy

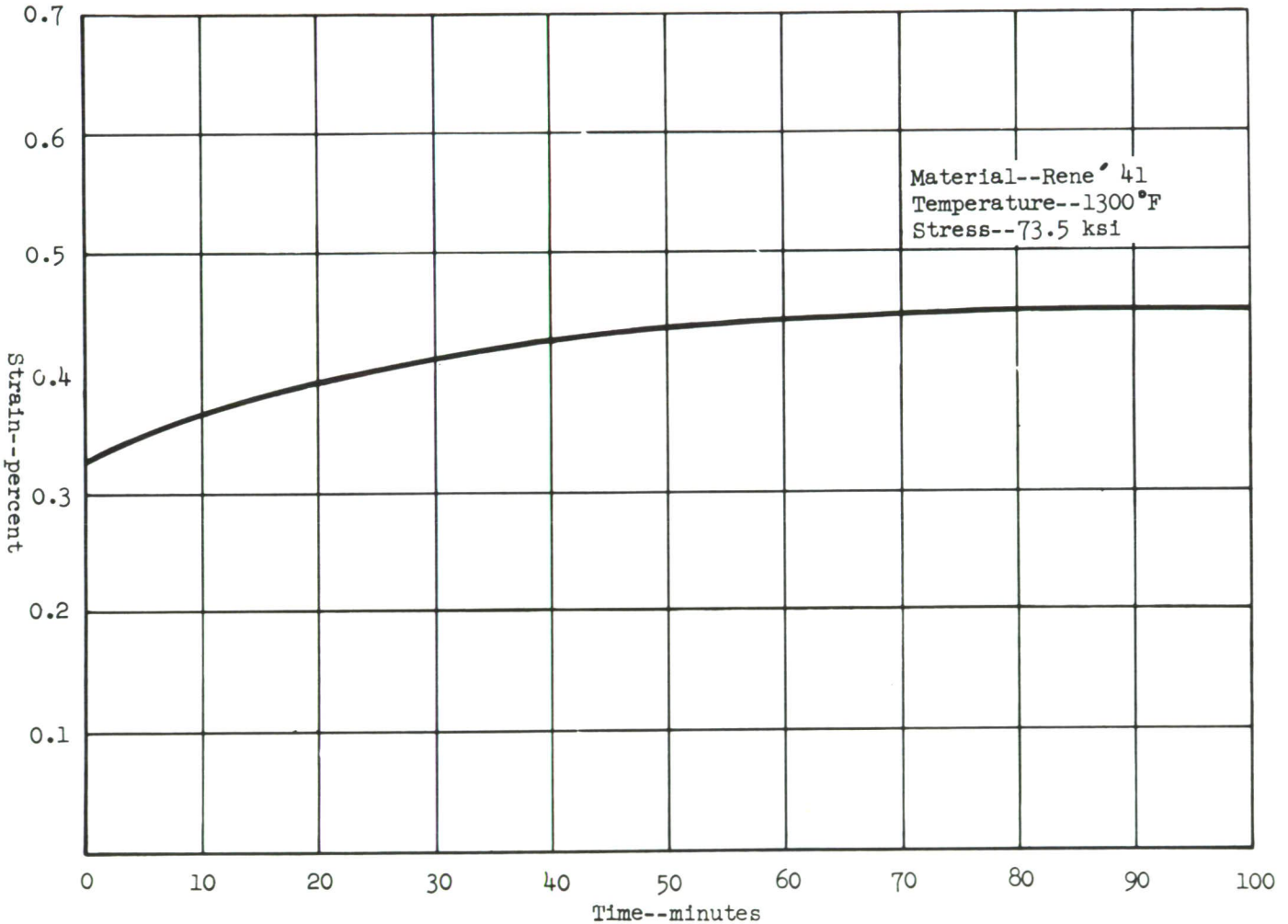


Figure 90. Creep Curve, Rene 41 Alloy, 1300°F

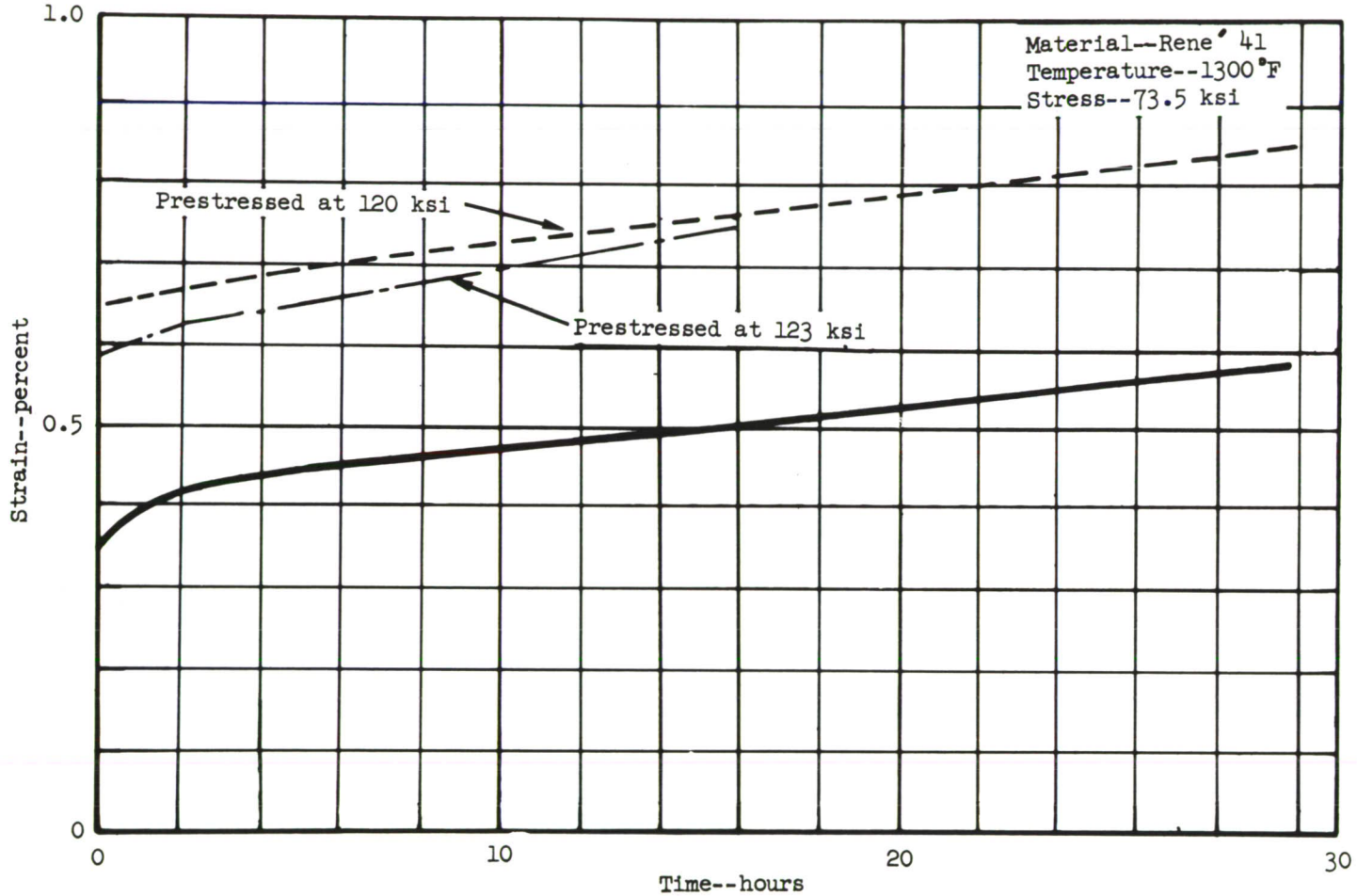


Figure 91. Creep Curves, Rene 41 Alloy, 1300°F

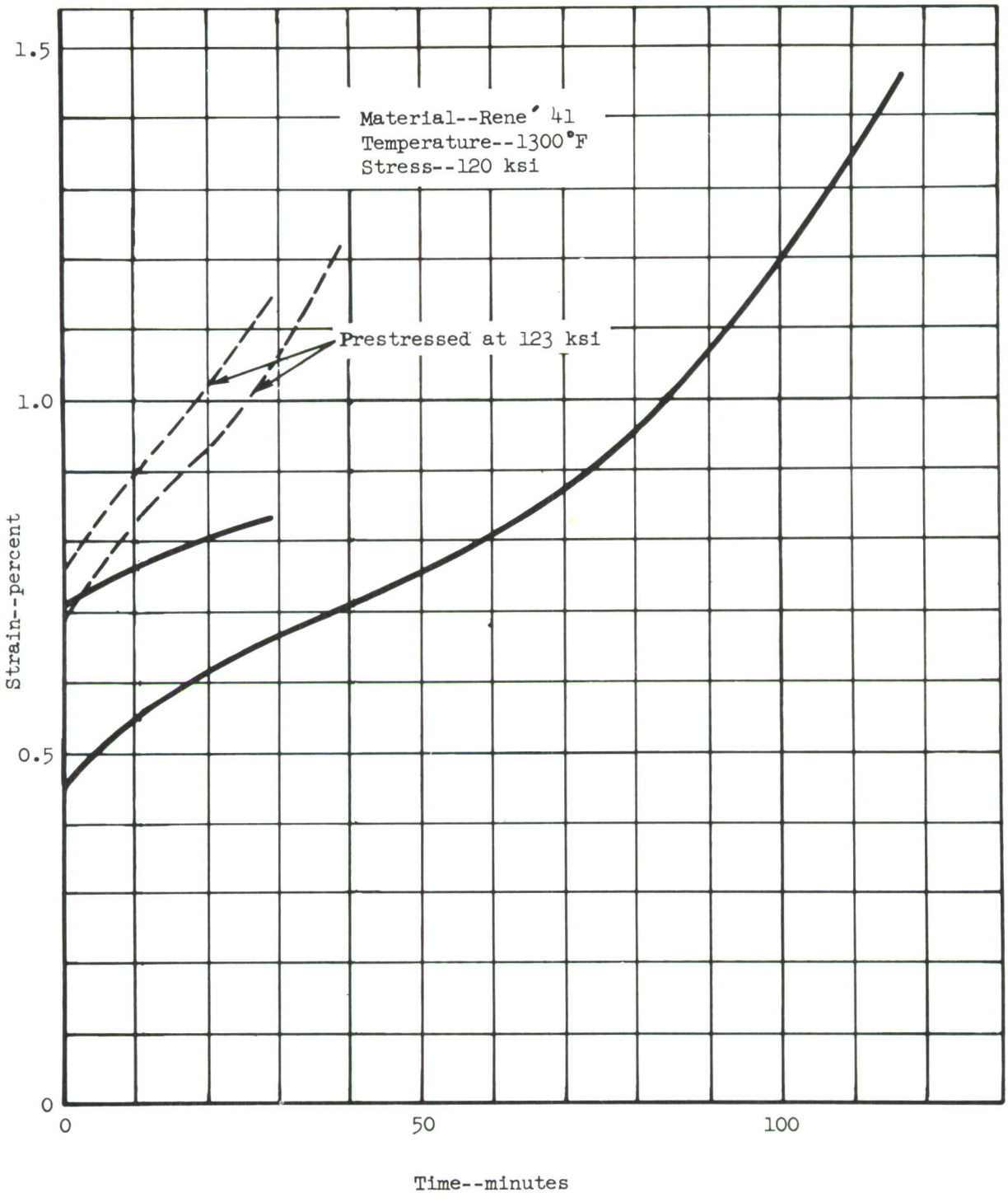


Figure 92. Creep Curves, Rene 41 Alloy, 1300°F

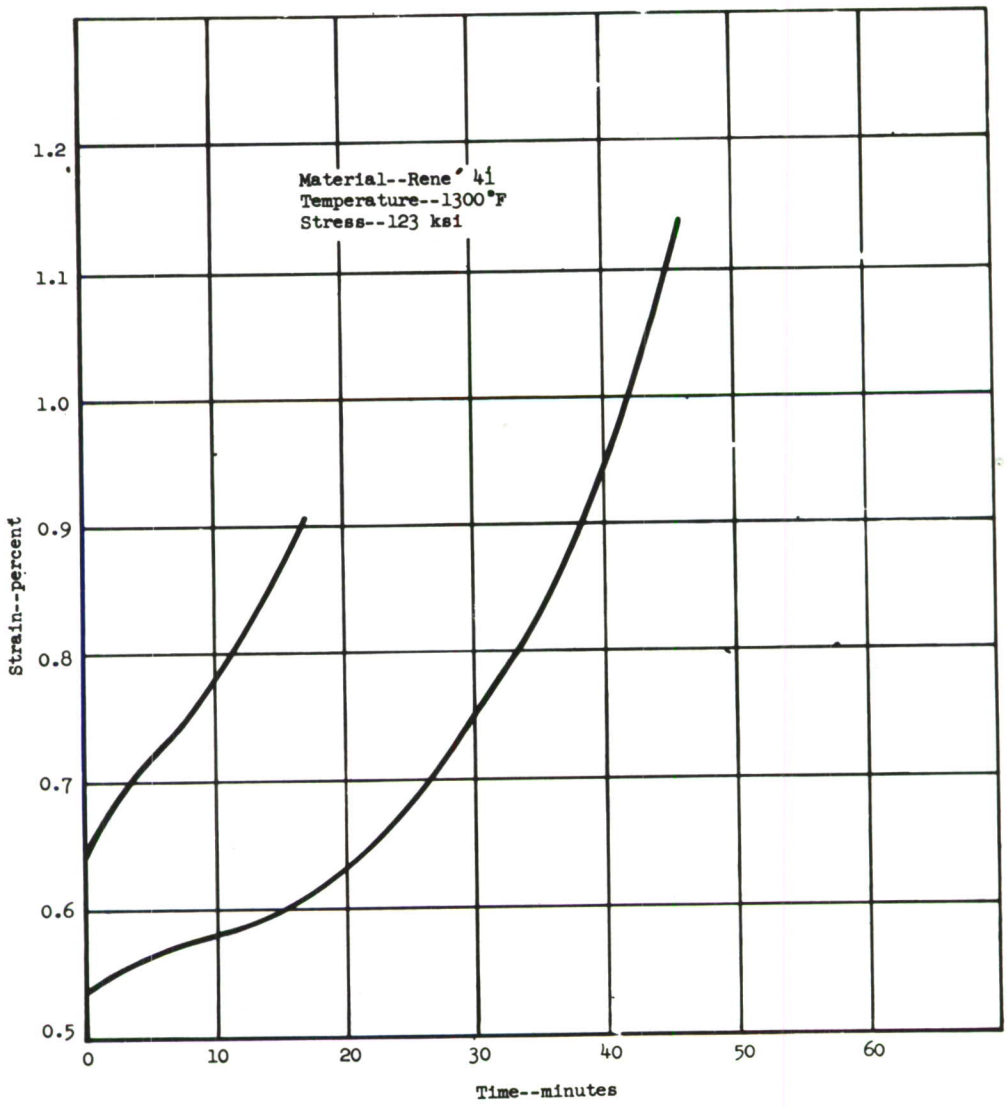


Figure 93. Creep Curves, Rene 41 Alloy, 1300°F

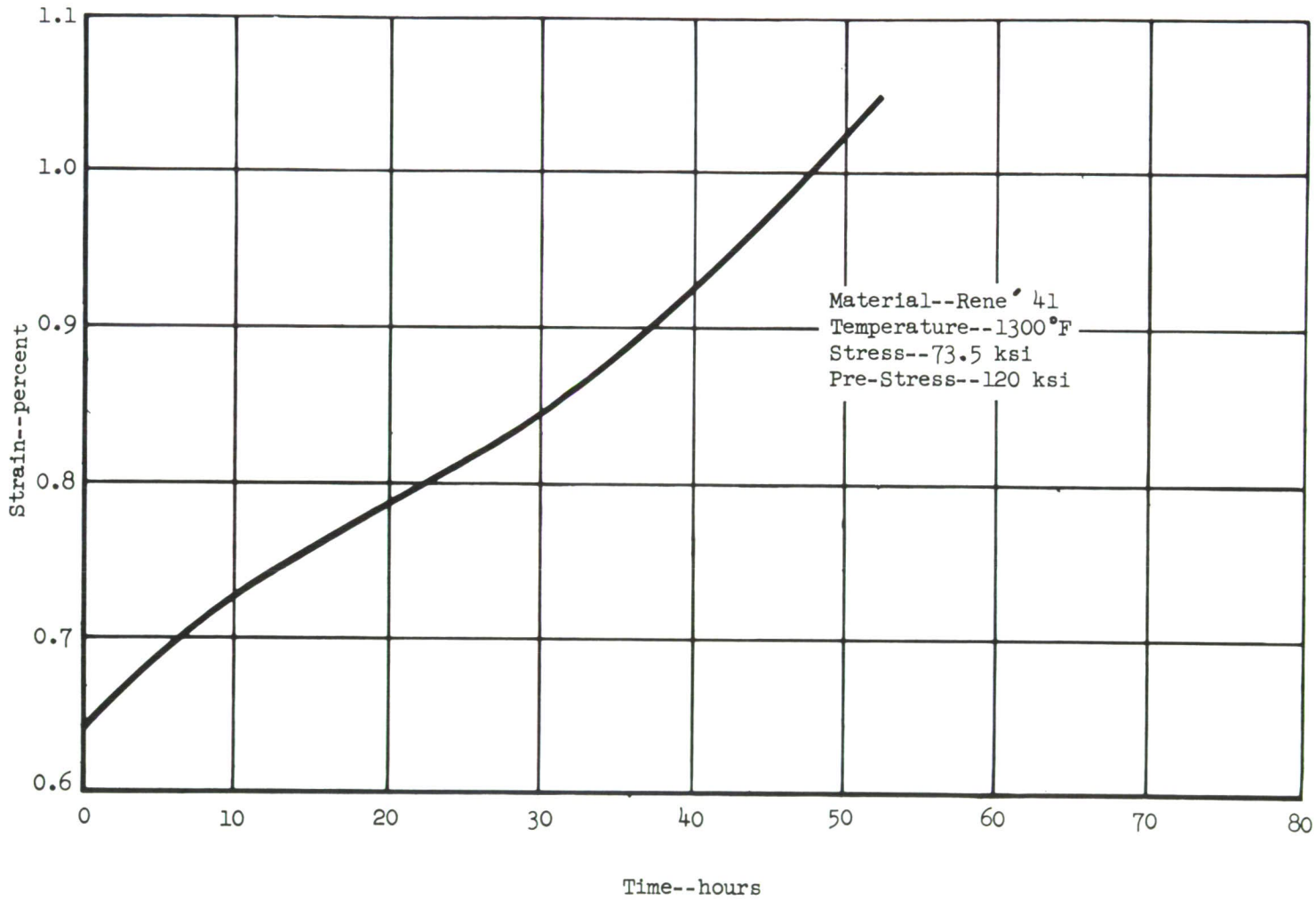


Figure 94. Creep Curve, Rene 41 Alloy, 1300°F

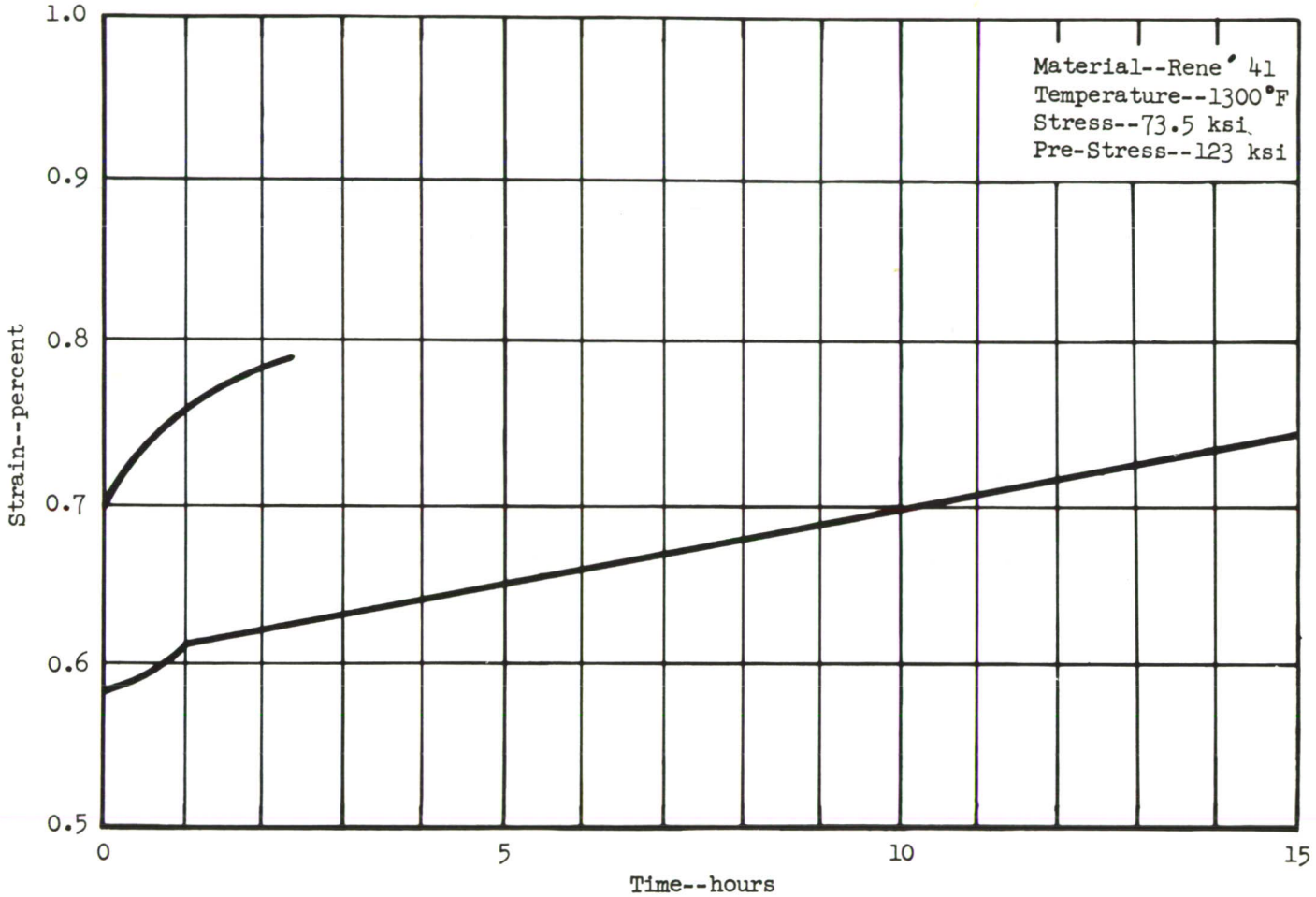


Figure 95. Creep Curves, Rene 41 Alloy, 1300°F

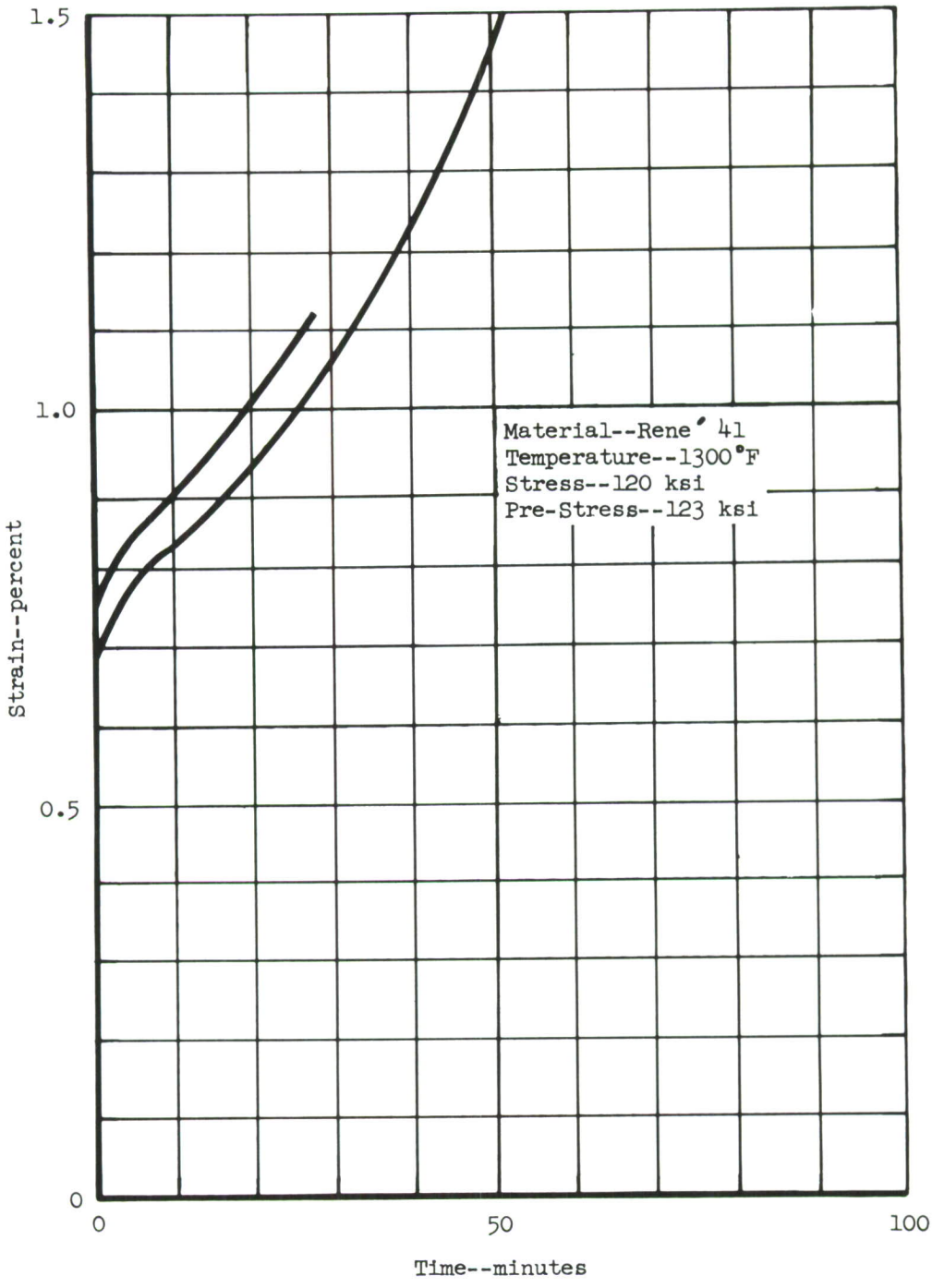


Figure 96. Creep Curves, Rene 41 Alloy, 1300°F

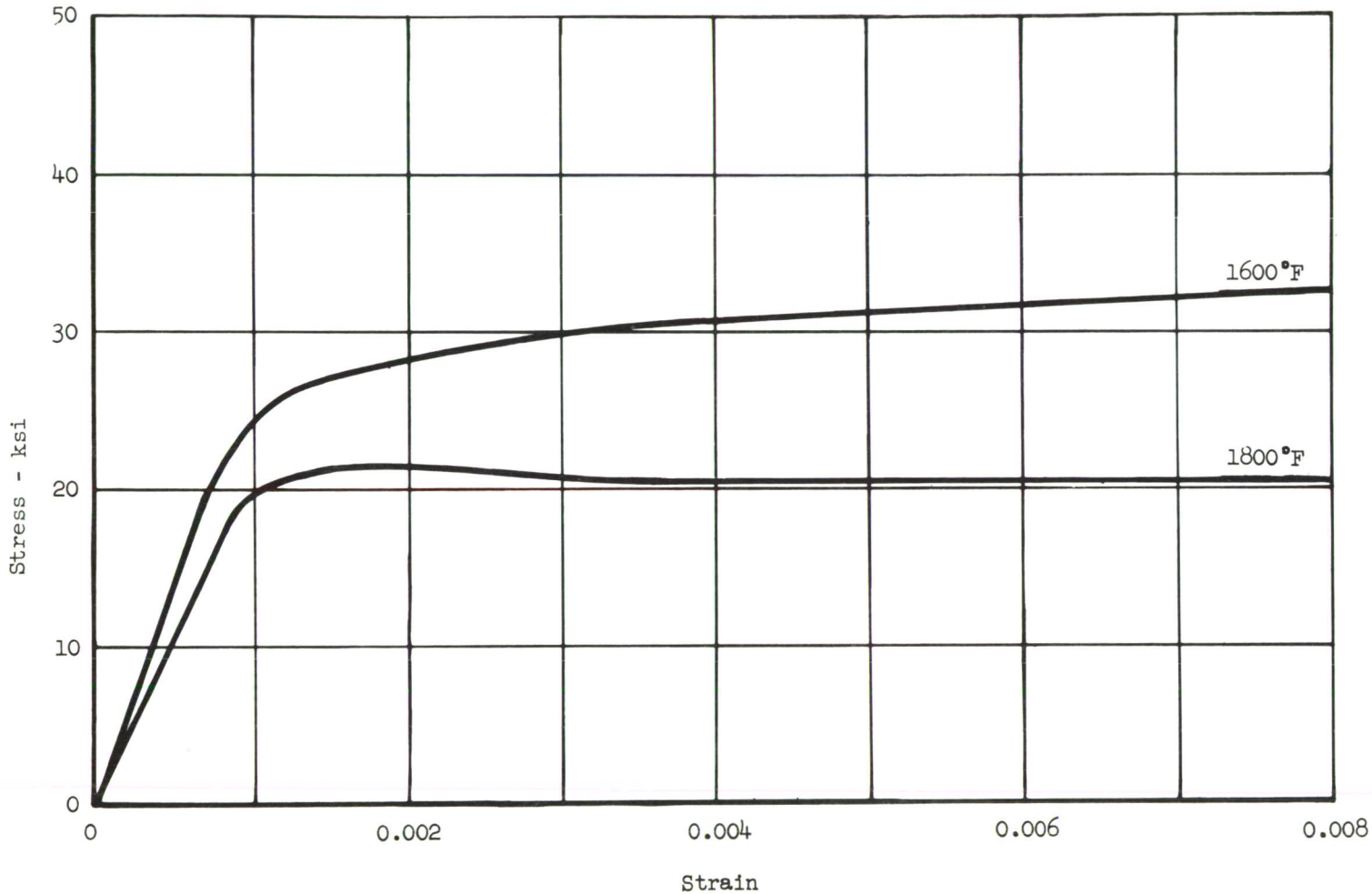


Figure 97. Stress Strain Curves, HS-25 Alloy

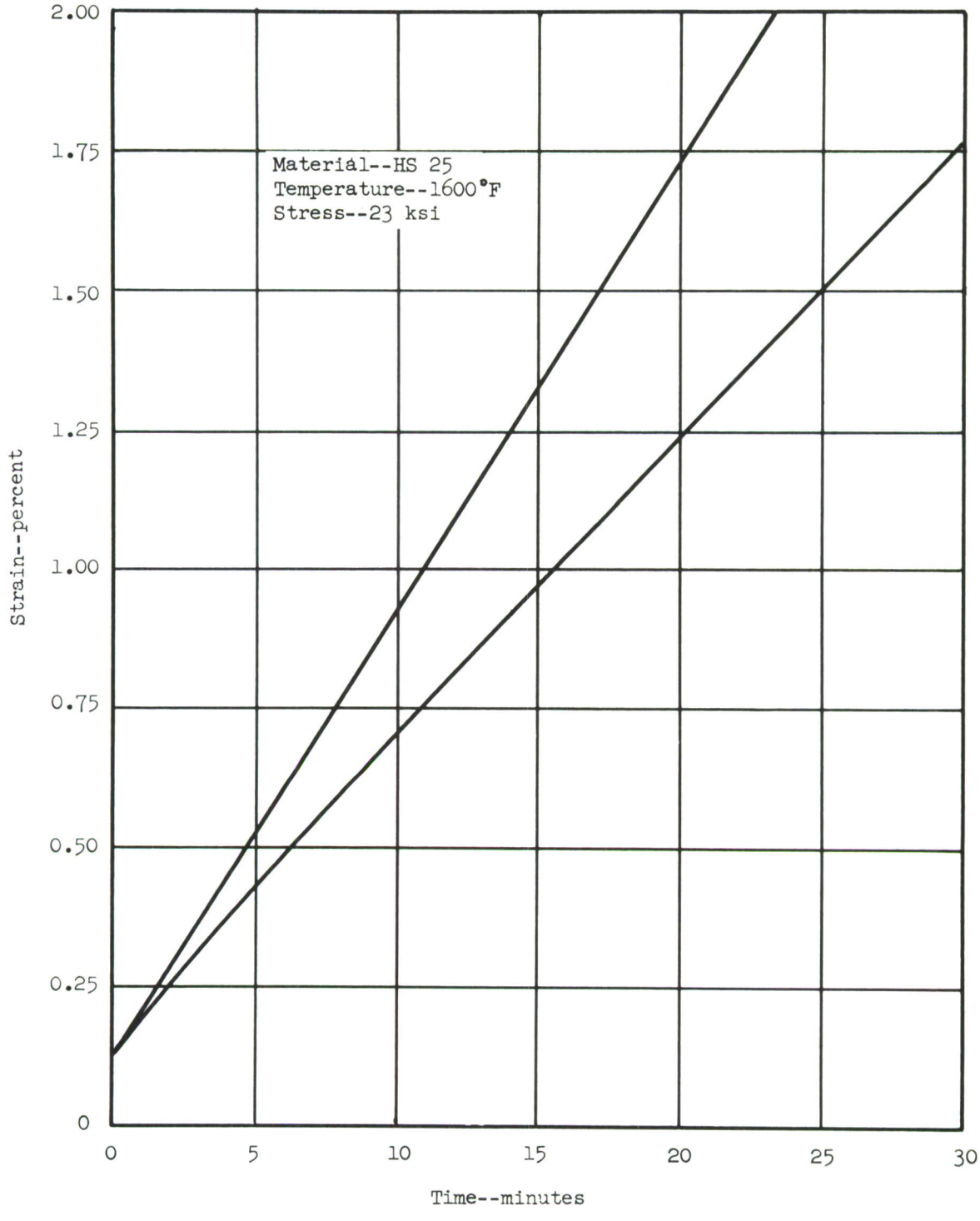


Figure 98. Creep Curves, HS-25 Alloy, 1600°F

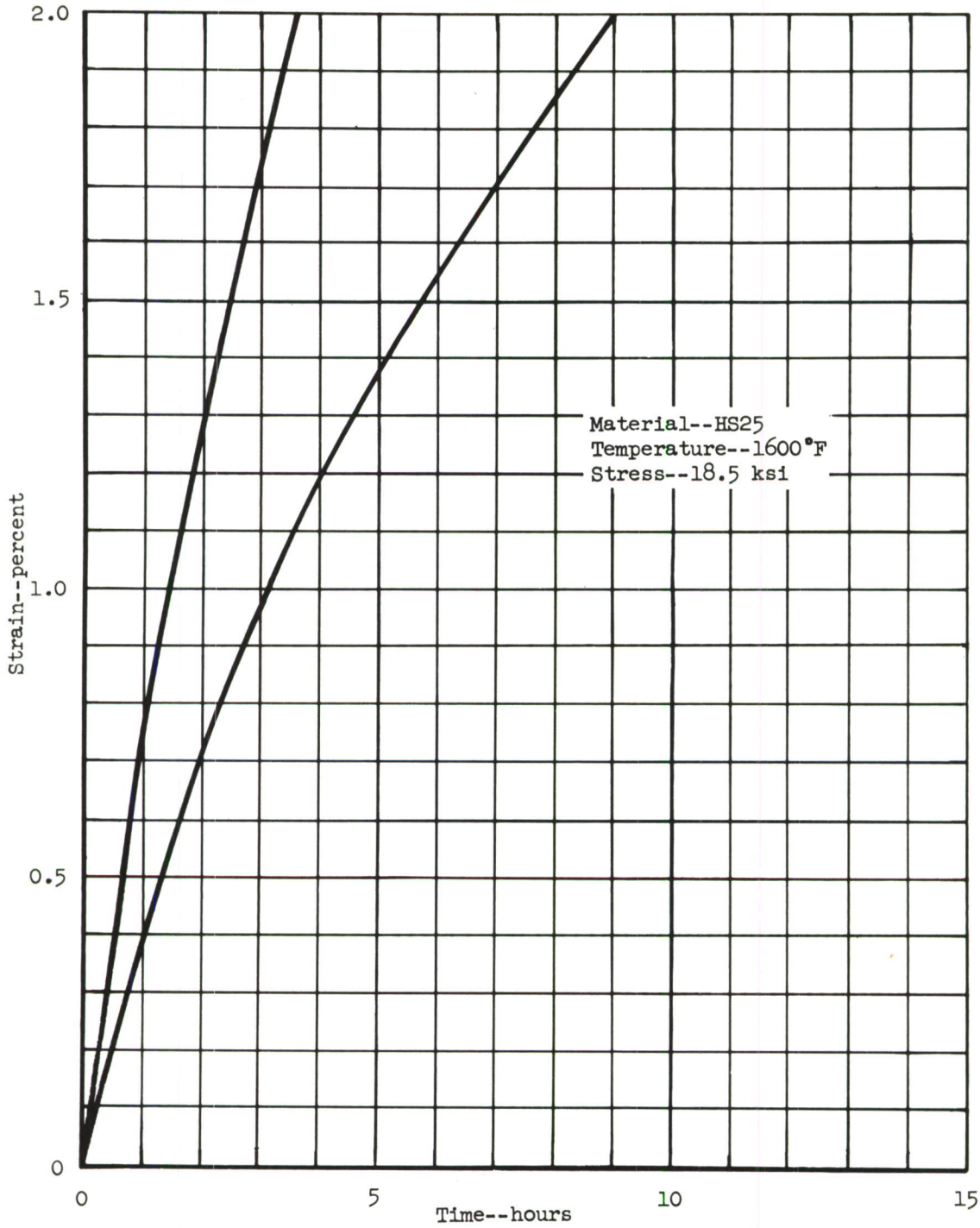


Figure 99. Creep Curves, HS-25 Alloy, 1600°F

Material - Armco PH 15-7 Mo,
Condition RH 950 Stainless Steel

Strain Gage - Type SSE-4C, Micro Test Inc.

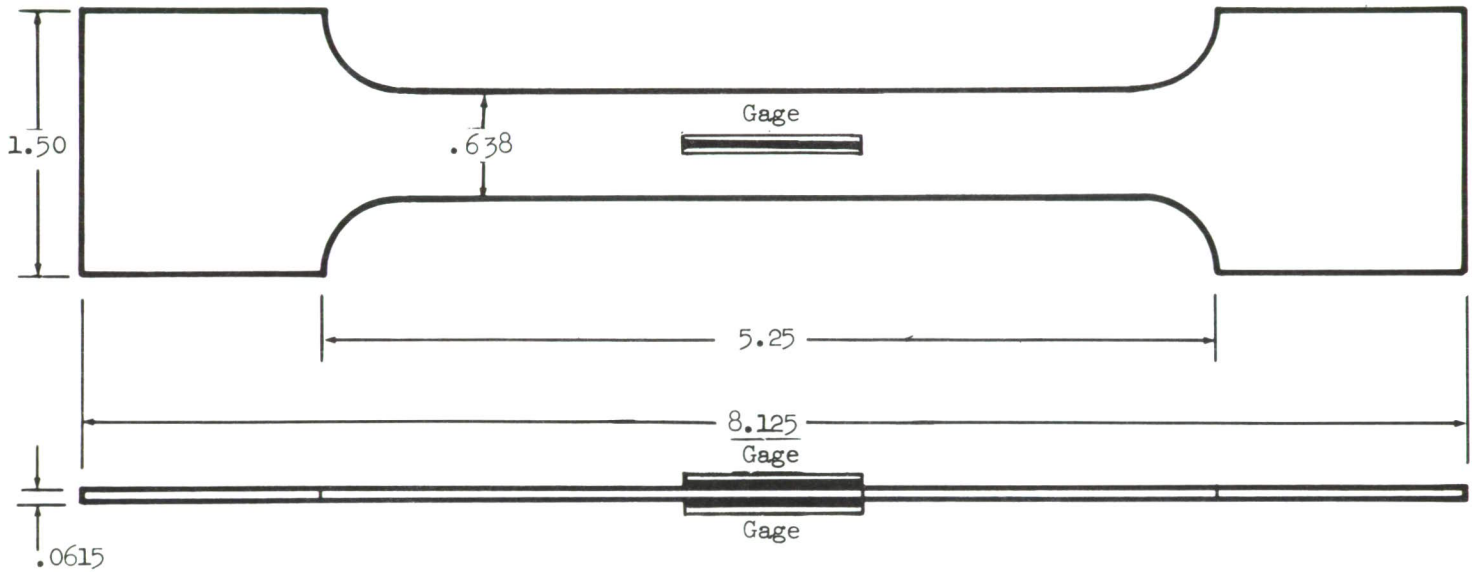


Figure 100. Electric Resistance Strain Gage Calibration Test Specimen

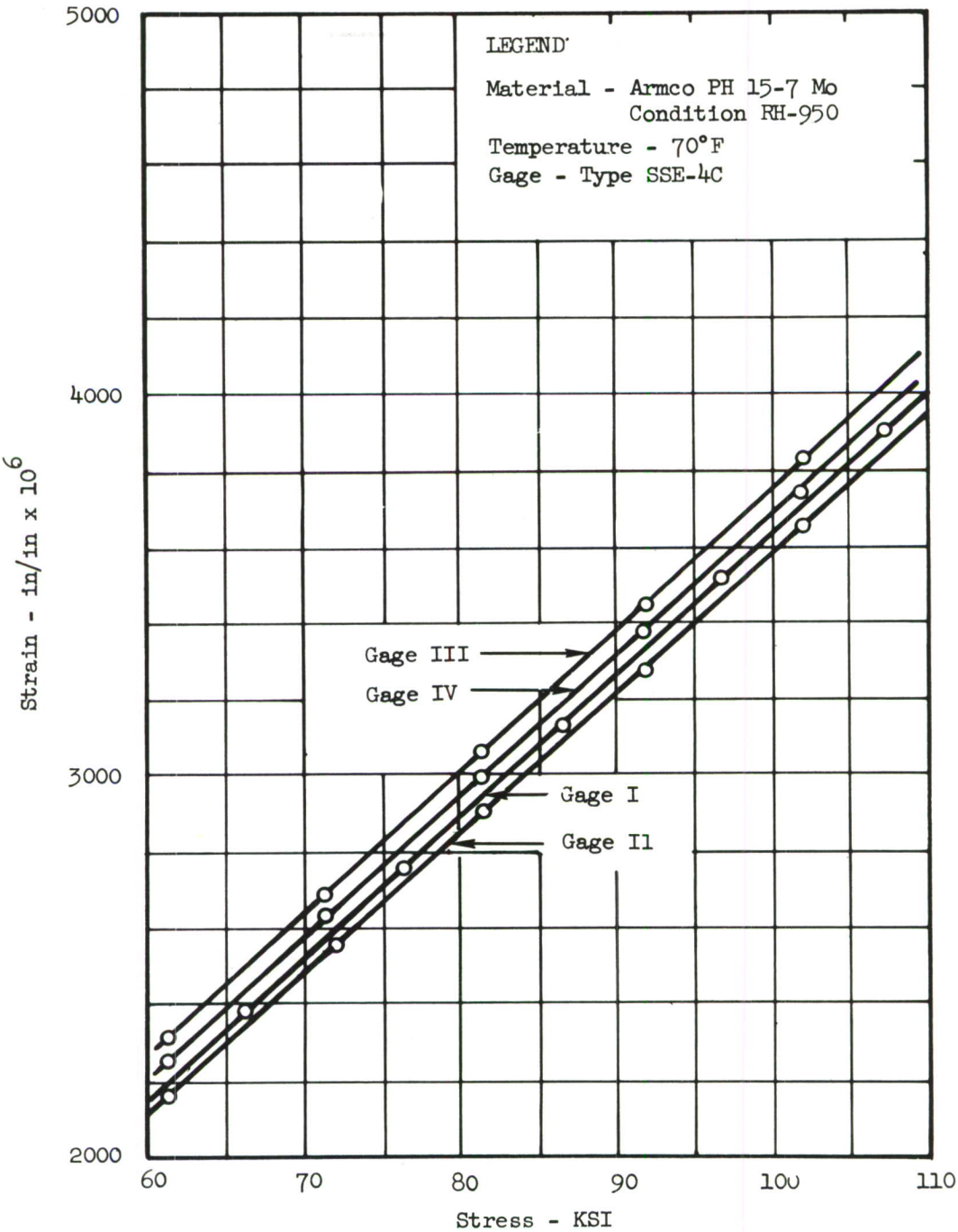


Figure 101. Strain Gage Calibration - Room Temperature

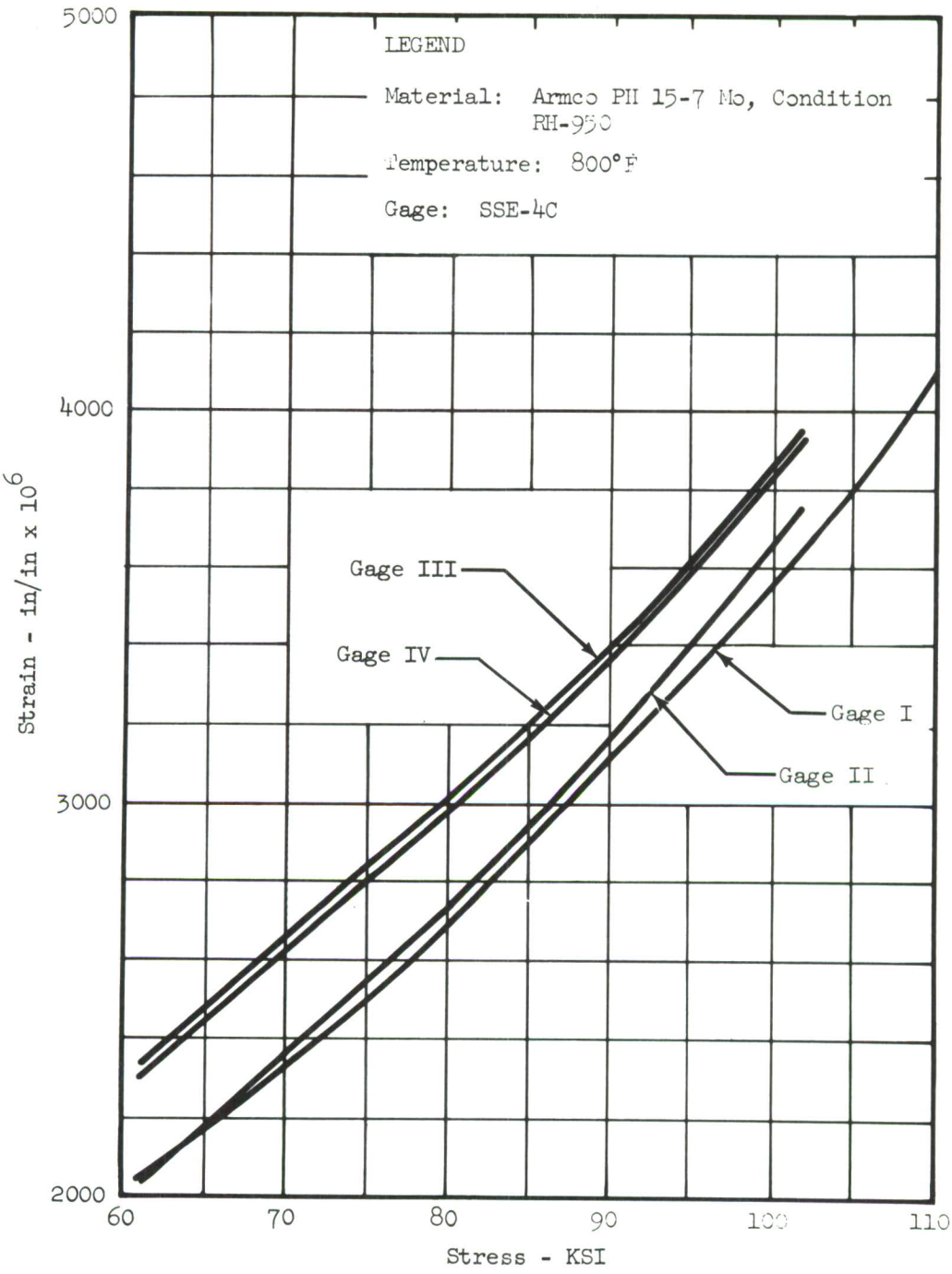
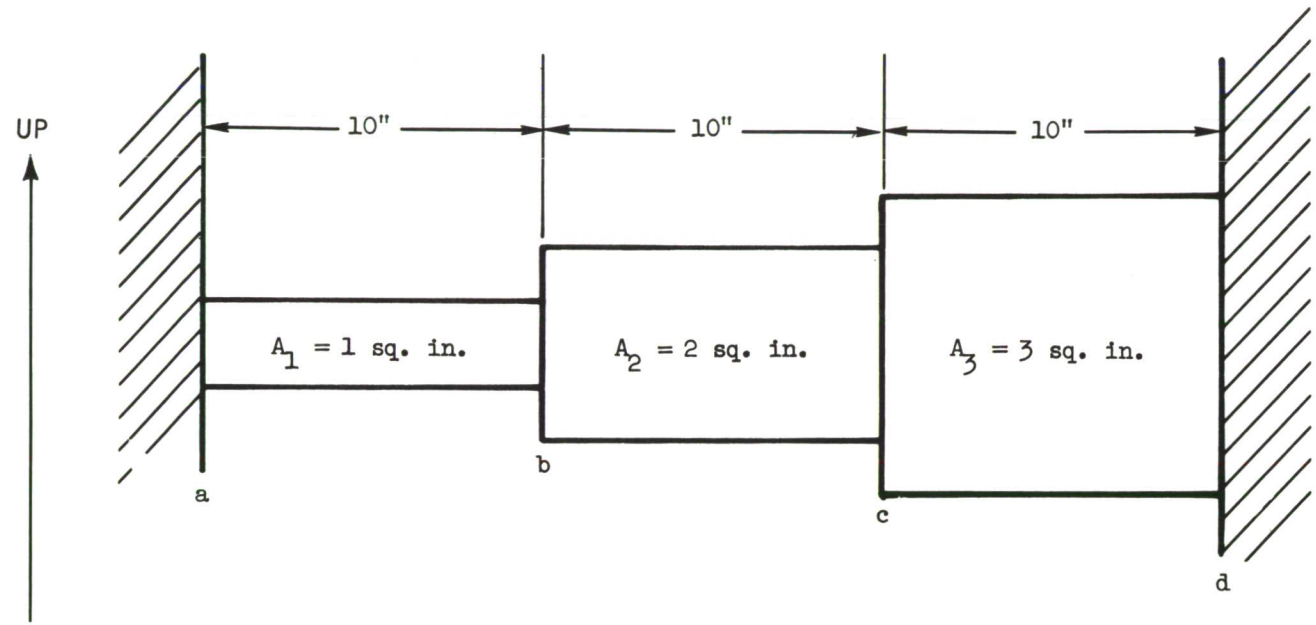


Figure 102. Strain Gage Calibration - 800°F



Material: Armco PH 15-7 Mo,
Condition TH-1050
Stainless Steel

Figure 103. Illustrative Example Scheme

APPENDIX I

VERIFICATIONS OF ELECTRIC RESISTANCE STRAIN GAGES FOR USE WITH STAINLESS STEEL AT ELEVATED TEMPERATURES

INTRODUCTION

According to manufacturer's specifications, the SSE-4C series of electric resistance strain gages manufactured by Micro-Test Incorporated, 1718 21st Street, Santa Monica, California were useful up to 900°F and 8000 micro-inches per inch strain. Prior to use in the present program these gages were not widely applied to a variety of stainless steels at temperatures approaching gage upper limit of utility. The verifications described below were thus performed to determine the presence of disturbances which would limit their operation at the relatively high temperatures involved in the present tests.

PROCEDURE

Four specimens of the dimensions and configuration shown in Figure 100 were fabricated from Armco PH 15-7 Mo, Condition RH 950 stainless steel. The strain gages shown in Figure 100 were attached to the specimens by resistance spot welding with a "one spot at a time" procedure. Gages were applied to two specimens which were not pre-loaded and to two specimens which were held under 65,000 psi stress.

In the initial calibration run all specimens were brought to an initial stress of 60,000 psi where readings were taken. Following this initial stress application, the stress was increased in 10,000 psi increments until a peak stress of 100,000 psi was attained. Readings were taken after attainment of each incremental load. After the room temperature calibration was done, all specimens were then heated to 800°F in induction furnaces. When temperature equilibrium between the specimens, gages and auxiliary equipment was established, the specimens were run through the same loading and observation programs that they were at room temperature. Figures 101 and 102 show strain gage calibration charts obtained for the room temperature and 800°F conditions.

CONCLUSIONS

1. The SSE-4C Micro-Test Incorporated electric resistance strain gages displayed non-linear calibration characteristics.

2. These gages show considerable variation in calibration when non-prestressed Armco PH 15-7 Mo, Condition RH 950 stainless steel is compared with the prestressed material. The strain indicated by gages prestressed to 60,000 psi at 800°F was about 270 micro-inches greater than that observed with gages which were not prestressed.

3. Those gages which were loaded in the prestressed condition showed greater non-linear tendencies than those which were loaded without prestress.

APPENDIX II

EXAMPLE PROBLEM ILLUSTRATING USE OF PROPOSED METHOD FOR INTRODUCING CREEP INTO AIRFRAME ANALYSIS

Figure 103 shows a shaft which is loaded and heated from 75°F to 700°F in a time approaching zero hours. The shaft material is Armco PH 15-7 Mo, Condition RH 950 stainless steel. This has, at 700°F, an elastic modulus, E, of 23.7×10^6 psi and a coefficient of expansion, α, of 6.5×10^{-6} in per in per deg F.

Using the stiffness or "unit deflection" concept, the stiffness matrix "K_n" for the constant sections are

$$K_n = \begin{bmatrix} k_n & -k_n \\ -k_n & k_n \end{bmatrix} \tag{139}$$

where $k_n = A_n (E_n/L_n)$

A = area

E = modulus of elasticity

L = length.

Then

$$K_1 = \begin{bmatrix} .1 & -.1 \\ -.1 & .1 \end{bmatrix} \times 23.7 \times 10^6 \tag{140}$$

$$K_2 = \begin{bmatrix} .2 & -.2 \\ -.2 & .2 \end{bmatrix} \times 23.7 \times 10^6$$

$$K_3 = \begin{bmatrix} .3 & -.3 \\ -.3 & .3 \end{bmatrix} \times 23.7 \times 10^6$$

and

$$K_{total} = K_1 + K_2 + K_3. \tag{141}$$

Therefore

$$K_{total} = \begin{bmatrix} .1 & -.1 & & \\ -.1 & [.1+.2] & -.2 & \\ & -.2 & [.2+.3] & -.3 \\ & & -.3 & .3 \end{bmatrix} \times 23.7 \times 10^{6} \tag{142}$$

The deflections at fixed points must be equal to zero. Hence the rows and columns representing them may be struck out.

$$K = \begin{bmatrix} .1 & -.1 & & \\ -.1 & .3 & -.2 & \\ & -.2 & .5 & -.3 \\ & & -.3 & .3 \end{bmatrix} \times 23.7 \times 10^{6} = \begin{bmatrix} .3 & -.2 \\ -.2 & .5 \end{bmatrix} \times 23.7 \times 10^{6} \tag{143}$$

The deflections are then

$$K^{-1} b = x \tag{144}$$

where

$$K^{-1} = \frac{10^{-6}}{.11 \times 23.7} \begin{bmatrix} .5 & .2 \\ .2 & .3 \end{bmatrix} = \begin{bmatrix} .191791 & .076717 \\ .076717 & .115075 \end{bmatrix} \times 10^{-6} \tag{145}$$

and b is a force generated at the sections by not letting them deflect.

The force, F, generated by heating is

$$F = E \alpha \Delta t \Delta A = 23.7 \times 10^{6} \times 6.5 \times 10^{-6} \times (700 - 75)\ .1 \tag{146}$$

$$= 96,281 \text{ lb.}$$

Then

$$\begin{bmatrix} x_b \\ x_c \end{bmatrix} = \begin{bmatrix} .191791 & .076717 \\ .076717 & .115075 \end{bmatrix} \times \begin{bmatrix} .096281 \\ .096281 \end{bmatrix} = \begin{bmatrix} .025854 \\ .018466 \end{bmatrix} . \tag{147}$$

The forces in the individual elements are

$$\begin{bmatrix} F_{1a} \\ F_{1b} \end{bmatrix} = \begin{bmatrix} 2.37 \times 10^6 & -2.37 \times 10^6 \\ 2.37 \times 10^6 & 2.37 \times 10^6 \end{bmatrix} \times \begin{bmatrix} 0 \\ .025854 \end{bmatrix} = \begin{bmatrix} 61274 \\ 61274 \end{bmatrix} \tag{148}$$

$$\begin{bmatrix} F_{2b} \\ F_{2c} \end{bmatrix} = \begin{bmatrix} 4.74 \times 10^6 & -4.74 \times 10^6 \\ -4.74 \times 10^6 & 4.74 \times 10^6 \end{bmatrix} \times \begin{bmatrix} .025854 \\ .018466 \end{bmatrix} = \begin{bmatrix} 35019 \\ -35019 \end{bmatrix} \tag{149}$$

$$\begin{bmatrix} F_{3c} \\ F_{3d} \end{bmatrix} = \begin{bmatrix} 7.11 \times 10^6 & -7.11 \times 10^6 \\ -7.11 \times 10^6 & 7.11 \times 10^6 \end{bmatrix} \times \begin{bmatrix} .018466 \\ 0 \end{bmatrix} = \begin{bmatrix} .131293 \\ -131293 \end{bmatrix} \tag{150}$$

The stress is then the superposition of the thermal stress and the redistribution stress where

$$\begin{aligned} \sigma_1 &= -96281 - 61274 = -157555 \\ \sigma_2 &= -96281 + 1/2\,(35019) = -78772 \\ \sigma_3 &= -96281 + 1/3\,(131293) = -52517 \end{aligned} \tag{151}$$

At this point it is advantageous to find a differential matrix expressing change of stress in the shaft with respect to creep in the different portions of the shaft. Since only section "1" is highly stressed, only the difference matrix expressing change of stress with creep in this section need be considered. The arbitrary unit value of creep is taken at one percent in per in strain. Then the force in the restrained system from one percent creep is

$$\begin{aligned} F_1 &= .01\ EA = -.237 \times 10^6 \text{ lbs} = F_b,\ F_c = 0 \\ F_2 &= .01\ EA = .474 \times 10^6 \text{ lbs} = F_b = -F_c \\ F_3 &= .01\ EA = .711 \times 10^6 \text{ lbs} = F_c, F_b = 0 \end{aligned} \tag{152}$$

When the restrained system is unlocked, the redistribution of deflections that occurs is

$$\begin{bmatrix} x_b \\ x_c \end{bmatrix} = \begin{bmatrix} .191791 & .076717 \\ .076717 & .115071 \end{bmatrix} \times \begin{bmatrix} -.237 \\ 0 \end{bmatrix} = \begin{bmatrix} -.0454545 \\ -.0181819 \end{bmatrix} \tag{153}$$

and the stress changes resulting are

$$\sigma_1 = (K_1X_1/A_1) - 0.01E = -107727.2 + 237000 = 129272.8$$

$$\sigma_2 = K_2X_2/A_2 = 64636.1 \text{ psi} \tag{154}$$

$$\sigma_3 = K_3X_3/A_3 = 43091.1 \text{ psi}$$

In a similar manner the stresses for one percent creep can be found for other sections and a different matrix can be written relating creep and stress. This matrix is

$$\begin{bmatrix} 129273.8 & 129271.9 & 129273.5 \\ 64636.1 & 64637.5 & 64635.8 \\ 43091.1 & 43090.6 & 43090.6 \end{bmatrix} \times \begin{bmatrix} \epsilon_1\%_c \\ \epsilon_2\%_c \\ \epsilon_3\%_c \end{bmatrix} = \begin{bmatrix} \sigma_1 c \\ \sigma_2 c \\ \sigma_3 c \end{bmatrix} \tag{155}$$

where $\epsilon_n\%_c$ is creep strain in percent in nth segment

$\sigma_n c$ is stress resulting from creep strain $\epsilon_n\%_c$.

Therefore a creep strain of .0001 in per in. in section 1 would result in the following stress distribution

$$\sigma_1 = -157,555 + 1292.7 = -156262.3$$

$$\sigma_2 = -78,772 + 643.4 = -78128.6 \tag{156}$$

$$\sigma_3 = -52,517 + 430.9 = 52086.1$$

If the increment of creep is small enough, an average stress could be used to predict the time required to arrive at the required strain. For purposes of illustration a strain of .0001 will be considered small enough to enable use of this average stress concept. Then

$$\sigma_{ave} = .5\ (-157555 - 156262) = -156908. \tag{157}$$

Time = 1.2 minutes

When the creep strain is allowed to increase .0001 in per in from .0001 in per in to .0002 in per in,

$$\sigma_1 = -156262 + 1293 = -154969$$

$$\sigma_2 = -78129 + 643 = -77486$$

$$\sigma_3 = -52086 + 431 = -51655 \qquad (158)$$

$$\sigma_{\ell\,\text{ave}} = .5\,(-156262 - 154969) = -155615$$

$$\text{Time} = 1.5 \text{ minutes}$$

The stresses arising out of several strain increments are shown in Table 26.

Since this problem is only illustrative, much larger steps of strain were used than would be used in a real problem. Also in a real problem a certain amount of time is required to apply loads. Sometimes a certain amount of strain is found to be almost time independent. In this case creep strain depends on stress and the rate of loading contains a certain amount of scatter, almost as if the creep flow were unstable. In this case the creep strain is included in a lump sum acting through zero time but the answers are only as good as the prediction of "time independent creep."

The formulation given in this example is only slightly different from that given in WADD TR 60-411 Part I. In this illustration the increment of strain was arbitrarily taken and the time required to produce this strain computed. In WADD TR 60-411 Part I the strain rate was taken from graphs and an arbitrary increment of time was used to estimate the creep strain. In WADD TR 60-411 Part I and in this example the change of stress resulting from creep strain is found. However, the creep rate used in WADD TR 60-411 Part I is based upon the stress at the beginning of the time increment and tends to be somewhat less accurate than use of an average stress as shown in this illustration.

APPENDIX III - BIBLIOGRAPHY

PERIODICALS

1. Andrews, K. W., "Some Observations on the Use of a Time-Temperature Parameter," Journal of the Iron and Steel Institute, Vol. 192, No. 3, p 291, 1959.

2. Ansell, G. S. and Weertman, J., "Creep of a Dispersion Hardened Aluminum Alloy." Transactions, Metallurgical Society, American Institute of Mining, Metallurgical and Petroleum Engineers, Vol. 215, No. 5, p 830, October 1959.

3. Arwidson, I., "Creep Resisting Materials," Jernkontorets Annaler, Vol. 143, No. 7, p 373, 1959.

4. Bailey, W. H., et al., "Creep Properties of Austenitic Nickel Chromium Steels Containing Niobium," Institution of Mechanical Engineers Proceedings, Vol. 171, No. 34, p 911, 1957.

5. Bieniek, M. P. and Freudenthal, A. M., "Creep Deformation and Stress in Pressurized, Long Cylindrical Shells," Journal of Aerospace Sciences, Vol. 27, p 763, October 1960.

6. Bleich, H. H. and Dillon, O. W. Jr., "Nonlinear Creep Deformations of Columns of Rectangular Cross Section," Transactions American Society of Mechanical Engineers, Vol. 81E, p 517, 1959.

7. Bychawski, Z., "Resolving Kernel of the Volterra Equation in the Case of the Generalized Creep Function," Arch. Mech. Stos., Warsaw, Vol. 9, No. 2, p 247, 1957.

8. Brookes, P. E., Kirby, N., and Burke, W. T., "Creep Deformation and Stress in Pressurized, Long Cylindrical Shells," Journal of the Aerospace Sciences, Vol 27, p 763, October 1960.

9. Child, H. C. et al., "Creep Strength of Some High Temperature Alloys at 1050° - 1200°C." Metallurgia, No. 61, p 51, February 1960.

10. Clauss, F. J., "What You Should Know About Creep Rupture," Materials in Design Engineering, Vol. 53, No. 1, p 89, January 1961.

11. Conrad, Hans, "Correlations of High Temperature Creep and Creep Rupture Data," American Society of Mechanical Engineers Transactions, Vol. 81D, p 617, December 1959.

12. Davis, E. A., "Relaxation of a Cylinder on a Rigid Shaft," American Society of Mechanical Engineers Transactions, No. 82E, No. 1, p 41, March 1960.

13. Davis, P. W. and Dennison, J. P., "Role of Voids in Creep and Fracture of a Pure Metal," Journal of the Institute of Metals, Vol. 88, No. 11, p 471, July 1960.

14. Dorn, J. E., "Fundamental Experiments on High Temperature Creep," Journal of Mechanics and Physics of Solids, Vol. 3, No. 2, p 85, January 1955.

15. Drucker, D. C., "A Definition of Stable Inelastic Material," American Society of Mechanical Engineers Transactions, Vol. 81E, No. 1, p 101, March 1959.

16. Duby, J., "Changes in Physical Properties and Microstructure of Metals Due to Rapid Straining," Canadian Mining and Metallurgical Bulletin, Vol. 53, p 408, June 1960.

17. Feltham, P. and Meakin, J. D., "Creep in Face-Centered Cubic Metals with Special Reference to Copper," Acta Metallurgia, Vol. 7, p 589, September 1959.

18. Fenn, R. W. Jr., and Gusack, J. A., "Effect of Strain Rate and Temperature on the Strength of Magnesium Alloys," Proceedings American Society for Testing Materials, Vol. 58, p. 685, 1958.

19. Findley, W. N., "Mechanism and Mechanics of Creep of Plastics," Journal of the Society of Plastics Engineers, Vol. 16, p 57, January 1960.

20. Findley, W. N. and Worley, W. J., "A Versatile High Temperature Testing Machine for Creep, Stress Relaxation and Static Tension Tests," Proceedings Society for Experimental Stress Analysis, Vol. XVII, No. 1, p 15, 1959.

21. Finnie, I., "Stress Analysis in the Presence of Creep," Applied Mechanics Review, Vol. 13, p 705, October 1960.

22. Finnie, I., "Steady State Creep of a Thick Walled Cylinder Under Combined Axial Load and Internal Pressure," Transactions American Society of Mechanical Engineers, Vol. 82D, No. 3, p 689 September 1960.

23. Fountain, R. W., and Korchinsky, M., "Phenomenon of Negative Creep in Alloys," Transactions American Society for Metals, Vol. 51, p 108, 1959.

24. Frederick, S. F., "Predicting Very Short Time Creep Behavior for Missiles," Metal Progress, Vol. 79, No. 3, p 88, March 1961.

25. Gemma, A. E., "The Creep Deformation of Symmetrically Loaded Circular Cylindrical Shells," Journal of the Aerospace Sciences, Vol. 27, No. 12, p 953 December 1960.

26. Gemma, A. E., "Ring with Edge Moments," Journal of the Aerospace Sciences, Vol. 27, No. 11, p 867, November 1960.

27. Glen, J., "Effect of Alloying Elements on Creep Behavior," Journal of the Iron and Steel Institute, Vol. 190, pt. 2, p 114, October 1958.

28. Glen, J., "New Approach to the Problem of Creep," Journal of the Iron and Steel Institute, Vol. 189, pt. 4, p 333, August 1958.

29. Gohlke, W., "On the Relationship of the Modulus of Elasticity to the Rate of Deformation," VDI Zeitschrift, Vol. 102, No. 13, p 516, May 1960.

30. Goodey, W. J., "Creep Deflection and Stress in a Beam," Aircraft Engineering, Vol. 30, No. 352, p 170, June 1958.

31. Green, A. E., Rivlin, R. S., Spencer, A. J. M., "The Mechanisms of Nonlinear Materials with Memory," Archives of Rational Mechanical Analytics, Vol. 1, No. 1, September 1959.

32. Green, W. V., "Short Time Creep-Rupture Behavior of Tungsten at 2250-2800°C," Transactions Metallurgical Society, American Institute of Mining, Metallurgical and Petroleum Engineers, Vol. 215, No. 6, p 1057, December 1959.

33. Greist, A. J., Sabroff, A. M. and Frost, P. D., "Effect of Strain Rate and Temperature on the Compressive Flow Stresses of Three Titanium Alloys," Transactions American Society for Metals, Vol. 51, p 935, 1959.

34. Hammel, R. L. and Uhrig, R. E., "Creep of Tantalum under Cyclic Elevated Temperatures," United States Energy Commission, IS-125, April 1960.

35. Harper, J. and Dorn, J. E., "Viscous Creep of Aluminum Near Its Melting Temperature," Acta Metallurgica, Vol. 5, p 654, 1957.

36. Hawthorne, R., "Predicting the Creep Strength of Joints," Space Aeronautics, Vol. 33, No. 3, p 99, March 1960.

37. Hengstenberg, T. F., "Vacuum Furnace for Creep Rupture Testing," Metal Progress, Vol. 77, No. 6, p 94, June 1960.

38. Hilton, H. H., "Divergence of Supersonic Linear Viscoelastic Lifting Surfaces Including Chordwise Bending," Journal of the Aerospace Sciences, Vol. 27, No. 12, p 926, December 1960.

39. Hwang, C., "Incremental Stress Strain Low Applied to Work Hardening Plastic Materials," Transactions American Society of Mechanical Engineers, Vol. 81E, p 594, December 1959.

40. Hwang, C., "Thermal Stresses in an Elastic, Work-Hardening Sphere," Transactions of the American Society of Mechanical Engineers, Vol. 82B, No. 4, p 629, December 1960.

41. Jacobowitz, J. L. and Mader, C. K., "Steady State Creep Analysis of the Weight Loadings of Furnace Tubes on Multiple Supports," Transactions American Society of Mechanical Engineers, Vol. 81B, No. 2, p 115, May 1959.

42. Johnson, A. E., Henderson, J. and Mather, V. D., "Complex Creep Relaxation of Metallic Alloys at Elevated Temperatures," Aircraft Engineering, Vol. 31, No. 361, p 75, March 1959.

43. Johnson, A. E., Henderson, J. and Mather, V. D., "Prediction of Relaxation Stress Time Curves from Static Tensile Test Data," Metallurgia, Vol. 59, p 215, May 1959.

44. Johnson, A. E., Henderson, J. and Mather, V. D., "Pure Torsion Creep Rates on Magnesium Alloy at 20°C and 0.2% C Steel at 450°C at Low Rates of Strain," Metallurgia, Vol. 58, No. 347, p 109, September 1958.

45. Johnson, A. E., Henderson, J. and Mather, V. D., "Complex Stress Creep Fracture of an Aluminum Alloy," Aircraft Engineering, Vol. 32, No. 376, p 61, June 1960.

46. Karpov, G. I., "Strain Distribution in the Compression of Cylinders at a High Rate of Deformation," Fiz. Metallov i Metallovedeniye, Vol. 2, No. 1, p 172, 1956.

47. Karpov, G. I., "Strain Inhomogeniety in Plastic Compression," Fiz. Metallov i Metallovedeniye, Vol. 2, No. 1, p 168, 1956.

48. Kennedy, C. R., Harns, W. O. and Douglas, D. A., "Multiaxial Creep Studies on Inconel at 1500°F., "Transactions American Society of Mechanical Engineers, Vol. 81D, No. 4, p 599, December 1959.

49. Kennedy, A. J., "Problems of Combined Creep and Fatigue Design," Engineer, Vol. 204, No. 5305, p 444, September 27, 1957.

50. Kirby, H. W., "The Creep Properties of Two Austenitic Molybdenum Bearing Steels," Alloy Metals Review, Vol. 9, No. 92, July 1959.

51. Korchynsky, M., "High Temperature Creep Rupture Data," Product Engineering, Vol. 31, No. 42, p 75, October 10, 1960.

52. Kostachkin, Y. V. and Odling, I. A., "Failure of Metals Due to Thermal Fatigue," American Rocket Society Journal, Vol. 30, No. 11, p 1062, November 1960.

53. Lawley, A., Coll, J. A. and Cahn, R. W., "Influence of Crystallographic Order on Creep of Iron-Aluminum Solid Solutions," Transactions Metallurgical Society, American Institute of Mining, Metallurgical and Petroleum Engineers, Vol. 218, No. 1, p 166, February 1960.

54. Lee, E. H., et al., "Stress Analysis for Linear Viscoelastic Materials," Transactions of the Society of Rheology, Vol. 3, 1959.

55. Ma, B. M., "A Further Creep Analysis for Rotating Solid Disks of Variable Thickness," Journal of the Franklin Institute, Vol. 269, No. 1613, pp 408, May 1960.

56. MacDonald, J. R., "Modifications of Lamnitz - Jeffreys Law of Creep," Journal of Applied Physics, Vol. 30, No. 3, p 453, March 1959.

57. Malinin, N. I., "The Regularity of Creep in Metals and Calculations of Creep in Design of Machine Elements," Vestnik Machino Strogeniya, Vol. 39, No. 1, January 1959.

58. Manjoine, M. J., "Combination Creep-Rupture Test Specimen," ASTM Bulletin, No. 222, p 26, May 1957.

59. Manson, S. S., Succop. G. and Brown, W. F. Jr., "Procedure for Application of Time Temperature Parameters to Accelerated Creep - Rupture Testing," Transactions American Society for Metals, Vol. 51, p 411, 1959.

60. Marin, J. and Griffith, J. E., "Creep Relaxation of Plexiglass II-A for Simple Stresses," Proceedings American Society of Civil Engineers, Vol. 82, No. EM3, Paper 1029, July 1956.

61. Marin, J., "Mechanics of Creep for Structural Analysis," Transactions of the American Society of Civil Engineers, Vol. 108, p 453, 1943.

62. Marin, J. and Pao, Y. H., "A Theory for Combined Creep Strain Stress Relations for Materials with Different Properties in Tension and Compression," Proceedings First National United States Congress on Applied Mechanics, American Society of Mechanical Engineers, p 585, 1952.

63. Marin, J. and Griffith, J. E., "Creep Relaxation in Torsion," Proceedings Ninth International Congress on Applied Mechanics, Vol. 8, p 316, 1957.

64. Marland, L. W. and Lee, E. H., "Stress Analysis for Linear Viscoelastic Materials with Temperature Variation," Brown University Applied Mathematics Technical Reports, September 1959.

65. Mead, H. W., "Effect of Annealing Treatment on the Structure and Tensile and Creep Properties of a Commercial Titanium Alloy (4% Al - 4% Mn)," Journal of the Institute of Metals, Vol. 87, pt 10, p 343, June 1959.

66. Melka, A. H. and Evershed, A. V., "The Dependence of Creep Behavior on the Duration of a Superimposed Fatigue Stress," Journal of the Institute of Metals, Vol. 88, No. 9, p 411, May 1960.

67. Melka, A. H., "Direct Stress Machine for Combined Fatigue and Creep Testing," Journal of Scientific Instruments, Vol. 36, p 468, November 1959.

68. Mendelson, A., Herschberg, M. H., and Manson, H. H., "A General Approach to the Practical Solution of Creep Problems," Transactions American Society of Mechanical Engineers, Vol. 81D, No. 4, p 585, December 1959.

69. Monkman, F. C. and Grant, N. J., "An Empirical Relation between Rupture Life and Minimum Creep Rate in Creep Rupture Tests," Proceedings American Society for Testing Materials, Vol. 56, p 593, 1956.

70. Naghdi, P. M. and Orthwein, W. C., "Response of Shallow Viscoelastic Spherical Shells to Time-Dependent Axisymmetric Loads," Quarterly of Applied Mathematics, Vol. 18, No. 2, p 107, July 1960.

71. Nowick, A. S., "On the Interpretation of Low Temperature Recovery Phenomena in Cold Worked Metals," Acta Metallurgica, Vol. 3, No. 4, p 321, July 1955.

72. Oding, I. A. and Lepin, G. F., "Calculation of Effective Stresses in a Ring Specimen Subjected to Creep and Relaxation," Industrial Laboratory, Vol. 24, No. 7, p 947, July 1959.

73. Ohara, H. and Doi, T., "Creep in Ni-Ti Alloy Wire," Proceedings Second Japan Congress on Testing Materials, Kyoto Japan, October 14-15, 1958, Japan Society for Testing Materials, p 47, Kyoto 1959.

74. Olds, G. C. E. and Michie, G. M., "Creep Resistant Magnesium Alloys for Nuclear Fuel Elements," Journal of the Institute of Metals, Vol. 88, No. 12, p 493, August 1960.

75. Palmer, K. B., "Creep Tests on a Flake Graphitic Cast Iron at 400°C," British Cast Iron Association Journal of Research and Development, Vol. 7, No. 14, p 839 October 1959.

76. Pao, Y. and Marin, J., "An Analytical Theory of the Creep Deformation of Materials," Journal of Applied Mechanics, Vol. 20, p 245, June 1953.

77. Perrone, N. and Hodge, P. G. Jr., "On Strain Hardened Circular Shells," Transactions of American Society of Mechanical Engineers, Vol. 81E, No. 4, p 594, December 1959.

78. Ree, F. M., Ree, T. and Eyring, H., "Relaxation Theory of Creep of Metals," Proceedings American Society of Civil Engineers, Vol. 86, No. EM-1, p 41, January 1960.

79. Reiner, M., "Plastic Yielding in Anelasticity," Journal of the Mechanics and Physics of Solids, Vol. 8, No. 4, p 255, November 1960.

80. Rimrott, F. P. J., "Creep of Thick Walled Tubes Under Internal Pressure Considering Large Strains," Transactions American Society of Mechanical Engineers, Vol. 81E, p 271, June 1959.

81. Rozovskii, M. I., "On the Non-Linear Integral Evaluation of Creep of Cylindrical Shells Under the Influence of External Pressure." Izv. Akad. Nauk, U.S.S.R. OTN Tech Nauk, No. 9, pp 139, September 1958.

82. Rudee, M. L., "Effect of Irridation on Creep," Journal American Society of Naval Engineers, Vol. 71, No. 3, p 453, August 1959.

83. Sackman, J. L., "Steady Creep Bending of a Non-Homogeneous Beam," Journal of the Aerospace Sciences, Vol. 28, No. 1, p 11, January 1961.

84. Shaninian, P. and Achter, M. R., "The Effect of Atmosphere on Creep Rupture Properties of a Nickel-Chromium-Aluminum Alloy," Proceedings American Society for Testing Materials, Vol. 58, p 761, 1958.

85. Saroja, B. V., "Creep Deformation, The Analysis of Creep in a Thin Rotating Disc with a Central Circular Hole," Aircraft Engineering, Vol. 32, No. 373, p 34, February 1960.

86. Sherby, O. D., Orr, R. L. and Dorn, J. E., "Creep Correlations of Metals at Elevated Temperatures," Journal of Metals, Vol. 6, No. 1, p 71, January 1954.

87. Sundstrom, E. N., "Creep Buckling in Cylindrical Shells," Transactions Royal Institute of Technology, No. 115, 1957, Stockholm.

88. Tao, L. N., "The Creep Deflection of a Rivet in Double Shear," Transactions American Society of Mechanical Engineers, Vol. 82E, p 208, March 1960.

89. Taira, S. Koterzawa, R. and Inoue, M., "Fatigue and Dynamic Creep Properties of a 13 Cr Steel at Elevated Temperatures under Combined Stresses of Static Tension and Alternating Bending," Bulletin Japanese Society of Mechanical Engineers, Vol. 2, No. 8, p 508, November 1959.

90. Van Buren, H. G., "Theory of Creep of Germanium Crystals," Physica, Vol. 25, p 775, 1959.

91. Vorhees, H. R., Sliepcevich, C. M. and Freeman, J. W., "Thick-Walled Pressure Vessels," Industrial and Engineering Chemistry, Vol. 48, No. 5, p 872, May 1956.

92. Wagner, P. and Driesner, A. R., "High Temperature Mechanical Properties of Graphite: Creep in Compression," Journal of Applied Physics, Vol. 30, No. 2, p 148, February 1959.

93. Wah, T. and Gregory, R. K., "Creep Collapse of Long Cylindrical Shells under High Temperature and External Pressure," Journal of the Aerospace Sciences, Vol. 28, No. 3, p 177, March 1961.

94. Warner, W. H. and Handleman, G. H., "A Modified Incremental Strain Law for Work Hardening Materials," Quarterly Journal of Mechanics and Applied Mathematics, Vol. 9, p 279, 1956.

95. Weertman, J., "Theory of Steady State Creep Based on Dislocation Climb," Journal of Applied Physics, Vol. 26, No. 10, p 1213, October 1955.

96. Weertman, J., "Dislocation Model of Low-Temperature Creep." Journal of Applied Physics, Vol. 29, p 1685, December 1958.

97. Wiesinger, F. W., "Creep Data on ASTM Type 302 Steel," Materials in Design Engineering, Vol. 50, No. 3, p 172, September 1959.

98. Wnuk, M., and Zyczkowski, M., "Application of the Puwein Formula to the Theory of Buckling," Arch. Mech. Stos., Warsaw, Vol. 9, No. 2, p 297, 1957.

99. Zama, W. A., Lang, D. D. and Brotzen, F. R., "Steady State Creep of Tin Near the Melting Point," Journal of the Mechanics and Physics of Solids, Vol. 8, No. 1, p 45, January 1960.